PHOSPHOLIPASE A_2 REGULATION OF GOLGI AND ENDOSOME STRUCTURE AND FUNCTION

A Dissertation

Presented to the Faculty of the Graduate School

of Cornell University

In Partial Fulfillment of the Requirements for the Degree of

Doctor of Philosophy

by

Marie Eileen Bechler

January 2011

PHOSPHOLIPASE A_2 REGULATION OF GOLGI AND ENDOSOME STRUCTURE AND FUNCTION

Marie Eileen Bechler, Ph. D.

Cornell University 2011

The transport mechanisms of secretory and endocytic pathways are responsible for the coordinated movement of proteins and lipids throughout the cell at the proper time and place. In mammalian cells, there are many proteins dedicated to maintaining organelles and the trafficking of materials between them, though the mechanisms that regulate these processes are far from being fully understood. For over a decade, the role of phospholipase and acyltransferase lipid-modifying enzymes in membrane trafficking has been described, but the identity of the proteins involved had not been determined. Inhibitor studies demonstrated that both PLA_2 and LPAT enzymes regulate trafficking events and membrane tubule formation from the Golgi complex and endosomes. In the last year, one LPAT and three PLA enzymes were found to contribute to trafficking and organelle maintenance of the Golgi and endosomes, including the work described here.

The function of the PLA_2 enzyme complex platelet activating factor acetylhydrolase Ib (PAFAH Ib) was investigated at both the Golgi complex and endosomes. Employing overexpression and knockdown of PAFAH Ib subunits in mammalian cells, I have found that the catalytic α subunits and the non-catalytic β subunit, LIS1, are important for the maintenance of an intact Golgi ribbon. The catalytic α subunits are important for the formation of membrane tubules and anterograde trafficking. I have also found that each

α subunit has distinct contributions to regulating Golgi morphology, assembly, and secretory trafficking. Knockdown of one subunit alone is not compensated by the presence of the other. At endosomes, both α subunits are important for membrane tubule formation and endocytic recycling pathways. Furthermore, the interaction of these subunits with LIS1 appears to regulate the distribution of endocytic compartments within the cell.

Additionally, I have used an in vitro Golgi membrane tubule reconstitution assay to investigate the regulation of membrane tubule formation by heterotrimeric Gβγ subunits. I utilized inhibitors of PLA_2 enzymes and the purified Gβ1γ2 protein complex to demonstrate that Gβ1γ2 can stimulate Golgi membrane tubules through a PLA_2 dependant pathway. This suggests that Gβ1γ2 may regulate the activity of PLA_2 enzymes important for the formation of membrane tubules or positive membrane curvature.

BIOGRAPHICAL SKETCH

Marie Eileen Bechler was born and raised just outside Milwaukee, in the town of Menomonee Falls, WI. She grew up under her parents Janice and David Bechler, with sister Bonnie and brother Daniel. She graduated from Menomonee Falls High School in 2000 and matriculated at the University of Wisconsin-Madison, majoring in biochemistry. While at UW-Madison, she participated in the Hawai'i club, performing hula at on- and off-campus events, was a member of the women in science and engineering organization, volunteered for charities, including the multiple sclerosis society, participated in concert band, and conducted undergraduate research. She first obtained a job in the lab of Dr. Sean Carroll, caring for the lab's butterfly colonies. Later she conducted research in Dr. Michael MacDonald's laboratory at the UW-Madison Medical School. Her project involved screening soil bacteria for reactivity with sera from type I diabetic patients, in hopes to find whether bacteria contribute to triggering the autoimmune response of this disease. Marie graduated in 2003 with a Bachelor of Science degree. She entered graduate school at Cornell University in Ithaca, NY in 2003, and joined the Brown lab in 2004, working to earn a doctoral degree in biochemistry, molecular, and cell biology in the department of Molecular Biology and Genetics. During graduate school years, besides research, she enjoyed several hobbies whenever she had the opportunity: cooking, photography, playing the flute, traveling, and backpacking. Marie will be continuing research, shifting to the cell biology of myelin sheath formation as a postdoctoral fellow in Charles ffrench-Costant's lab at the University of Edinburgh.

ACKNOWLEDGEMENTS

I would like to acknowledge and thank my advisor, Bill Brown, for many years of guidance and support in my graduate research. He has fostered my ability to become an independent scientist. I would like to thank the Brown lab members, committee members Tony Bretscher and Andrea Quaroni for helpful discussions of this work. I would like to acknowledge Amy Antosh, Ina Chen, Anne Doody, Jim Garrison, Bret Judson, Lin Lin, Kelvin Lee, and Esther Racoosin for contributions to these projects by assisting with electron microscopy, plasmid preparation, protein purification, antibody production, and experiments cited within this dissertation. I would also like to thank the Bretscher lab for use of instrumentation.

I appreciate the support and encouragement from my family and friends over the years. In addition, I am grateful to Ryan Lewis, who has challenged me to try my crazy ideas (many of which inevitably would not work) and for thoughtful discussions of this work. He has been an extraordinarily positive influence.

TABLE OF CONTENTS

LIST OF FIGURES

LIST OF TABLES

LIST OF ABBREVIATIONS

AAG	1-*O*-alkyl-2-acetyl-glycero phospholipids
AGPAT	1-acylglycerol-3-phosphate *O*-acyltransferase
AP	adaptor protein
ARF1	ADP-ribosylation factor 1
ATP	adenosine triphosphate
BBC	bovine brain cytosol
BFA	brefeldin A
BGS	bovine growth serum
BSA	bovine serum albumin
BTRD	Bovine transformed testicular cell line
CERT	ceramide transfer protein
CFTR	cystic fibrosis transmembrane conductance regulator
CHAPS	3-[(3-cholamidopropyl)dimethylammonio]-1-propanesulfonate
CoA	coenzyme A
COPI	coat protein complex I
COPII	coat protein complex II
Cos7	African green monkey kidney cell line
$cPLA_2$	cytoplasmic phospholipase A_2 enzyme family
DAG	diacylglycerol
DMEM	Dubelcco's modified eagle medium
DTT	dithiothreitol
EDTA	ethylenediamine tetraacetic acid
EEA1	early endosome antigen1
EGF	epidermal growth factor
EGTA	ethylene glycol tetraacetic acid
EHD/Rme1	Eps15-homology-domain protein/receptor mediated endocytosis protein 1
EM	electron microscopy

Eps15	EGF receptor pathway substrate 15
ER	endoplasmic reticulum
ERC	endocytic recycling compartment
ERES	endoplasmic reticulum exit sites
ERGIC	ER-Golgi-intermediate compartment
ESCRT	endosomal sorting complex required for transport
FA	fatty acid
FAPP2	four-phosphate adaptor protein 2
FITC	fluorescein isothiocyanate
GalT	galactosyltransferase
GDP	guanine nucleotide diphosphate
GF	gel filtration
GFP	green fluorescent protein
GGA	Golgi-localized, γ-ear-containing, ADP-ribosylation factor-binding proteins
GPCR	G protein coupled receptor
GPP130	Golgi phosphoprotein 130 kD
GST	glutathione S-transferase
GTP	guanine nucleotide triphosphate
GUV	giant unilamellar vesicle
HA	hemagglutinin
HeLa	human epithelial cell line
HRP	horseradish peroxidase
Hrs	hepatocyte-growth-factor-regulated tyrosine kinase substrate
IC_{50}	concentration required for 50% inhibition
$iPLA_1$	intracellular phospholipase A_1 enzyme family
$iPLA_2$	Ca^{2+}-independent phospholipase A_2 enzyme family
ITD	isotetrandrine
KDEL	ER retention signal-amino acid sequence
LAMP	lysosome associated membrane protein

LDL	low density lipoprotein
LPA	lysophosphatidic acid
LPAAT	lysophosphatidic acid acyltransferase
LPAT	lysophospholipid acyltransferase
LPC	lysophosphatidylcholine
LPL	lysophospholipid
$LPLA_2$	lysosomal phospholipase A_2 enzyme family
LPP	lipid phosphate phosphatase
$LpPLA_2$	lipoprotein associated phospholipase A_2
M6PR	mannose-6-phosphate receptor
MALDI	matrix assisted laser desorption/ionization
ManII	mannosidase II
MEM	minimal essential media
MTOC	microtubule organizing center
MVB	multivesicular body
NDE1	nuclear distribution protein
Ndel1	nuclear distribution protein nudE-like1
NSF	N-ethylmaleimide-sensitive factor
NTE	neuropathy target esterase
ONO-RS-082	2-(*p*-amylcinnamoyl) amino-4 chlorobenzoic acid
PA	phosphatidic acid
PAF	platelet activating factor (1-*O*-alkyl-2-acetyl-*sn*-glycero-3-phosphocholine)
PAFAH	platelet activating factor acetylhydrolase
PAFR	platelet activating factor receptor
PBS	phosphate buffered saline
PC	phosphatidylcholine
PE	phosphatidylethanolamine
PI	phosphatidylinositol
PIP	phosphatidylinositol phosphate
PKC	protein kinase C

PKD	protein kinase D
PKD-KD	protein kinase D kinase dead
PL	phospholipid
PLA_1	phospholipase A_1
PLA_2	phospholipase A_2
PLAA	phospholipase A_2 activating protein
PLC	phospholipase C
PLD	phospholipase D
PMSF	phenylmethylsulfonyl fluoride
PNPLA	patatin-like phospholipase domain containing proteins
Rab	Ras superfamily GTPase
RER	rough endoplasmic reticulum
RNAi	RNA interference
SEM	standard error of the mean
SNAP	soluble NSF attachment protein
SNARE	SNAP receptors
SNX	sorting nexin
$sPLA_2$	secreted phospholipase A_2 enzyme family
ssHRP	signal sequence horseradish peroxidase
TAG	triacylglycerol
Tf	transferrin
TfR	transferrin receptor
TGN	*trans* Golgi network
TMB	3, 3′, 5, 5′-tetramethylbenzidine
TOF	time of flight
TRITC	tetramethyl rhodamine isothiocyanate
VLDLR	very low density lipoprotein receptor
VSV-G ts045	vesicular stomatitis virus G-protein temperature sensitive
VTC	vesicular tubular cluster
YFP	yellow fluorescent protein

CHAPTER 1

General Introduction

For every organism, the coordinated movement of macromolecules within the cell is a constant and critical part of life. Eukaryotic cells are physically compartmentalized to enclose components for particular metabolic pathways within membrane-bound organelles, including: the nucleus, mitochondria, peroxisomes, lipid droplets, the endoplasmic reticulum, the Golgi complex, endosomes, and lysosomes. Many macromolecules—e.g. proteins, lipids, carbohydrates, DNA, etc.—require a specific environment and localization to properly function. If a protein involved in transport of nutrients across the plasma membrane is misrouted to any other location it could be devastating to cell homeostasis. Additionally, the transport of lipids is essential for all cells. Lipid trafficking is particularly critical in specialized cells, such as Schwann cells, which insulate the electrical signals of neurons by producing massive membrane sheets that wrap vertebrate neurons in the form of a myelin sheath. Eukaryotic cells have developed tightly regulated spatial and temporal trafficking mechanisms to permit cellular processes to become more complex and specialized.

The Secretory Pathway

An estimated one quarter to one third of proteins encoded in the human genome are synthesized at the endoplasmic reticulum (ER) and shuttled through the secretory pathway (1), as depicted in Figure 1-1. Newly synthesized proteins in the rough ER and lipids from the smooth ER are packaged and delivered to the Golgi complex, traverse the Golgi stack to the

Figure 1-1: A depiction of the secretory and endocytic organelles and related trafficking pathways. Transport intermediates carrying both proteins and lipids between the membrane bound organelles occurs via various membrane bound vesicles—COPI, COPII, clathrin (AP-1 or AP-2)—or membrane tubules. Microtubule motor proteins are shown (dynein and kinesin) at respective transport steps. Red arrows indicate transport that can occur by membrane tubules. TGN = *trans* Golgi network, RER = rough endoplasmic reticulum, VTC = vesicular tubular cluster, ERGIC = ER-Golgi-Intermediate Compartment, MVB = multivesicular body.

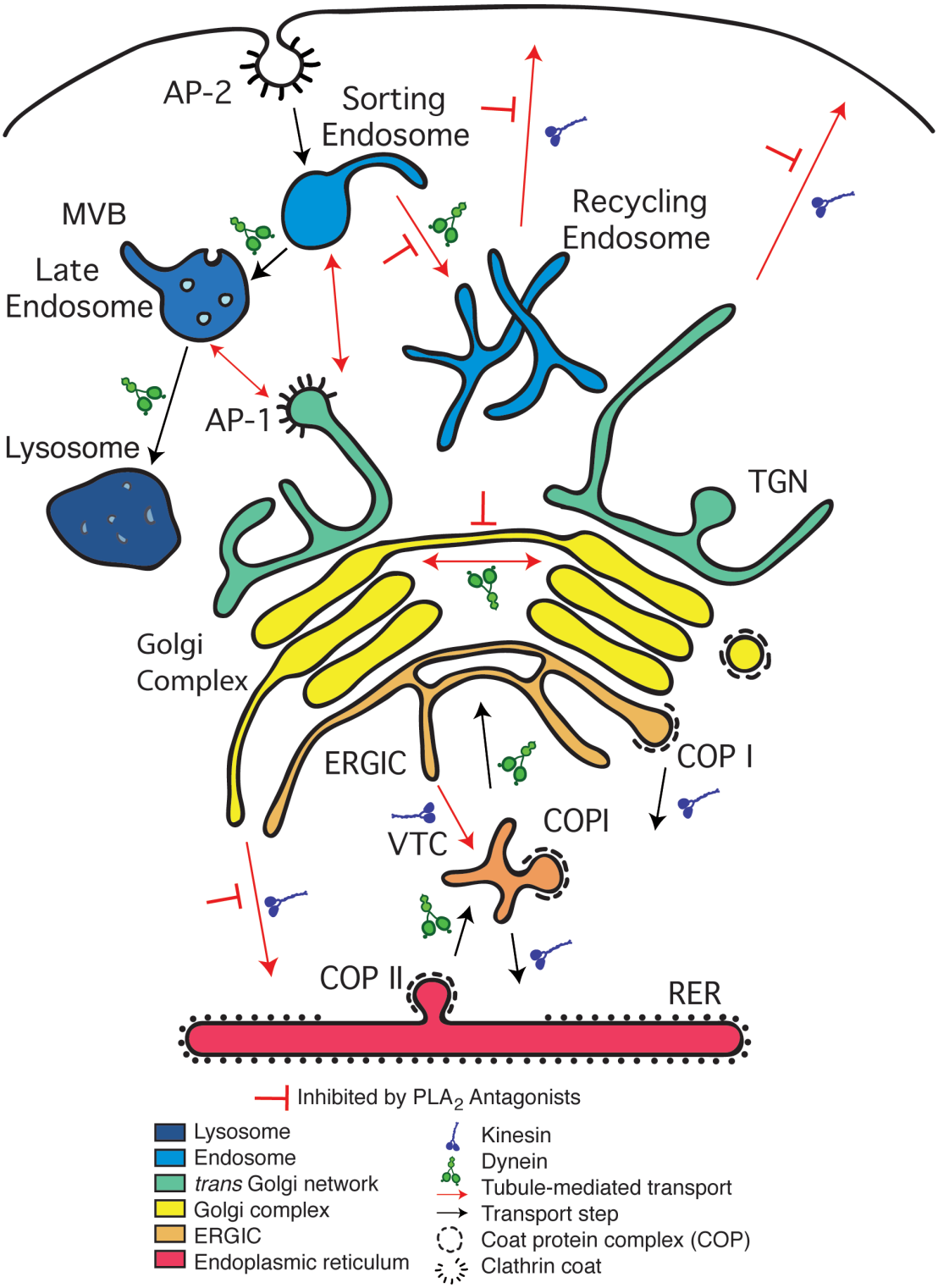
AP-2
Sorting Endosome
MVB
Late Endosome
Recycling Endosome
AP-1
Lysosome
TGN
Golgi Complex
ERGIC
COP I
COPI
VTC
COP II
RER
Inhibited by PLA2 Antagonists
Lysosome
Endosome
trans Golgi network
Golgi complex
ERGIC
Endoplasmic reticulum
Kinesin
Dynein
Tubule-mediated transport
Transport step
Coat protein complex (COP)
Clathrin coat

trans Golgi network (TGN), where they are sorted and packaged for delivery to their site of function outside the cell, on the plasma membrane, in endosomes, or in lysosomes. Since the first description of the secretory pathway by George Palade (2), there have been many advances in our understanding of how proteins and lipids are sorted and shuttled through these organelles, but many details and regulatory mechanisms have yet to be revealed.

Endoplasmic Reticulum

The endoplasmic reticulum (ER) is an expansive organelle of membrane sheets and a tubular network reaching from the nuclear envelope to the outer edges of mammalian cells (3). The mRNA of transmembrane or luminal proteins destined for the secretory pathway initially begin translation in the cytoplasm and are quickly recognized and shuttled to the surface of the rough ER by the signal recognition particle, which recognizes a signal sequence on the nascent polypeptide as it is generated by an associated ribosome (4). Upon reaching the ER, the polypeptide chain is co-translationally directed into the lumen or membrane of the ER by the translocon. The process of nascent chain recognition and ER insertion is reviewed in (4-6). Upon arrival in the ER, an assortment of chaperone proteins aid in proper protein folding, disulfide isomerases assist in correctly forming disulfide bonds, and resident glycosylation enzymes modify the proteins. Once properly folded, these proteins are targeted for packaging into membrane-bound vesicles that bud from specific ribosome-free subdomains of the ER known as ER exit sites (ERES) (7, 8).

The smooth ER is a major site of cell membrane biosynthesis,

containing many of the enzymes that convert storage lipids (such as triacylglycerol, TAG) into certain types of glycerophospholipids. Lipids generated in the ER additionally must exit the ER and progress to the Golgi complex. These membrane lipids can undergo movement to the Golgi complex either in membrane-bound transport intermediates or are shuttled by specific transfer proteins (e.g. CERT, FAPP2) to the Golgi and TGN, as is the case for lipids such as ceramide (9).

At ERES, a specific set of proteins has been identified that regulate sorting of cargo into membrane buds and form spherical vesicles. Several of these proteins, known as coat protein complex II (COP II) components, bind to transmembrane cargo and coat the surface of budding ER membranes (10-12). COPII coated vesicles shed their coat shortly after budding, allowing the vesicles to fuse with other membranes that form vesicular tubular clusters (VTC), structures also known as the ER Golgi Intermediate Compartment (ERGIC), that are shuttled to the Golgi complex (13-19).

While exported proteins and lipids progress to the Golgi complex (i.e. move in an anterograde direction), ER resident proteins that escape are captured and retrieved by specific receptors, such as the KDEL receptor at the ERGIC compartment as well as early Golgi compartments (i.e. move in an retrograde direction). These receptors recognize specific amino acid sequences, such as KDEL (20), that act as ER retention signal sequences for their retrieval back to the ER. The process of sorting these ER proteins for retrieval is aided by the subsequent packaging of KDEL receptors by another class of coat proteins that are part of the coat protein complex I (COPI) (20-24). In addition to these spherical vesicle transport carriers, proteins and lipids returned to the ER by this retrograde pathway can be seen to move through

long membrane extensions known as membrane tubules (21, 25-27). The sorting and packaging of both anterograde and retrograde cargo into vesicles at the ER and Golgi interface is also reviewed in (1). Once arriving at the ERGIC, proteins and lipids are transported to the anterograde 'arrival center' of the Golgi complex, the *cis* cisternae of the Golgi complex. While some evidence suggests that COPI may be involved in anterograde transport from the ERGIC to the *cis* Golgi (28), the ERGIC is alternatively thought to grow and mature into or fuse with the *cis* cisternae of the Golgi complex, thereby moving cargo forward as ER proteins are packaged by COPI and returned to the ER (14, 18, 29, 30).

The Golgi Complex

The Golgi complex is believed to be the central hub of trafficking in mammalian cells, critical for processing and sorting newly synthesized lipids and proteins from the ER to endosomes, lysosomes, the ER, the plasma membrane and out of the cell. At the same time, the Golgi complex also receives lipids and proteins from endosomes. As cargo from the ER passes through the stacked/layered membrane subdomains called cisternae in an anterograde direction (*cis* to *trans*), they are exposed to unique enzymes, decreasing pH, and changes in lipid compositions (e.g. increasing cholesterol and sphingolipids) (31-35). The realization that the Golgi complex is the major site of protein glycosylation (36) led to the discovery that unique subdomains in the Golgi complex exist. The Golgi cisternae *cis*, *medial*, *trans*, and the TGN, each have sequential glycosylating enzymes and lipid metabolism enzymes that are resident to that compartment (37-40).

Constant departure and arrival of proteins and lipids creates a complex

organelle architecture that is highly fenestrated with numerous vesicles and tubules on both the *cis* and *trans* most sides of the Golgi complex (13, 41-44). In between the outermost cisternae, relatively compact membrane stacks of *cis*, *medial*, and *trans* cisternae are present, often bridged into a ribbon-like structure with membrane tubules between and across cisternae (45-49). Numerous vesicles have been seen emanating from less compact regions within the Golgi complex (50).

The Golgi ribbon structure is seen in most animal cells, however in plants, Drosophila, and certain yeast species such as *Schizosaccharomyces pombe* and *Pichia pastoris* the Golgi complexes are mini-stacks, physically separate and distributed throughout a cell rather than in a centralized Golgi ribbon (51-54). Strikingly, the number of cisternae within a cell remains constant, but between cells and cell types this number varies (35). Most animal cells have a total of 3-8 individual cisternae, whereas plant cells can exceed 100 (35, 53). Another deviation in Golgi structure is found in the yeast *Saccharomyces cerevisae*, which do not have stacked Golgi and have separated cisternae scattered throughout the cell (51, 54). It is unclear if a stacked or ribbon structure is important for enzymatic function or transport and whether the Golgi complex structure found in mammalian cells has evolved to become more efficient to accommodate increasingly complex or extensive trafficking. A more detailed review of Golgi evolution in eukaryotes can be found in (55).

In mammalian cells, the Golgi complex structure is maintained by the constant flux of proteins and lipids, tethering proteins, as well as microtubule and dynein-dependent anchoring to the centrosome (the convergence point for the minus ends of radial-positioned microtubules). The Golgi cisternae may vary greatly in volume, expanding or shrinking accordant to the

flux/secretory load of proteins and lipids through the Golgi complex (56-58). The tethering, protein-dense meshwork surrounding the Golgi (aka Golgi matrix) (59-62) is maintained by golgins (reviewed by (63)), which bind to cisternae and vesicle membranes, keeping cisternae as a stacked structure and aiding in the capture of vesicles. The mammalian Golgi complex is held close to the centrosome (within 1-3 μm) by the microtubule motor dynein (35, 64-66). Dynein and microtubules are important for maintenance and the formation of Golgi ribbon structure (64, 67, 68).

During mitosis the Golgi complex disassembles, either redistributing its contents to the ER (69-73) or becoming fragmented and scattered upon the disassembly of the microtubule network (74-77). After cell division, the Golgi first appears as small, distinct stacked cisternal units, mini-stacks, that are disconnected and scattered throughout the cell. These mini-stacks eventually converge into a single stacked Golgi complex located adjacent to the centrosome. This process has been shown to be dependent on microtubules and involves the microtubule motor dynein (67, 75). The reassembly of the Golgi and continual maintenance of Golgi ribbon structure are also dependent on membrane tubules (78, 79).

Transport through the Golgi (intra-Golgi transport) has been a topic of debate for many years. Several models exist to address how cargo moves forward while the enzyme and lipid compositions of cisternal sub-compartments is maintained. The two primary models, cisternal maturation model and vesicular transport model, suggest that either the cisternae itself carries cargo forward while enzymes are recycled back, or the cargo is packaged into transport carriers that move forward while enzymes stay in distinct cisternae (80, 81). Much of the argument lies in the inconsistencies

between studies (82-84), such as reports that COPI vesicles contain Golgi resident enzymes (23, 85), while other reports suggest that COPI vesicles contain secretory cargo and not resident enzymes (86, 87). The predominant model of the field is that of cisternal maturation: the ERGIC matures into the *cis* Golgi, which matures into *medial*, *trans* and then peels away from the Golgi stack turning into the TGN, which is consumed by the creation of transport vesicles and tubules (88, 89). In this model, COPI vesicles (or membrane tubules) would recycle enzymes to newer cisternae. Recent work using live imaging of fluorescently tagged cargo and distinct cisternae resident enzymes in *S. cerevisiae* showed that resident enzymes rapidly change from *cis*, *medial*, to *trans* in each cisterna spot (90, 91). These results indicate that a cisterna acquires the next set of enzymes from a more 'mature' cisterna, strongly supporting the maturation model. The cisternal maturation model is also supported by the movement of pro-collagen and algae scales through the Golgi stack. These molecules stay within the cisternae as they traverse the Golgi complex (92, 93). Other models, besides cisternal maturation and the vesicular transport model, suggest that compartments of the Golgi are not always distinct, and tubules interconnect cisternae to provide a route for cargo to progress forward or enzymes to be transferred to new cisternae (47). A new and controversial model of 'rapid-partitioning' suggests that cargo and enzymes separate/partition laterally across cisternae (94). This model accounts for the kinetics of cargo transport seen in live-cell imaging studies, which are not consistent with the maturation model, and addresses disputes on the direction of movement for enzymes in transport carriers, indicating the carriers are bidirectional. This model also incorporates the role of lipids in sorting and partitioning transmembrane proteins. However, the rapid

partitioning model is difficult to reconcile with the foundation that resident enzymes are enriched in particular cisternae and are in sequential order to which glycosylation reactions take place (33). A more comprehensive discussion of recent work on transport through the Golgi complex can be found in (95).

Irrespective of the exact route for cargo to be modified and traverse the Golgi complex, proteins and lipids requiring export from the Golgi complex to the plasma membrane and endosomes reach the TGN. The TGN is considered the major sorting and packaging site for cargo traversing the Golgi complex. The TGN additionally receives proteins and lipids transported from endosomes, a process that is believed necessary for the homeostasis of the TGN. The gradual anterograde enrichment of particular proteins and lipids across the Golgi stack combined with the arrival of lipids and proteins from endosomes creates a distinct TGN composition rich in cholesterol, sphingolipids, and enriched in enzymes for the synthesis of sphingomyelin (96, 97).

At the TGN, it is believed that sorting can occur through the formation of lipid domains and cargo segregation by vesicle coat proteins. The TGN sorts and packages cargo for delivery to endosomes using a particular class of vesicle coat proteins known as clathrin and clathrin adaptor proteins (96-98). At the TGN, both AP1 and GGA (Golgi-localized, γ-ear-containing, ADP-ribosylation factor-binding proteins) clathrin adaptor proteins recognize cargo for transport to the endocytic/lysosomal system. Endosome/lysosome destined cargo are believed to contain sorting signals that aid in their recognition and packaging into endosome-destined clathrin coated vesicles (99). Sorting events at the TGN are also important for segregation of cargo

destined for apical versus basolateral membranes in polarized cells, reviewed in (100-102). One example of TGN sorting in polarized cells is through the use of the clathrin adaptor AP1B, which may recognize sorting signals within the cargo for packaging into basolateral-destined vesicles (102-106).

Other cargo destined for the plasma membrane is found in clathrin-independent transport carriers: secretory granules for regulated secretion, non-clathrin or -COP coated vesicles, and larger tubular carriers. The mechanisms for selective cargo transport from these alternative transport carriers are not well understood. The tubular carriers do not appear to concentrate cargo at the TGN and are thought to allow for bulk, constitutive secretion (107-109). However, membrane tubules seen at the TGN exclude resident enzymes, suggesting some level of segregation exists (108, 110). Cargo segregation may be partly controlled by the partitioning of cholesterol and sphingolipids into domains on the TGN membrane, which has been suggested for glycosylphosphatidylinositol (GPI)-anchored protein transport to the apical plasma membrane (111, 112). Further discussion of TGN exit mechanisms can be found in (96, 97).

Endocytic Trafficking Pathways

Cell surface proteins and material internalized into a eukaryotic cell is often packaged into small inward-budding vesicles at the plasma membrane. Once budded into the cell, the nutrients, proteins, and lipids are delivered to sorting stations known as early sorting endosomes, where machinery further packages the material for degradation in the lysosome or recycling back to the plasma membrane (113). The endocytic pathway is depicted in Figure 1-1. Mammalian cells internalize their entire plasma membrane contents once

every 1-5 hours, therefore it is critical that a balance of internalization, delivery, and recycling exists (114).

Like most organelles, the types of endocytic organelles are defined by enriched proteins and lipids that compose them. However, the composition of endosomes is dynamic, and the presence of lipids and proteins is continually changing (115, 116). Therefore the classification of endosomes based on the presence of different protein and lipid components only identifies a transient stage of endocytic organelles. Endosomes are constantly sorting, enriching, and exchanging molecules with other membrane bound compartments and the cytoplasm.

Proteins and lipids to be endocytosed are segregated prior to internalization. Particular types of cargo are internalized in specific plasma membrane domains and by specific sets of machinery. These endocytic processes are subdivided into clathrin-dependent and clathrin-independent, which includes caveolae, phagocytosis, pinocytosis and other membrane invaginations. Endocytic events are extensively reviewed in (117, 118). Clathrin-mediated endocytosis is the best understood route of endocytosis, involving recognition of dileucine and tyrosine-based sorting signals/motifs in plasma membrane receptors by clathrin adaptor AP2 (99).

Vesicles and tubular invaginations from the plasma membrane fuse with each other and with early sorting endosome membranes, which are occupied sequentially with components involved in regulating fusion, sorting of cargo, and budding of cargo (116, 119, 120). Early endosomes are defined as the receiving compartments for plasma membrane internalized cargo. These compartments are enriched in specific Rab GTPases, Rab5 and Rab4, which are involved in regulating the fusion and transport of cargo from the

plasma membrane and delivery to the endocytic recycling compartment (ERC), respectively (115, 119, 121, 122). Early endosomes are also enriched in proteins and lipids involved in the recruitment of fusion and sorting machinery, upstream and downstream of Rab protein recruitment and activation, such as the phosphoinositide-3-P kinase (PI(3)P kinase), the phosphoinositide-3-phosphate (PI(3)P), and EEA1 (early endosome antigen 1, a Rab5 effector protein) (119, 123).

The predominant model for endocytic sorting is through a process of endosome maturation. Membrane tubules sort away cargo destined for the recycling pathway at early endosomes, while cargo to be degraded remains in early endosomes as the endosomes change their composition by recruitment of proteins from the cytosol and 'kiss-and-run' or fusion events with other endocytic compartments to gradually exchange early endosome proteins for late endosome machinery (119, 122, 124, 125). Early endosome membrane tubules have been shown to concentrate or sort transmembrane proteins and lipids away from soluble, luminal cargo (126, 127). This process occurs as the endosomes move on dynein motors towards the minus end of microtubule tracks (116, 128, 129). Concomitantly, transmembrane proteins that are destined for degradation are tagged with ubiquitin and recognized by Hrs and ESCRT (endosome sorting complex required for transport) machinery that sorts these proteins into invaginating domains on the endosome (130-134). These domains eventually turn into small inward budding vesicles enriched in the lipid lysobisphosphatidic acid (bis(monoacylglycero)phosphate) and bud into the lumen of an endosome, which can be seen in late endosome multi-vesicular bodies (MVBs) (120, 135, 136). These endosomes mature into late endosomes or MVBs by losing early endosome components and acquiring late

endosome proteins and lipids such as Rab7, Rab9, CD63, PI(3,5)P (by phosphoinositide kinase PIKFyve activity) (119, 137-139). They also increase amount of vacuolar H^+-ATPase pumps that lower the pH from ~6 to pH ~5 and receive lysosomal hydrolases delivered from the TGN (122, 140). Further enrichment of LAMPs (lysosomal associated membrane proteins), acquisition of lysosomal enzymes, and decrease in pH down to pH 4-5 occurs as late endosomes and MVBs merge with lysosomes, the terminal destination for cargo to be degraded (122, 140-142). The low pH activates hydrolases that degrade the luminal soluble and internal vesicles at the lysosome.

Cargo destined for recycling to the plasma membrane can travel directly from early endosomes to the plasma membrane in a 'rapid/short' recycling pathway (143, 144), but it is believed that the majority of recycled components travel from the early sorting endosomes to the ERC. The actual fraction of cargo traveling in the short recycling versus the 'long,' ERC-mediated pathway is not known (115). Proteins involved in the regulation of endocytic recycling pathways can be found reviewed in more detail in (121). The vast majority of recycled cargo can be seen traveling from early endosomes to the ERC by membrane tubules (113, 145). Upon reaching the ERC, which is a more stationary tubulovesicular network often adjacent to the TGN, cargo is sorted to the plasma membrane in membrane tubule carriers (115, 146). In polarized cells, the ERC may play a pivotal role in transcytosis and the regulation of sorting apical versus basolateral cargo to the correct plasma membrane surface (100, 147). The transport of cargo from the ERC to the plasma membrane is regulated by Rab11 and EHD/RME1 (Eps15-homology-domain protein/receptor-mediated endocytosis protein) (115, 121). Rab11 is the most common marker for the ERC due to its fairly stable

association with these membranes. Both EHD family members and sorting nexins (SNX) have been shown to be involved at specific endocytic transport steps, and both families have been shown to either stimulate or stabilize membrane tubules from endocytic compartments (121, 148-150).

As previously mentioned, there are also retrograde pathways from endosomes to the TGN that aid in recycling membrane and proteins required for TGN functions. One such pathway is mediated by the retromer complex, which forms either vesicles or tubules from endosomes (early to late) that move from these endosomes to the TGN (151-154). The retromer complex aids in recycling TGN-based proteins such as the mannose-6-phosphate receptor (M6PR), so it may be used for additional rounds of transport from the TGN to the endocytic pathway. The retrograde endosome-to-TGN pathway is reviewed in (152, 155). Additional reviews on endocytic trafficking pathways can be found in (115, 121, 122, 152, 156).

Transport Carriers: Vesicles and Membrane Tubules

While both membrane bound vesicles and membrane tubules have been seen emanating from organelles of the secretory and endocytic pathways, it is still unclear what the relative contributions are of these two types of cargo carriers. These transport carriers exist at the ER, Golgi complex, and endosomes and aid in the sorting of cargo by both lipid-based and protein-based mechanisms (24, 157-159). Each of these carriers bud from a donor membrane, travel along cytoskeletal tracks, and then fuse with the target organelle for proper delivery. General mechanisms fundamental to this process can be found reviewed by (24, 160).

Vesicles

Vesicles were originally hypothesized to be the major route of protein trafficking between organelles, starting from the early studies of the secretory pathway by George Palade (2). Shortly after these studies the first vesicle coat protein, clathrin, was purified (161). Much has been revealed about the molecular mechanisms of vesicular transport in the 30 years since the initial vesicle transport hypothesis and the identification of clathrin, including mechanisms of vesicle formation, fission, targeting, and fusion. A temperature-sensitive yeast mutant screen by the Scheckman lab was a pivotal point in the identification of specific proteins involved in the secretory pathway. These proteins were coined 'Sec' proteins (162, 163). Studies by the Rothman lab using an in vitro reconstitution system and biochemical approach identified the contribution of key proteins such as COPI and SNAREs in transport (24, 164-166). These initial studies led to a large expansion of research into the mechanisms of vesicle-mediated transport in cells.

There are three main types of coated vesicles in mammals: COPI, COPII, and clathrin. Each of these types of coated vesicles requires protein complexes for their assembly and budding. The COPII, COPI, and clathrin coats are multi-subunit complexes containing proteins that bind to cargo and form cage-like scaffolding believed to aid in inducing membrane curvature (12, 160, 167). These vesicles bud from membranes, load onto cytoskeletal tracks by motor proteins, shed their protein coat, dock to the receiving membrane through tether proteins and SNARE machinery, and then fuse with the target membrane (24, 160, 166). Many of these steps, including that of initial assembly, uncoating, docking, and fusion are regulated by small GTPases

(such as Sar1, Arf1, and Rabs) that aid in the recruitment of proteins involved in each of these processes or by directly interacting with vesicle machinery (24). The selectivity of transport for these vesicles is believed to partially lie in the particular coat proteins used to form the vesicles. Clathrin coated vesicles associate with particular adaptor protein complexes (AP1, AP2, AP3 or GGA), which are found on vesicles budding from and transported to specific membranes. For example, AP2 adaptor proteins are specifically found at the plasma membrane and involved in clathrin-mediated endocytosis (160). The AP1 and GGA subunits are associated with clathrin at the TGN for transport to late endosomes. AP1 subunits recognize tyrosine-based sorting signals (such as YXXØ) in cargo and GGAs assist in sorting the M6PR through acidic clustered dileucine motifs (99). Similarly, coatamer complexes have recently been acknowledged to contain isoforms of subunits that can be found in distinct vesicles. For example, particular COPII Sec24 isoforms have been found to localize with specific subsets of cargo molecules (168-170). COPI subunit isoforms have been implicated in forming distinct vesicles at different locations within the Golgi complex (171).

Membrane Tubules

Electron microscopy studies long ago noted long membrane extensions, 60-100 nm in diameter, from organelles (41, 48, 49, 172-175), but these structures were not recognized as a mode of transport between organelles until live-cell imaging studies of fluorescent proteins and lipids. Initially, studies of the fungal metabolite brefeldin A (BFA) demonstrated dramatic tubule formation, carrying Golgi resident enzymes in a retrograde direction to the ER (176). The belief that vesicles were the sole transport carrier in

membrane trafficking changed when real time, live-cell imaging of transport intermediates containing green fluorescent protein (GFP)-tagged proteins and fluorescent lipids revealed the presence of long, thin membrane extensions that protrude from organelles, extend, break off and fuse with other organelles (177-182). These results showed that membrane tubules were not restricted to the presence of BFA and that membrane tubules appear to carry cargo (179-181, 183). Additionally, membrane tubules have been seen to occur regardless of vesicle inhibition by BFA or RNAi of vesicle components (180, 184) and exist with or without accompanying budding vesicles (180, 185, 186).

Like vesicles, tubules require an initial outward protrusion and extension from the donor membrane of an organelle, fission from the donor membrane, linkage to motor proteins and the cytoskeleton (which they have been shown to move along) (177, 178), and eventual fusion with the target compartment (158). Membrane tubules have been proposed to contribute to the sorting of protein and lipid cargo at many steps of trafficking: *cis* to *trans* intra Golgi transport (47), retrograde cargo trafficking to the ER (26, 178, 180, 187), ER to Golgi transport (11, 16, 179, 183, 188), TGN to cell surface trafficking (181, 185, 186, 189), and in endocytic recycling pathways (113, 115, 145, 152, 190). Additionally, endocytic cargo is shown to be concentrated within tubules (126, 191-193), likely from sorting of protein and lipid cargo via the tubule shape, which increases the membrane to lumen ratio (194-196). These observations suggest that tubules are a distinct and cooperative component of sorting and trafficking. The mechanisms of formation and regulation of these transport carriers are only now beginning to be identified.

Transport Intermediates: Bending a Membrane

To shuttle proteins and lipids between the various organelles of the secretory and endocytic pathway, domains on organelle membranes must first bend into spherical and tubular shapes to create vesicles and tubules, which then undergo constriction/pinching for their fission and release. This bulging and constriction may be achieved by several means: proteins that bind to the membrane surface and generate forces that bend, stretch, and pinch off the carriers, proteins that insert into membranes, or via changes in the lipid composition of the membrane itself. These mechanisms are reviewed in (167).

Proteins can generate force to bend membranes in a number of ways. Linking motor proteins to membranes can generate force to pull or stretch the membrane; the kinesin motor protein has been shown to pull tubes from giant unilamellar vesicles (GUVs) in vitro (197). Many proteins have been implicated in bending membranes by forming scaffolds that force the membrane to adopt their particular shape (167). For example, proteins of coated vesicles, such as COPII, form curved, cage-like scaffolding that may contribute to the bending energy needed to form vesicles (167, 198-200). Certain BAR-domain containing proteins, such as SNXs, have an intrinsic crescent-shaped structure and dramatic tubulation of membranes occurs when these proteins are overexpressed in cells or with liposomes in vitro (148, 198, 201-204). However, it is unclear whether these SNXs and other BAR-domain containing proteins induce the curvature or stabilize curvature that already exists, as they preferably bind to curved membranes and form scaffolds on their surfaces (201, 205-208).

Membrane curvature can also be achieved by the insertion of amphipatheic or hydrophobic regions of proteins, such as caveolin, reticulons,

Arf1, Sar1 and certain BAR domain containing proteins, into the outer leaflet of the membrane bilayer (12, 167, 209-212). Many of these proteins have been shown to generate tubules from liposomes in vitro in addition to being important for membrane trafficking events, vesicle, and/or membrane tubule formation in cells (213-216). Changes in membrane composition on one leaflet of the membrane bilayer can generate changes in membrane curvature. This membrane bilayer couple hypothesis was proposed by Sheetz and Singer in the 1970s (217) and has progressed over the years to aid in understanding how membrane bilayer asymmetry can generate membrane curvature.

The lipid composition itself also has a fundamental role in providing the framework for membrane bending, fission and fusion (159, 198, 218, 219). Lipids can contribute in several ways, by changing the fluidity/rigidity of the membrane, making it easier or more difficult to stretch, bend and push the bilayer, by generating an intrinsic curvature, or by creating domains that allow for regulatory protein binding. Specific lysophospholipids (LPLs), phosphatidic acid (PA), and diacylglycerol (DAG) all have spontaneous (intrinsic) positive or negative curvature that can bend membranes as well as increase or decrease fusion and fission events (198, 220, 221). Several lipid species have been shown to recruit effector proteins to membranes, such as DAG, which recruits fission factors such as protein kinase D (PKD) (222). Another well-studied class of lipid signaling/targeted binding molecules is phosphoinositides. Phosphoinositol (PI) can be phosphorylated at several specific points in the inositol ring, allowing for several phosphoinositol phosphate (PIPs) species. These PIPs have been shown to be enriched in specific organelle membranes and therefore contribute to organelle 'identity', allowing for proteins to specifically bind to one organelle membrane and not

others (223-226). PI(4,5)P2 and PI(3,4,5)P3 are enriched at the plasma membrane, PI(3)P on early endosomes, PI(4)P at the Golgi or TGN, and PI(3,5)P at late endosomes (227).

Regulation of Membrane Trafficking by Lipid Composition

There is growing realization that lipids can have a dramatic impact on the behavior of proteins, protein recruitment to membrane surfaces, and the formation transport intermediates (159, 210). Lipid composition has been shown to create environments that proteins can partition into or exclude themselves from, generate binding surfaces to recruit effector proteins involved in regulation of trafficking, or change intrinsic curvature to aid in membrane bending, fission, and fusion (159, 219-221). Additionally, asymmetric changes in membrane composition can generate changes in membrane curvature (217). Thus, lipid-modifying enzymes are crucial to intracellular trafficking. Many phospholipid-modifying enzymes exist in mammals to create an enormous variety of phospholipid species with varying head groups, acyl chains, and covalent bonds between the fatty acid chains and glycerol. The membrane composition—the specific phospholipids, fatty acids, and sterol content—can have a profound effect on the fluidity/rigidity, curvature, and binding affinity for proteins (159); all of which regulate organelle architecture and membrane trafficking. Several general classes of proteins contribute to generating membrane bilayer asymmetry in the bilayer, including lipases and acyltransferases—both of which directly alter individual phospholipids—as well as flippases which can move phospholipid species between the two leaflets.

Lipid-modifying Enzymes

Several classes of phospholipid altering enzymes have been implicated in organelle architecture and membrane trafficking, particularly phospholipases and acyltransferases, which cleave or reacylate phospholipids as depicted in Figure 1-2. Phospholipase C member PLCβ3 was implicated in TGN to plasma membrane transport by generation of DAG, which recruits the fission factor PKD (228). Phopshoinositide lipids (PIs, PI(4,5)P2 and PI(4)P) are cleaved by specific PLC enzymes to generate DAG, which is a negative curvature inducing PL that also recruits fission factors such as PKD to the TGN (220, 222, 229, 230). Phospholipase D (PLD) has been shown to generate DAG indirectly by converting PC to PA, which can then be converted into DAG by lipid phosphate phosphatase (LPP). Both PLD1 and PLD2 are thought to partially localize to Golgi membranes (231, 232) and in vitro increase secretory vesicle release from Golgi membranes (233). PLD2 has also been implicated in endocytic recycling transport carrier formation (234, 235). Cells with reduced PLD levels show decreased export of secretory cargo, specifically CFTR (cystic fibrosis transmembrane conductance regulator) (236) and inhibition of PLD by 1-butanol shows decreased VSV-G trafficking both the ER to Golgi and TGN to plasma membrane, as well as altering Golgi complex structure (237). Further review of PLD and the Golgi complex can be found in (238).

The generation of PA by the lysophospholipid acyltransferase (LPAT, AGPAT) AGPAT3 was shown to be important for Golgi architecture and Golgi membrane trafficking (239). PA is also a negative curvature inducing PL and is critical for membrane trafficking events through its intrinsic negative curvature-promoting shape (220, 229, 230) or by the conversion of PA

Figure 1-2: Role of lipid-modifying enzymes. (**A**) Simplified phospholipid metabolism pathways pertinent to trafficking and structures of the lipids involved are shown (based on (250)). PC = phosphatidylcholine, LPC= lysophosphatidylcholine, PA = phosphatidic acid, LPA= lysophosphatidic acid, DAG = diacylglycerol, PI(4)P = phosphatidylinositol 4-phosphate, PLC = phospholipase C, PLD = Phospholipase D, DAGK = DAG kinase, LPP = lipid phosphate phosphatase, PLA = phospholipase A, LPAT = lysophospholipid acyltransferase. (**B**) Putative roles for PLA and LPAT enzymes in generating membrane curvature. PLA enzymes remove an acyl chain (fatty acid, FA) from phospholipids (PL), generating an inverted cone shaped lysophospholipid (LPL). LPAT enzymes can reacylate LPA, generating PA, a cone-shape, negative curvature inducing PL.

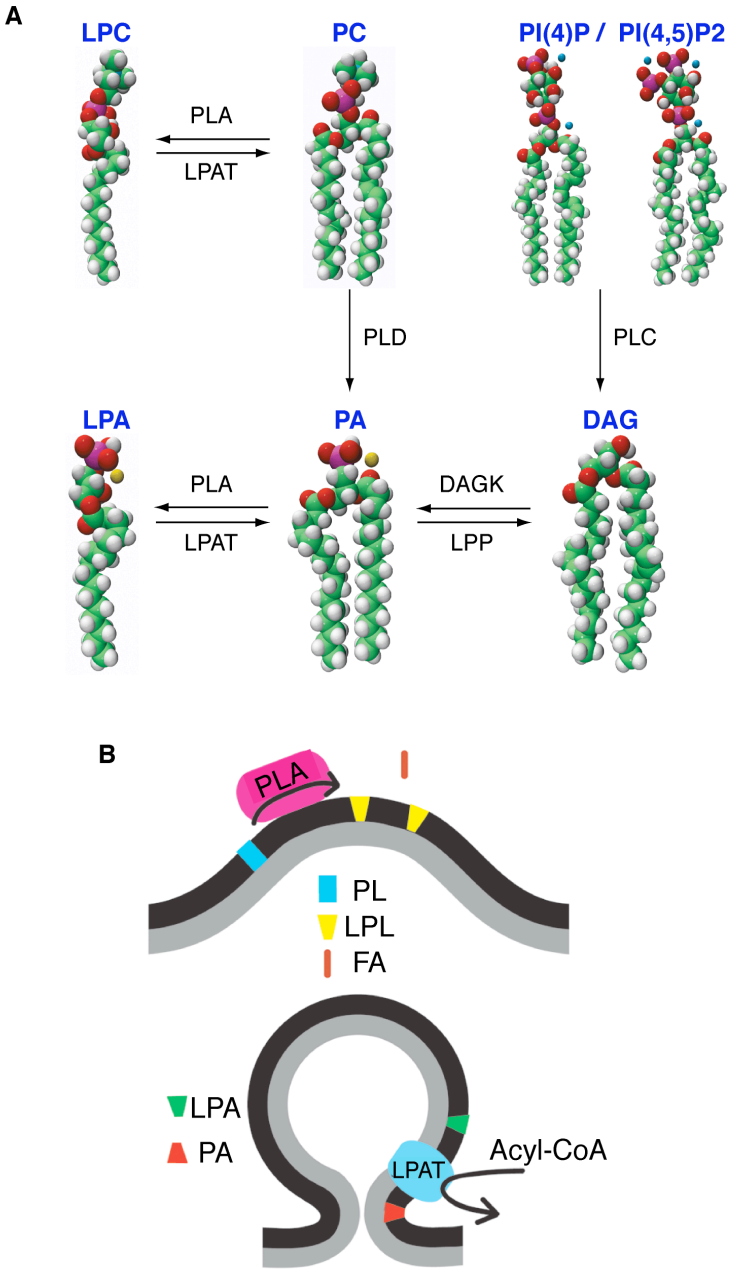
A
LPC
PC
PI(4)P / PI(4,5)P2
PLA
LPAT
PLD
PLC
LPA
PA
DAG
PLA
LPAT
DAGK
LPP
B
PLA
PL
LPL
FA
LPA
PA
LPAT
Acyl-CoA

to DAG (230, 240, 241) (Figure 1-2).

Phospholipase A (PLA) enzymes have also been implicated in generating shape changes in phospholipids to induce positive curvature in membranes (242). PLA enzymes are divided into PLA_1 and PLA_2, designated as such for the fatty acyl chain cleaved from the phospholipids, either from the *sn-1* or *sn-2* position, respectively. PLA hydrolysis of phospholipids to generate lysophospholipids may change the shape of PLs from a cylindrical shape to an inverted-cone shape LPL. The local generation of lysophospholipids on the cytosolic leaflet of membranes would change the shape of the membrane (217, 242), depicted in Figure 1-2. Such a change in local phospholipids has been demonstrated by treating erythrocyte membranes with a PLA_2, yielding numerous membrane protrusions (243). In contrast, reversing outward curvature or inducing negative/inward curvature has been hypothesized to occur by the action of LPAT enzymes as described above.

A number of studies have suggested that PLA enzymes are important for membrane tubule formation at the Golgi complex and endosomes. A pharmacological screen of enzyme antagonists found that cytosolic PLA_2 inhibitors abolished BFA-stimulated tubules from Golgi and endosomes in vivo as well as cytosol-stimulated tubules from isolated Golgi and endosomes in an in vitro reconstitution assay (244, 245) (Figure 1-1). It was further demonstrated that LPL and FA chain products from PLA_2 activity are primarily responsible for the generation of these membrane tubules, as arachidonic acid and other downstream metabolites of LPLs and FAs were shown to have no effect on tubule formation and membrane trafficking (244). In addition to membrane tubule formation and fusion events, PLA_2 inhibitors affected organelle architecture, BFA-stimulated retrograde transport, as well

as retrograde trafficking of KDEL receptor chimeras (246). In the presence of PLA_2 inhibitors, Golgi complexes become fragmented and the assembly of Golgi ribbons after BFA washout is also inhibited (78, 247). An in vitro reconstitution assay with PLA_2 antagonists also demonstrated that intra-Golgi transport is dependent on PLA_2 enzyme activity (248). Conversely, activators of PLA_2 enzymes promote Golgi membrane tubule formation (249). In addition, PLA_2 enzymes appear to aid in cargo transport at the TGN, as PLA_2 inhibitors block membrane tubule formation at the TGN, and decrease TGN to plasma membrane transport of VSV-G (250). Beyond the Golgi complex, PLA_2 antagonists decrease endocytic recycling of transferrin (Tf) and transferrin receptors (TfRs) as well as reduce LDL/LDL receptor, bulk fluid phase cargo, and EGF/EGF receptor endocytic transport (245, 251).

Since studies with PLA_2 antagonists, several specific PLA enzymes have been identified to have a role in Golgi complex membrane trafficking. A specific cytoplasmic, Ca^{2+}-dependent PLA_2, $cPLA_2\alpha$, was demonstrated to translocate to the Golgi complex upon increased intracellular calcium (252-255), or with increased secretory load at the Golgi after temperature shift with the model cargo VSV-G (256). Additionally, in epithelial cells $cPLA_2\alpha$ translocates to the Golgi shortly after cell-to-cell contacts are formed (257, 258) and regulates trafficking of cell junction proteins from the Golgi complex to the cell-cell contacts, as shown by RNAi of $cPLA_2\alpha$ (258). $cPLA_2\alpha$ was also shown in non-epithelial cell lines, by RNAi and antibody micro-injection studies, to contribute to intra-Golgi tubule connections, resulting in fragmentation of the Golgi stack and correlated with the reduced transport of VSV-G through the cisternae (256). However, cells from $cPLA_2\alpha$ knockout mice showed no defect in VSV-G transport and only demonstrated inhibition

of trafficking upon RNAi knockdown of one other cytoplasmic PLA_2 enzyme, the α1 subunit of PAFAH Ib (256). This indicates there is redundancy or compensation between PLA enzymes in Golgi trafficking. As described in chapter 2, I have found that PAFAH Ib is a PLA_2 involved in membrane tubule formation and is important for Golgi membrane trafficking and architecture (259).

A third PLA enzyme, $iPLA_1\gamma$, was shown to be involved in a different step of Golgi membrane trafficking, retrograde transport to the ER (260). $iPLA_1\gamma$ was localized to *cis* Golgi compartments and ERGIC membranes and was shown to have no effect on anterograde transport, but knockdown of $iPLA_1\gamma$ rather reduced BFA-stimulated retrograde membrane tubules and the transport of cholera toxin B from the Golgi to the ER. However, $iPLA_1\gamma$ showed no effect on cargo that uses COPI vesicle retrograde transport (ERGIC-53) or on Rab6-dependent movement of cargo (shiga toxin), indicating $iPLA_1\gamma$ forms specific transport carriers for retrograde Golgi to ER trafficking (260).

Phospholipase A Enzymes

There are three identified mammalian intracellular PLA_1 enzymes: PA-PLA ($iPLA_1\alpha$), p125 ($iPLA_1\beta$), and KIAA0725p ($iPLA_1\gamma$) (260). The substrates and functions of these $iPLA_1$ enzymes are just beginning to be discovered. $iPLA_1\alpha$ shows preference for PA but can also act on other phospholipids; its role in cells is unclear (261, 262). $iPLA_1\beta$ was identified to interact with Sec23, a COPII component, and affect ER exit sites (ERES) as well as transport to the Golgi complex (263, 264). $iPLA_1\gamma$ was recently shown to be important for the formation of COPI- and Rab6-independent transport intermediates from the

Golgi to the ER (260).

The PLA_2 enzyme superfamily is broken down into 15 groups based on protein sequence, molecular weight, localization, calcium dependency, function, disulfide bonds, and active site residues and further subdivided into five categories: secreted PLA_2s ($sPLA_2$), cytoplasmic PLA_2s ($cPLA_2$), calcium independent PLA_2s ($iPLA_2$), PAF acetylhydrolases (PAFAH), and lysosomal PLA_2s ($LPLA_2$) (265-267) (Table 1-1). The majority of known PLA_2 enzymes are categorized as secreted enzymes ($sPLA_2$s, groups I, II, III, V, IX, X, XI, XII, XIII, and XIV), which are found in various venoms, function in the immune system, and are involved in inflammatory signaling. More information on the thoroughly studied $sPLA_2$ family can be found in reviews (268, 269). Much less is known about the remaining groups, with detailed studies only existing for one or two proteins from each category of PLA_2 enzymes.

A single lysosomal PLA_2 ($LPLA_2$, group XV) contains both a signal sequence and glycosylation sites indicative of secretory pathway transport (270). This enzyme is optimally active at pH 4.5 and localizes with other lysosome-resident enzymes, supporting the role of this PLA_2 in lysosome degradation functions (270). $LPLA_2$ contains active site residues of Ser, His, Asp (same as PAFAH enzymes) and was originally shown to esterify ceramide with acyl chains from phospholipid 'donors' (271, 272). However, knockout mice of $LPLA_2$ showed accumulated PC and PE, which were also shown to be preferred substrates of $LPLA_2$ (273). This accumulation was seen in macrophages and had increased foam cell formation, appearing to have phospholipidosis (265).

The $cPLA_2$s (group IV) are generally calcium dependent, have a Ser Asp dyad catalytic site, and are believed to be cytosolic. Within the $cPLA_2$ family,

Table 1-1: Phospholipase A_2 enzyme families.

Family	Group	Name(s)	Localization & features	Catalytic Residues	Ca^{2+} dependent	Molecular Mass (kDa)
$sPLA_2$	IA-B		secreted	H/D dyad	for activity	13-15
	IIA-F		secreted	H/D dyad	for activity	13-17
	III		secreted	H/D dyad	for activity	13-18, 55
	V		secreted	H/D dyad	for activity	14
	IX		secreted	H/D dyad	for activity	14
	X		secreted	H/D dyad	for activity	14
	XIA-B		secreted	H/D dyad	for activity	12.4-12.9
	XII		secreted	H/D dyad	for activity	19
	XIII		secreted	H/D dyad	for activity	<10
	XIV		secreted	H/D dyad	for activity	13-19
$LPLA_2$	XV	lysosomal PLA_2	lysosome lumen	S/H/D triad		45
$cPLA_2$	IVA	$cPLA_2\alpha$	cytosol, translocates to ER and Golgi	S/D dyad	for lipid binding	85
	IVB	$cPLA_2\beta$	cytosol, translocates to membranes	S/D dyad	for lipid binding	114
	IVC	$cPLA_2\gamma$	prenylated, membrane-associated	S/D dyad	none	61
	IVD	$cPLA_2\delta$	cytosol, translocates to ER and Golgi	S/D dyad	for lipid binding	92-93
	IVE	$cPLA_2\varepsilon$	cytosol, lysosome	S/D dyad	for lipid binding	100
	IVF	$cPLA_2\zeta$	cytosol	S/D dyad	for lipid binding	96
$iPLA_2$	VIA-1	$iPLA_2$	cytosol	S	none	84-85
	VIA-2	$iPLA_2\beta$	cytosol, membrane-associated	S	none	88-90
	VIB	$iPLA_2\gamma$	prenylated, membrane-associated	S	none	88-91
	VIC	$iPLA_2\delta$, NTE	transmembrane protein	S	none	146
	VID	$iPLA_2\varepsilon$, PNPLA3, adiponutrin	lipid droplets	S	none	53
	VIE	$iPLA_2\zeta$, $PNPLA_2$, ATGL	lipid droplets	S	none	57
	VIF	$iPLA_2\eta$, PNPLA4	cytosol	S	none	28
PAFAH	VIIA	plasma PAFAH, $LpPLA_2$	secreted	S/H/D triad	none	45
	VIIB	PAFAH II	myristoylated, translocates to membranes	S/H/D triad	none	40
	VIIIA	PAFAH Ib α1	cytosol, Golgi	S/H/D triad	none	29
	VIIIB	PAFAH Ib α2	cytosol, Golgi	S/H/D triad	none	30

enzymes have slightly different *sn-2* fatty acid specificity. cPLA$_2\alpha$ is specific for arachidonic acid, a well-known molecule in inflammatory signaling pathways, whereas other cPLA$_2$ members preferentially act on linoleic acid, but can also cleave oleic acid and arachidonic acid (274, 275). All cPLA$_2$s, except cPLA$_2\gamma$, are Ca^{2+}-dependent, requiring Ca^{2+} for the C2 domain of these enzymes to bind lipids (276-278). cPLA$_2\gamma$ is instead prenylated and constitutively associates with membranes (277). The best characterized cPLA$_2$ is cPLA$_2\alpha$, which is the only PLA$_2$ with preference for phospholipids having arachidonic acid in the *sn-2* position (267, 275). This enzyme also behaves as a lysophospholipase and a transacylase enzyme (279, 280). cPLA$_2\alpha$ translocates to ER and Golgi membranes upon: an increase in cellular calcium, an acute increase in Golgi secretory load, an increase in PIP2 and PIP3 levels, upon cPLA$_2\alpha$ binding of ceramide-1-phosphate, and upon MAP kinase phosphorylation of cPLA$_2\alpha$ (256, 281-285). cPLA$_2\alpha$ knockout mice primarily show changes in inflammatory signaling, likely through decreased production of arachidonic acid for generation of inflammatory eicosanoids (266). cPLA$_2\alpha$ knockout mice and/or human patients with defects in cPLA$_2\alpha$ also have increased intestinal ulcers, decreased damage from acute lung or brain injury, decreased anaphylaxis, spermatozoa with impaired mobility, and lower birth rate (286-290).

iPLA$_2$s (group VI) are generally Ca^{2+}-independent and vary in their substrate specificity as well as their intracellular distribution. These enzymes share a GXSXG lipase consensus motif, with a catalytic Ser residue and do not appear to have much if any selectivity for *sn-2* fatty acids (291-293). The enzymes in this group primarily act as PLA$_2$ enzymes, but iPLA$_2$ and iPLA$_2\beta$ appear to also have lysophospholipase and transacylase activity (294). Several

iPLA$_2$s, including iPLA$_2\varepsilon$ (PNPLA3), iPLA$_2\zeta$ (PNPLA2), and iPLA$_2\eta$ (PNPLA4) were found to additionally have roles in energy homeostasis and triacylglycerol metabolism, for which they are being extensively studied (293, 295). The iPLA$_2$s involved in metabolism are also known as patatin-like phospholipase domain containing proteins (PNPLAs), which are reviewed in (295). iPLA$_2$s have many intracellular distributions, from cytoplasmic iPLA$_2$ and iPLA$_2\beta$, to lipid droplet associated iPLA$_2\zeta$, and membrane-bound iPLA$_2\gamma$ (265, 295). The integral membrane iPLA$_2\delta$ has been shown to be involved in neuropathies such as Wallerian degeneration, also known as neuropathy target esterase (NTE) (266, 296). NTE was identified as the Drosophila swiss cheese mutant protein, which shows glial cell hyperwrapping of axons and eventual axonal degeneration (297). iPLA$_2\delta$ cleaves acyl chains at the *sn-2* position of PC, then subsequently cleaves the *sn-1* position acyl chains (266, 298).

The family of PLA$_2$ enzymes known as PAFAHs (group VII and VIII) contain intracellular and secreted enzymes, both of which share a common Ca^{2+}-independent activity through a Ser, His, Asp catalytic triad and act on platelet activating factor (PAF) as a substrate (299-302). PAF is a phosphatidylcholine ether lipid, with an ether linked acyl chain in the *sn-1* position (1-*O*-alkyl-2-acetyl-sn-glycero-3-phosphocholine) (303). Similar to ether linked plasmologen lipids (which have a vinyl-ether *sn-1* linkage), PAF is most prevalent in endothelial cells and cells of the immune system but can also be found in extremely small quantities in other cell types (303-305). PAF is both intracellular and extracellular; PAF levels have been measured in blood, saliva, amniotic fluid during labor, and urine (303). PAF has been implicated in many signaling functions: inducing acute inflammatory

reactions, anaphylaxis responses, platelet aggregation, roles in neuronal and testicular function, as well as chemotaxis and granule secretion of neutrophils and monocytes (299, 303, 306-310). Several of the signaling roles for PAF can be attributed to its binding and activation of transmembrane PAF receptors (PAFR), which are G protein coupled receptors (GPCRs) found in cells of the innate immune system and central nervous system that bind to extracellular PAF (299, 311).

Group VII PAFAH enzymes can cleave the *sn-1* or *sn-2* position acyl chain of a broad array of substrates, which includes PAF, TAG and DAG with varying fatty acid chain lengths, phospholipids with short *sn-2* position fatty acids as well as on oxidized lipids (265, 312). Group VIIA consists of a single secreted PLA_2 also known as lipoprotein-associated lipase ($LpPLA_2$) or plasma PAFAH (266, 313, 314). This PAFAH has been studied extensively for its role in lipoprotein association, possible role in cardiovascular disease, and as a marker of coronary heart disease (315, 316). The enzyme of group VIIB shares similar specificity to group VIIA but is intracellular with myristoylation at its N-terminus; it can translocate from the cytosol to membranes during oxidative stress (265, 317). Group VIII PLA_2 PAFAH Ib is discussed in detail in the following section.

Platelet Activating Factor Acetylhydrolase Ib

This phospholipase complex of group VIII PLA_2 enzymes consists of two catalytic subunits that share a GXSXV lipase motif and a Ser, His, Asp catalytic triad (318, 319). PAFAH Ib forms homo- or heterodimers of α1 (*Pafah1b3*) and/or α2 (*Pafah1b2*). Dimerization is needed for catalytic activity (320), as the catalytic triad lies within a cleft between the two subunits

(Figure 1-3) (321). Mutations of the catalytic Ser for either subunit yield a catalytically inactive enzyme (322). PAFAH Ib catalytic subunits were originally identified for their ability to cleave the PAF *sn-2* position acetyl group, or acyl chains less than six carbons in length, to generate a lyso-PAF (319, 322). However, in vitro studies that examined cleavage of 1-*O*-alkyl-2-acetyl-glycerophospholipids (AAG phospholipids) with different head groups suggest that α1 and α2 have other possible phospholipid substrates depending on the dimer composition. Dimers of α1/α1 or α1/α2 show activity for cleaving PAF, and AAG PA (phosphatidic acid head group), but had little activity for AAG PE (ethanolamine head group). Homodimers of α2/α2 had considerably higher PAF acetylhydrolase activity, AAG PE activity, and moderate AAG PA activity (323).

Human and bovine PAFAH Ib α1 and α2 are 63% identical at the amino acid level and within subunits have 95-100% conservation of amino acid sequence among mammalian species. Studies in rats and mice indicate both α1 and α2 mRNAs are expressed in fetal development, but α1 mRNA expression progressively declines until undetectable in adulthood (324, 325). PAFAH Ib α1 and α2 protein levels were ubiquitous in mouse tissues (326), however, α1 showed higher expression during development, α1 and α2 were highest in brain and testis, and α2 also showed higher expression in lung tissue (326). Expression levels of α1 and α2 subunits in bovine tissues were ubiquitous, and did not demonstrate the decrease in α1 mRNA expression observed in adult mice. The highest amounts of bovine α1 mRNA expression were found in fetal brain, but significant levels were found in adult bovine kidney, human kidney, thymus and colon (327, 328). Conservation among non-mammalian species has only been confirmed in *Drosophila melanogaster*,

Figure 1-3: Structure of PAFAH Ib. (**A**) Space filling structure of an α1/α2 (blue/yellow) heterodimer with the catalytic pocket showing the Ser, His, Asp catalytic triad in red. Based on (331). (**B**) Structure of the PAFAH Ib complex with a dimer of LIS1 in turquoise bound to an α2/α2 homodimer (yellow/orange). The catalytic pocket is facing downward in this structure. Based on (341). (**C**) Structure of an α2/α2 homodimer, with catalytic serines (Ser 48) highlighted in red and LIS1-binding important E39 residues highlighted in white. The catalytic pocket is facing downward.

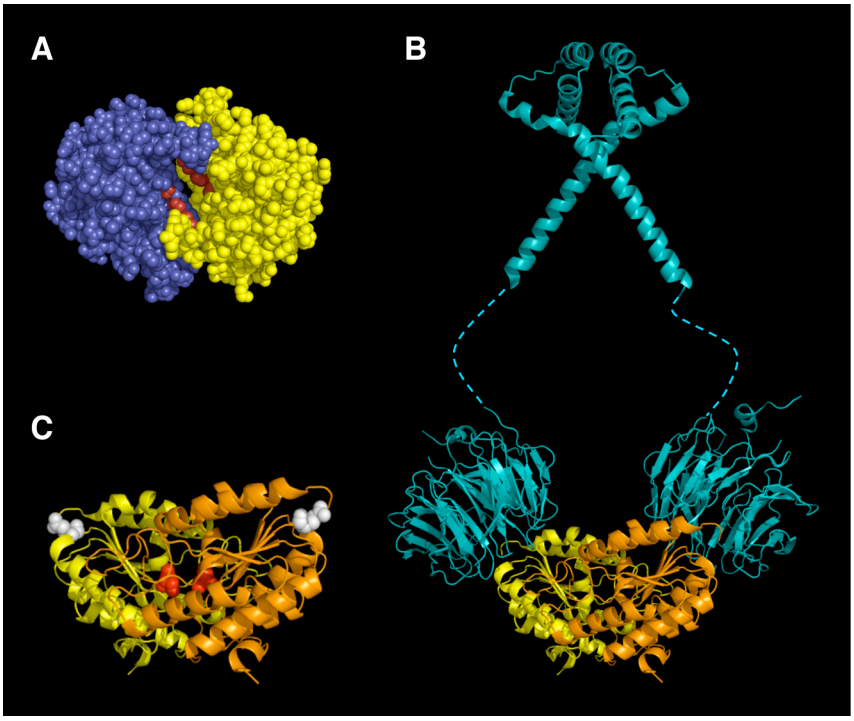
A
B
C

whose homologues lack two of the three catalytic residues, hence do not have catalytic activity (329). The exact function for the PAFAH Ib catalytic subunits has been unclear, particularly because knockout mice of α1 and α2 subunits had limited phenotypes. PAFAH Ib $\alpha1^{-/-}$ mice were grossly normal, $\alpha2^{-/-}$ mice had reduced testes weight and inconsistent germ cell defects. Double mutants of $\alpha1^{-/-}/\alpha2^{-/-}$ had increased apoptosis in cells of seminiferous tubules leading to more severe spermatogenic phenotypes (326, 330).

PAFAH Ib α subunits can be isolated in a protein complex, as it was originally purified as a trimer of two α subunits and a β subunit. The third β subunit was predicted to be regulatory (322). Later studies determined that α1 and α2 form a tetrameric structure with a homo or heterodimer of α1 and/or α2 and a dimer of LIS1 subunits (Figure 1-3) (331). The β subunit was later identified to have 99% amino acid identity with the protein LIS1 (gene *Pafah1b1*), a protein involved in dynein regulation (discussed more below). LIS1 has been investigated extensively for its association with a severe neural development disease known as lissencephaly, which is Greek for smooth brain. Mutations in *Pafah1b1* subdivide into two types of congenital, autosomal dominant lissencephaly: Miller-Dieker syndrome and type 1 isolated lissencephaly (332, 333). Loss of both copies of LIS1 is lethal (334). While neurons appear to be extremely sensitive to levels of LIS1, it has functions in all cell types. LIS1 is conserved within eukaryotes, and amino acid sequences of LIS1 are >99% identical within mammalian species. Expression of LIS1 is ubiquitous (326, 333) but found at higher levels during development, and in brain, testis, and lung of mice (326).

The relevance of catalytic α1 and α2 subunit interactions with LIS1 is still unclear. The catalytic subunits have not been associated with

lissencephaly and have been found to function independently of LIS1 binding (318). Binding to LIS1 appears to increases the catalytic activity four-fold specifically for α2/α2 dimers but not other dimer combinations in vitro (323). Interactions between LIS1 and α1 and α2 have only been found in mammals; these proteins do not interact in *Drosophila* (329) and α1 and α2 homologues have not been identified in other species where LIS1 homologues exist. Heterozygous loss of LIS1 combined with loss of α2 ($\alpha2^{-/-}$ $Lis1^{-/+}$) in mice showed fewer spermatogenic defects than $\alpha2^{-/-}$ (330). The reason for this reduced phenotype severity with α2 loss is not understood.

Differences between α1 and α2, beyond catalytic preference and increased activity with LIS1, were found in studies of PAFAH Ib subunits with the reelin receptor pathway. *Reeler* mice, which have loss of functional reelin, a ligand for both VLDLR and ApoER2 receptors, show neuronal phenotypes of abnormal cortical neuritogenesis. $Ndel^{-/-}/Lis1^{+/-}$ mice phenocopy reelin disruption ($Reln^{-/-}$) in *reeler* mice, with cortical layer disruption, cerebellar hypoplasia and ataxia (335). Both LIS1, α1, and α2 have been shown to interact with components of the reelin receptor pathway, and mouse knockouts indicate that α1 versus α2 have different effects on LIS1 genetic interactions with the reelin receptor pathway. Surprisingly, $LIS1^{-/+}$ in combination with loss of reelin pathway components showed exacerbated phenotypes with loss of α1 ($\alpha1^{-/-}$) and suppressed phenotypes with loss of α2 ($\alpha2^{-/-}$) (336). This adds another layer of complexity to the functional roles of α1 and α2 and how α subunits affect LIS1 functions.

PAFAH Ib α subunits have been shown to affect LIS1 function. α1 and α2 compete for binding to LIS1 with Ndel1, another dynein regulatory protein (331). In this study, α2 appeared to be a better competitor, indicating that α2

may bind LIS1 with higher affinity than α1 (331). The overexpression of α1, but more dramatically α2, was shown to reduce LIS1 binding to dynein, resulting in delayed mitosis due to spindle formation defects as well as disorganized microtubules during interphase (337). This reduction in LIS1-dynein interaction was no longer seen when overexpressing α1 E38D or α2 E39D mutants that abolish LIS1 binding (337). Other studies have confirmed this delay in mitosis and further found that overexpression of α1 or α2 resulted in Golgi fragmentation and a peripheral distribution of endosomes as seen by labeling with wheatgerm agglutinin (338). Overexpression of α subunits also impaired migration of cortical neurons (338). Similar to the studies by Yamaguchi et al (337), these effects were found to be dependent on titration of LIS1 from Ndel1 and dynein by overexpression of α1 or α2 (338). Both of these reports indicate that there is a balance between LIS1 binding to dynein and LIS1 binding to the catalytic subunits of PAFAH Ib. This additionally suggests that α1 and α2 can regulate LIS1-activation of dynein.

LIS1 and Dynein Function in Membrane Trafficking

While it is debated exactly how LIS1 contributes to dynein function, it is generally accepted that LIS1 aids in activating dynein minus-end directed microtubule transport (339). Dynein motors form complexes with a variety of regulatory proteins including LIS1, the dynactin complex, CLIP-170, Bicaudal D, Spindly, Rod/ZW10/Zwilch, Ndel1, and NDE1 (340). Current research is examining which dynein functions are regulated by these proteins.

There are at least three members of the cytoplasmic dynein family (341, 342); dynein1 is the most abundant member. Dynein1 is important for the positioning of microtubules in cells, spindle orientation during mitosis,

organelle positioning, and transport of cargo in several intracellular trafficking events (dynein functions are reviewed in (68, 340, 343). Dynein1 binds to the activator protein complex dynactin, which is a multi-subunit complex consisting of Arp1 (actin related protein), Arp11, $p150^{Glued}$, dynamitin (p50), CapZ α or β, actin, p62, p25, p24, and p27 (344). The dynactin complex is believed to link dynein to the cargo it carriers (344-346) and may help facilitate long-range movement (347, 348).

The steady state distribution of the ER, Golgi, endosomes, and lysosomes has been shown to be dependent on microtubule motor protein function. Bidirectional movement of endosomes occurs along microtubule tracks involving both kinesin motors to move cargo to the cell periphery (towards microtubule + ends) and dynein, which generally moves organelles and cargo toward the (microtubule - ends) microtubule organizing center (MTOC, aka centrosome) at the cell center. Dynein and dynactin have been shown to be critical for the position of endosomes, lysosomes, and the Golgi complex (65, 66). Inhibition of dynein activity by dynamitin overexpression, which interferes with the dynactin complex formation, shows Golgi fragmentation and relocation of early endosomes, recycling endosomes (ERC), late endosomes, and lysosomes to the cell periphery (66, 349).

Dynein and kinesin split responsibilities in the movement of transport intermediates between organelles (Figure 1-1). Transport from the Golgi complex to the ER is dependent on kinesin, while ER to Golgi trafficking is dynein/dynactin dependent (179). Studies demonstrate dynein/dynactin transport of cargo from early to late endosomes, but dynein/dynactin does not affect Tf recycling out of the cell (349). These results were confirmed with antibody microinjection, dynamitin overexpression, and dynein knockout

mouse studies (65, 66, 349). Dynein is important for early endosome to ERC transport (350). Kinesin motors are believed to mediate the movement of cargo from endosomes to the plasma membrane. For more details on kinesins, see (351).

LIS1 contributes to many roles of the dynein/dynactin complex (352-355) and is consistently shown localized to plus ends of microtubules, to the centrosome, and to kinetochores during cell division (352, 356). LIS1 contributes to dynein-dependent connections of the nucleus to the centrosome and the microtubule network (353, 357), which is critical for cell migration. Decreased levels of functional LIS1 lead to a loss of these connections, which may contribute to the defects in neuronal migration observed in lissencephaly (339).

Additionally, LIS1 expression levels impact the mitotic spindle, centrosome position, radial microtubule arrays and both the morphology and localization of secretory and endocytic organelles, including the Golgi complex (352, 358, 359). Increased or decreased levels of LIS1 generate spindle abnormalities that result in defective chromosomal alignment (352). High expression levels of LIS1 shift the distribution of dynein and $p150^{Glued}$ (dynactin component) to the cell center, indicating that LIS1 increases the minus-end directed transport of dynein (358). LIS1 levels affect the distribution of the Golgi complex, as $Lis1^{+/-}$ fibroblasts showed dispersed Golgi, and the addition of LIS1 to these cells returned the Golgi to a more centrally clustered organelle (358). Conversely, the overexpression of LIS1 in Cos7 cells resulted in a more compact Golgi (358). LIS1 has also been shown to affect the positioning of endosomes and lysosomes, irrespective of the microtubule organization, indicating that LIS1 must regulate dynein-

dependent transport of these organelles (360). This is not an exhaustive review of LIS1 and the multitude of LIS1 studies is reviewed in (339, 361).

Research Goals

Previous work demonstrated that PLA_2 activity is important for membrane tubule formation as well as secretory and endocytic trafficking steps (78, 79, 244, 245, 250, 251) (Figure 1-1). The specific PLA_2 enzyme(s) involved in these processes was unknown. The co-fractionation of PAFAH Ib with Golgi membrane tubule-stimulating activity from cytosol led to the hypothesis that PAFAH Ib is involved in Golgi membrane tubule formation and membrane trafficking events. I set out to examine the potential role of PAFAH Ib subunits in Golgi membrane tubule formation, Golgi complex structure, and trafficking (Chapter 2). As α1 and α2 subunits form both homo- and hetero-dimers, which have been shown to genetically and biochemically differ (323, 331, 336), I also investigated whether α1 and α2 have overlapping or distinct roles at the Golgi complex (Chapter 3). The role for PAFAH Ib in endocytic trafficking was also investigated (Chapter 4). Additionally, to determine how PLA_2 activity in Golgi membrane tubule formation is regulated, I investigated the role of heterotrimeric G protein Gβγ subunits, as Gβγ subunits have been implicated in Golgi complex structure, tubule formation, and trafficking (97, 362) (Chapter 5).

CHAPTER 2

The Phospholipase Complex PAFAH Ib Regulates the Integrity and Trafficking of the Golgi Complex[1]

Abstract

We report that Platelet Activating Factor Acetylhydrolase (PAFAH) Ib, comprised of two phospholipase A_2 (PLA_2) subunits, α1 and α2, and a third subunit, the dynein regulator LIS1, mediates the structure and function of the Golgi complex. Both α1 and α2 partially localize on Golgi membranes, and purified catalytically active, but not inactive, α1 and α2 induce Golgi membrane tubule formation in a reconstitution system. Overexpression of wild type or mutant α1 or α2 revealed that both PLA_2 activity and LIS1 are important for maintaining Golgi structure. Knockdown of PAFAH Ib subunits fragment the Golgi complex, inhibit tubule-mediated reassembly of intact Golgi ribbons, and slow secretion of cargo. Our results demonstrate a cooperative interplay between the PLA_2 activity of α1 and α2 with LIS1 to facilitate the functional organization of the Golgi complex, thereby suggesting a model that links phospholipid remodeling and membrane tubulation to dynein-dependent transport.

Introduction

An unresolved feature of the Golgi complex is the role of membrane tubules in trafficking and maintenance of Golgi architecture (96, 97, 363). Within the Golgi, membrane tubules are implicated in *cis* to *trans* cargo

cisternal transport (46, 47), retrograde trafficking to the endoplasmic reticulum (ER) (14, 176), transport from the *trans* Golgi network (TGN) to the cell surface and endosomes (96, 97, 186, 189), and in the assembly and maintenance of intact Golgi ribbons (78, 244).

Pharmacological studies have shown cytoplasmic phospholipase A_2 (PLA_2) enzymes regulate the formation of Golgi membrane tubules that contribute to retrograde trafficking, and the assembly and maintenance of an intact Golgi ribbon in mammalian cells (78, 242, 244, 246, 249, 364). Here we identify Platelet Activating Factor Acetylhydrolase Ib (PAFAH Ib) as a cytoplasmic PLA_2 complex that regulates membrane tubule formation, organization and function of the Golgi complex. PAFAH Ib was originally purified based on its ability to hydrolyze the *sn*-2 position acetyl group of the signal transducing, phosphatidylcholine derivative, Platelet Activating Factor (PAF) (318, 322, 365). PAFAH Ib consists of homo- or hetero-dimers of two closely related catalytic subunits, α1 (*Pafah1b3*) and α2 (*Pafah1b2*), and a non-catalytic dimer of β subunits (*Pafah1b1*) (302, 321, 331). The β subunit is better known as LIS1, the causative agent of the fatal brain disorder Miller-Dieker lissencephaly (366). LIS1 is a highly conserved protein involved in dynein-mediated processes including nuclear and neuronal migration, centrosomal function, and mitotic spindle orientation (339, 367). Although PAFAH Ib has been implicated in a variety of processes, including the regulation of PAF and LIS1 functions, its exact biological function is unclear, as $\alpha1^{-/-}/\alpha2^{-/-}$ double knockout mice, while exhibiting defects in spermatogenesis, are otherwise normal (326, 330).

Using multiple *in vitro* and *in vivo* approaches, we find that all three subunits of PAFAH Ib contribute to the structure of the mammalian Golgi

complex, and the catalytic subunits independently contribute to secretion. Our results suggest a model whereby the PLA_2 activity of α1 and α2 remodel membrane phospholipids to form Golgi tubules, which are linked via LIS1 to dynein-mediated, microtubule transport.

Materials and Methods

Reagents

Sprague-Dawley male rats were obtained from Charles River Breeding Laboratories, Inc. BFA and cycloheximide were from Biomol Research Laboratories, Inc. Antibodies were as follows: guinea pig anti-α1 antibody (A. Doody); rabbit anti-bovine CI-M6PR (by us (368)); rabbit anti-dynamin (MC63) (M. McNiven, Mayo Clinic, Rochester, MN); rabbit anti-human GPP130 (A. Linstedt, Carnegie Mellon Univ., Pittsburgh, PA); rabbit anti-ManII (K. Moremen, Univ. of Georgia, Athens, GA); chicken anti-α2 (Abcam, Inc.); mouse anti-LIS1 (Sigma Chemical Co.); mouse anti-HA (Covance); mouse anti-β-COP (BioMakor), mouse anti-α tubulin (Sigma Chemical Co.), rabbit anti-γ-adaptin (Santa Cruz), rabbit anti-Sec31A (W. Balch, Scripps Research Institute, La Jolla, CA) fluorescent secondary antibodies (Jackson Immuno-Research Laboratories and Invitrogen); HRP-conjugated goat anti-chicken (Aves Laboratories), anti-guinea pig (Pocono Rabbit Farm and Laboratory), anti-rabbit (GE Healthcare), and anti-mouse (Gibco).

Preparation of Plasmids

The protein purification vectors pGEX6P1-α1-S47A and pGEX6P1-α2-S48A were generated by Anne Doody and Lin Lin ((259); Anne Doody dissertation). The protein purification vectors pGEX4T1-α1 and pGEX4T1-α2

were gifts of Dr. Z. Derewenda (University of Virginia, Charlottesville, VA). pGEX4T1-α1-E38D and pGEX4T1-α2-E39D were generated by site-directed mutagenesis with the Quickchange II Site-directed mutagenesis kit (Stratagene) using the following primers (mutations are bold):

α1: 5′-GAAGACGACTTCGGG**A**TCCTTATCTTTGCTGTCG-3′

5′-CGACAGCAAAGATAAGGA**T**CCCGAAGTCGTCTTC-3′

α2: 5′-GGACATCCGGG**T**CTTTGTCTTTGCAGTCCAGG -3′

5′-CCTGGACTGCAAAGACAAAGA**C**CCGGATGTCC-3′

Although our polyclonal antibodies were useful for Western blots, we were unsuccessful in localizing endogenous α1 and α2 with many different polyclonal antibodies (made in rabbit, guinea pig, chicken, rat). Therefore, Anne Doody and Lin Lin generated mammalian expression constructs containing internally HA-tagged α1 and α2 (pEN1-α1-HA, pEN1-α2-HA, and pEN1-α2-S48A-HA) by insertion on surface loops (α1 G165 and α2 P130) based on (321), that would not interfere with dimer or LIS1 interactions mammalian expression vectors.

Mammalian expression plasmid pEN1-α1-S47A-HA was made by site-directed mutagenesis using Quickchange II (Stratagene) with the following primers: 5′-TCGTCTTCATCGGTGACGCCTTGGTCCAGCTGATGC-3′ and 5′-GCATCAGCTGGACCAAGGCGTCACCGAATGAAGACGA-3′. RNAi resistant pEN1-α1-HA, pEN1-α1-S47A-HA, pEN1-α2-HA, and pEN1-α2-S48A-HA were generated by making two silent mutations in the dsRNA target sequence, using primers:

α1: 5′-GTGTTCCAGCTC**G**CC**G**TTCTCCAGACGCCAC-3′

5′-GTGGCGTCTGGAGAA**C**GG**C**GAGCTGGAACAC-3′

α2: 5′-GGTTTAATATTCTCCAG**C**TC**G**CCATTCTTTAGTCTCC-3′

5′-GGAGACTAAAGAATGG**C**GA**G**CTGGAGAATATTAAACC-3′

LIS1 binding mutants α1 E38D or α2 E39D (337) were generated, with the help of Ina Chen, by site-directed mutagenesis of RNAi resistant pEN1-α1-HA, pEN1-α2-HA, pEN1-α1-S47A-HA, and pEN1-α2-S48A-HA with the following primers:

α1: 5′-GAAGACGACTTCGGG**A**TCCTTATCTTTGCTGTCG-3′

5′-CGACAGCAAAGATAAGGA**T**CCCGAAGTCGTCTTC-3′

α2: 5′-GGACATCCGG**G**TCTTTGTCTTTGCAGTCCAGG -3′

5′-CCTGGACTGCAAAGACAAAGA**C**CCGGATGTCC-3′

pCMV-HA-LIS1 was a gift from Dr. R. Vallee (Columbia University, New York, NY). The sequence of this LIS1 contained a point mutation A166T that was reverted back to alanine using site-directed mutagenesis using primers: 5′-GCGGCAAGCTTCTGGCTTCCTGTTCTGC-3′ and 5′-GCAGAACAGGAAGCCAGAAGCTTGCCGC-3′. RNAi-resistant pCMV-HA-LIS1 was created by site-directed mutagenesis to generate two silent mutations in the dsRNA target sequence using primers: 5′- GGATTACAAGAACAAGCG**C**TG**T**ATGAAGACCCTCAATGCGC -3′ and 5′-GCGCATTGAGGGTCTTCAT**A**CA**G**CGCTTGTTCTTGTAATCC -3′**.**

Protein Purification

Vectors were prepared as described above and transformed into the competent BL21 *E. coli* strain. Proteins were purified and cleaved from GST using the GST-3C-Pro system or thrombin (Sigma Chemical Co.) as described by GE Healthcare (also found in detail A. Doody dissertation).

In Vitro Golgi Tubulation Assay and Mass Spec Protein Identification

Reconstitution of Golgi membrane tubule formation and fractionation of BBC was as described (369). Briefly, BBC was fractionated by a series of centrifugations to remove particulate material and several ammonium sulfate precipitations. A soluble fraction was subjected to a series of chromatographic separations including phenyl-sepharose, DE52 ion exchange, Affi-Gel blue, and finally gel filtration (GF) on Sephadex G100 that yielded a GF highly enriched in tubulation activity. GF fraction proteins were separated and identifiec using MALDI TOF-TOF as described in (259) (A. Doody, K. Lee). BBC was combined with antibodies or purified proteins as described in the Results.

PAFAH Activity Assay

The PAFAH assay was used to confirm activity of PAFAH Ib α1 and α2 purified proteins, using substrate 2-Thio PAF, was performed as described by the supplier (Cayman Chemical).

Cell Culture, Transfection and RNAi

BTRD bovine testicular and HeLa cells were cultured in MEM (Mediatech, Inc.) with 10% bovine growth serum (BGS) or NuSerum in a 37°C, 95% humidity, and 5% CO_2 incubator. Lipofectamine 2000 (Invitrogen) was used with modifications: DNA and reagent were reduced to a quarter. Experimentation was 24-48 h later. Double stranded RNA targeting bovine α1 mRNA and bovine α2 mRNA were from Dharmacon: AGAAUGGAGAGCUGGAACAUU and GGAGAACUGGAGAAUAUUAUU, for α1 and α2 respectively. LIS1 dsRNA was from Dharmacon, sequence from

Tsai et al., 2005: GAACAAGCGAUGCAUGAAG. Control RNA was siGenome non-targeting siRNA #1 and #2 (Dharmacon). RNA was transfected on two consecutive days with Lipofectamine RNAiMax (Invitrogen) and 30 nM RNA. Experiments were 48 h or 72 h after the initial RNA transfection.

Cell Fractionation

Linear sucrose gradients were prepared by repeated freeze-thaw cycles of a 4-step sucrose gradient, containing 1.5 mL 48%, 4 mL 39%, 4 mL 35%, and 4 mL 29% sucrose with 10 mM Tris, pH 7.4. BTRD cells were grown to confluency in six 24 x 24 cm dishes, washed with PBS (pH 7.4), harvested by scraping, and kept at 4°C or on ice. Cells were pelleted by low speed centrifugation and washed 3 times in homogenization buffer (0.25 M sucrose, 1 mM EDTA, 10 mM Tris, pH 7.4). Cells were homogenized in a Balch-Rothman apparatus, followed by a low speed centrifugation to obtain post-nuclear supernatant. The post-nuclear supernatant (~5 mL) was loaded on top of a linear 20-49% sucrose (10 mM Tris, pH 7.4) gradient and centrifuged in a SW28.1 rotor in a Beckman Coulter Optima LE-80K ultracentrifuge (Beckman Instruments) at 25,000 rpm for 2 h at 4°C with no brake. One-milliliter fractions were collected from the cell fractionation gradient, prepared for SDS-PAGE and subsequent Western blotting. Fractions from a second parallel gradient were collected and used to measure sucrose concentration with an Abbe refractometer (Bausch & Lomb).

Fluorescence Microscopy

For direct fluorescence of GFP or YFP tagged proteins, cells were fixed in

3.7% formaldehyde in PBS for a minimum of 10 min at room temperature, washed in PBS three times for 5 min each, mounted with Vectashield (Vector Laboratories) mounting media, and stored at -20ºC until imaged. For immunofluorescence, cells were fixed in 3.7% formaldehyde in PBS for a minimum of 10 min at room temperature, washed in PBS for 5 min three times and permeabilized with 0.1% Triton X-100 in PBS for 10 min. Cells were then incubated for one hr at room temperature or overnight at 4ºC with primary antibodies diluted in PBS, followed by three washes in PBS and secondary antibody incubation for 1 h at room temperature. Coverslips were mounted with Vectashield (Vector Laboratories) mounting media, stored at -20ºC until imaged. Primary antibodies were diluted as follows: anti-HA, anti-Sec31A anti-ManII, anti-β-COP, anti-α tubulin, and anti-γ-adaptin 1:100; anti-bovine CI-M6PR 1:200; and anti-GPP130 1:1000. Secondary antibodies conjugated to Alexa 488, DyLight 488, fluorescein isothiocyanate, tetramethylrhodamine isothiocyanate, or Cy5 were used, diluted in PBS 1:500 for Alexa488 and 1:100 for all other secondary antibodies. Wide-field epifluorescence was with Zeiss Axioscope II, Zeiss 40x or 100x Plan-Apochromat NA1.4 oil objective lenses, a Hamamatsu Orca II digital camera, and Openlab software (Improvision). Spinning disk confocal images were taken with a Nikon Eclipse TE2000-U, Nikon Plan-Apo 60xA/N1.4 or Nikon Plan-Apo100x/N1.4 oil objectives, with Perkin-Elmer Ultraview LCI, a Hamamatsu 1394 ORCA-ER camera, and Perkin-Elmer Ultraview software. A Leica DMI6000B microscope equipped with a Leica oil 63x/NA1.4 objective, 3i Marianas spinning disk system, Photometrics HQII CCD camera, and 3i Slidebook 5.0 software was also used (Intelligent Imaging Innovations).

VSVG-YFP and ssHRP-Flag

ts045VSVG-YFP pixel intensities of the juxtanuclear Golgi region and total cell were measured per cell from confocal images using ImageJ (NIH), with appropriate background fluorescence subtraction (per area). Kinetic equations for ts045VSVG-YFP transport were fit by least squares non-linear regression using Origin 3.5 software, based on first order kinetic equations (181). For ssHRP-Flag measurements, media and lysate HRP activity was quantified by absorbance, using 3, 3', 5, 5'-tetramethyl-benzidine reagent (Sigma), and normalized to total HRP expression.

Electron Microscopy

Cells were fixed in the dish using 1.5% glutaraldehyde fixative (with 5% sucrose and 0.1 M Na cacodylate) for 1 h, followed by three 15 min 4ºC 0.1 M Na cacodylate washes, and post-fix in osmium tetroxide (1% OsO4, 1% KFeCN, 0.1 M Na cacodylate) for 1 h at 4ºC. Cells were washed three times for 15 min in 4ºC 0.1 M Na cacodylate then stained with 0.25% uranyl acetate for 30 min, followed by an additional three Na cacodylate washes. Cells were dehydrated using 70%, 95%, and 100% ethanol washes then removed from the dish with propylene oxide. Cells were pelleted in a micro-centrifuge and infiltrated with 1:1 propylene oxide and Spurs for 30 min. The supernatant was removed and replaced with 100% Spurs overnight. The Spurs was replaced twice more and polymerized at 60°C for 24 h. The polymerized block was sectioned and stained with lead citrate and uranyl acetate. For electron microscopy images, a FEI Morgagni 268 transmission EM was used.

Image Analysis and Statistics

The Golgi disruption indices were by categorizing Golgi as diffuse, fragmented, or intact. For most experiments, $\geq$ 300 cells were counted for each condition, and each was repeated independently $\geq$ three times. The statistical significance between control and knockdown cells was with a two-tailed, unequal variance T-test. The significance of overexpression phenotypes was by Behrens-Welch testing. Images and z-projections were cropped, brightness adjusted, or contrast adjusted using ImageJ, Photoshop CS3, or using 3i Slidebook 5.0 software. Three-dimensional reconstruction was done using Volocity software (Improvision). Line intensity plots were done using 3i Slidebook 5.0 software (Intelligent Imaging Innovations).

Results and Discussion

PAFAH Ib α1 and α2 are Cytoplasmic Membrane Tubulation Factors

Previous studies showed that a preparation of bovine brain cytosol (BBC) contains PLA_2 activity that stimulates Golgi membrane tubule formation in a cell-free system (78). In collaboration with other members of the Brown lab, we identified a specific PLA_2 responsible for this tubulation activity. Biochemical fractionation of BBC yielded a final gel filtration (GF) fraction highly enriched (~5,400 fold) in tubulation activity, with native molecular weight of 150-170 kD (369), and containing co-fractionating proteins of ~80, 66, 45, 40, 30 and 18 kD (Figure 2-1). MALDI TOF-TOF and Western blotting identified the 45 kD band as LIS1 and the 29-30 kD bands as α1 and α2 catalytic subunits of PAFAH Ib (Figure 2-1). Other proteins identified in the GF fraction were Hsc70, PLA_2 activating protein (PLAA), and fructose bis-phosphate aldolase. A variety of experiments showed that aldolase is a contaminant; the role of Hsc70 and

PLAA in tubule formation, if any, remains to be determined.

To determine if PAFAH Ib is directly involved in membrane tubule formation, purified α1 or α2 were added to isolated Golgi complexes *in vit*ro. Alpha subunits alone were unable to stimulate membrane tubules in the absence of BBC (Figure 2-2; A. Doody dissertation). However, when α1 or α2 were mixed with sub-threshold amounts of BBC, catalytically active α1 and α2, but not inactive enzymes with single amino acid changes in active site serines (α1 S47A; α2 S48A) (318), significantly induced Golgi membrane tubule formation (Figure 2-1 D, E). This cytosol requirement was not due to LIS1, because α1 or α2 mutants that do not bind to LIS1 (α1 E38D and α2 E39D) (337) stimulated membrane tubules (Figure 2-2). Consistent with these results, antibodies against α1 and α2 (but not pre-immune antisera) inhibited BBC-dependent *in vitro* Golgi membrane tubulation (Figure 2-1 F), whereas the addition of LIS1 antibodies had no effect (data not shown). These results show that PAFAH Ib catalytic activity is required for stimulating membrane tubules from isolated Golgi complexes.

PAFAH Ib α1 and α2 Partially Localize to Golgi Membranes and Tubules

In mildly expressing cells, catalytically active HA-tagged α1 or α2 (Figure 2-1 C) were found diffuse throughout the cytoplasm, in the nucleus, on punctate structures, and clearly on intracellular structures in the juxtanuclear region that co-localized with Golgi markers including Rab6-GFP (*cis*), GPP130 (*cis*), mannosidase II (ManII, *medial*), and mannose 6-phosphate receptors (M6PR, TGN) (Figure 2-3 A, B; Figure 2-4; data not shown). A similar distribution was seen by Caspi et al. in cells expressing GFP-α1 (356). Catalytically inactive α1 S47A and α2 S48A, as well as α1 E38D and α2 E39D,

Figure 2-1: PAFAH Ib catalytic subunits are cytosolic Golgi tubulation factors. (**A**) Peak Golgi tubule-stimulating activity (determined by an *in vitro* reconstitution assay) co-fractionates with PAFAH activity and PAFAH Ib subunits (Western blot) in final bovine brain cytosol (BBC) fractionation steps. (data from Dr. Esther Racoosin) (**B**) Silver stain of final fractions with the minimal components that stimulate Golgi tubules *in vitro*. The components identified by MALDI TOF-TOF and/or Western blot are labeled (NS = non specific). (Data shown from Dr. Anne Doody based on mass spec results from Dr. Kelvin Lee's laboratory.) (**C**) Coomassie-stained gel and PAFAH activity of purified subunits. (data from Dr. Anne Doody) (**D**) EM of negative stain Golgi from *in vitro* tubulation reconstitution assays incubated with BBC and purified subunits as indicated. Bars, 500 nm. (Images from M.E. Bechler) (**E**) Quantitation of tubulation assays using purified α1 and α2 subunits (7.5 μg/ml), with subthreshold BBC (Low BBC, 0.25 mg/ml) compared to saturating BBC (1.5 mg/ml). svPLA$_2$ = snake venom PLA$_2$. Results are the percentage of control (BBC), n = 4, error bars = SD. (Data shown from Dr. Anne Doody.) (**F**) Anti-α1 and/or anti-α2 antibodies, but not pre-immune IgG (PI-α1, PI-α2), inhibit cytosol-stimulated Golgi membrane tubules *in vitro*. BSA = bovine serum albumin. Results are percent of control (BBC), n = 4, error bars = SD. (Data shown from Dr. Anne Doody.)

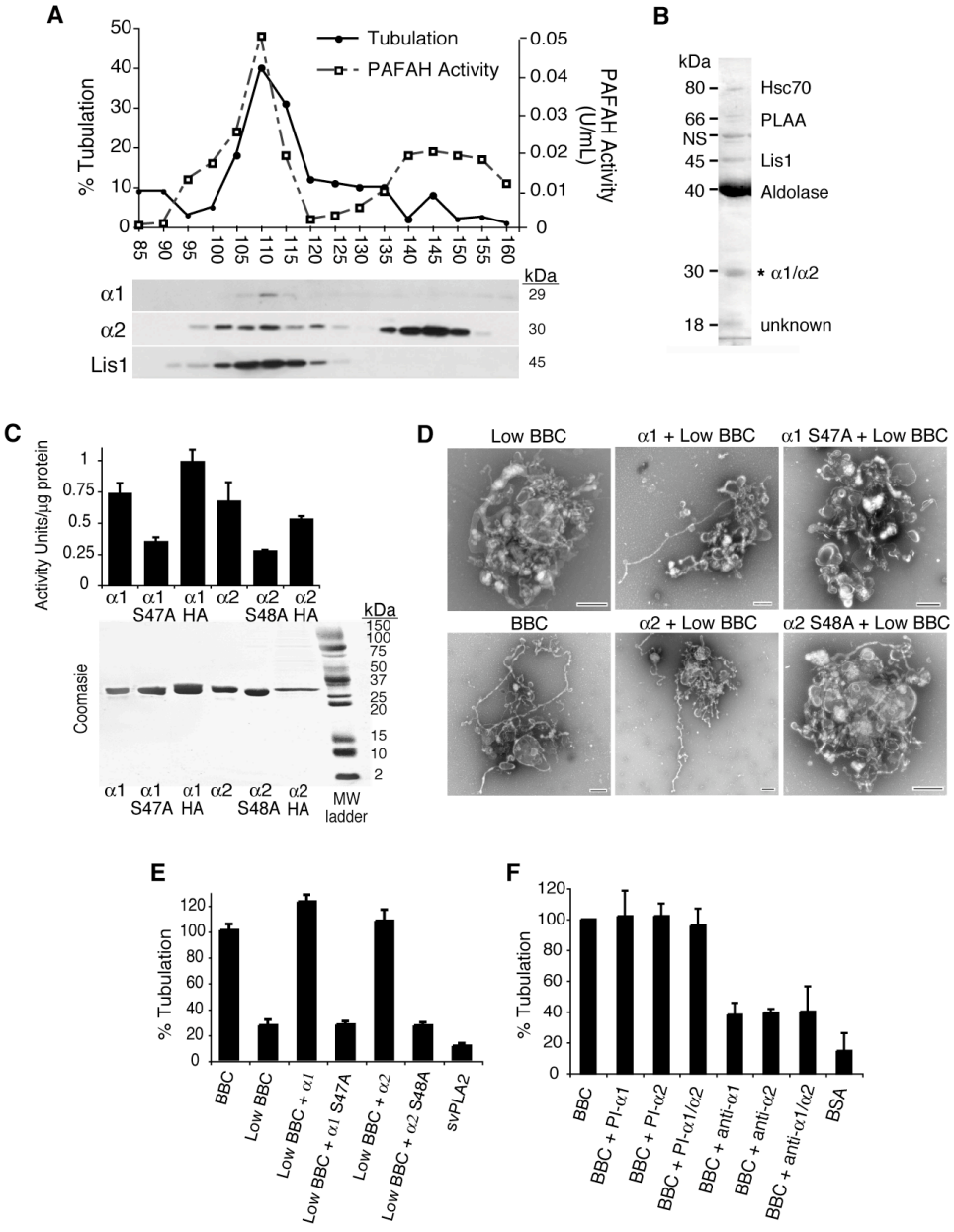
A
Tubulation
PAFAH Activity
% Tubulation
PAFAH Activity (U/mL)
kDa
α1
α2
Lis1
29
30
45
B
kDa
80
66
NS
45
40
30
18
Hsc70
PLAA
Lis1
Aldolase
* α1/α2
unknown
C
Activity Units/μg protein
α1
α1 S47A
α1 HA
α2
α2 S48A
α2 HA
Coomasie
MW ladder
D
Low BBC
α1 + Low BBC
α1 S47A + Low BBC
BBC
α2 + Low BBC
α2 S48A + Low BBC
E
% Tubulation
BBC
Low BBC
Low BBC + α1
Low BBC + α1 S47A
Low BBC + α2
Low BBC + α2 S48A
svPLA2
F
% Tubulation
BBC
BBC + PI-α1
BBC + PI-α2
BBC + PI-α1/α2
BBC + anti-α1
BBC + anti-α2
BBC + anti-α1/α2
BSA

Figure 2-2: α1 and α2 stimulate Golgi membrane tubules via catalytic activity, independently of LIS1 binding. Quantification of isolated Golgi complexes with membrane tubules in the reconstitution assay. Golgi were incubated with purified wild type or LIS1 binding-defective α1 E38D and α2 E39D (7.5 μg/ml), in the presence or absence of Low BBC. Results are percentage of control (BBC), n = 3, error bars = SEM. svPLA$_2$ = snake venom PLA$_2$.

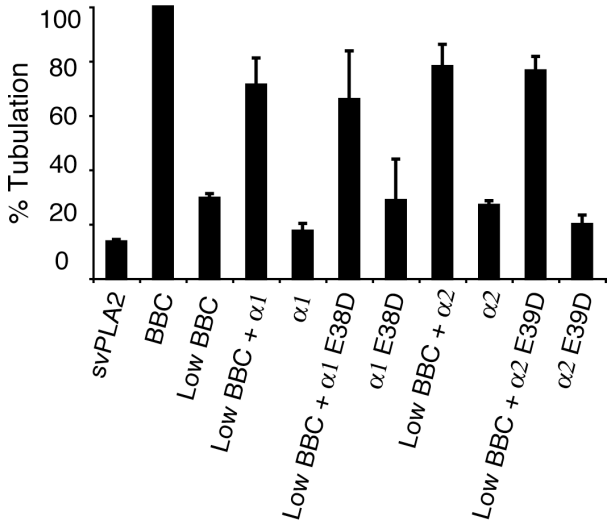
% Tubulation
100
80
60
40
20
0
svPLA2
BBC
Low BBC
Low BBC + α1
α1
Low BBC + α1 E38D
α1 E38D
Low BBC + α2
α2
Low BBC + α2 E39D
α2 E39D

Figure 2-3: PAFAH Ib partially localizes to Golgi membranes. (**A**) Confocal microscopy of BTRD cells mildly overexpressing α1 (HA tagged) and Rab6-GFP. Box indicates the region in lower panels. (**B**) Fluorescence intensity line plot of α1 and Rab6-GFP from the line shown in the merge image of lower panel of (A). (**C**) Western blot showing α1 and LIS1 co-migrate with the Golgi (ManII) by sucrose-density cell fractionation. Bracket indicates non-specific bands. (**D**) Confocal slice shows HA-LIS1 localizes around the Golgi (ManII). (**E**) Line fluorescence intensity plot of LIS1 concentrated around Golgi complexes (from line in merge image of D). Scale bars: A lower, E = 5 μm; A upper, D = 10 μm.

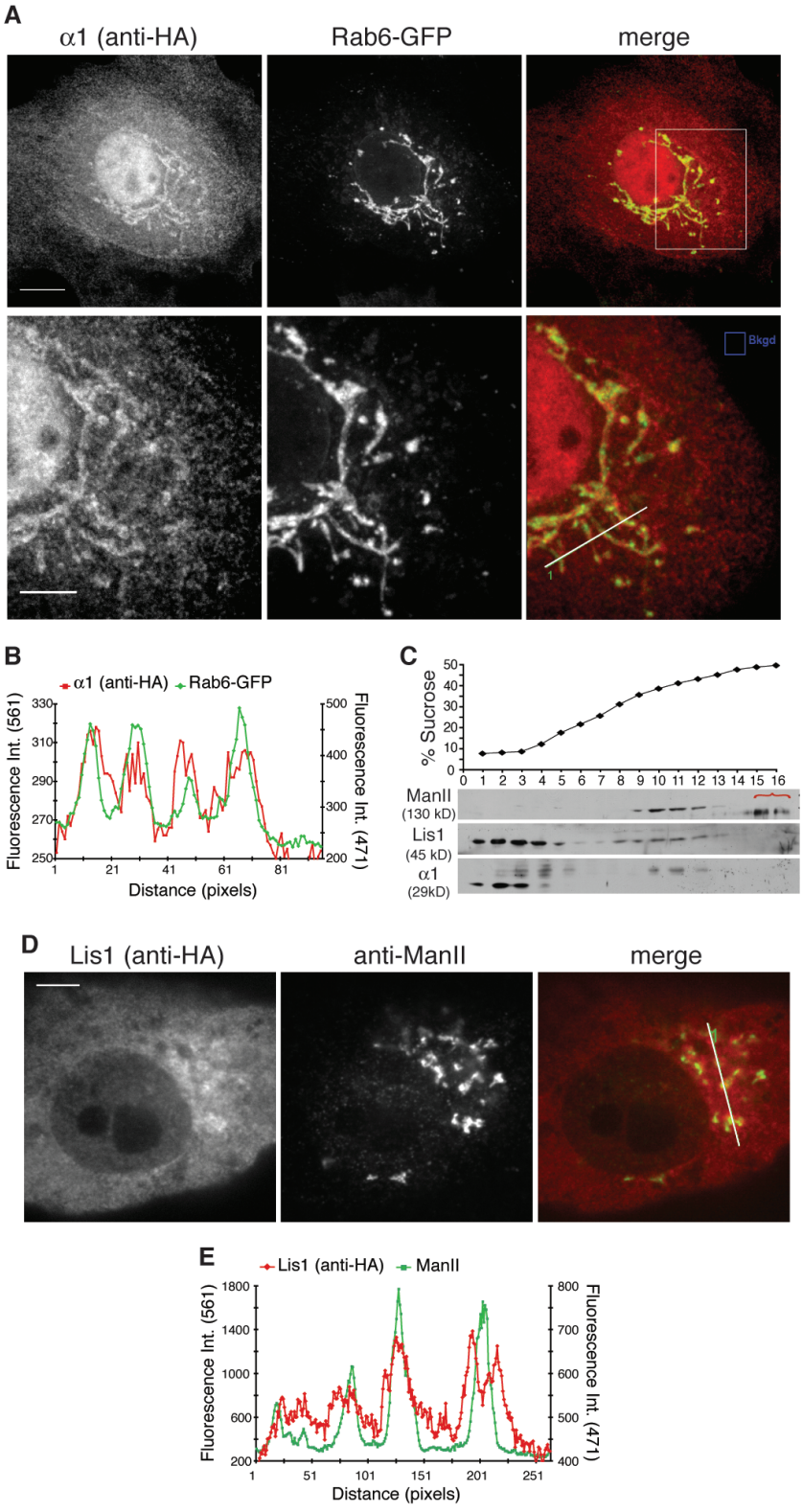
A
α1 (anti-HA)
Rab6-GFP
merge
Bkgd
B
α1 (anti-HA)
Rab6-GFP
Fluorescence Int. (561)
Fluorescence Int. (471)
Distance (pixels)
C
% Sucrose
ManII
(130 kD)
Lis1
(45 kD)
α1
(29kD)
D
Lis1 (anti-HA)
anti-ManII
merge
E
Lis1 (anti-HA)
ManII
Fluorescence Int. (561)
Fluorescence Int. (471)
Distance (pixels)

Figure 2-4: Wild type and mutant α1 and α2 colocalize to multiple Golgi cisternae as well as the TGN. Representative images of BTRD cells show the localization of α1, α2, α2 S48A catalytic mutant to *medial* Golgi, as seen by anti-ManII. Representative image showing the double LIS1 binding mutant and catalytic inactive α1 S47A/E38D localizes to the TGN, as seen by anti-M6PR. Scale bars = 2 μm.

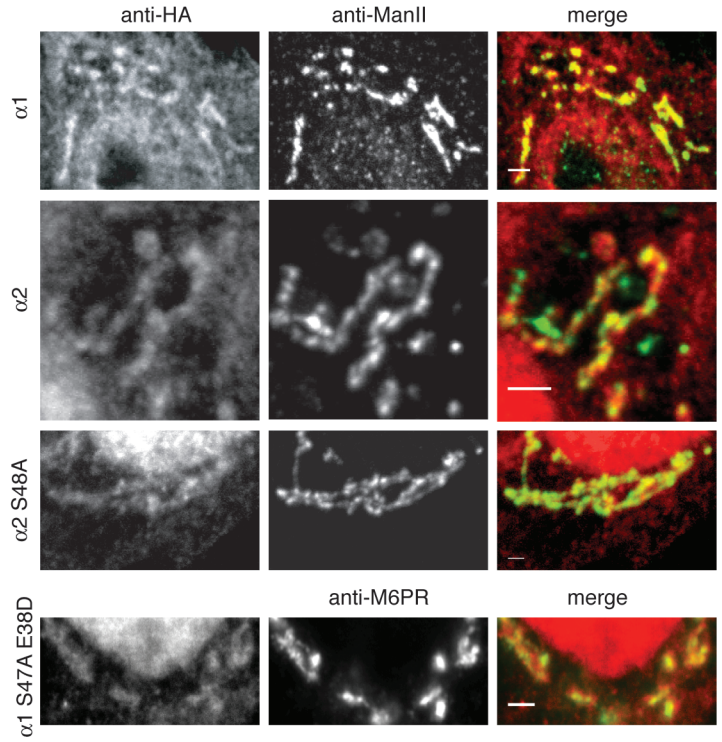
anti-HA
anti-ManII
merge
α1
α2
α2 S48A
anti-M6PR
merge
α1 S47A E38D

were similarly localized (Figure 2-4; data not shown), indicating that catalytic activity and LIS1 binding are not required for α1 or α2 association with Golgi membranes. In addition to centrosomal and cytoplasmic localization, HA-tagged LIS1 was observed to surround the Golgi complex (Figure 2-3 D, E), consistent with reports that a small fraction of LIS1 is membrane associated (360). PAFAH Ib α1 could also be found localized to membrane tubules (Figure 2-5). Consistent with the imaging results, we found that a fraction of both α1 and LIS1 co-fractionated with Golgi membranes in sucrose gradients (Figure 2-3 C).

PAFAH Ib α1 and α2 Overexpression Reveals a Connection Between PLA_2 Activity and LIS1-Mediated Regulation of Golgi Structure

Overexpression of α1 or α2 resulted in a fragmented or completely dispersed Golgi and TGN (Figures 2-6; 2-7; 2-8), which was more severe in α2 overexpressing cells (Figure 2-7 A, D, E). Changes in Golgi structure were not observed when cells overexpressed an unrelated cytoplasmic PLA_2, $iPLA_2\alpha$ (E. Racoosin, data not shown). Overexpression of catalytically inactive α1 S47A or α2 S48A also caused the Golgi and TGN to become fragmented or diffuse (Figures 2-6; 2-7; 2-8). Overexpression of catalytically inactive α1 or α2 may produce a dominant negative effect by forming poisonous dimers, competing with endogenous α1 and α2 for binding to membranes, and/or by titrating LIS1, thus inhibiting the ability of LIS1 to regulate dynein (339, 367). Microtubules and dynein-mediated centripetal positioning are required for the maintenance of an intact mammalian Golgi near the centrosome (64). To determine if overexpression of α1 and α2 affected Golgi structure by binding to and influencing LIS1 function, cells were transfected with the LIS1-binding

Figure 2-5: α1 colocalizes with Golgi and TGN membrane tubules. (**A**) α1 (HA) localizes to Golgi tubules as seen in confocal images of BTRD cells. Arrowheads indicate colocalization with Rab6-GFP membrane tubules. (**B**) Line fluorescence intensity of α1 on membrane tubules (from line in merge image of A). (**C**) Confocal stacks of BTRD cell overexpressing HA tagged α1 PKD-KD-GFP shows α1 localizes to a subset of TGN tubules (arrowheads). Box indicates region shown in lower panel.

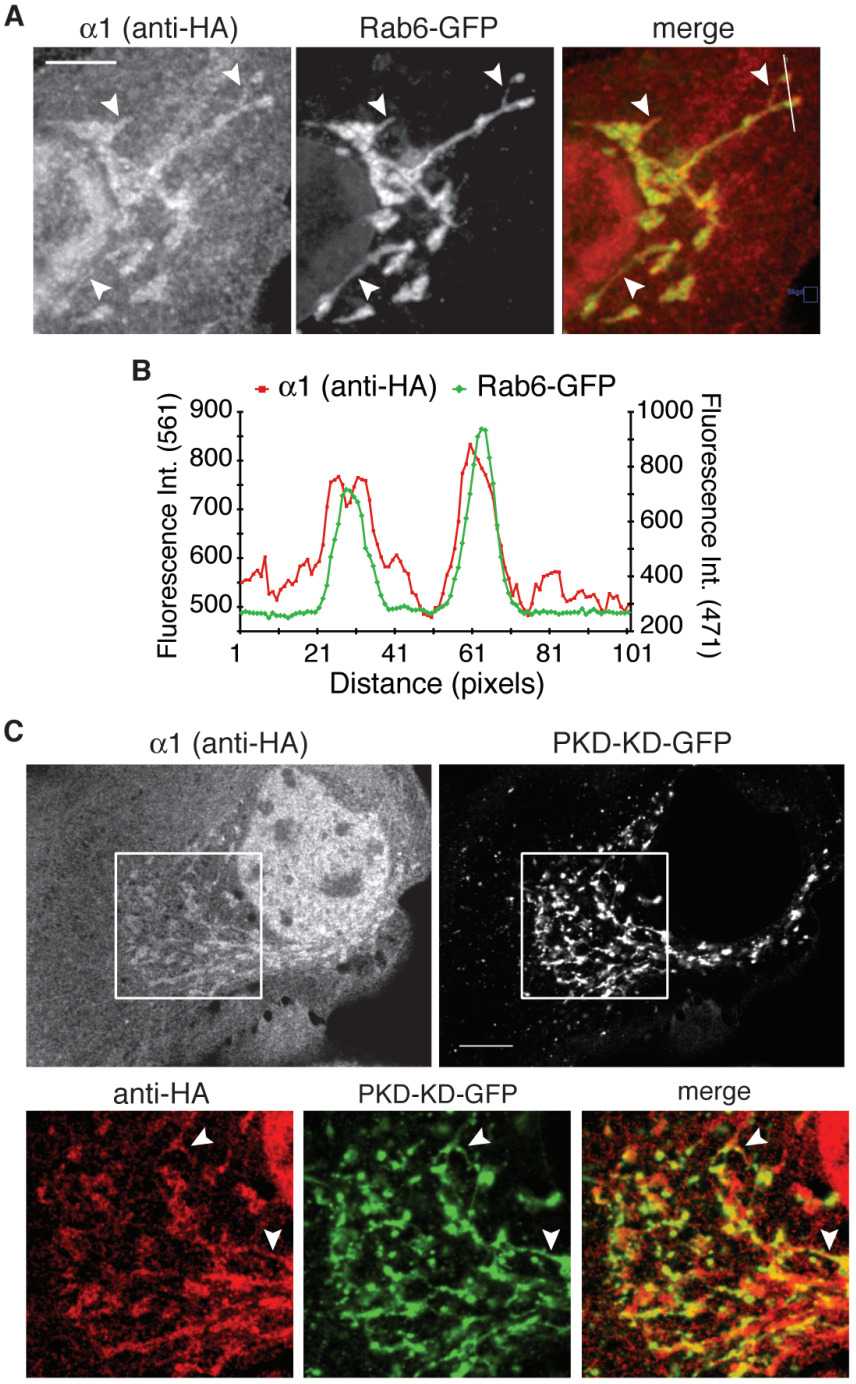
A
α1 (anti-HA)
Rab6-GFP
merge
B
α1 (anti-HA)
Rab6-GFP
Fluorescence Int. (561)
Fluorescence Int. (471)
900
800
700
600
500
1000
800
600
400
200
1
21
41
61
81
101
Distance (pixels)
C
α1 (anti-HA)
PKD-KD-GFP
anti-HA
PKD-KD-GFP
merge

Figure 2-6: Overexpression of PAFAH Ib alpha subunits perturbs Golgi and TGN structure. (**A**) HeLa cells transfected with the indicated α1 (HA tagged) and double labeled for HA and either a Golgi (GPP130) or TGN marker (M6PR). Overexpression of α1 wild type, α1 S47A (catalytic mutant), or α1 S47A/E38D (catalytic and LIS1 binding mutant) disrupted the structure of the Golgi and the TGN. Asterisks and arrowheads indicate transfected and untransfected cells, respectively. (**B**) Quantitation of HeLa and BTRD cells with disrupted Golgi structure in cells transfected as indicated. Weighted means shown, n = 3, error bars = SEM, *= $p < 0.05$ compared to untransfected cells, **= $p< 0.001$ compared to α1 E38D (Behrens-Welch test). Scale bars = 10 μm.

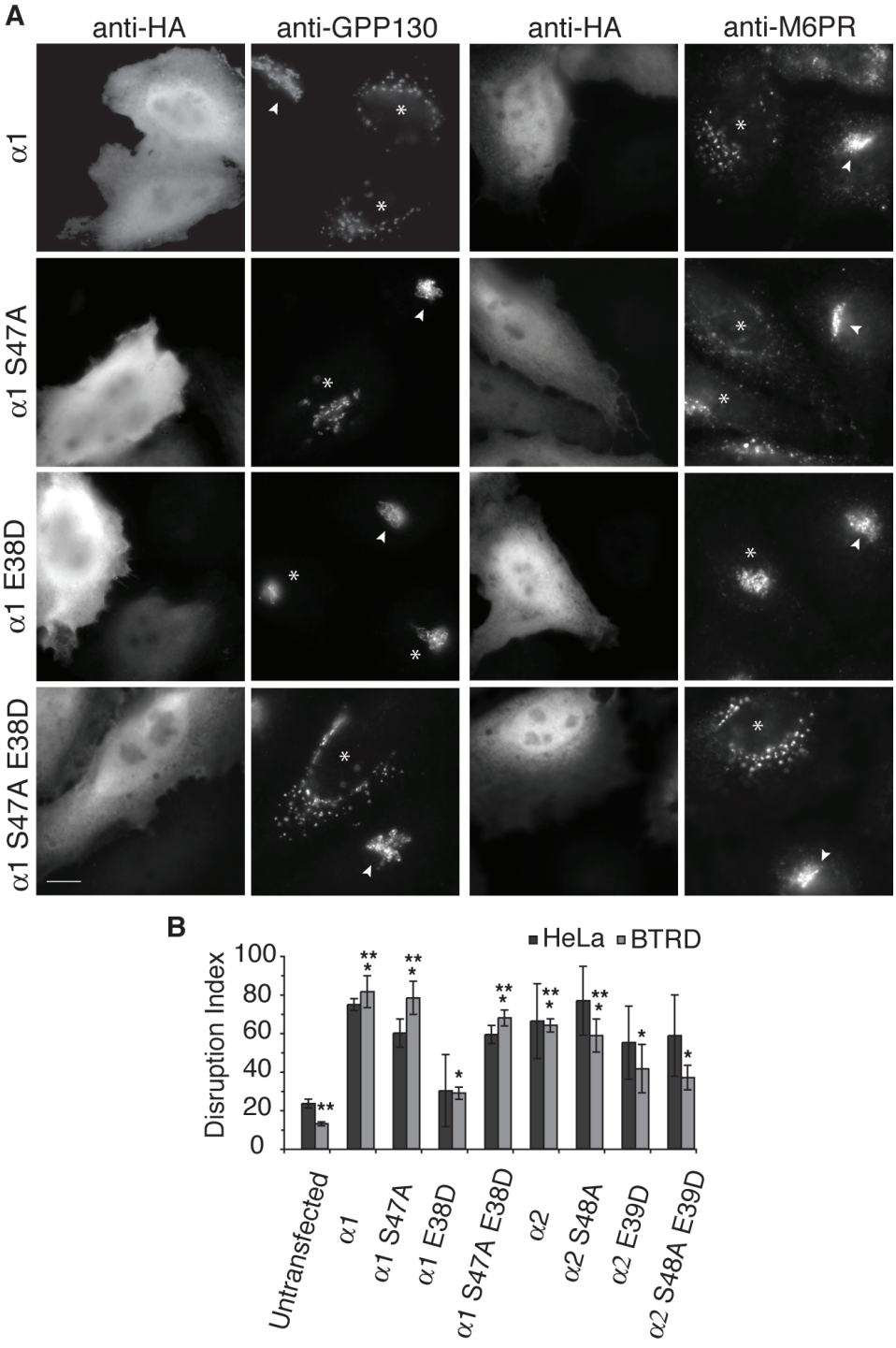
A
anti-HA
anti-GPP130
anti-HA
anti-M6PR
α1
α1 S47A
α1 E38D
α1 S47A E38D
B
HeLa
BTRD
Disruption Index
100
80
60
40
20
0
Untransfected
α1
α1 S47A
α1 E38D
α1 S47A E38D
α2
α2 S48A
α2 E39D
α2 S48A E39D

Figure 2-7: PAFAH Ib α1 and α2 disrupt Golgi structure. (**A**) Wide field fluorescence images showing HeLa cells overexpressing α2 (HA, *) wild type or mutants disrupt Golgi (GPP130) structure as compared to untransfected cells. (**B, C**) Overexpression of α1 or α2 (HA, *) and indicated mutants, except a1 E38D, disrupt Golgi (ManII) structure, as compared to neighboring untransfected BTRD cells. (**D, E**) The severity of Golgi disruption was quantified in untransfected and overexpressing cells (as indicated), categorized as intact, fragmented, or diffuse Golgi, n = 3. All scale bars = 10 μm.

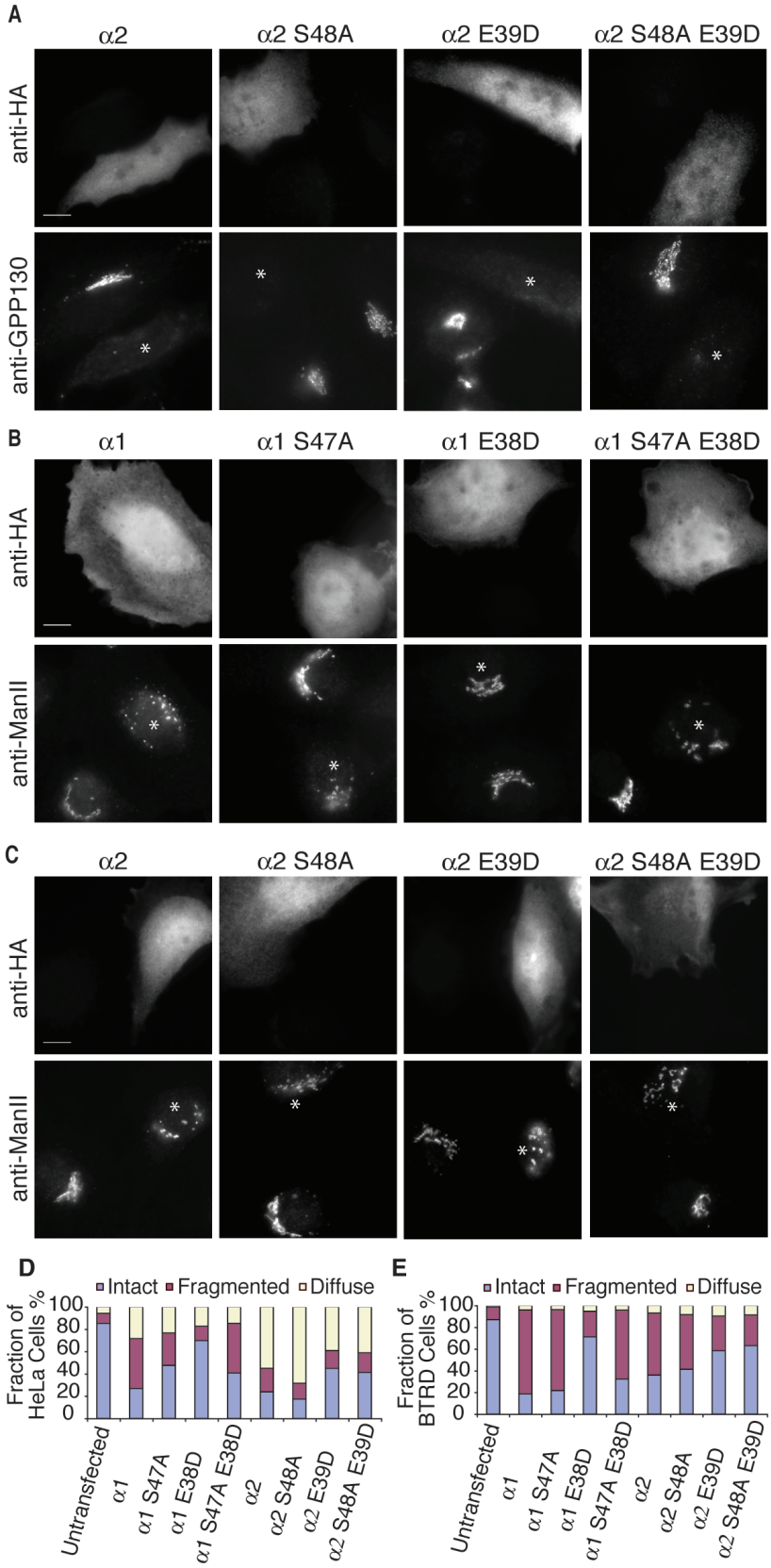
A
α2
α2 S48A
α2 E39D
α2 S48A E39D
anti-HA
anti-GPP130
B
α1
α1 S47A
α1 E38D
α1 S47A E38D
anti-HA
anti-ManII
C
α2
α2 S48A
α2 E39D
α2 S48A E39D
anti-HA
anti-ManII
D
Intact
Fragmented
Diffuse
Fraction of HeLa Cells %
100
80
60
40
20
0
Untransfected
α1
α1 S47A
α1 E38D
α1 S47A E38D
α2
α2 S48A
α2 E39D
α2 S48A E39D
E
Intact
Fragmented
Diffuse
Fraction of BTRD Cells %
100
80
60
40
20
0
Untransfected
α1
α1 S47A
α1 E38D
α1 S47A E38D
α2
α2 S48A
α2 E39D
α2 S48A E39D

Figure 2-8: PAFAH Ib α1 and α2 disrupt TGN structure. (**A**) Wide field fluorescence images of HeLa cells overexpressing indicated constructs of α2 (HA, *) disrupt TGN (M6PR) structure in comparison to untransfected cells. (**B, C**) Overexpression of the indicated α1 or α2 (HA, *) constructs, except α1 E38D, disrupts TGN (M6PR) structure in BTRD cells. All scale bars = 10 μm.

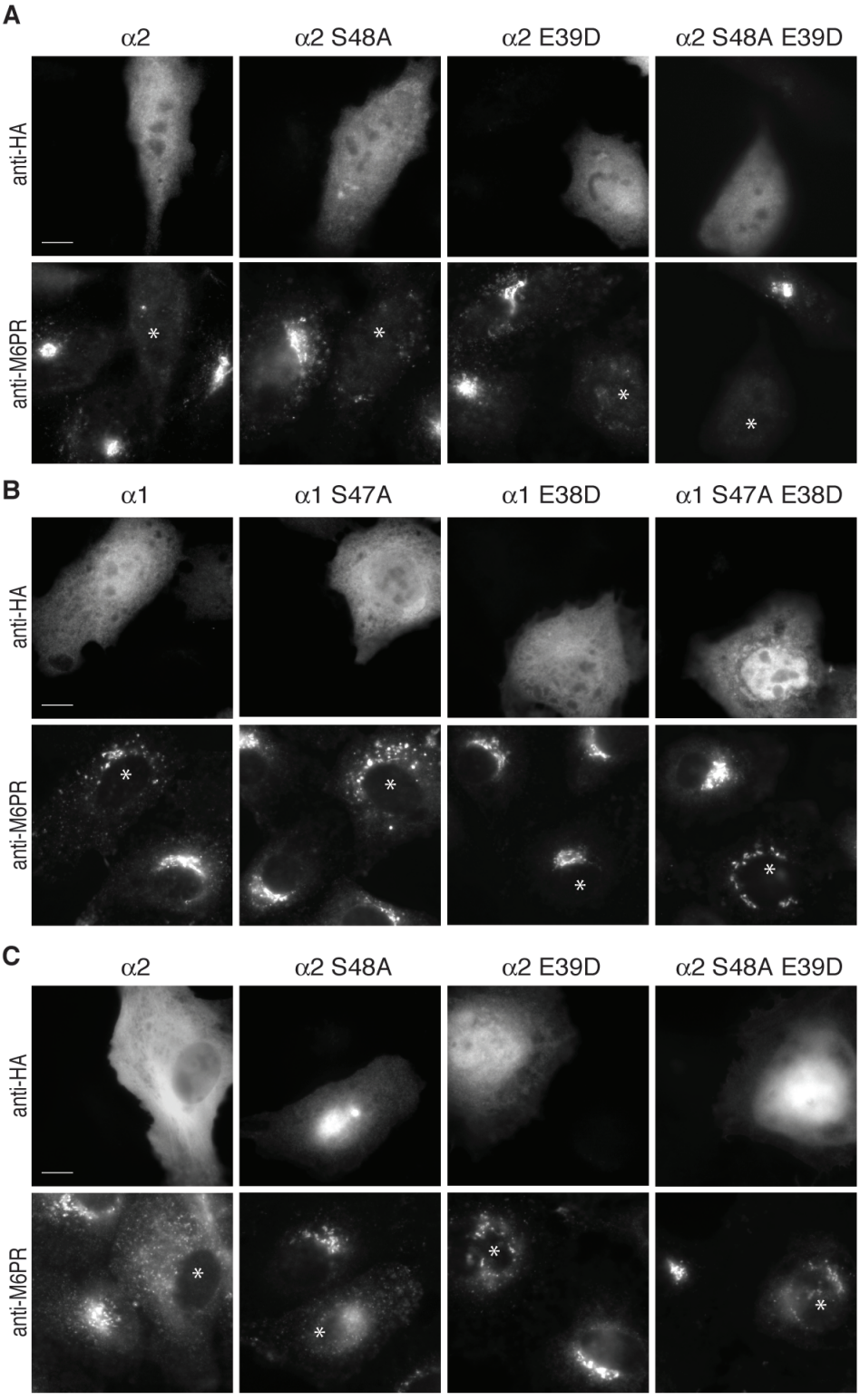
A
α2
α2 S48A
α2 E39D
α2 S48A E39D
anti-HA
anti-M6PR
B
α1
α1 S47A
α1 E38D
α1 S47A E38D
anti-HA
anti-M6PR
C
α2
α2 S48A
α2 E39D
α2 S48A E39D
anti-HA
anti-M6PR

mutants α1 E38D or α2 E39D. α2 E39D did disrupt the Golgi and TGN, albeit less severely than α2 wild type or α2 S48A (Figures 2-7; 2-8). In contrast to wild type and catalytically inactive α1, overexpression of equivalent levels of α1 E38D did not significantly disrupt the Golgi or TGN (Figures 2-6; 2-7; 2-8; 2-9), indicating that the Golgi disruption produced by α1 and α1 S47A are partially due to interactions with LIS1.

To determine if catalytic activity of α1 and α2 is also important for maintaining Golgi structure *in vivo*, independent of LIS1, cells were transfected with a double mutant, which is both catalytically inactive and unable to bind LIS1 (α1 S47A/E38D; α2 S48A/E39D). These constructs also disrupted the Golgi and TGN (Figures 2-6; 2-7; 2-8).

The LIS1 binding mutant results suggest that catalytic activity is important, and that α subunits also compete for binding to LIS1 to regulate dynein-dependent Golgi structure, in agreement with previous reports (338). In addition, our results agree with Ding et al., who found that overexpression of α2 had a more dramatic effect on Golgi positioning. A role for LIS1 in Golgi structure has been suggested; $LIS1^{+/-}$ mouse embryonic fibroblasts had mild Golgi dispersal, and Cos-7 cells overexpressing LIS1 had more compact Golgi complexes (358).

Our results suggest a model whereby PAFAH Ib provides a link between the initiation of membrane tubule formation and the subsequent movement of these tubules along microtubules. PAFAH Ib α1 and α2, bound to LIS1, may initiate membrane curvature by intrinsic PLA_2 activity, thus forming membrane tubules. Subsequently, LIS1 may switch to a LIS1-Ndel1-dynein complex, facilitating the minus end movement of membrane tubules along microtubules to the centrosome (339). This provides a mechanism to

couple the formation of Golgi membrane tubules to dynein motors for the formation and maintenance of a centrally located, intact Golgi ribbon.

Loss of PAFAH Ib Fragments the Golgi Complex, Inhibits Tubule-Mediated Golgi Assembly, and Reduces Anterograde Trafficking

To determine if PAFAH Ib α1 and α2 are required for Golgi structure and function, siRNA-mediated knockdown experiments were conducted. PAFAH Ib α1 and α2 can form catalytically active homo- and heterodimers (323). Therefore we used mixed siRNAs targeting both α1 and α2, reducing expression by 85.7 $\pm$ 3.3% and 81.8 $\pm$ 3.8% (n = 7 and 6; $\pm$ SEM), respectively, which did not affect levels of LIS1 (Figure 2-9). As a consequence of α1 and α2 loss, the Golgi complex, ER-Golgi-Intermediate Compartment (ERGIC), and the TGN became fragmented (Figures 2-10; 2-11). Confocal microscopy revealed that fragmented Golgi puncta contained multiple cisternal markers, indicating that loss of α1 and α2 resulted in the formation of mini-stacks (Figure 2-10; 2-11), which was confirmed by transmission EM (Figure 2-10 D). Similar fragmentation was seen with knockdown of LIS1, which could be rescued by expressing RNAi-resistant HA-LIS1 (Figure 2-12), similar to other recent studies (360).

Membrane tubule-mediated assembly and maintenance of an intact Golgi ribbon is inhibited by PLA_2 antagonists (78). To determine if knockdown of PAFAH Ib subunits similarly inhibits these tubules, we examined the reassembly of the Golgi during recovery from brefeldin A (BFA). Following washout of BFA, the Golgi reassembles into separate mini-stacks that subsequently coalesce via membrane tubules into an intact ribbon (78). Knockdown of α1 and α2 or LIS1 had no apparent effect on BFA-stimulated

Figure 2-9: Relative expression of α1. (**A**) Western blot of α1 in control BTRD cells, BTRD cells overexpressing α1 and mutants, α1 & α2 siRNA treated cells or α1 & α2 knockdown cells expressing an RNAi-resistant α1 or α1 S47A. (**B**) Relative expression levels—fold expression relative to endogenous—of α1 when knocked down or overexpressed. (**C**) Western blot of PAFAH Ib subunits in control and α1 and α2 siRNA treated (72 h) BTRD cells.

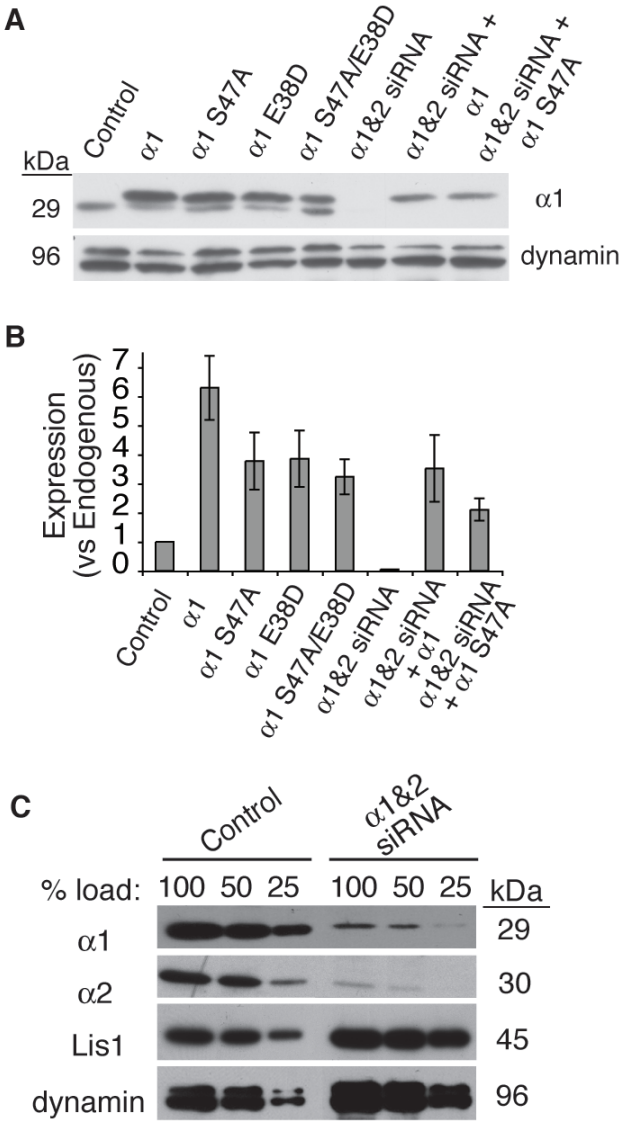
A
Control
α1
α1 S47A
α1 E38D
α1 S47A/E38D
α1&2 siRNA
α1&2 siRNA + α1
α1&2 siRNA + α1 S47A
kDa
29
96
α1
dynamin
B
Expression (vs Endogenous)
0
1
2
3
4
5
6
7
Control
α1
α1 S47A
α1 E38D
α1 S47A/E38D
α1&2 siRNA
α1&2 siRNA + α1
α1&2 siRNA + α1 S47A
C
Control
α1&2 siRNA
% load: 100 50 25 100 50 25
kDa
α1
α2
Lis1
dynamin
29
30
45
96

Figure 2-10: PAFAH Ib subunits are important for maintaining an intact Golgi ribbon. (**A**) Confocal stack of the Golgi (ManII) in control BTRD and α1/α2 siRNA transfected BTRD cells. (**B**) The fraction of cells with fragmented Golgi. n = 7, error bars = SEM, $p < 0.001$ by T-test. (**C**) 3-D reconstructions of Golgi from confocal z-series of control and α1/α2 siRNA treated cells visualized with anti-ManII (medial marker, red) and GalT-GFP (*trans* marker, green). (**D**) Electron micrographs from control and α1/α2 siRNA knockdown cells. Scale bars: A = 2 μm; C, D = 500 nm.

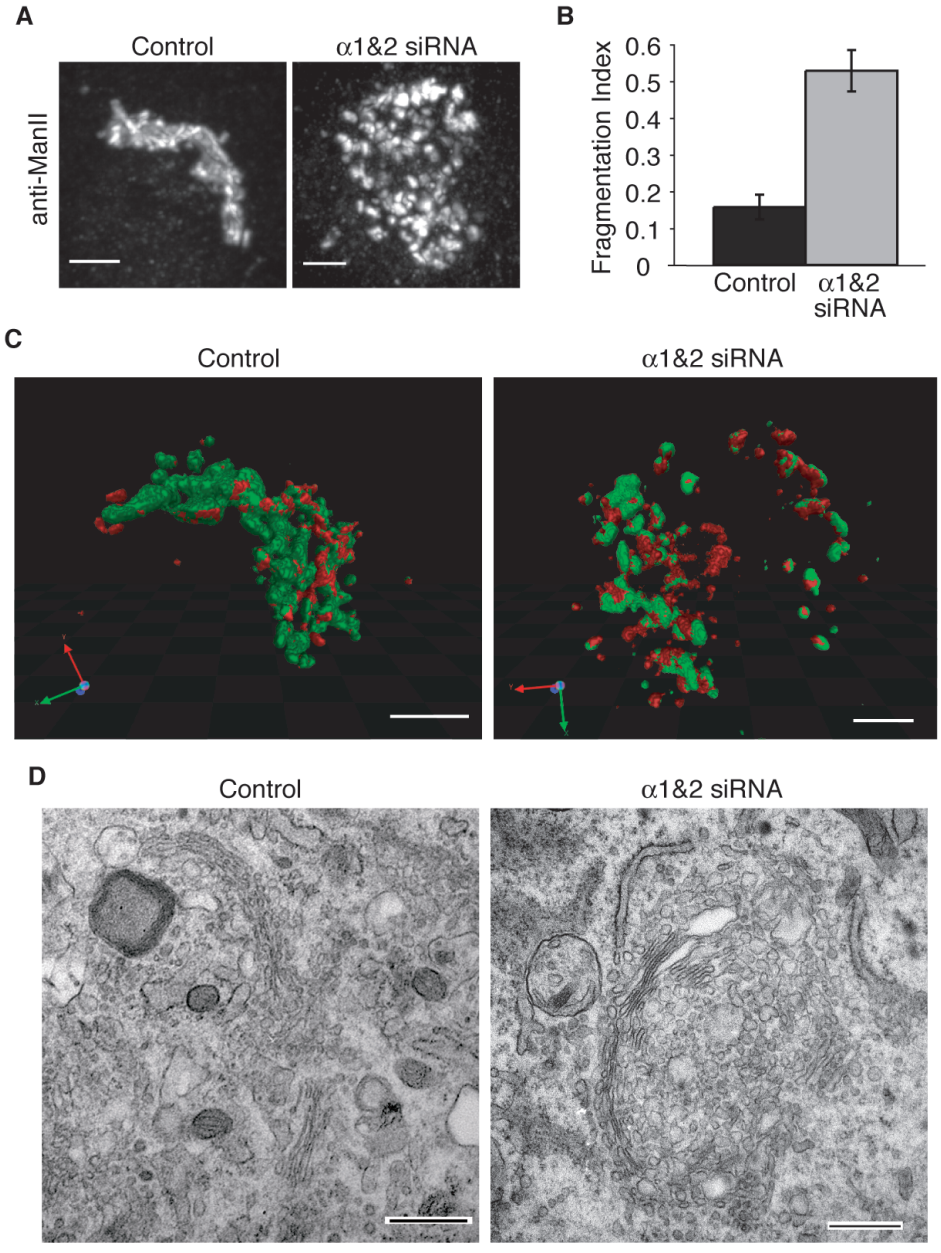
A
Control
α1&2 siRNA
anti-ManII
B
Fragmentation Index
0.6
0.5
0.4
0.3
0.2
0.1
0
Control
α1&2 siRNA
C
Control
α1&2 siRNA
D
Control
α1&2 siRNA

Figure 2-11: The ERGIC and TGN are perturbed in α1 and α2 knockdown cells, and the TGN is associated with mini-stacks. Loss of α1 and α2 fragments the ERGIC and TGN into mini-stacks. (**A**) Reduced α1 and α2 levels disrupts ERGIC structure. Control or α1 & α2 siRNA transfected BTRD cells transiently transfected with ERGIC53-GFP under a low expression promoter. (**B**) Knockdown of α1 & α2 in BTRD cells fragments the TGN (M6PR). (**C**) The TGN in α1 & α2 siRNA transfected BTRD cells is present in mini-stacks, as seen by the overlap of M6PR (red) and expressed GalT-GFP (green) in confocal images. Scale bars: A = 5 μm; B, C = 2 μm.

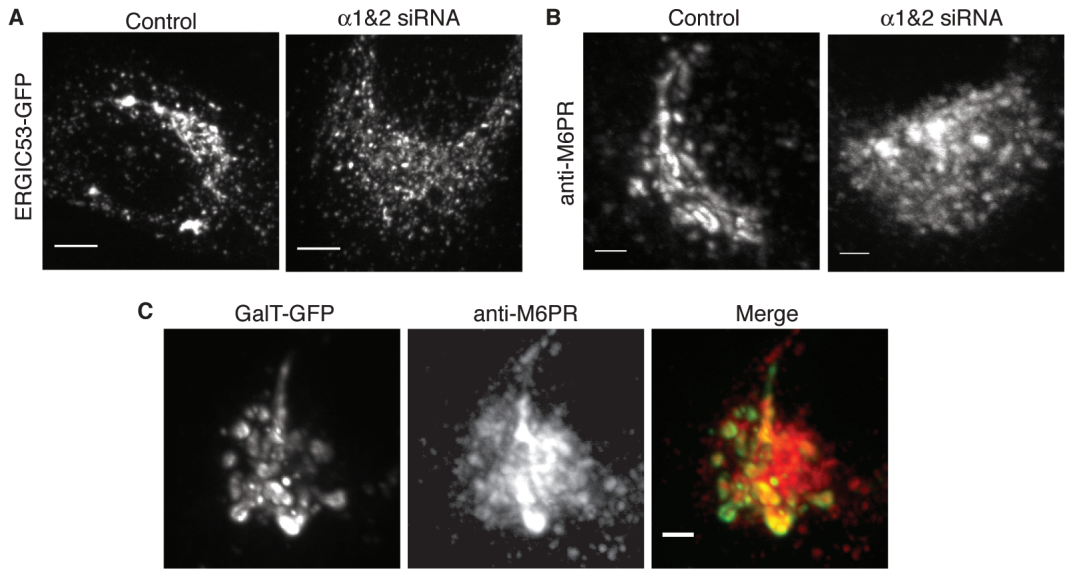
A
Control
α1&2 siRNA
ERGIC53-GFP
B
Control
α1&2 siRNA
anti-M6PR
C
GalT-GFP
anti-M6PR
Merge

Figure 2-12: Golgi structure is perturbed with LIS1 knockdown. (**A**) Western blot of LIS1 expression with siRNA knockdown and rescue 48 h after transfection of control BTRD cells, LIS1 siRNA transfected cells, and LIS1 knockdown cells overexpressing RNAi resistant HA-LIS1. (**B**) Wide field fluorescence image of the Golgi (ManII) in control and LIS1 siRNA transfected BTRD cells. (**C**) Fraction of cells with fragmented Golgi. n = 3, error bars = SEM. Scale bars = 10 μm.

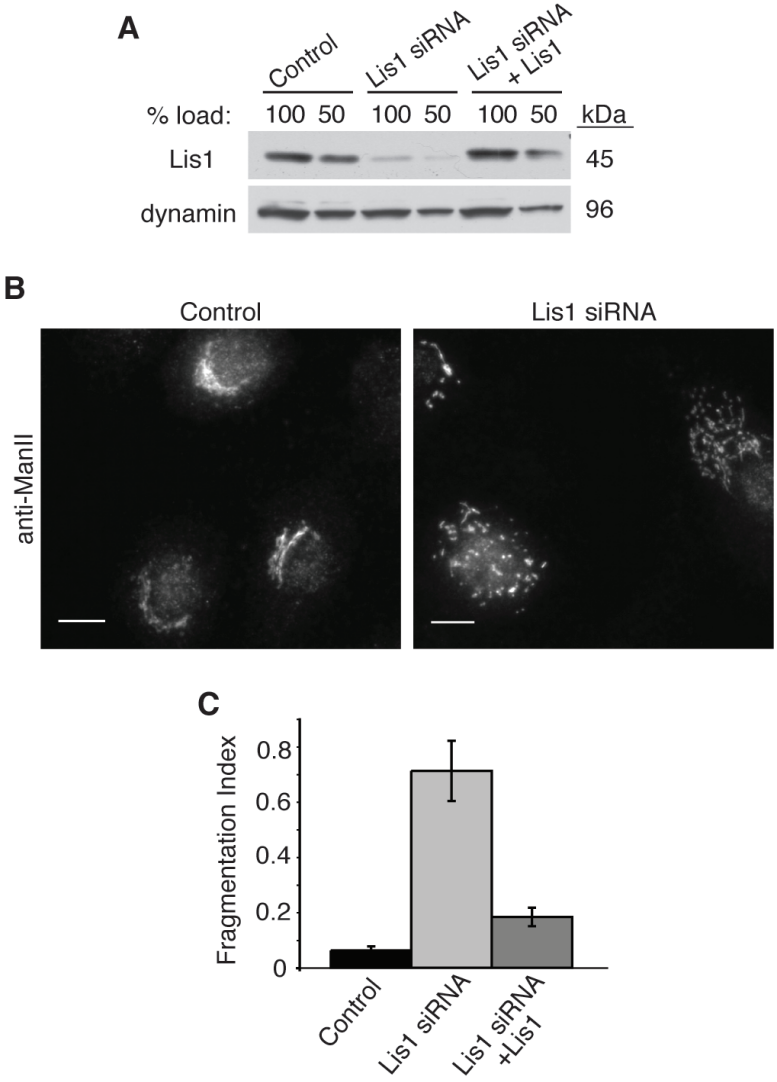
A
Control
Lis1 siRNA
Lis1 siRNA + Lis1
% load:
100 50 100 50 100 50
kDa
Lis1
45
dynamin
96
B
Control
Lis1 siRNA
anti-ManII
C
Fragmentation Index
0.8
0.6
0.4
0.2
0
Control
Lis1 siRNA
Lis1 siRNA +Lis1

retrograde movement of Golgi enzymes to the ER (data not shown). Upon washout, the emergence of separate Golgi mini-stacks was unaffected by knockdown of PAFAH Ib subunits. In contrast, knockdown of α1 and α2 or LIS1 significantly inhibited subsequent coalescence into intact ribbons (Figure 2-13; 2-14), which could be rescued by expressing RNAi-resistant LIS1 (Figure 2-14 C, D). Importantly, unlike α1 and α2 knockdown, LIS1 knockdown Golgi mini-stacks displayed numerous membrane tubules, which were no longer seen when all three subunits were knocked down (Figure 2-15). These results are consistent with our *in vitro* and overexpression studies and further support the conclusion that the catalytic α1 and α2 subunits of PAFAH Ib are capable of inducing membrane tubules *in vivo*. The membrane tubules that form in LIS1 knockdown cells are dependent on α1 and α2, but directed movement for mini-stack coalescence is inhibited in the absence of LIS1-mediated dynein interactions.

In addition to reassembly of the Golgi complex, membrane tubules are implicated in export from the TGN and secretion (96, 97). Using ts045VSV-G as a transmembrane cargo, we found that transport from the ER to the Golgi complex was unaffected in α1 and α2 knockdown cells (Figure 2-16). In contrast, export of ts045VSV-G from the TGN to the cell surface was significantly slowed in α1 and α2 knockdown cells (Figure 2-17). VSV-G transport was unchanged with LIS1 knockdown (Figure 2-18), suggesting α1 and α2 have LIS1-independent roles in TGN to plasma membrane trafficking. The reduced transport of VSV-G with α1 and α2 knockdown could be partially rescued by the re-introduction of equivalent levels of RNAi resistant α1, but not RNAi resistant α1 S47A, indicating the PLA_2 activity is important for regulating the transport of Golgi to plasma membrane cargo (Figure 2-17

Figure 2-13: Golgi ribbon reassembly is significantly delayed in α1 and α2 knockdown cells. (**A**) Confocal images of the Golgi (anti-ManII) before BFA, after 20 min in BFA (0 min), and 20, 45 or 90 min after BFA washout in control or α1 & α2 siRNA transfected cells. (**B**) Percent of cells with reassembled Golgi ribbons after BFA washout. n = 4, error bars = SEM, at 90 min $p < 0.01$ by a T-test. Scale bars =10 μm.

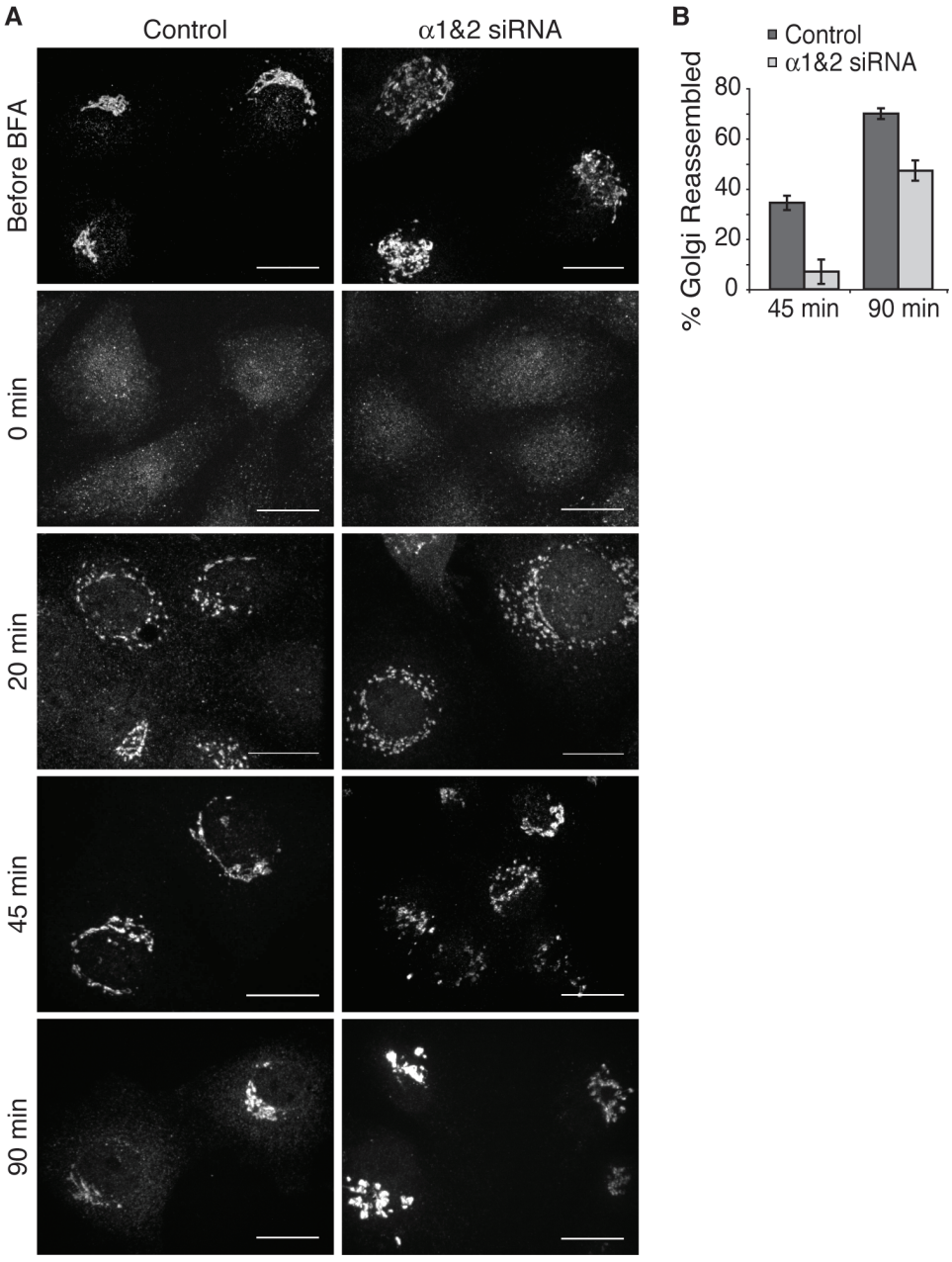
A
Control
α1&2 siRNA
Before BFA
0 min
20 min
45 min
90 min
B
Control
α1&2 siRNA
% Golgi Reassembled
80
60
40
20
0
45 min
90 min

Figure 2-14: Golgi ribbon reassembly is impaired in LIS1 knockdown cells. (**A**) Wide field fluorescence images of the Golgi (anti-ManII) before BFA treatment, and after 0, 20, 45, or 60 min of BFA washout. RNAi-resistant HA-LIS1 expression is shown in insets (anti-HA). (**B**) Percent of cells with reassembled Golgi ribbons, n = 3, error bars = SEM. Scale bars =10 μm.

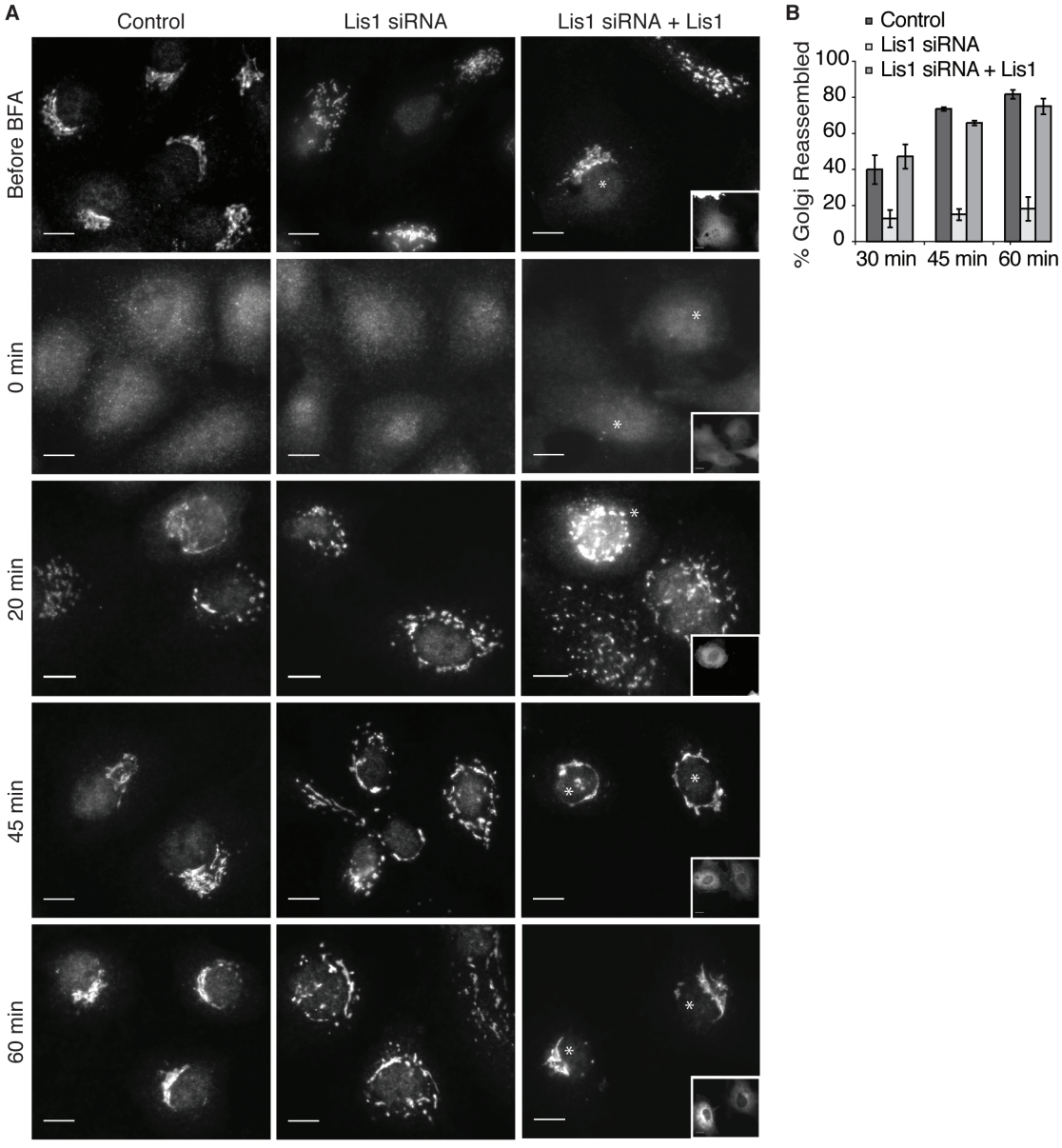
A
Control
Lis1 siRNA
Lis1 siRNA + Lis1
Before BFA
0 min
20 min
45 min
60 min
B
Control
Lis1 siRNA
Lis1 siRNA + Lis1
% Golgi Reassembled
100
80
60
40
20
0
30 min
45 min
60 min

Figure 2-15: α1 and α2, but not LIS1 are important for membrane tubules in Golgi reassembly. (**A**) Confocal images of Golgi ministacks (anti-ManII) after 30 min of BFA recovery for α1 & α2 siRNA or LIS1 siRNA, or α1/α2/LIS1 siRNA (triple) treated BTRD cells. LIS1 knockdown cells show extensive membrane tubules, which are not seen in α1 & α2 or triple knockdown cells. (**B**) Percent of cells with Golgi tubules after 30 min of BFA washout. n=3, error bars = SEM. Scale bars = 5 μm.

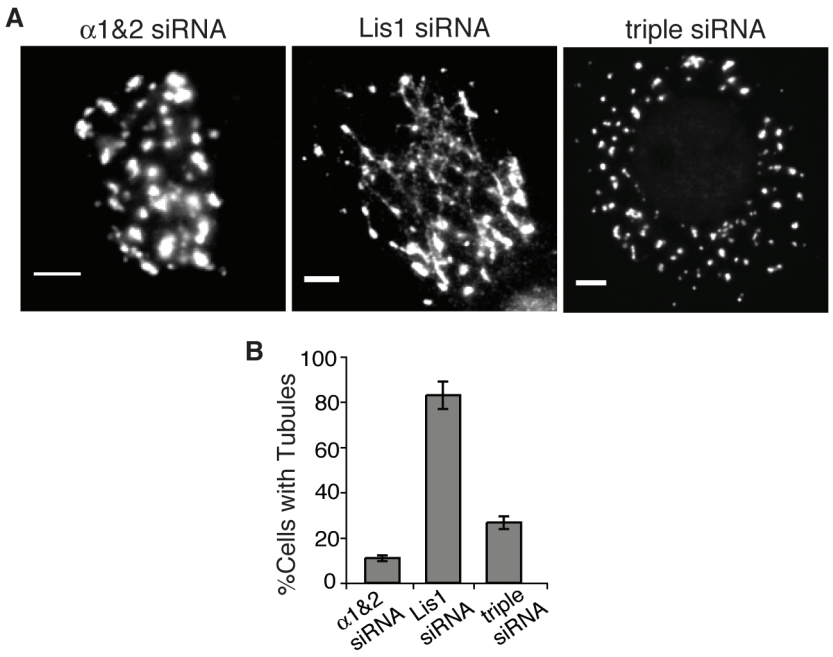
A
α1&2 siRNA
Lis1 siRNA
triple siRNA
B
%Cells with Tubules
100
80
60
40
20
0
α1&2 siRNA
Lis1 siRNA
triple siRNA

Figure 2-16: α1 and α2 knockdown does not affect anterograde transport of $_{ts045}$VSV-G from the ER to the Golgi. Control and α1 and α2 siRNA treated BTRD cells were transfected with VSV-G-YFP. VSV-G-YFP fluorescence in the Golgi after release from a 40°C block to 20°C. Lines correspond to first order kinetic equations: control $k = 0.10 \pm 0.02$ and siRNA $k = 0.07 \pm 0.02$, ± SEM. Difference in kinetic constants was not statistically significant, $p < 0.25$ (T-test).

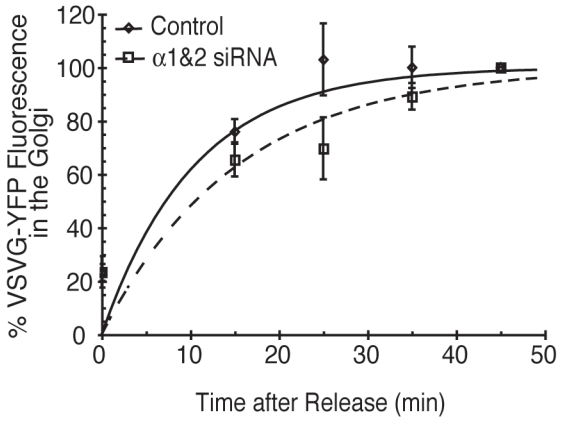
Control
α1&2 siRNA
% VSVG-YFP Fluorescence in the Golgi
120
100
80
60
40
20
0
0
10
20
30
40
50
Time after Release (min)

Figure 2-17: PAFAH Ib α1 and α2 are important for the transport transmembrane cargo ts045 VSV-G-YFP. (**A**) Confocal stacks of ts045VSV-G-YFP after release from a 20°C TGN block in control, α1 & α2 siRNA transfected, and either α1&2 siRNA + RNAi resistant α1 or catalytic mutant α1 S47A transfected BTRD cells. Insets show anti-HA, indicating α1 or α1 S47A transfected cells. (**B**) Fluorescence intensity of post-TGN VSV-G-YFP fluorescence after release from 20°C. Lines correspond to first order kinetic equations, control $k = 0.027 \pm 0.005$ and siRNA $k = 0.013 \pm 0.003$, ± SEM, $p < 0.05$ (T-test). (**C**) Fluorescence intensity of post-TGN VSV-G-YFP fluorescence after release from 20°C for control, α1 & α2 siRNA, and siRNA cells transfected with RNAi resistant α1 or α1 S47A (catalytic mutant). A-C, n = 3-4, error bars = SEM. Scale bars = 10 μm.

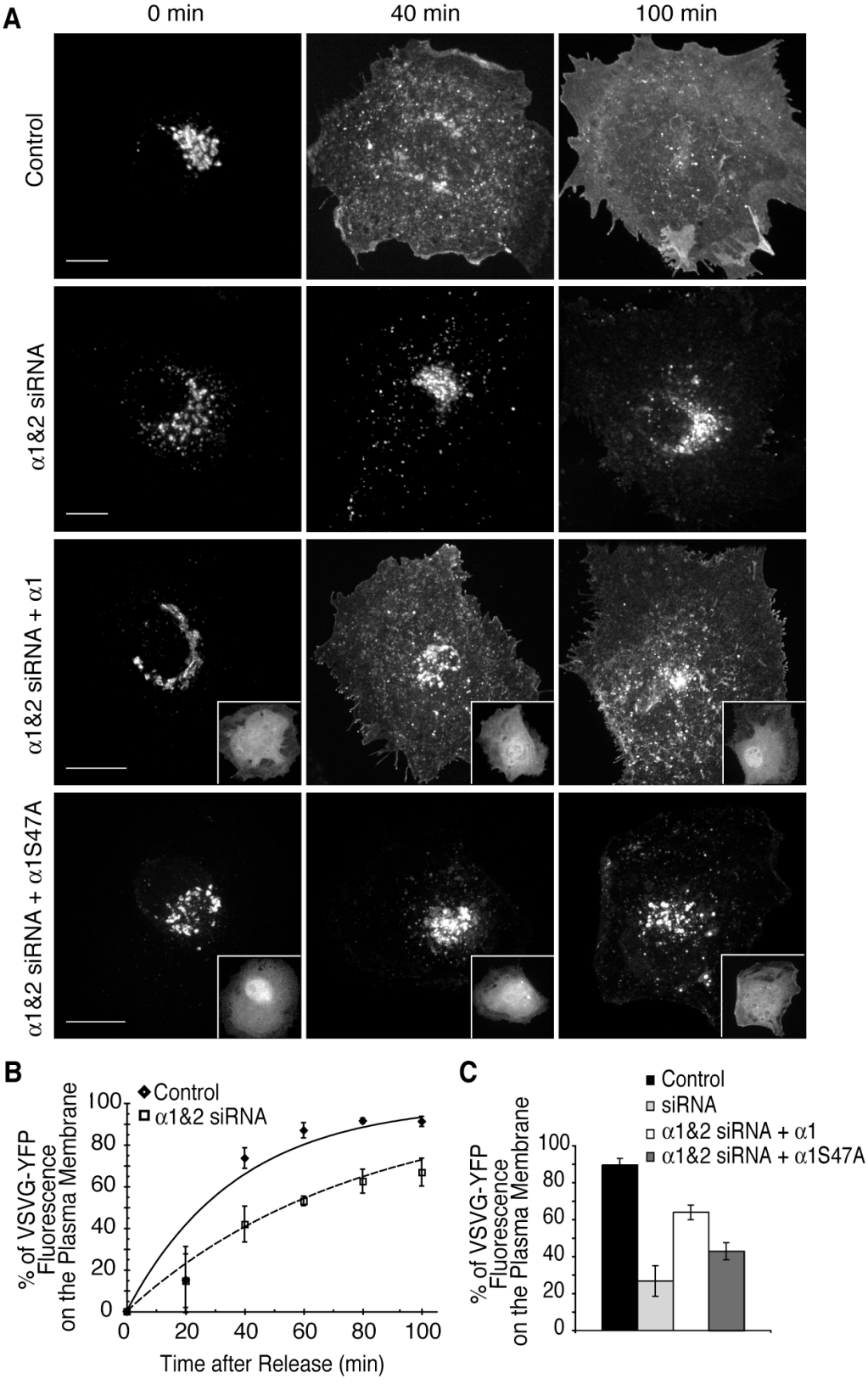
A
0 min
40 min
100 min
Control
α1&2 siRNA
α1&2 siRNA + α1
α1&2 siRNA + α1S47A
B
Control
α1&2 siRNA
% of VSVG-YFP Fluorescence on the Plasma Membrane
Time after Release (min)
C
Control
siRNA
α1&2 siRNA + α1
α1&2 siRNA + α1S47A
% of VSVG-YFP Fluorescence on the Plasma Membrane

Figure 2-18: VSV-G-YFP is transported from the Golgi to the plasma membrane in LIS1 siRNA treated BTRD cells with rates similar to control cells, as seen by wide field fluorescence. Scale bars = 10 μm.

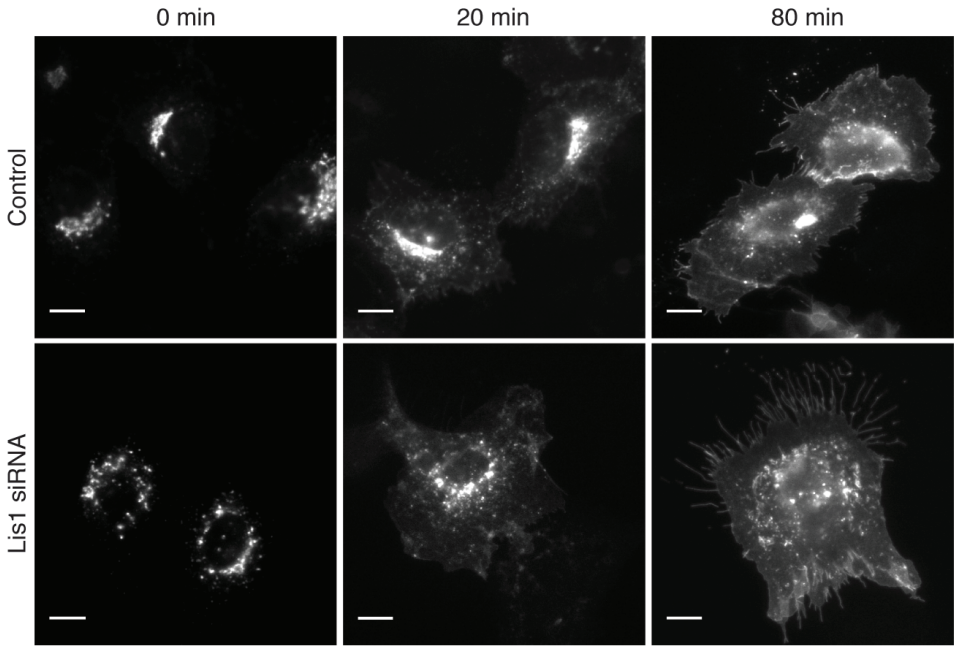
0 min
20 min
80 min
Control
Lis1 siRNA

A, C). Likewise, secretion of soluble cargo, ssHRP, was significantly inhibited in α1 and α2 knockdown cells (Figure 2-19). Thus, loss of α1 and α2 may directly decrease TGN to plasma membrane tubulo-vesicular carriers (96, 97).

Loss of α1 and α2 could also influence Golgi trafficking by affecting any number of components that require specific lipids for binding. Export from the TGN requires protein kinase D (PKD), which binds to membranes via diacylglycerol (222). A kinase dead (KD) version of PKD, which inhibits TGN tubule fission (97), is a convenient marker for PKD association with the TGN. In α1 and α2 knockdown cells, PKD-KD-GFP underwent redistribution from the TGN to the cytoplasm and plasma membrane (Figure 2-20 A). The structure and function of the Golgi and TGN is also dependent on COPI vesicles, AP-1 clathrin coated vesicles, and microtubules; however, we found that knockdown had no discernable effect on β-COP, AP-1, or tubulin (Figure 2-20 B, C). Similarly, the COPII vesicle component Sec31 was unaffected (Figure 2-20 B). These results suggest that α1 and α2 contribute to phospholipid remodeling that is important for PKD association with the TGN.

It is becoming clear that Golgi structure and membrane trafficking require constant and complex phospholipid remodeling. In addition to PAFAH Ib, cPLA$_2$α has recently been shown to influence the Golgi by regulating tubule-mediated, *cis* to *trans*, inter-cisternal trafficking. Interestingly, loss of cPLA$_2$α can be compensated by PAFAH Ib α1 (256). cPLA$_2$α was also shown to regulate export from the TGN (258). Other recent studies found that another phospholipase, iPLA$_1$γ, contributes to tubule-mediated retrograde trafficking from the Golgi (260). Although the molecular mechanisms are unclear, continual phospholipid remodeling by PLA$_1$, PLA$_2$, and lysophosphatidyl acyltransferase enzymes, such as LPAAT3/AGPAT3

Figure 2-19: PAFAH Ib α1 and α2 are important for the transport soluble cargo. Secretion of ssHRP-Flag in control and α1 & α2 siRNA treated BTRD cells. Media HRP activity was measured and normalized to total HRP expression, expressed as a fraction of secreted HRP at 8 h in control cells. The rates of secretion were: control = 0.121 ± 0.003, α1 & α2 siRNA = 0.068 ± 0.008, ± SEM. n = 8, error bars = SEM.

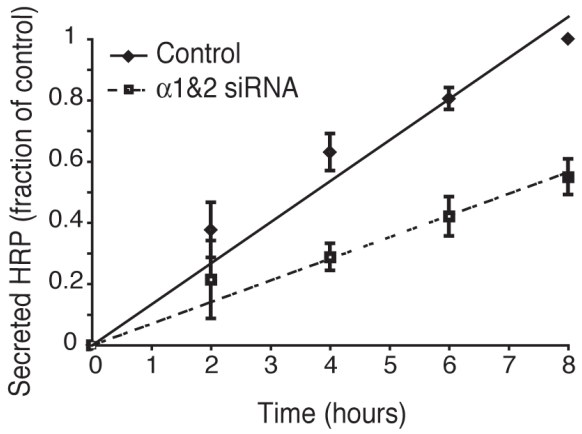
Secreted HRP (fraction of control)
1
0.8
0.6
0.4
0.2
0
Control
α1&2 siRNA
0
1
2
3
4
5
6
7
8
Time (hours)

Figure 2-20: α1 and α2 knockdown does not affect vesicle coat protein or microtubule distribution but alters protein kinase D localization. (**A**) The localization of vesicle proteins COPII (Sec31), COPI (β-COP), and AP1 clathrin (γ-adaptin) is unchanged by α1 & α2 knockdown, as seen by confocal microscopy. (**B**) PKD kinase dead-GFP (PKD-KD-GFP) distribution is affected by α1 & α2 siRNA knockdown. (**C**) Microtubules (α tubulin) are unaffected with α1 & α2 knockdown. Scale bars: A (except Sec31) = 5 μm;
B, C, and Sec31 in A = 10 μm.

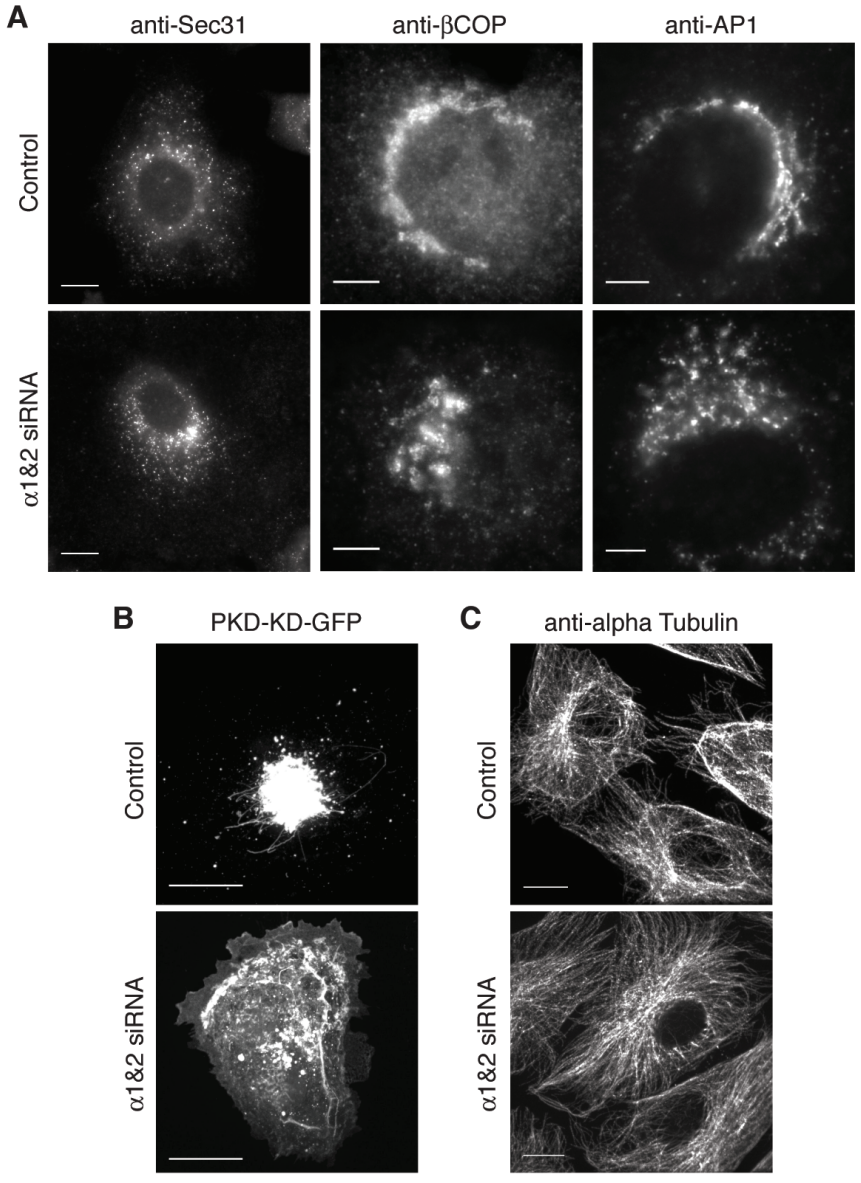
A
anti-Sec31
anti-βCOP
anti-AP1
Control
α1&2 siRNA
B
PKD-KD-GFP
Control
α1&2 siRNA
C
anti-alpha Tubulin
Control
α1&2 siRNA

(239), may be critical for regulating the availability of curvature-altering lipids such as lysophospholipids, phosphatidic acid, diacylglycerol, and/or for the recruitment of other membrane trafficking proteins, such as PKD (240).

Our results demonstrate a novel role for PAFAH Ib $PLA_2\alpha$ subunits, which appear to be multi-functional, regulating PAF signaling, LIS1 function in dynein-mediated processes, and, as shown here, the formation of membrane tubules and the function of the Golgi complex. Our studies reveal a novel relationship of PAFAH Ib PLA_2 activity with dynein-dependent processes that are coupled by LIS1 to regulate Golgi structure. Additionally, our results show that α1 and α2 have a LIS1-independent role in export from the TGN.

CHAPTER 3

PAFAH Ib Catalytic Subunits Have Distinct Roles in Maintaining Golgi Structure and Function

Abstract

Recent studies have shown that the phospholipase subunits of Platelet Activating Factor Acetylhydrolase (PAFAH) Ib, α1 and α2, partially localize to the Golgi complex and regulate its structure and function. PAFAH Ib consists of homo- and heterodimers of α1 and α2, together with a third subunit, the dynein regulator LIS1. Using siRNA knockdown of individual subunits, we find that α1 and α2 perform overlapping and unique roles in regulating Golgi morphology, assembly, and secretory cargo trafficking. Knockdown of either α1 or α2 reduced secretion of soluble HRP, but neither single knockdown reduced secretion to the same degree as knockdown of both. Knockdown of α1 or α2 also inhibited reassembly of an intact Golgi complex following recovery from brefeldin A to the same extent as knockdown of both α1 and α2. Interestingly, transport of VSV-G was slowed with subunit knockdown but at different steps in the secretory pathway: reduction of α1 slowed TGN to plasma membrane transport, whereas α2 loss reduced ER to Golgi trafficking. Similarly, knockdown of either subunit alone disrupted the Golgi complex but with markedly different morphologies. Finally, knockdown of α1, or double knockdown of α1 and α2, resulted in a significant redistribution of kinase dead protein kinase D from the Golgi to the plasma membrane, whereas loss of α2 alone had no such effect. These studies reveal an unexpected complexity in the regulation of Golgi structure and function by PAFAH Ib.

Introduction

A series of pharmacological studies originally suggested that cytoplasmic phospholipase A (PLA) activities regulate the structure and function of the Golgi complex (78, 242, 244, 249). More recent studies have revealed an unexpectedly large number of cytoplasmic PLA enzymes involved in these processes, with a common theme of partial localization to the Golgi complex and functional regulation of the Golgi complex by controlling the shape and formation of cisternal membranes as well as transport carriers exiting the Golgi (256, 258-260). The calcium-dependent enzyme $cPLA_2\alpha$ was shown to translocate to the Golgi during times of increased secretory load. It is also involved in forming membrane tubules that bridge between Golgi cisternae for intra-cisternal trafficking of secretory cargo and is implicated in export from the *trans* Golgi network (TGN) (256, 258). An unrelated cytoplasmic phospholipase, $iPLA_1\gamma$ is located on *cis* Golgi and ERGIC membranes and is required for tubule-mediated, COPI- and Rab6-independent retrograde trafficking from the Golgi to the ER (260). Recent studies have determined that a third, unrelated phospholipase, platelet activating factor acetylhydrolase Ib (PAFAH Ib), also regulates the functional organization of the Golgi complex (259). PAFAH Ib regulates membrane tubule formation that leads to the coalescence of the Golgi complex into an intact ribbon structure and regulates export from the TGN. Thus, at least three different PLA enzymes function at different domains of the Golgi to regulate its structure and function.

In addition to its role in Golgi structure and function, PAFAH Ib appears to be a multifunctional enzyme with varied biological roles in cells. It consists of homo- or heterodimers of two PLA_2 subunits $\alpha1$ and $\alpha2$, and a third

subunit, LIS1/β (321, 331, 365). PAFAH Ib was first discovered by its ability to hydrolyze the extracellular signaling lipid, PAF, which plays a role in platelet activation and inflammation (322). LIS1/β, the causative agent of the fatal brain disorder Miller-Dieker lissencephaly, functions independently of the α subunits to regulate the activity of cytoplasmic dynein (339, 366, 367). Although the functional relationship between PAFAH Ib and LIS1/dynein is unclear, several studies strongly suggest that altering the cytoplasmic levels of α1 and α2 controls the amount of LIS1 that is available for functional interactions with dynein (259, 337, 338).

Another area of uncertainty concerns the functional roles of the α1 and α2 subunits. Human α1 and α2 are 63% identical at the amino acid level and can form catalytically active homo- and hetero-dimers (323). However, numerous studies have established that α1 and α2 have differences in substrate preferences (323), catalytic rates when bound to LIS1/β (323), developmental expression patterns (325), and neurological phenotypes in different mutant backgrounds (370).

Previous studies have suggested a role for PLA_2 activity in regulating the formation of membrane tubules that facilitate cargo export from the Golgi complex and endosomes (242). Using a cell-free in vitro reconstitution system and biochemical fractionation of bovine brain cytosol (369), we discovered that PAFAH Ib was able to induce tubule formation from Golgi membranes, and in vivo studies showed that α1 and α2 are partially localized to Golgi membranes (259). Unable to find a cell line that expresses only one of the a subunits, we performed double knockdown experiments of PAFAH Ib α1 and α2 subunits, which resulted in the fragmentation of the Golgi/TGN ribbon into smaller, disconnected cisternal stacks (mini-stacks) and significantly

decreased export from the TGN. However, these studies left the open question of the relative roles of α1 and α2 in regulating the functional organization of the Golgi complex. Here we report that single knockdown of either α1 or α2 results in significant differences in Golgi morphology and function. We conclude that α1 and α2 have overlapping and distinct functions in regulating the Golgi, which suggest an additional level of complexity for the role of these enzymes at the Golgi complex.

Materials and Methods

Reagents

BFA and cycloheximide were from Biomol Research Laboratories, Inc. Antibodies and GFP-tagged constructs were obtained as follows: guinea pig anti-α1 antibody (by us (259)); chicken anti-α2 (Abcam, Inc.); mouse anti-HA (Covance); rabbit anti-dynamin (MC63) (M. McNiven, Mayo Clinic, Rochester, MN); rabbit anti-ManII (K. Moremen, Univ. of Georgia, Athens, GA); mouse anti-β-COP (BioMakor), mouse anti-α tubulin (Sigma Chemical Co.), rabbit anti-γ-adaptin (Santa Cruz), rabbit anti-Sec31A (W. Balch, Scripps Research Institute, La Jolla, CA) fluorescent secondary antibodies (Jackson Immuno-Research Laboratories and Invitrogen); HRP-conjugated goat anti-chicken (Aves Laboratories), anti-guinea pig (Pocono Rabbit Farm and Laboratory), anti-rabbit (GE Healthcare), and anti-mouse (Gibco). ERGIC53-GFP was from C. Fromme (Cornell University, Ithaca, NY); ts045 VSVG-YFP was from B. Storrie (University of Arkansas for Medical Sciences, Little Rock, AR); ssHRP-Flag (in pEN1) and PKD-KD-GFP (in pEGFP) were from V. Malhotra (Centre de Regulació Genòmica, Barcelona, Spain).

Preparation of Plasmids

An RNAi-resistant version of pEN1-α1-HA was generated as described in Chapter 2.

Cell Culture, Transfection and RNAi

BTRD bovine testicular were cultured in MEM (Mediatech, Inc.) with 10% BGS in a 37°C, 95% humidity, and 5% CO_2 incubator. Double stranded RNA purchased from Thermo Scientific were: AGAAUGGAGAGCUGGAACAUU and GGAGAACUGGAGAAUAUUAUU, for α1 and α2, respectively (8). The control double stranded RNA was siGenome non-targeting siRNA #1 and #2 from Thermo Scientific. 30 nM of RNA was transfected on two consecutive days with Lipofectamine RNAiMax (Invitrogen). DNA transfection was carried out 48 h after the first RNA transfection, using Lipofectamine 2000 (Invitrogen) with ¼ the amount of reagent and DNA indicated by the manufacturer. Experiments were conducted 72 h after the initial RNA transfection.

Cell Lysates and Immunoblotting

Cells were lysed by scraping dishes in the presence of 0.05% TritonX-100 in phosphate buffered saline, pH 7.4 and complete protease inhibitor cocktail (Roche Applied Science). Lysates and purified proteins were run by SDS-PAGE, transferred to PVDF membranes, and Western blotted with the following antibodies: guinea pig anti-α1 (1:2,000); chicken anti-α2 (1:1000); Detection rabbit anti-dynamin (1:10,000) was used as an internal loading control. HRP-conjugated antibodies were: goat anti-guinea pig (1:2,500); goat anti-chicken (1:2,500); and goat anti-rabbit (1:10,000). HRP was detected with

Millipore Corporation enhanced chemilluminescent reagent. Band intensities were quantified using NIH ImageJ software, background intensity was subtracted, and normalized to the corresponding anti-dynamin band for each lane.

Fluorescence Microscopy

For direct fluorescence of GFP or YFP tagged proteins, cells were fixed in 3.7% formaldehyde in PBS for a minimum of 10 min at room temperature, washed in PBS three times for 5 min each, mounted with Vectashield (Vector Laboratories) mounting media, and stored at -20ºC until imaged. For immunofluorescence, cells were fixed in 3.7% formaldehyde in PBS for a minimum of 10 min at room temperature, washed in PBS for 5 min three times and permeabilized with 0.1% Triton X-100 in PBS for 10 min. Cells were then incubated for one hour at room temperature or overnight at 4ºC with primary antibodies diluted in PBS, followed by three washes in PBS and secondary antibody incubation for 1 h at room temperature. Coverslips were mounted with Vectashield (Vector Laboratories) mounting media, stored at -20ºC until imaged. Primary antibodies were diluted as follows: anti-HA, anti-Sec31A anti-ManII, anti-β-COP, anti-α tubulin, and anti-γ-adaptin 1:100. Secondary antibodies conjugated to Alexa 488, DyLight 488, fluorescein isothiocyanate, or tetramethylrhodamine isothiocyanate were used, diluted in PBS 1:500 for Alexa488 and 1:100 for all other secondary antibodies. Wide-field epifluorescence images were taken with a Zeiss Axioscope II, a Zeiss 40x Plan-Apochromat NA1.4 oil objective lens, a Hamamatsu Orca II digital camera, and Openlab software (Improvision). Spinning disk confocal images were taken with a Nikon Eclipse TE2000-U, a Nikon Plan-Apo 60xA/N1.4 or Nikon

Plan-Apo100x/N1.4 oil objectives, with Perkin-Elmer Ultraview LCI, a Hamamatsu 1394 ORCA-ER camera, and Perkin-Elmer Ultraview software.

Electron Microscopy

Cells were fixed in a culture dish using 1.5% glutaraldehyde fixative, containing 5% sucrose and 0.1 M Na cacodylate for 1 h, followed by three 15 min 4ºC 0.1 M Na cacodylate washes, and post-fixing in osmium tetroxide (1% OsO4, 1% KFeCN, 0.1 M Na cacodylate) for 1h at 4ºC. Cells were washed in 4ºC 0.1 M sodium cacodylate three times for 15 min followed by staining with 0.25% uranyl acetate for 30 min, and an additional three sodium cacodylate washes. Cells were dehydrated using sequential 70%, 95%, and 100% ethanol washes and removed from the dish by scoring and propylene oxide. Cells were pelleted in a centrifuge, infiltrated for 30 min with equal part mixture of Spurs and propylene oxide, which was replaced with 100% Spurs overnight. The Spurs was replaced twice more and polymerized at 60°C for 24 h. For electron microscopy images, a FEI Morgagni 268 transmission EM was used.

VSV-G-YFP and ssHRP-Flag

The pixel intensities of ts045 VSV-G-YFP for entire cells and the juxtanuclear Golgi region were measured from confocal images using ImageJ (NIH), with background fluorescence subtraction (per area). For ssHRP-Flag measurements, HRP activity was quantified by absorbance using 3, 3', 5, 5'-tetramethylbenzidine reagent from Sigma (TMB). Collected media and cell lysates were used for measurements, which were normalized to total HRP expression (total activity in the media + lysate). All reactions with TMB were done in duplicate or triplicate and the absorbencies were measured at 450 nm

with a SpectraMax 190 (Molecular Devices) 96-well plate reader.

Image Analysis and Statistics

For experiments, ≥ 100 cells were counted for each condition, and each experiment was repeated independently ≥ three times. The statistical significance between control and knockdown cells was determined with a two-tailed, unequal variance T-test. Images and z-projections were cropped, brightness adjusted, or contrast adjusted using ImageJ or Photoshop CS3.

Results

Knockdown of α1 or α2 Subunits Fragments the Golgi Complex with Dramatically Different Morphologies

To examine the contribution of individual PAFAH Ib catalytic subunits to regulation of Golgi structure, we performed single knockdown studies of α1 or α2. Cultured BTRD cells express PAFAH Ib α1 and α2 subunits at approximately equal levels, composing 0.025-0.05% of the total soluble protein weight (Figure 3-1). Knockdown of either α1 or α2 alone resulted in a significant loss of the appropriate subunit but not the other (Figure 3-2). Similar to double knockdown, loss of either α1 or α2 resulted in fragmentation of the Golgi ribbon but with qualitatively different morphologies. As visualized by immunofluorescence with the medial marker α-mannosidase II (ManII), the Golgi in α1 knockdown cells were often dilated, ranging from distinct rounded fragments to web-like or highly fenestrated membranes, although still clustered in the juxtanuclear region (Figure 3-3; 3-4). Thin section transmission electron microscopy (TEM) revealed that the fragments seen by fluorescence microscopy were relatively a normal stacked (mini-stack)

Figure 3-1: Relative endogenous expression of α1 and α2 in BTRD cells. Western blots of α1 and α2 from BTRD cell lysate (soluble proteins) compared to either α1 or α2 purified protein dilutions. The approximate total protein loaded in each lane is indicated.

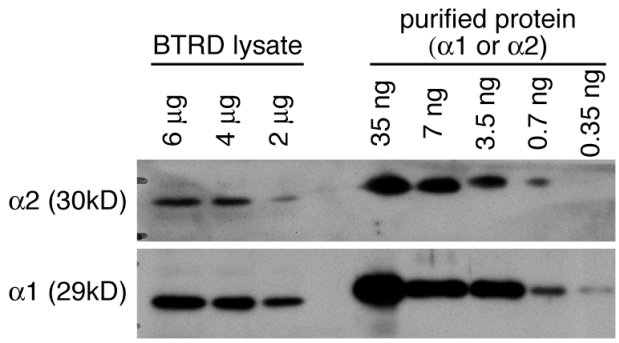
BTRD lysate
purified protein
(α1 or α2)
6 µg
4 µg
2 µg
35 ng
7 ng
3.5 ng
0.7 ng
0.35 ng
α2 (30kD)
α1 (29kD)

Figure 3-2: siRNA-treated BTRD cells with siRNAs targeting either α1 or α2 siRNA show appropriate subunit reduction. Western blots showing amounts of α1 and α2 in control, single, or double siRNA-treated BTRD cells 72 h after initial siRNA transfection. Dynamin served as a loading control.

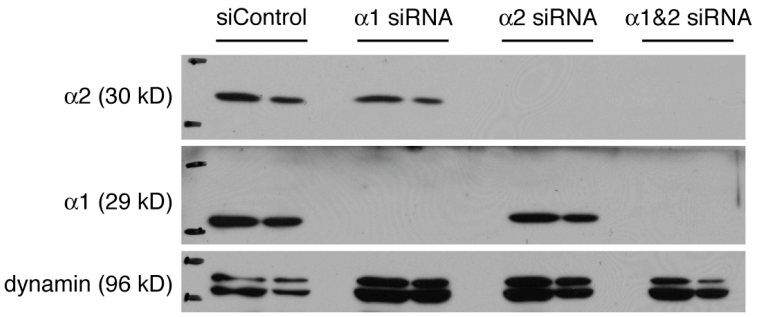
siControl
α1 siRNA
α2 siRNA
α1&2 siRNA
α2 (30 kD)
α1 (29 kD)
dynamin (96 kD)

Figure 3-3: Single knockdown of either PAFAH Ib α1 or α2 causes differential fragmentation of the Golgi complex. (**A**) Confocal z-series of the Golgi (anti-ManII immunofluorescence) and direct fluorescence of ERGIC53-GFP (**B**) in control, single, and double knockdowns. Two images of α1 siRNA-treated cells are shown for anti-ManII to demonstrate the range in phenotype. Scale bars = 5 μm. (**C**) Transmission electron microscopy of thin sections from control and single knockdown BTRD cells. Scale bars = 500 nm.

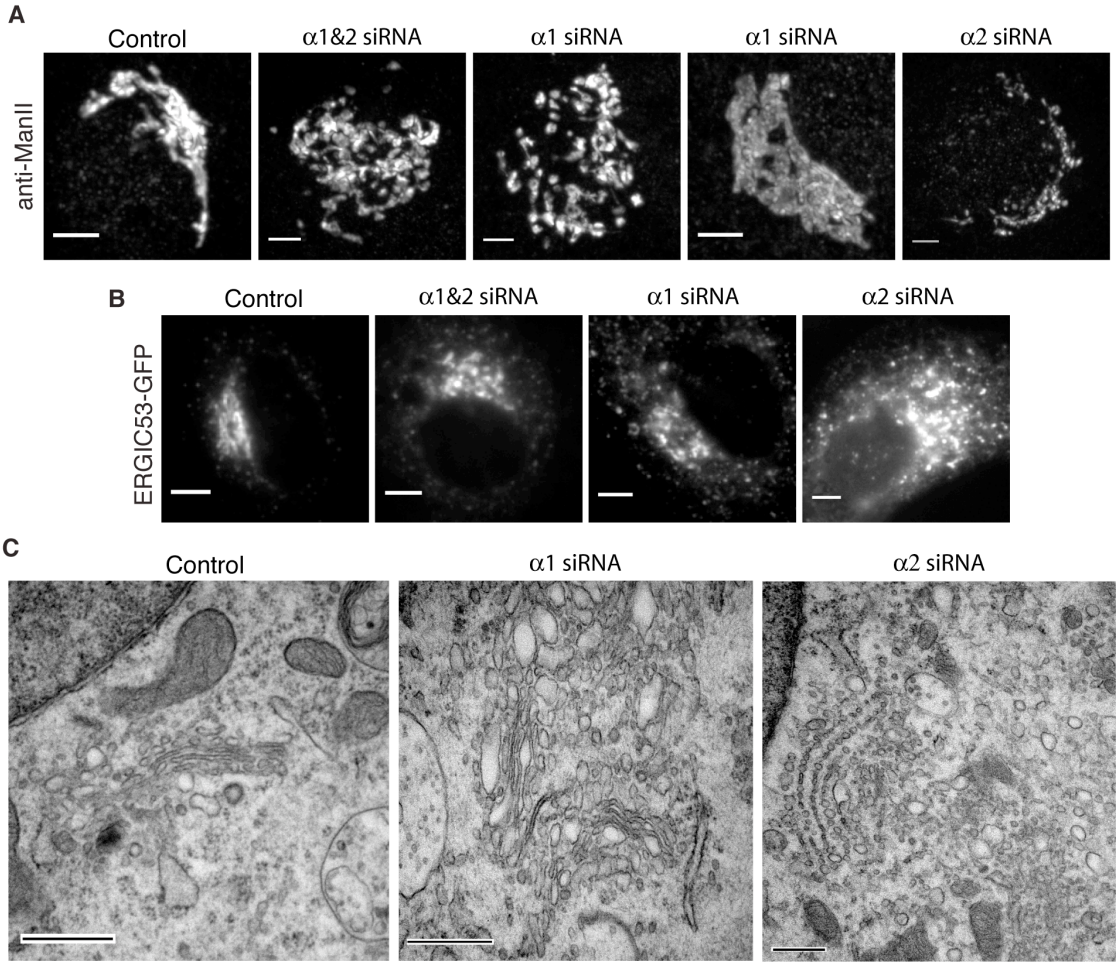
A
Control
α1&2 siRNA
α1 siRNA
α1 siRNA
α2 siRNA
anti-ManII
B
Control
α1&2 siRNA
α1 siRNA
α2 siRNA
ERGIC53-GFP
C
Control
α1 siRNA
α2 siRNA

Figure 3-4: Organelle morphologies in single knockdown. Additional wide-field and EM micrographs illustrating the range in Golgi and ER morphologies following single knockdown of either PAFAH Ib α1 or α2. Scale bars = 2 μm and 500 nm (EM).

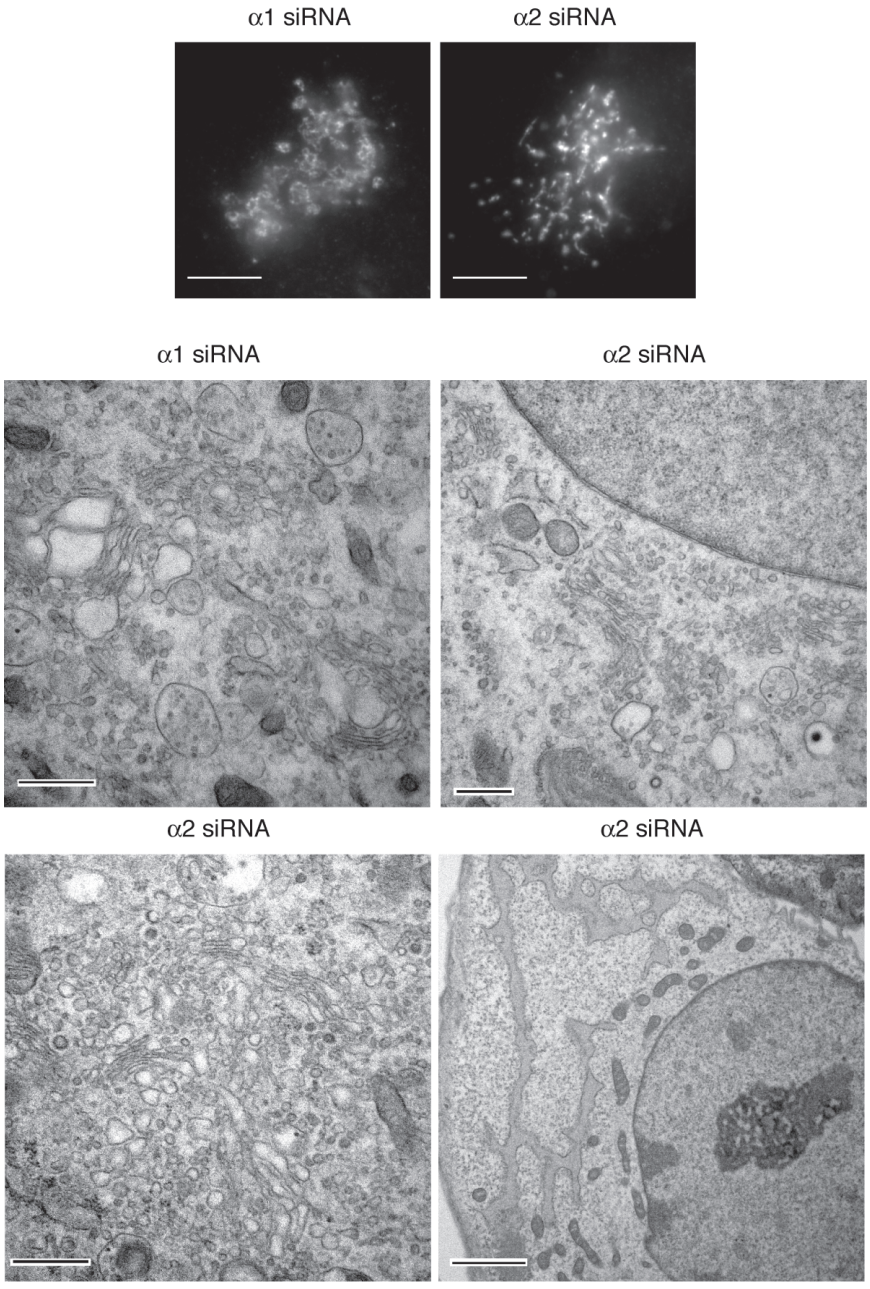
α1 siRNA
α2 siRNA
α1 siRNA
α2 siRNA
α2 siRNA
α2 siRNA

structure but with obviously dilated cisternae (Figure 3-3; 3-4). In contrast, Golgi fragments in α2 knockdown cells appeared as short linear and punctate or vesiculated elements by immunofluorescence (Figure 3-3; 3-4). By TEM, these fragments were also part of mini-stacks but with cisternae that appear to be significantly vesiculated (Figure 3-3). Strikingly, α2 knockdown cells also exhibited fairly dilated ER morphology as seen by EM (Figure 3-4).

Knockdown of α1 or α2 appeared to have a less dramatic effect of ER-Golgi-Intermediate Compartment (ERGIC) fragmentation as seen by localization of ERGIC53-GFP in comparison to α1 and α2 knockdown but still appeared more fragmented than control cells (Figure 3-3 B). Additionally, α2 knockdown cells appeared to have a higher proportion of ERGIC53-GFP fluorescence in ER-like structures compared to control and other knockdown cells (Figure 3-3 B).

Reduced α1 or α2 Levels Slow Secretory Trafficking But at Different Steps of the Pathway

Loss of both α1 and α2 inhibits transport through the secretory pathway, at least at the level of export from the TGN (259). To determine the relative contribution of each subunit, knockdowns of individual subunits were performed, revealing an unexpected difference between the two with regard to secretory trafficking. When measuring bulk soluble protein transport through the secretory pathway, by assaying soluble secreted HRP (ssHRP) in transfected cells, knockdown of either α1 or α2 resulted in a loss of secretion that was approximately 50% that of double knockdown (Figure 3-5 A). To more accurately assess the location of secretory protein trafficking inhibition by α1 or α2 knockdown, we employed the ts045 VSV-G-YFP protein.

Figure 3-5: Secretory protein trafficking is inhibited at different steps in single PAFAH Ib α1 or α2 knockdown cells. (**A**) Kinetics of ssHRP secretion, measured by HRP activity in the media of control or siRNA-treated (as indicated) BTRD cells. Values were normalized to expression levels of HRP and HRP activity in control cells at 8 h. (**B**) Confocal images of ts045 VSV-G-YFP transport in single knockdown cells. Transfected cells were incubated at 40°C to accumulate ts045 VSV-G-YFP in the ER, shifted to 20°C for 20 or 120 min to allow export from the ER and transport to the TGN, and then shifted to 32°C for 80 min to allow export from the TGN and transport to the cell surface. (**C**) Quantification of the percent of total ts045 VSV-G-YFP fluorescence on the PM following shift to 32°C for 80 min. For α2 knockdown cells, only cells with VSV-G outside the ER (~80% of cells) were measured.

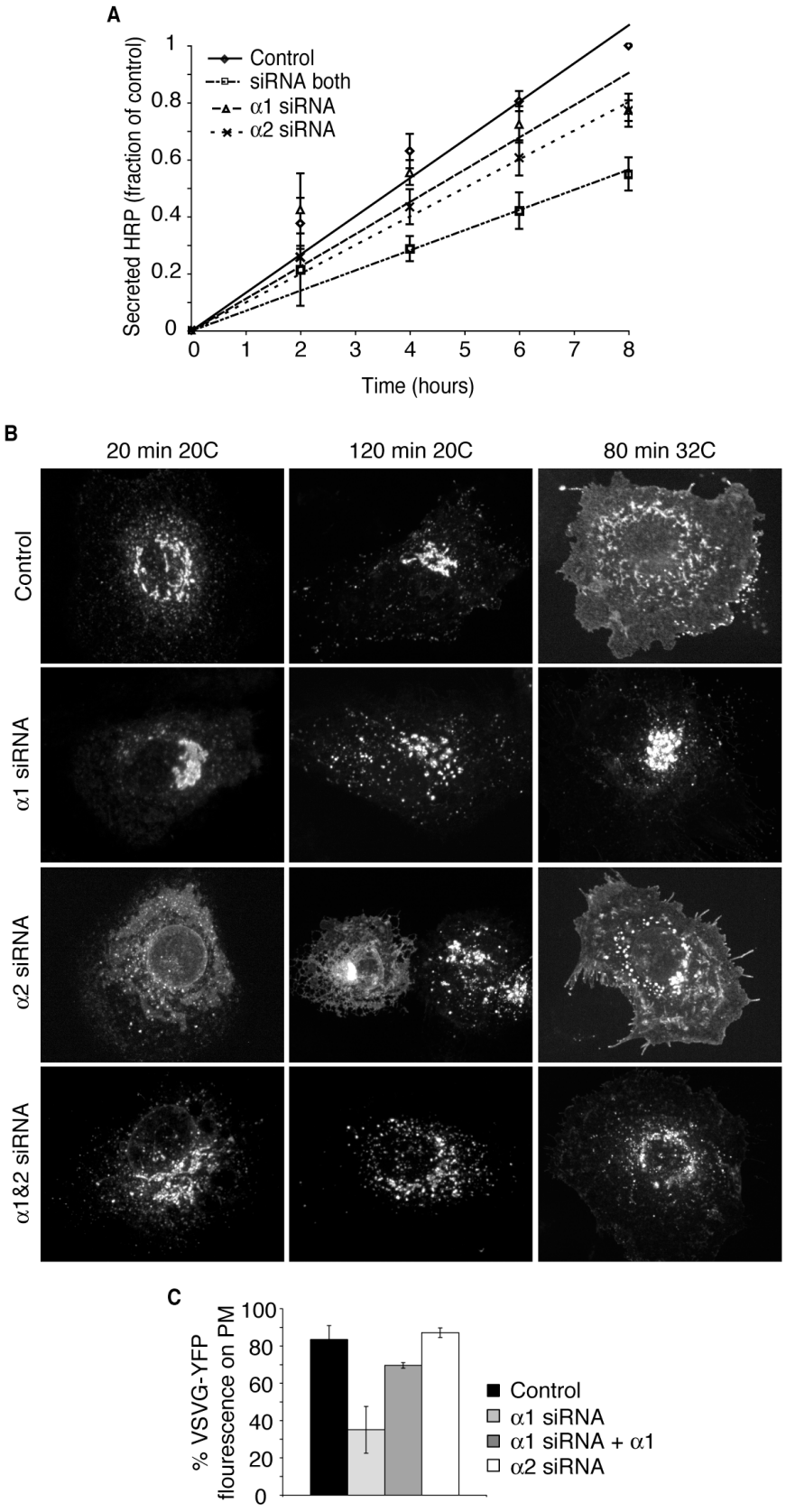
A
Secreted HRP (fraction of control)
Time (hours)
Control
siRNA both
α1 siRNA
α2 siRNA
B
20 min 20C
120 min 20C
80 min 32C
Control
α1 siRNA
α2 siRNA
α1&2 siRNA
C
% VSVG-YFP flourescence on PM
Control
α1 siRNA
α1 siRNA + α1
α2 siRNA

ts045 VSV-G-YFP was allowed to accumulate in the ER at the restrictive temperature (40°C), shifted to 20°C to allow export from the ER and accumulation in the TGN, and then shifted again to the permissive temperature (32°C) to allow export from the TGN and delivery to the cell surface. In control cells, ts045 VSV-G clearly accumulated in the intact, ribbon-like TGN by 120 min following shift to 20°C, and was then delivered to the plasma membrane following shift to 32°C for 80 min (Figure 3-5 B). In α1 knockdown cells, ts045 VSV-G similarly accumulated in the fragmented TGN and was significantly slowed in export and delivery to the plasma membrane following shift to 32°C (Figure 3-5 B, C). This inhibition was rescued by expression of siRNA-resistant α1 construct after knockdown (Figure 3-5 C). In contrast to α1, knockdown of α2 resulted in a significant inhibition of ts045 VSV-G reaching the TGN following shift to 20°C, and a prolonged presence in the ER (Figure 3-5 B). After 120 min at 20°C ~40% of α2 siRNA-treated cells had a substantial amount of VSV-G in the ER. However, once in the TGN, transport to the plasma membrane was not noticeably slowed (compare control versus α2 siRNA at the 80 min time point) (Figure 3-5 B, C). Even at 80 min following shift to 32°C, ~15-20% of cells still had VSV-G in the ER. Thus, it would appear that α1 and α2 affect different trafficking steps to regulate transport dynamics.

Knockdown of α1 or α2 Does Not Affect Coat Protein Localization But Has Differential Effects on the Localization of Protein Kinase D

We previously found that knockdown of both α1 and α2 did not significantly impact the localization of various trafficking proteins such as the COPI subunit β-COP, clathrin AP-1 adaptor, or the COPII subunit Sec31 (259).

Likewise, single knockdown did not influence these markers (Figure 3-6 A). Protein kinase D (PKD) is a regulator of TGN secretory vesicle fission (97). A kinase dead version of PKD (PKD-KD) localizes to the TGN and induces a dominant negative effect on vesicle fission thereby causing the formation of extensive membrane tubules (371). We found that double knockdown appeared to inhibit PKD-KD-induced TGN tubule formation, and resulted in a significant relocation of PKD-KD from the TGN to the plasma membrane (259) (Figure 3-6 B). Interestingly, cells subjected to single knockdown of α1, but not α2, exhibited a similar phenotype (Figure 3-6 B). Thus, α1 subunits alone play a role in maintaining PKD-KD at the TGN.

Both α1 and α2 Are Required for Assembly of an Intact Golgi Ribbon

In addition to secretory trafficking, PLA_2 activity controls the biogenesis and maintenance of an intact Golgi ribbon. Biogenesis of the Golgi complex has often been studied using recovery from brefeldin A (BFA) treatment as a model system (78), and we have previously shown that knockdown of both α1 and α2 inhibits the coalescence of mini-stacks into an intact ribbon (259). Similarly, following knockdown of either α1 or α2 and recovery from BFA treatment, the Golgi complex reassembled into separate mini-stacks, but their coalescence into intact ribbons was inhibited (Figure 3-7 A, B). In each case, the Golgi reassembled into mini-stacks during recovery from BFA, but the Golgi did not form intact ribbon morphology (Figure 3-7), demonstrating that reassembly of the Golgi requires both subunits.

Discussion

In previous studies, we found that double knockdown of the two

Figure 3-6: Localization of vesicle markers and protein kinase D in single knockdown cells. (**A**) Knockdown of PAFAH Ib α1 or α2 does not detectably affect clathrin AP-1 adaptor, COPI subunit β-COP, or the COPII subunit Sec31a in BTRD cells. Scale bars = 5 μm. (**B**) Knockdown of α1, but not α2, causes a loss of PKD-KD-GFP from the TGN and redistribution to the plasma membrane. Scale bars = 10 μm.

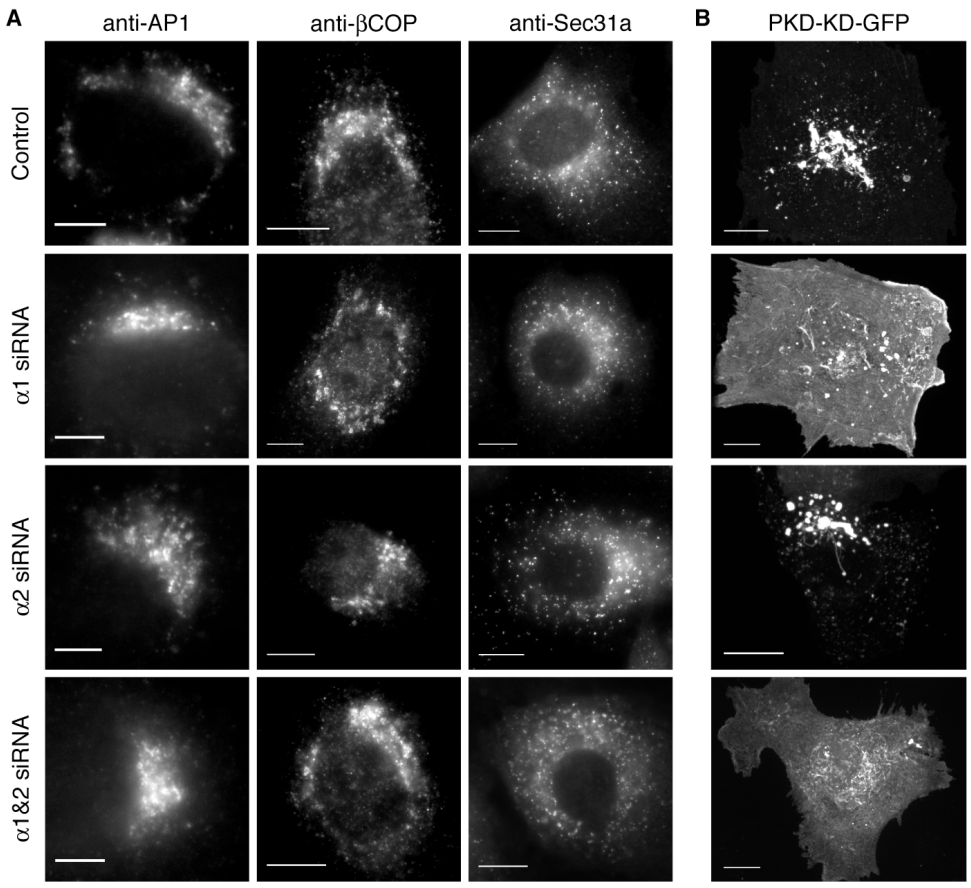
A
anti-AP1
anti-βCOP
anti-Sec31a
B
PKD-KD-GFP
Control
α1 siRNA
α2 siRNA
α1&2 siRNA

Figure 3-7: Golgi reassembly following BFA washout is inhibited in PAFAH Ib α1 or α2 single knockdown cells. (**A**) Confocal images of control and cells treated with siRNA against individual or both subunits. BTRD cells were treated with media containing 5 μg/mL BFA for 20 min, followed by replacement with BFA-free media to allow reassembly of the Golgi. Cells were fixed at the indicated time points (after BFA removal) and processed for immunofluorescence with anti-ManII. Scale bars = 10 μm. (**B**) Quantification of reassembly into an intact Golgi ribbon in control and siRNA-treated cells. (**C**) Confocal micrographs illustrating the morphology of the Golgi complex (anti-ManII immunofluorescence) during recovery from BFA in control and siRNA treated cells. Scale bars = 2 μm.

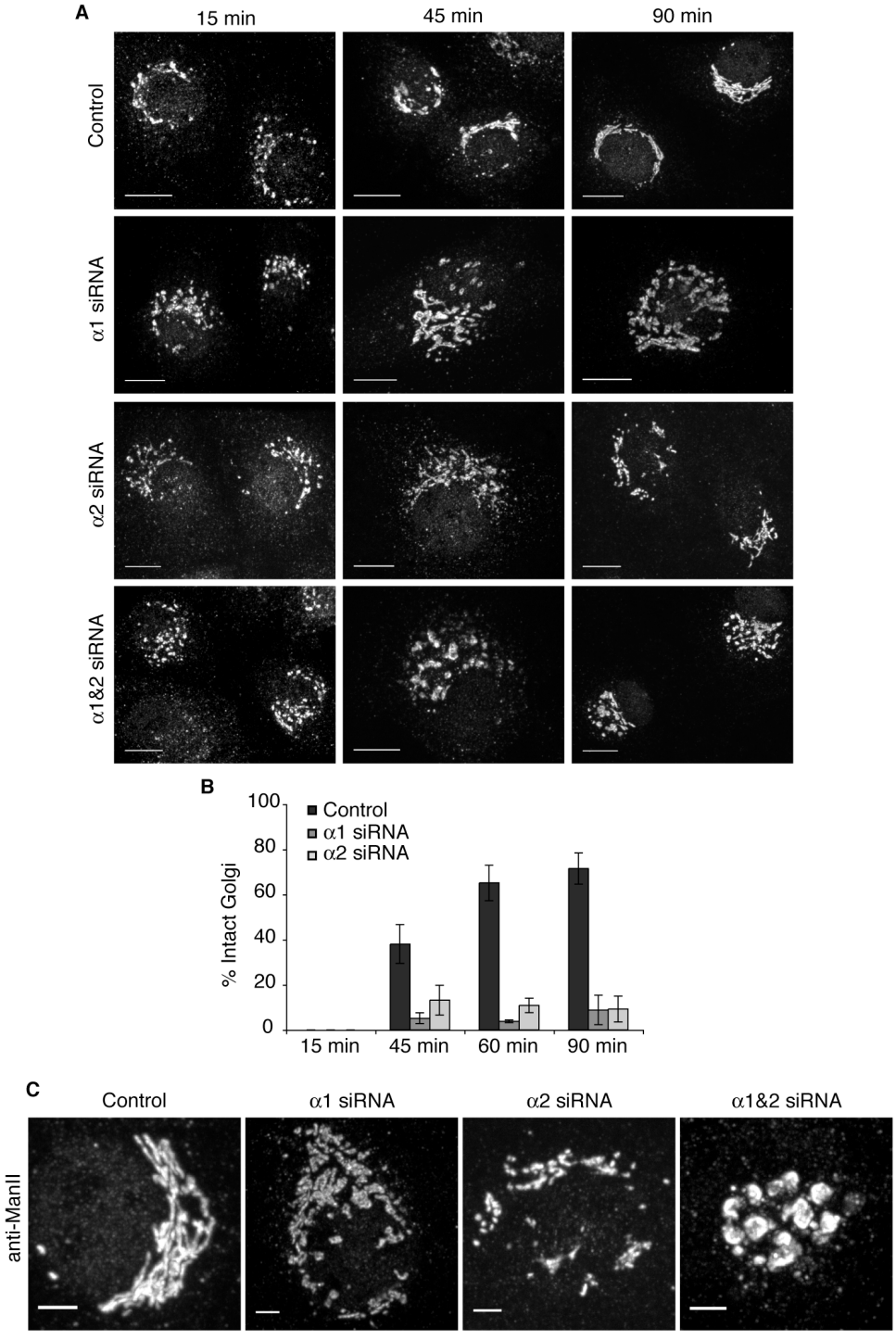
A
15 min
45 min
90 min
Control
α1 siRNA
α2 siRNA
α1&2 siRNA
B
100
80
60
40
20
0
% Intact Golgi
Control
α1 siRNA
α2 siRNA
15 min
45 min
60 min
90 min
C
Control
α1 siRNA
α2 siRNA
α1&2 siRNA
anti-ManII

catalytic subunits of PAFAH Ib, α1 and α2, produced a severely fragmented Golgi and inhibited secretion (259). Here we examine α1 and α2 subunits individually and show that these subunits play overlapping but also distinct roles in regulating Golgi structure and function. This is a surprising result because α1 and α2 can form both functional homo- and heterodimers, all of which form competent complexes with LIS1 (323).

Loss of either α subunit produces distinctly different Golgi morphologies: the Golgi complexes in α1 knockdown cells are swollen and highly fenestrated, whereas α2 knockdown cells exhibit a severe vesiculated phenotype. Interestingly, the Golgi morphologies in single knockdown cells are not exactly the same as those in double knockdown cells, in which the fragmented Golgi complexes do not show the same degree of cisternal dilation or vesiculation (259). These results strongly suggest that Golgi morphology requires a tight balance between the levels of both α1 and α2 subunits. The reason for the differences in single knockdown cells is not clear. One possibility could be based on the fact that α2 appears to have a higher affinity for LIS1 (based on the relative abilities of α1 and α2 to compete with Ndel for binding to LIS1) (338). These differences are likely relevant in vivo for regulation of LIS1 and dynein function; however, cells with reduced α2 have smaller, vesiculated Golgi and more dilated ER, which is not consistent with α2 knockdown simply effecting dynein activation. Dynein activity is important for anterograde ER to Golgi trafficking (179), which hypothetically should increase in the absence of α2 competition for binding LIS1. On the contrary, α2 knockdown phenotypes suggest decreased ER to Golgi transport. A second possibility to explain differing phenotypes between α1 and α2 knockdown is by their relative substrate preferences. In vitro studies suggest

that heterodimers and α1/α1 homodimers are more selective for phosphatidic acid (1-*O*-alkyl-2-acetyl-3-*sn*-glycero-phosphoric acid) species and exhibit little to no activity on phosphatidylethanolamine, whereas α2/α2 homodimers have much lower phosphatidic acid catalytic activity and had preference for platelet activating factor, a phosphatidylcholine derivative (1-alkyl-2-acetoyl-*sn*-glycero-3-phosphocholine), and phosphatidylethanolamine species (1-*O*-alkyl-2-acetyl-3-*sn*-glycero-phosphorylethanolamine) (323). The generation of distinct lysophospholipid species may help to account for changes in membrane architecture by changing membrane shape and/or feeding into different lipid metabolic pathways (159, 240).

Loss of either α1 or α2 inhibited soluble protein secretion to ~50% that achieved by double knockdown, initially suggesting that each has overlapping functions in secretion. However, the second surprising finding was that α1 or α2 appear to facilitate protein trafficking at different stages of the secretory pathway—loss of α2 resulted in slowed export from the ER and delivery to the TGN, whereas loss of α1 inhibited binding of PKD-KD to the TGN and export from the TGN. These observations are consistent with previous pharmacological studies showing that PLA_2 antagonists have similar effects on ER and TGN export (372). This result is also consistent with the dilated ER and Golgi morphologies for α2 and α1 knockdown, respectively. These results strongly suggest that α2 homodimers function early in the secretory pathway and α1 homodimers later. Moreover, it is possible that these different effects on trafficking could be indirectly related to the differences in Golgi morphology produced by single knockdowns. Our localization studies of expressed subunits are not helpful in this regard because we observed no significant difference in the intracellular distributions of α1 and α2, with both

being cytosolic, nuclear, and Golgi-associated (259).

PAFAH Ib α1 and α2 subunits both have profound effects on secretory trafficking, Golgi structure, and the assembly of the Golgi complex. BFA washout studies show that reduced levels of either subunit delays the reassembly of an intact Golgi ribbon to the same extent as knockdown of both subunits. Interestingly, α2 knockdown, while having an effect on cargo export from the ER does not show an observable difference in the appearance of Golgi mini-stacks from the ER. Instead, either α1 knockdown or α2 knockdown inhibits reassembly at the stage of mini-stack coalescence into Golgi ribbon morphology, a stage that has been observed to require dynein-mediated membrane tubule transport (78, 79).

Importantly, cells did not compensate for single knockdowns by increasing expression of the other subunit. Even though single knockdowns still expressed wild type levels of the other subunit, it was not enough to overcome the loss of one subunit. Thus, the overall functional organization of the Golgi is very sensitive to total α1 and α2 levels.

Work from several laboratories in the past year has revealed an unexpected level of complexity with regard to phospholipase regulation of the Golgi complex. In addition to PAFAH Ib, two other phospholipases have recently been shown to regulate different aspects of Golgi structure and function. These include iPLA$_1$γ, which regulates retrograde trafficking to the ER (260), and cPLA$_2$α, which regulates tubule-mediated, *cis* to *trans*, inter-cisternal trafficking (256) as well as export from the TGN (258). Our studies here strongly suggest that PAFAH Ib α1 and α2 homodimers have some distinct functions, indicating that the Golgi is influenced by four phospholipases. The extent to which these phospholipases function

independently to control Golgi structure and function is unclear. Although, previous studies indicate that loss of cPLA$_2\alpha$ can be compensated by PAFAH Ib α1: VSV-G trafficking in cells from cPLA$_2\alpha^{-/-}$ mice is only decreased with the additional reduction of α1 levels by RNAi (256). It is evident that future studies will be required to dissect the individual and combined roles of these enzymes.

The molecular mechanisms by which PAFAH Ib, iPLA$_1\gamma$, or cPLA$_2\alpha$ regulate the functional organization of the Golgi complex is unclear. The combined evidence strongly suggests that all three can influence the shape of Golgi membranes by controlling membrane tubule formation. Moreover, it would appear that continual phospholipid remodeling by PLA$_1$, PLA$_2$, and lysophospholipid acyltransferase enzymes, such as LPAAT3/AGPAT3 (239), may be critical for regulating the availability of curvature-altering lipids such as lysophospholipids, phosphatidic acid, diacylglycerol, and/or for the recruitment of other membrane trafficking proteins, such as PKD and vesicle-associated coat proteins (240).

CHAPTER 4

PAFAH Ib Regulates Endosome Positioning, Membrane Tubule Formation and Transferrin Recycling

Abstract

Previous studies have shown that membrane tubule-mediated export from endosomal compartments requires a cytoplasmic phospholipase A_2 (PLA_2) activity. Here we report that the catalytic subunits of Platelet Activating Factor Acetylhydrolase (PAFAH) Ib, α1 and α2, which are cytoplasmic Ca^{2+}-independent PLA_2 enzymes, are located on early sorting endosomes and the central endocytic recycling compartment (ERC). Overexpression of catalytically active α1 and α2, but not their catalytically inactive counterparts, induced endosome membrane tubules. In addition, overexpression α1 and α2 altered normal endocytic trafficking; transferrin was recycled back to the plasma membrane directly from peripheral early sorting endosomes, instead of making an intermediate stop in the ERC. Consistent with these results, siRNA-mediated knockdown of α1 and α2 significantly inhibited the formation of endosome membrane tubules and delayed the recycling of transferrin. Additionally, our results agree with previous reports that PAFAH Ib α1 and α2 expression levels affect the distribution of endosomes within the cell through interactions with the dynein regulator LIS1. These studies characterize a novel PLA_2-dependent mechanism for mediating endocytic membrane trafficking and identify a function for PAFAH Ib in this process.

Introduction

Trafficking through the endocytic pathway involves an ordered set of transport steps that move both membrane-bound and soluble cargo between different compartments (24, 115). In mammalian cells, most endocytic compartments, especially early sorting endosomes and the endocytic recycling compartment (ERC), are morphologically complex tubulo-vesicular structures, consisting of a mosaic of phosphoinositides, regulatory proteins, and other effectors (115, 175, 373, 374). Sorting and export out of endocytic compartments has long been recognized to involve membrane tubules that emanate from the main vacuolar domain (193). Based on geometry alone, thin membrane tubules (60-80 nm in diameter) serve as efficient sorting structures to separate membrane lipids and proteins from soluble internal contents (195). Early studies showed that many itinerant receptors become concentrated into tubular domains of endosomes for efficient export (126, 127, 375). These tubular extensions may function as platforms for the budding of coated vesicles or may detach to serve as trafficking intermediates (152).

The molecular mechanisms that mediate the formation of endosome membrane tubules are unclear. Rabs and other molecules have been shown to be involved in the formation of tubular domains on endosomes and to function in export from these organelles. For example, sorting nexins (SNX) (148) and Rab7 (376) facilitate the tubule-mediated sorting of itinerant endocytic cargoes. In addition, pharmacological and biochemical studies have suggested that phospholipid remodeling by cytoplasmic phospholipase A_2 (PLA_2) enzymes plays an important role in the formation of endosome membrane tubules (242). For example, a broad spectrum of PLA_2 antagonists inhibit the formation of endosome membrane tubules in vivo and in a cytosol-

dependent in vitro reconstitution system (245). In addition, these PLA_2 antagonists inhibit the export of transferrin (Tf) and Tf receptors (TfR) from early sorting endosomes and the ERC. These results strongly suggest that a cytoplasmic PLA_2 functions in tubule-mediated export at each of these endosomal compartments.

The identity of cytoplasmic PLA_2 enzymes involved in the formation of endosomal membrane tubules has remained elusive. Here we show that the catalytic subunits of platelet activating factor acetylhydrolase (PAFAH) Ib are endosome-associated PLA_2 enzymes that mediate tubule formation and routing endocytic receptors for recycling. PAFAH Ib was originally purified based on its ability to hydrolyze an acetyl group in the *sn-2* position of the signal transduction phospholipid, platelet activating factor (PAF) (322). It is a multi-subunit complex consisting of a dimer of two highly conserved catalytic subunits, α1 (*Pafah1b3*) and α2 (*Pafah1b*2), and an associated non-catalytic subunit, β (*Pafah1b1*) (302). Within a species, α1 and α2 subunits share ~60% amino acid identity and by themselves can form catalytically active homo- or heterodimers (323). The β subunit, also known as LIS1, is highly conserved from yeast to humans, and mutations in it lead to the fatal brain disorder Miller-Dieker lissencephaly (366). Recent studies have shown that, independent of binding to α1 or α2, LIS1/β regulates the location of dynein on microtubules through the combined activities of a host of accessory proteins including NudE, and NudEL (377). LIS1/β, NudE, and NudEL are responsible for cytoplasmic nuclear trafficking in yeasts, spindle orientation, and neuronal migration in mammals, the latter being compromised in human lissencephaly (339, 367).

Although PAFAH Ib has been implicated in a wide array of processes, its

exact biological function is unclear. Mice with targeted disruption of both *Pafah1b2* and *Pafah1b3* genes ($\alpha1^{-/-}/\alpha2^{-/-}$) exhibit defects in spermatogenesis but are otherwise normal (326, 330). In contrast, recent studies using overexpression and siRNA-mediated knockdown of α1 and α2 in cultured cells showed that PAFAH Ib α1 and α2 function to mediate the functional organization of the Golgi complex and secretion (256, 259). These results show that PAFAH Ib has an unexpected role in intracellular membrane trafficking. Here we show that this role is not limited to secretion. We found that α1 and α2 are partially localized to endosomes and that overexpression of either subunit induces endosome membrane tubule formation and alters the recycling route of endocytosed Tf and TfRs. Conversely, siRNA-mediated knockdown of α1 or α2 in cultured cells inhibited endosome tubule formation and delayed the recycling of Tf. These results demonstrate a novel mechanism for mediating endosome membrane trafficking and a new physiological role for PAFAH Ib enzymes.

Materials and Methods

Reagents

Brefeldin A (BFA) was obtained from Biomol Research Laboratories, Inc. The stock solution of BFA (10 mg/mL in ethanol) was stored at -20°C and diluted to working concentrations of 5 μg/mL in MEM just prior to use. Alexa 488-Tf (Molecular Probes) and bovine holo-transferrin were purchased from Invitrogen. Fluorescein isothiocyanate (FITC) was from Sigma.

Mouse monoclonal anti-human influenza virus hemagglutinin (HA) was purchased from Covance. Rabbit polyclonal anti-early endosomal antigen 1 (EEA1) was purchased from Affinity Bioreagents and Cell Signaling.

Mouse anti-human transferrin receptor was obtained from Boehringer-Mannheim and Zymed (Invitrogen). Rabbit polyclonal and mouse monoclonal antibodies against the late endosome/lysosome marker CD63 and rabbit anti-Cathepsin D were prepared and characterized as described (378-380). The secondary fluorescent antibodies goat anti-mouse or goat anti-rabbit conjugated to FITC, TRITC, Cy5 or DyLight were purchased from Jackson ImmunoResearch Laboratories. The anti-mouse conjugated to Alexa488 was from Molecular Probes (Invitrogen).

Plasmids for Mammalian Expression

PAFAH Ib plasmids were prepared as described in chapter 2. Human cDNA of Rab11 and Rab4 in pEGFP vectors, GFP-Rab11 and GFP-Rab4, were the kind gifts of Dr. M. Scidmore (Cornell University). Human Rab5A cDNA in the pGreenLantern vector, GFP-Rab5, was the gift of Dr. C. Roy (Yale University).

Cell Lysates and Immunoblotting

Lysate preparation and immunoblotting was conducted as described in chapter 3.

Cell Culture, Transfection, and Immunocytochemistry

HeLa and BTRD cells were cultured and transfected as described in chapter 2. Cells were processed for indirect immunofluorescence as described in chapter 3. Primary antibodies used were diluted as follows in PBS: monoclonal mouse anti-HA at 1:100; polyclonal rabbit anti-EEA1 at 1:100 (ABR) or 1:50 (Cell Signaling); monoclonal anti-TfR at 1:200; polyclonal rabbit

or mouse monoclonal anti-CD63 at 1:200; and polyclonal rabbit anti-Cathepsin D at 1:200. Secondary antibodies were used at the following dilutions: FITC-, TRITC-, or Cy5-labeled anti-mouse IgG or anti-rabbit IgG at 1:100; Alexa 488-labeled anti-mouse IgG at 1:500; and DyLight anti-rabbit at 1:100.

Transferrin Preparation and Trafficking Experiments

For use in BTRD cell experiments, bovine holo-transferrin was conjugated to FITC. A 257 μM solution of FITC was made in 50 mM borate buffer, pH 9.2. A 4 mg/mL transferrin solution was made in 5 mL of 50 mM borate buffer and was placed into dialysis tubing. The dialysis tubing containing Tf was kept in the FITC solution at 4ºC for 24 h. The FITC-Tf in dialysis tubing was then placed in 3 L PBS, pH 7.4 at 4ºC. The PBS was exchanged 6 times over three days. The resulting FITC-Tf was stored in aliquots at 4ºC and spun briefly by low speed centrifugation before use.

For Tf experiments, HeLa cells or BTRD cells were grown on coverslips for a minimum of two days, washed 15 min three times in 37ºC MEM or DMEM without serum, and incubated for the indicated pulse time points with 40 μg/mL FITC-Tf in 37ºC MEM or DMEM. Cells were then washed three times in 37ºC MEM + 10% BGS, with subsequent incubation for chase time points. FITC-Tf florescence was measured from 40x Zeiss wide-field images using ImageJ (NIH) to measure cell total fluorescence intensity, central (ERC) fluorescence intensity and background fluorescence. For each image, the background fluorescence intensity (per pixel) was subtracted from the corresponding cell fluorescence measurements.

Microscopy

Wide-field epifluorescence imaging was done using a Zeiss Axioscope II, with a Zeiss 40x or 100x Plan-Apochromat NA1.4 oil objective, a Hamamatsu Orca II digital camera, and Openlab software (Improvision). Spinning disk confocal images were taken with a Nikon Eclipse TE2000-U, Nikon Plan-Apo 60xA/N1.4 or Nikon Plan-Apo100x/N1.4 oil objectives, with Perkin-Elmer Ultraview LCI, a Hamamatsu 1394 ORCA-ER camera, and Perkin-Elmer Ultraview software.

Statistics

Error bars on graphs represent standard error of the mean values for a minimum of one hundred cells and a minimum of three independent experiments. Two-tailed, unequal variance student T-tests were used to determine significance.

Results

PAFAH Ib α1 and α2 are Found on Early Sorting Endosomes and the Endocytic Recycling Compartment

The intracellular location of PAFAH Ib α1 and α2 has not been well documented. One study found GFP-tagged α1 diffuse in the cytoplasm, in the nucleus, and on juxtanuclear structures that resemble the Golgi complex (358). We have confirmed this localization pattern in cells transfected with HA-tagged α1 and α2 (259). In addition, we found that α1-HA and α2-HA were located on peripheral cytoplasmic puncta that colocalized with the early endosome proteins EEA1 and GFP-Rab5 (Figure 4-1 A, B; 4-2 A). At higher magnifications, the mosaic nature of this compartment was revealed as

Figure 4-1: Localization of α1 to early and recycling endosomes. (**A**) HA-tagged α1 (anti-HA) was expressed and partially colocalized with the early sorting endosome protein GFP-Rab5 in BTRD cells. Lower panel shows a higher magnification of the cell. (**B**) Line fluorescence intensity plot of α1 and GFP-Rab5 from the merged confocal slice in A, line shown in merge. (**C**) Cells expressing both α1-HA and GFP-Rab11 show α1 colocalizes to the ERC. Lower panel shows a higher magnification of the cell. (**D**) Line fluorescence intensity plot of α1 and GFP-Rab11, from the line shown in the merged confocal slice of (C). Scale bars = 10 μm.

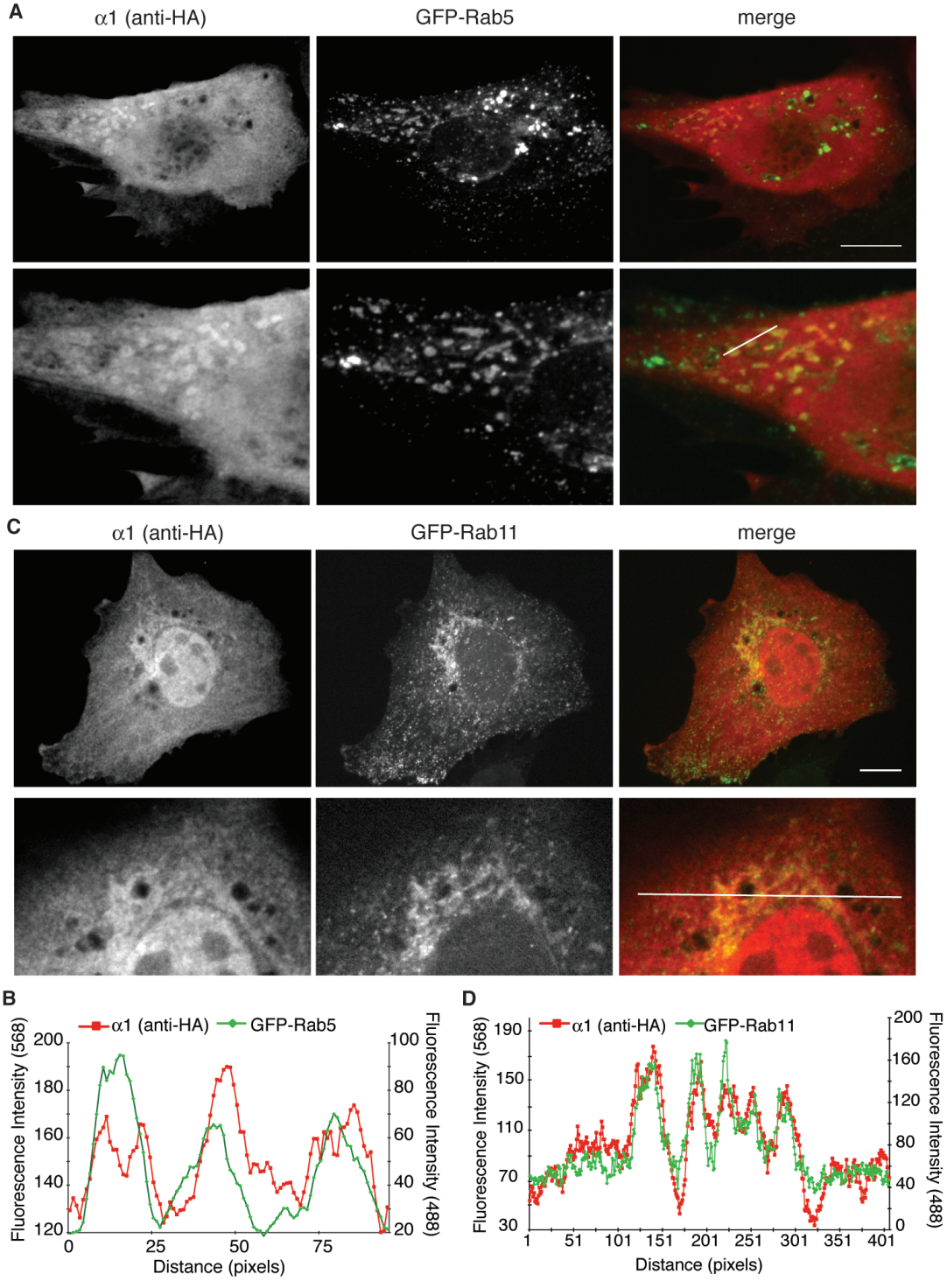
A
α1 (anti-HA)
GFP-Rab5
merge
C
α1 (anti-HA)
GFP-Rab11
merge
B
α1 (anti-HA)
GFP-Rab5
Fluorescence Intensity (568)
Fluorescence Intensity (488)
Distance (pixels)
D
α1 (anti-HA)
GFP-Rab11
Fluorescence Intensity (568)
Fluorescence Intensity (488)
Distance (pixels)

Figure 4-2: Localization of α1 and α2 to early but not late endosomes. Representative images of the localization the subunits are shown with either α1 or α2. (**A**) HA-tagged α1 (anti-HA) was expressed and partially colocalized with the early sorting endosome protein EEA1 (anti-EEA1) in BTRD cells. Box shows region in lower panel with magnified view of early sorting endosomes labeled with both α1-HA and EEA1. Arrow indicates a tubule-projection seen with anti-HA but not anti-EEA1. (**B**) Catalytically inactive and HA-tagged α1 S47A localizes to early sorting endosomes. (**C**) HA-tagged α2 was expressed and did not overlap with labeling for late endosomes, anti-CD63.

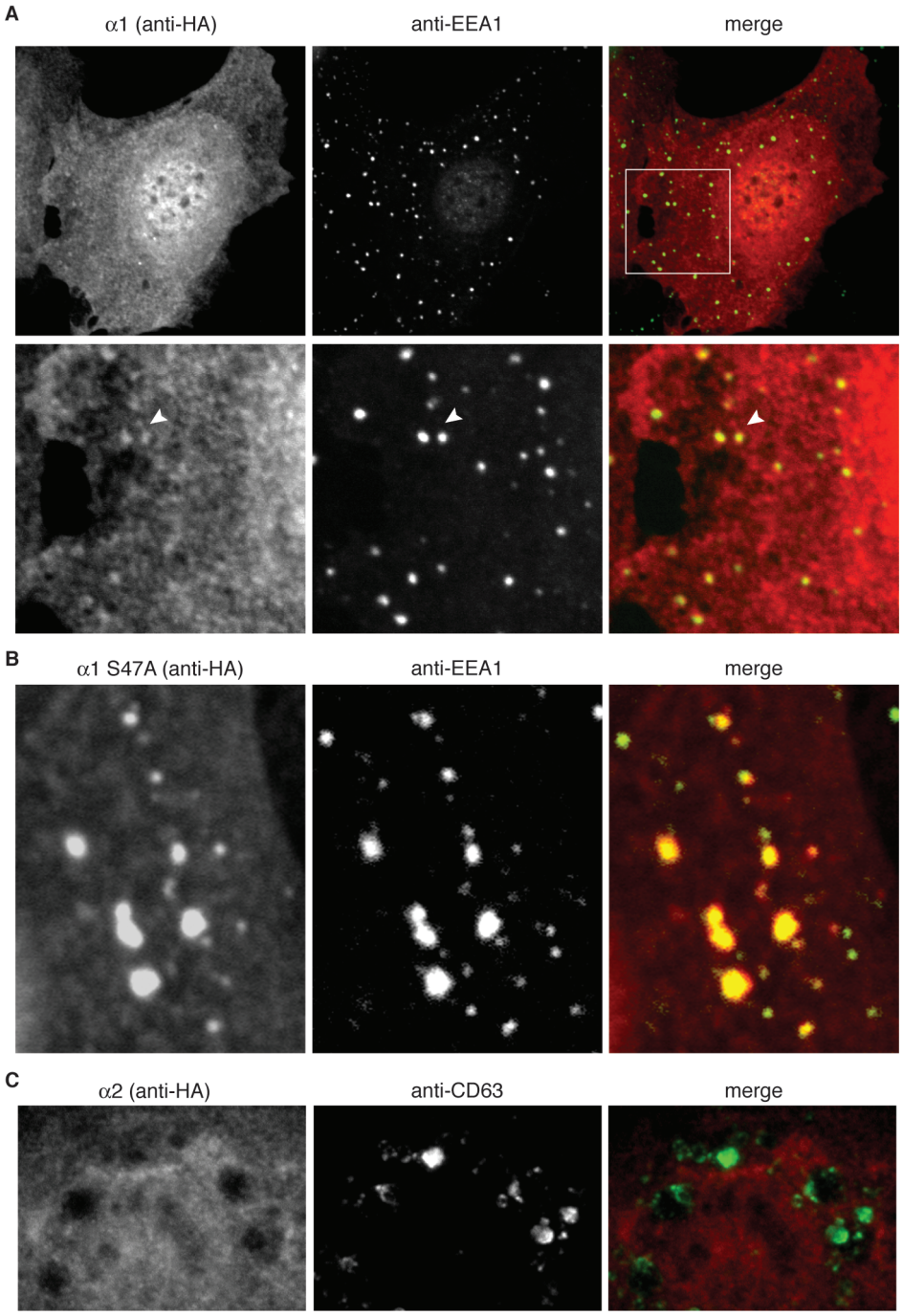
A
α1 (anti-HA)
anti-EEA1
merge
B
α1 S47A (anti-HA)
anti-EEA1
merge
C
α2 (anti-HA)
anti-CD63
merge

EEA1 was confined to the spherical domain whereas α1-HA could also be found on tubular extensions (Figure 4-2 A). PAFAH Ib α1 and α2 have conserved lipase motifs, and changing the serine residues in these motifs (α1 S47A; α2 S48A) renders the subunits catalytically inactive (318). We found that α1 S47A and α2 S48A were still partially localized to EEA1-positive early sorting endosomes in transfected cells, demonstrating that catalytic activity is not required for organelle targeting (Figure 4-2 B; data not shown).

In addition to peripheral early sorting endosomes, HA-tagged α1 and α2 were found on the centrally located ERC, as determined by colocalization with the ERC marker GFP-Rab11 (Figure 4-1 C, D). Localization of α1 or α2 on late endosomes/lysosomes was not observed (Figure 4-2 C).

Overexpression of α1 or α2 Alters the Location of Endocytic Compartments

While α1 and α2 were found on early sorting endosomes and recycling endosomes, we observed that the distribution of early and late endosomes, but not recycling endosomes, was altered by overexpression (Figure 4-3). Both early and late endosomes appeared to be dispersed to the periphery, similar to defects in dynein-dependent endosome transport to the centrosome (65, 66, 349, 381). The overexpression of α1 or α2 has been shown to affect LIS1-dynein interactions by sequestering LIS1 away from dynein (337), resulting in dispersed membrane organelles labeled by wheat germ agglutinin (338). However, the exact endocytic organelles affected by this and the contribution of α1 and α2 catalytic activity was not explored.

To test whether this redistribution is dependent on α1 and α2 catalytic activity, LIS1 binding, or both, we expressed α1 S47A, α1 E38D (337), or the double mutant α1 S47A/E38D. The overexpression of both catalytically active

Figure 4-3: Overexpression of α1 or α2 redistributes early and late endosomes to the cell periphery. (**A**) Wide-field images of untransfected BTRD cells side-by-side with cells expressing either wild type α1, catalytic inactive α1 S47A, LIS1 binding mutant α1 E38D, or double mutant α1 S47A/E38D (HA-tagged) and co-labeled with early (EEA1), late (CD63) and recycling endosomes (GFP-Rab11) markers. * indicates transfected cells. Scale bar = 10 μm.
(**B**) Quantification of the percent of cells with endosomes, early (EEA1) or late (CD63), dispersed toward the cell periphery. (Quantification by Ina Chen)

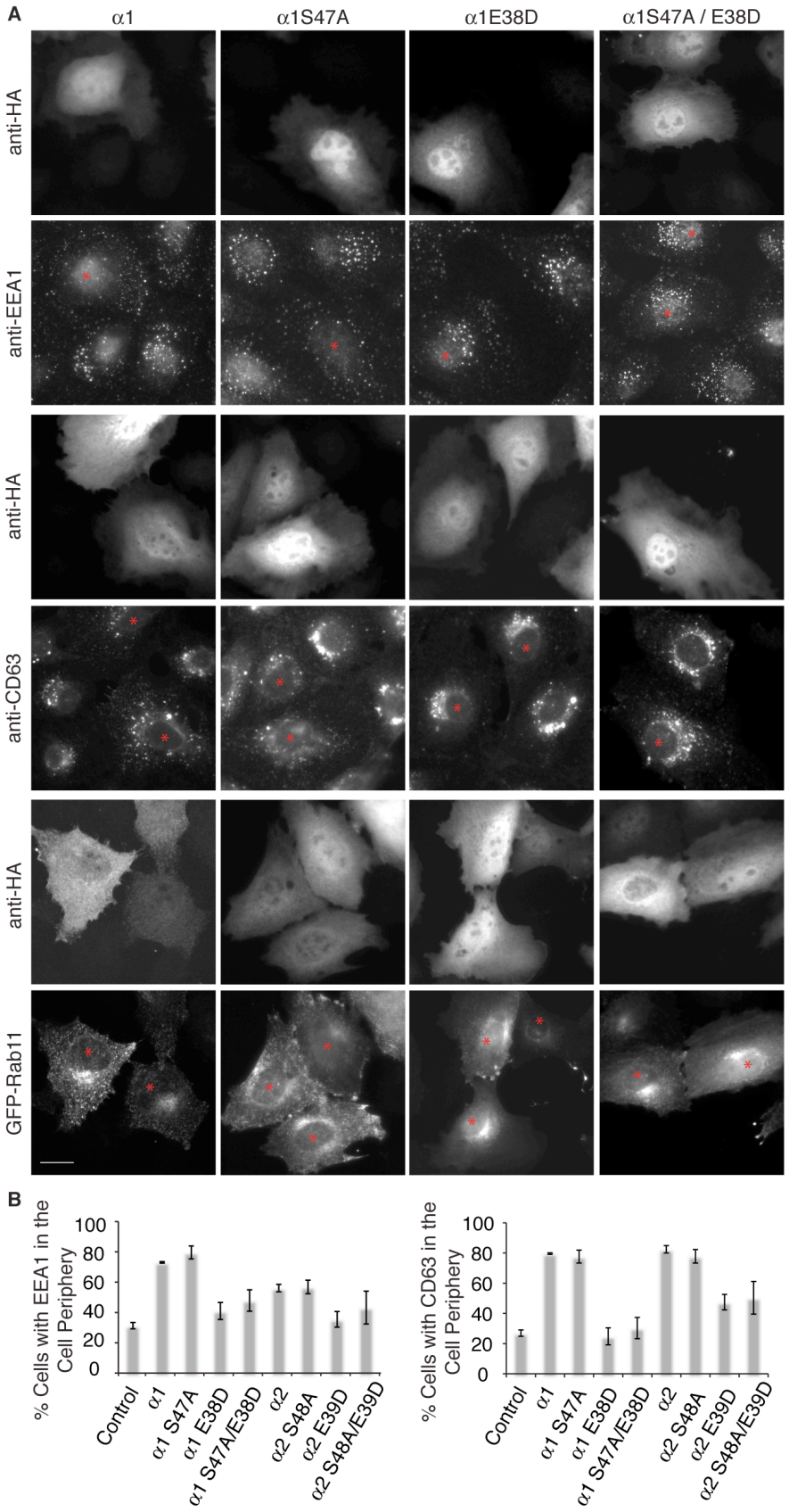
A
α1
α1S47A
α1E38D
α1S47A / E38D
anti-HA
anti-EEA1
anti-HA
anti-CD63
anti-HA
GFP-Rab11
B
% Cells with EEA1 in the Cell Periphery
100
80
60
40
20
0
Control
α1
α1 S47A
α1 E38D
α1 S47A/E38D
α2
α2 S48A
α2 E39D
α2 S48A/E39D
% Cells with CD63 in the Cell Periphery
100
80
60
40
20
0
Control
α1
α1 S47A
α1 E38D
α1 S47A/E38D
α2
α2 S48A
α2 E39D
α2 S48A/E39D

and inactive α1 S47A resulted in a peripheral distribution of late and early endosomes, whereas—consistent with Ding et al. (338)—expression of α1 E38D had normal endosome distribution. Likewise, the LIS1-binding defective and catalytically inactive α1 S47A/E38D, showed normal distribution of early and late endosomes (Figure 4-3). The endocytic recycling compartment, as seen by GFP-Rab11, appeared unaffected by the expression of α1 or the various α1 mutants. These overexpression results are also consistent with knockdown experiments (see below), indicating the expression levels of α1 and α2 impact the location of early endosomes.

siRNA-Mediated Knockdown of α1 and α2 Alters the Localization of Endocytosed Transferrin and Delays Transferrin Recycling

Previous studies have shown that PLA_2 antagonists inhibit the trafficking of Tf through the endocytic recycling pathway (245). To investigate the potential role of PAFAH Ib PLA_2 subunits, α1 and α2, in endocytic recycling, siRNA-mediated knockdown was conducted with siRNAs targeting both α1 and α2. A large assortment of cell lines was found to express both α1 and α2, therefore it was necessary to transfect cells with an siRNA mixture to knockdown both proteins. In BTRD cells, the mixed siRNAs reproducibly generated a >80% reduction in α1 and α2 levels (Chapter 2, Figure 2-9).

Tf trafficking in cells with reduced α1 and α2 was monitored over a pulse-chase time course with FITC-Tf. Within 5 min of endocytosis, the amount of FITC-Tf was equivalent between α1 and α2 knockdown and control cells (Figure 4-4 A, B), indicating that knockdown did not affect endocytosis. Within 15 min of FITC-Tf endocytosis, there was an apparent difference between knockdown and control cells. In knockdown cells, the FITC-Tf was

Figure 4-4: siRNA-mediated knockdown of α1 and α2 delays the recycling of transferrin. BTRD cells were transfected with control or α1 and α2 siRNAs 72 h before experimentation. (**A**) Pulse-chase experiments were conducted with FITC-Tf in control and α1 and α2 siRNA-treated cells. Cells were pulse-labeled with FITC-Tf for 45 min, followed by chase in media containing unlabelled (non-fluorescent) Tf for 15 min. Representative confocal images are shown for the indicated time points. (**B**) Total FITC-Tf fluorescence was measured at 5 and 15 min after addition of FITC-Tf to the media (pulse). (**C**) At the indicated chase time points, transferrin fluorescence remaining in cells was quantified and is shown as a percent of the total transferrin fluorescence after 45 min pulse (maximum Tf fluorescence). At 30 min, $p < 0.05$ by a T-test. (**D**) The fluorescence intensity of the juxtanuclear, central FITC-Tf was measured at the indicated pulse and chase time points in control or α1 and α2 siRNA-treated cells. n = 4, error bars = SEM.

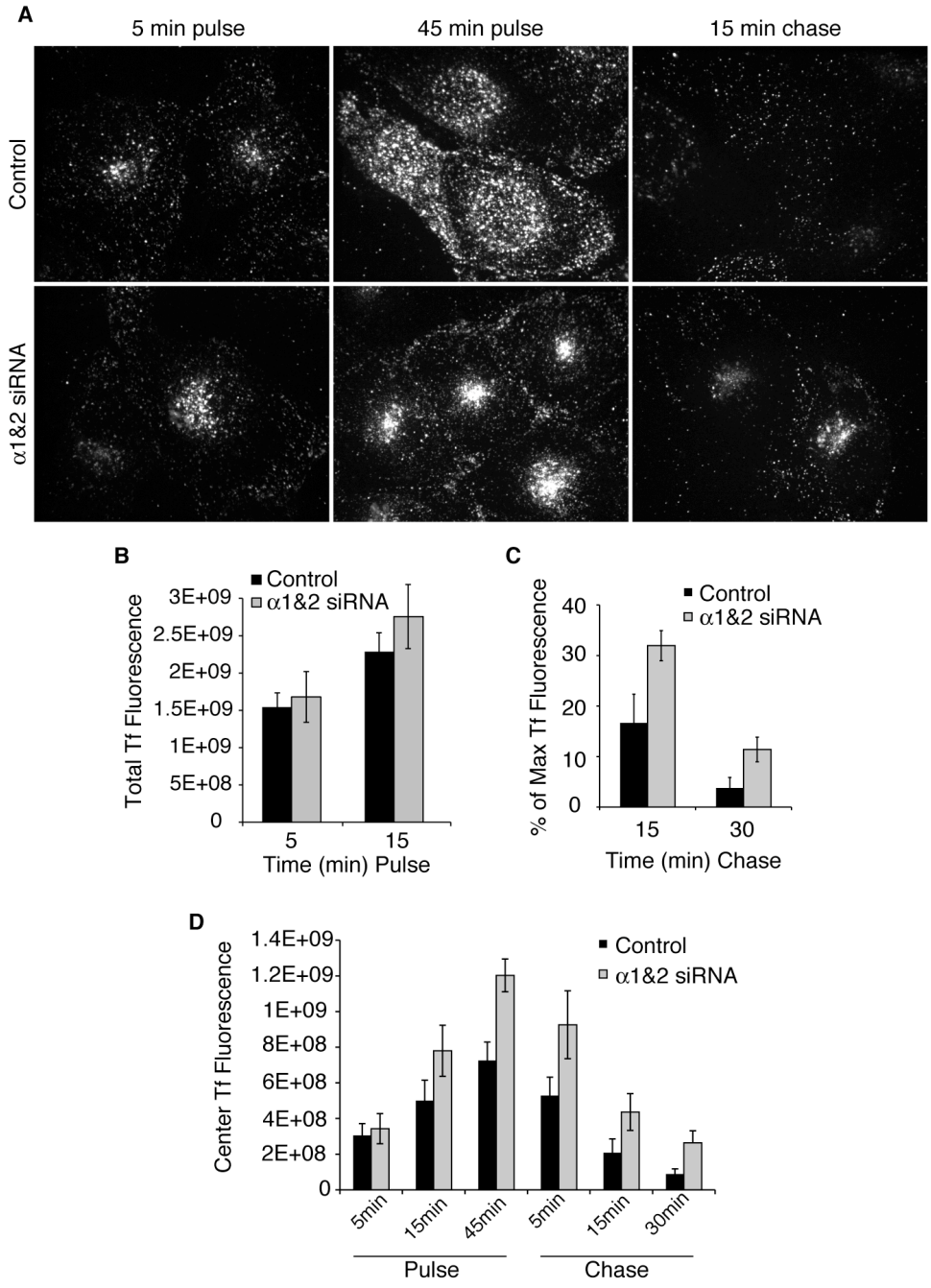
A
5 min pulse
45 min pulse
15 min chase
Control
α1&2 siRNA
B
Control
α1&2 siRNA
Total Tf Fluorescence
3E+09
2.5E+09
2E+09
1.5E+09
1E+09
5E+08
0
5
15
Time (min) Pulse
C
Control
α1&2 siRNA
% of Max Tf Fluorescence
40
30
20
10
0
15
30
Time (min) Chase
D
Control
α1&2 siRNA
Center Tf Fluorescence
1.4E+09
1.2E+09
1E+09
8E+08
6E+08
4E+08
2E+08
0
5min
15min
45min
5min
15min
30min
Pulse
Chase

clustered in a tight, central ERC-like location, with very few peripherally labeled endosomes (Figure 4-4 A, D). This became more evident by 45 min pulse. This distribution of FITC-Tf was also evident during chase of FITC-Tf out of the cells (Figure 4-4 A, D). Additionally, during chase time points, α1 and α2 knockdown cells appeared to retain FITC-Tf fluorescence over a longer period of time, indicating the recycling of FITC-Tf was slowed (Figure 4-4 A, C).

Knockdown of α1 and α2 Alters the Distribution of Early and Late Endosomes But Not the Endocytic Recycling Compartment

Since the distribution of FITC-Tf was affected by α1 and α2 knockdown, and overexpression affects the distribution of endosomes, we wanted to address whether the physical location of endosomes was affected with the reduction of α1 and α2. Therefore, we analyzed the distribution of early endosomes, late endosomes, recycling endosomes, and lysosomes in α1 and α2 knockdown BTRD cells. Endosomes labeled with EEA1, CD63, and Cathepsin D, but not GFP-Rab11, were more clustered in the cell center with reduced α1 and α2 (Figure 4-5). To determine whether this phenotype was due to decreased α1 and α2 PLA_2 activity or a consequence of reduced binding to LIS1, which regulates dynein activity (331, 340), we expressed RNAi-resistant versions of α1 wild type, catalytic inactive (α1 S47A), and LIS1 binding mutants α1 E38D or α1 S47A/E38D in cells that were treated with α1 and α2 siRNAs. Cells expressing RNAi-resistant α1 or α1 S47A rescued the distribution of early and late endosomes, as well as lysosomes. In contrast, cells expressing LIS1-binding mutant versions displayed similar phenotypes to α1 and α2 knockdown cells (Figure 4-6), suggesting that endosome

Figure 4-5: Reduced levels of α1 and α2 redistributes early endosomes, late endosomes, and lysosomes to the cell center. Confocal images of early endosomes (EEA1), late endosomes (CD63), lysosomes (Cathepsin D), the transferrin receptor (TfR), or recycling endosomes visualized with expression of GFP-Rab11 in BTRD cells transfected with control RNA or siRNA targeting α1 and α2.

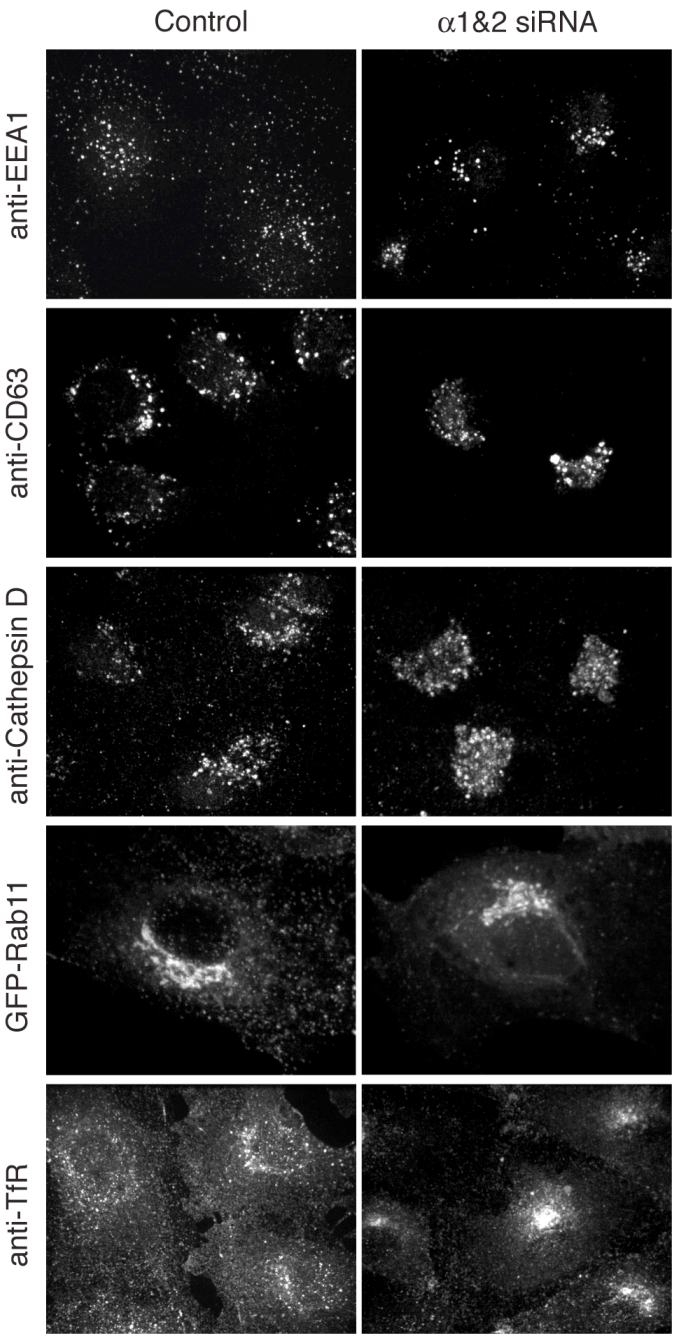
Control
α1&2 siRNA
anti-EEA1
anti-CD63
anti-Cathepsin D
GFP-Rab11
anti-TfR

Figure 4-6: Endosome positioning is altered in α1 and α2 knockdown cells due to lost interactions with LIS1. (**A**) Confocal images of α1 and α2 siRNA-treated BTRD cells transfected with RNAi-resistant α1, catalytic inactive α1 S47A, LIS1 binding mutant α1 E38D, or double mutant α1 S47A/E38D. Wild type α1 and catalytic inactive α1 S47A rescued endosome clustering seen with α1 and α2 knockdown, but LIS1 binding mutant (E38D) versions did not rescue changes in endosome distribution. * indicates cells transfected with α1 RNAi-resistant constructs, as determined by anti-HA staining.
(**B**) Quantification of early and late endosome clustering in knockdown and RNAi-resistant α1 transfected cells as indicated. n = 3-4, error bars = SEM.

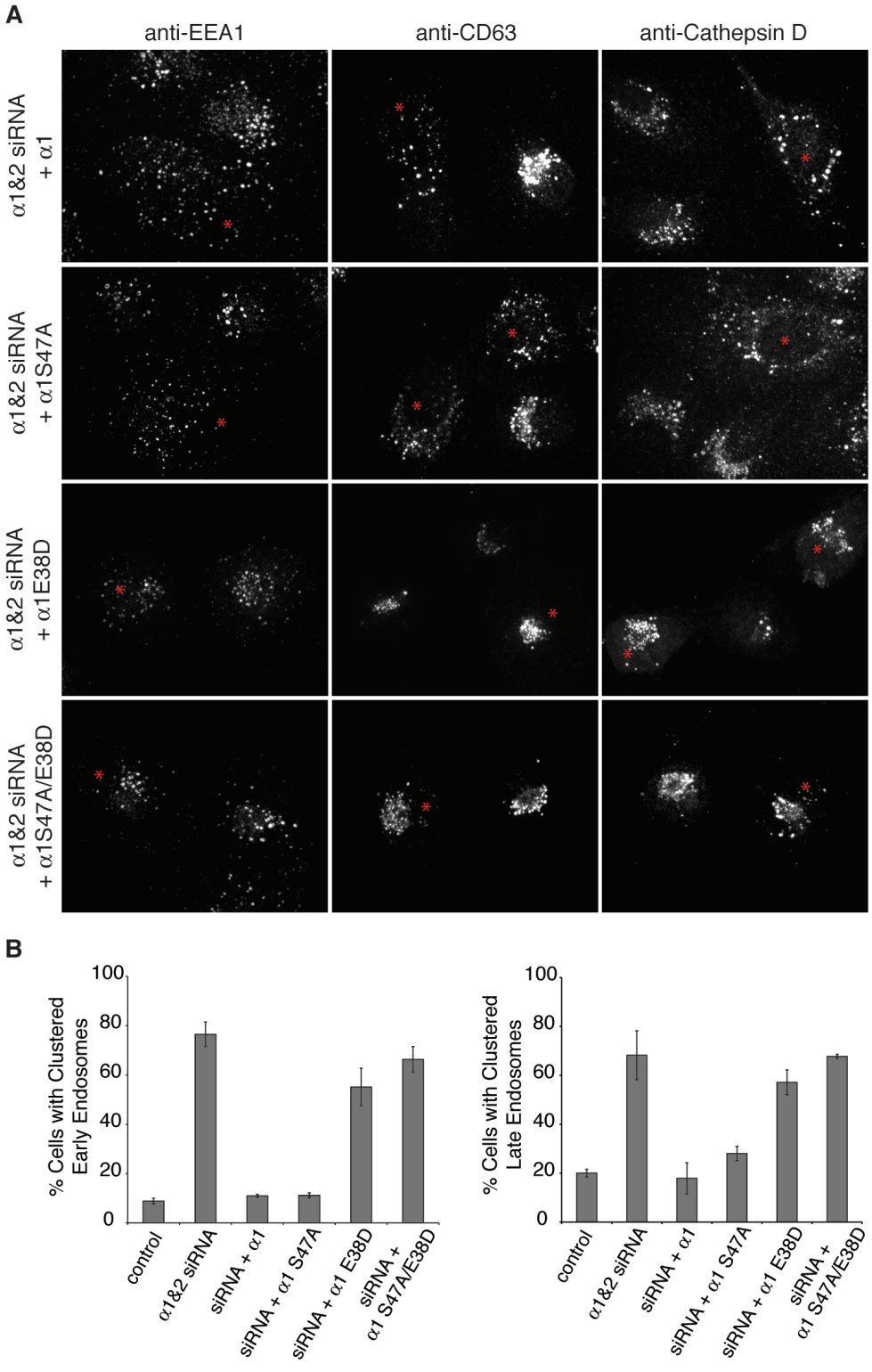
A
anti-EEA1
anti-CD63
anti-Cathepsin D
α1&2 siRNA + α1
α1&2 siRNA + α1S47A
α1&2 siRNA + α1E38D
α1&2 siRNA + α1S47A/E38D
B
% Cells with Clustered Early Endosomes
% Cells with Clustered Late Endosomes
100
80
60
40
20
0
control
α1&2 siRNA
siRNA + α1
siRNA + α1 S47A
siRNA + α1 E38D
siRNA + α1 S47A/E38D

clustering is a result of lost α1 and α2 interactions with LIS1.

This redistribution of endocytic markers could result from physical relocation of endosomes, mis-targeting of endocytic proteins, or enhanced fusion of early endosomes with late endosomes. To determine whether the endosome markers still appropriately localize to distinct early and late endosome organelles in α1 and α2 knockdown cells, double- and triple-labeling with Rab proteins was conducted. The reduction of α1 and α2 levels did not affect the colocalization of EEA1 with GFP-Rab4 or GFP-Rab5 (Figure 4-7). Conversely, EEA1 did not localize to GFP-Rab7 or CD63 late endosomes (Figure 4-7 A; data not shown). Additionally, CD63 did not colocalize with GFP-Rab4 (Figure 4-7 A) but did colocalize appropriately with GFP-Rab7 (not shown).

As a second test of endosome identity, we examined whether Tf is delivered to EEA1-labeled endosomes shortly after endocytosis. Within 5 min of internalization from the plasma membrane, proteins arrive in EEA1-labeled early endosomes but are not yet sorted to the ERC or late endosomes (115). Control and α1 and α2 knockdown cells were immunostained for EEA1 to determine if FITC-Tf internalized for 5 min was localized with EEA1-labeled early endosomes. In both control and α1 and α2 knockdown cells FITC-Tf colocalized with a subset of EEA1-labeled puncta. In α1 and α2 knockdown cells, the majority of FITC-Tf was localized to central EEA1 puncta, indicating that Tf did reach early endosomes (Figure 4-7 C).

Knockdown of α1 and α2 Inhibits Endosome Tubule Formation

Early sorting endosomes and the ERC are complex tubulo-vesicular organelles. At steady state, the tubular elements are difficult to image and

Figure 4-7: Endosome identity is not affected by α1 and α2 knockdown. (**A**) Early endosome Rab4 tagged with GFP was expressed in control or α1 and α2 siRNA-treated cells and triple labeled to compare the localization with early endosome marker EEA1 and late endosome marker CD63 by confocal microscopy. GFP-Rab4 labeled endosomes that contain EEA1, but not CD63, in control and knockdown cells. Scale bars = 10μm. (**B**) Early endosome GFP-tagged Rab5 was expressed in control or α1 and α2 knockdown cells and co-stained with anti-EEA1 antibodies. GFP-Rab5 labeled endosomes that contain EEA1 in control and knockdown cells. Scale bars = 10μm. (**C**) BTRD cells treated with either control siRNA or α1 and α2 siRNA were exposed to FITC-Tf at 4ºC to allow binding to TfRs, then shifted to 37ºC for 5 min to permit endocytosis and delivery to early endosomes. Both control and knockdown cells show partial colocalization between FITC-Tf and anti-EEA1.

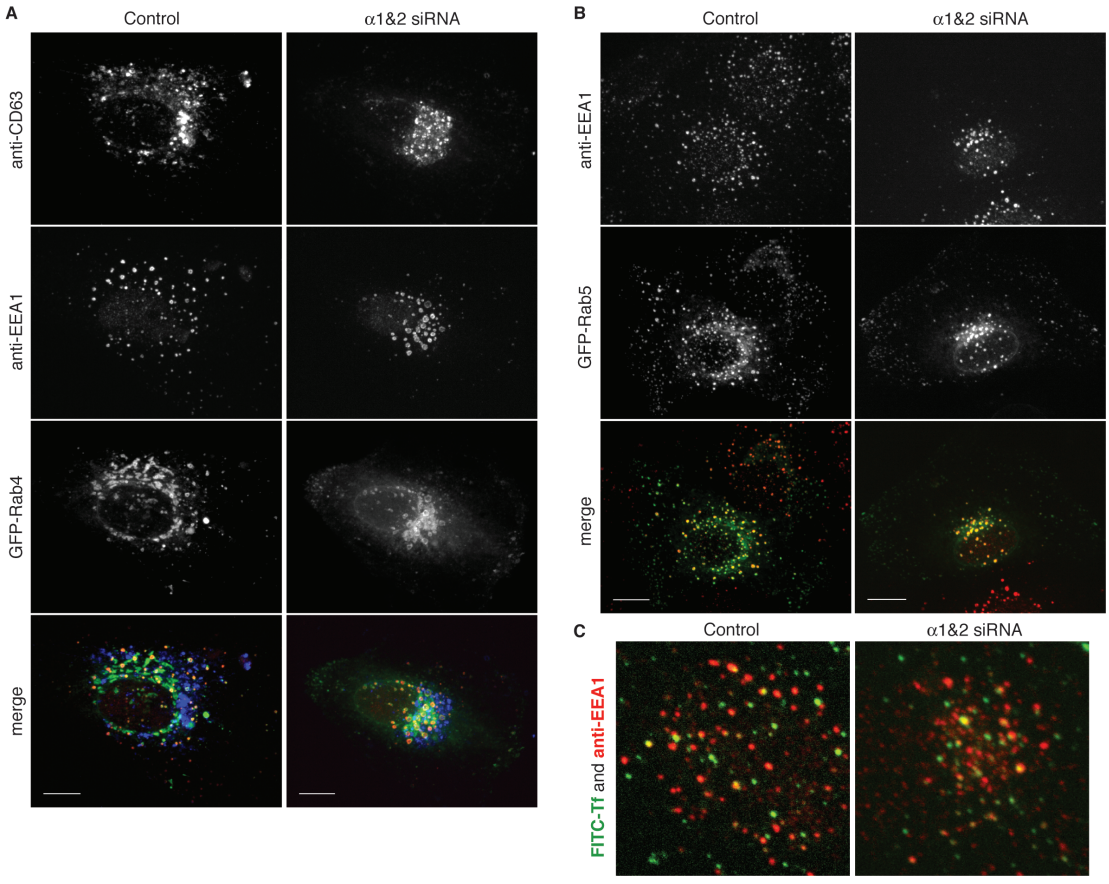
A
Control
α1&2 siRNA
anti-CD63
anti-EEA1
GFP-Rab4
merge
B
Control
α1&2 siRNA
anti-EEA1
GFP-Rab5
merge
C
Control
α1&2 siRNA
FITC-Tf and anti-EEA1

quantify, because they are highly dynamic. However, the tubular domains of endosomes become greatly enhanced when treated with brefeldin A (BFA), an inhibitor of coated vesicle formation (382-384). BFA provides a useful tool for investigating the molecular mechanisms required to make tubules. For example, previous studies showed that PLA_2 antagonists inhibit BFA-stimulated endosome tubule formation (245). Therefore, we asked if α1 and α2 are required for BFA-stimulated tubule formation by performing siRNA-mediated knockdown experiments. In control cells, early endosomes and the ERC labeled with FITC-Tf rapidly undergo extensive tubule formation following addition of BFA, whereas the endosomes in siRNA-treated cells displayed many fewer tubules (Figure 4-8). Quantification of these results revealed that the extent of membrane tubule formation was reduced in knockdown cells (Figure 4-8 B).

Overexpression of PAFAH Ib α1 or α2 Induces Endosome Tubule Formation

To determine if, conversely, overexpression of α1 or α2 increased endosome tubule formation, Bret Judson, a former member of the Brown laboratory, measured the percentage of endosomes that had tubular morphology in transfected and non-transfected cells that had internalized TRITC-Tf for 45 min, which labels both early and recycling endosome compartments. For these experiments, he primarily measured the peripheral endosomes, which correspond to early sorting endosomes. Overexpression of wild type α1 or α2, caused peripheral endosomes to become more tubular. Long axis lengths of sorting endosomes in untransfected cells were 1.04 ± 0.2 μm versus 1.41 ± 0.3 μm in transfected cells (Figure 4-9). In addition, the percentage of total endosomes with tubules was increased (Figure 4-9 B). This

Figure 4-8: α1 and α2 knockdown inhibits BFA-stimulated tubulation of endosomes. (**A**) Cells transfected with control RNA or siRNAs against α1 and α2 were incubated with FITC-Tf for 45 min to label all early sorting endosomes and the ERC, and then treated with BFA (5 μg/ml) in the continuous presence of FITC-Tf for the indicated times. Scale bar = 10μm. (**B**) Magnified images of FITC-Tf-labelled endosomes in control and α1&2 siRNA treated cells after 5 min of BFA treatment. (**C**) Quantification of BFA-stimulated tubulation in control and α1 and α2 siRNA treated cells. n = 4, error bars = SEM.

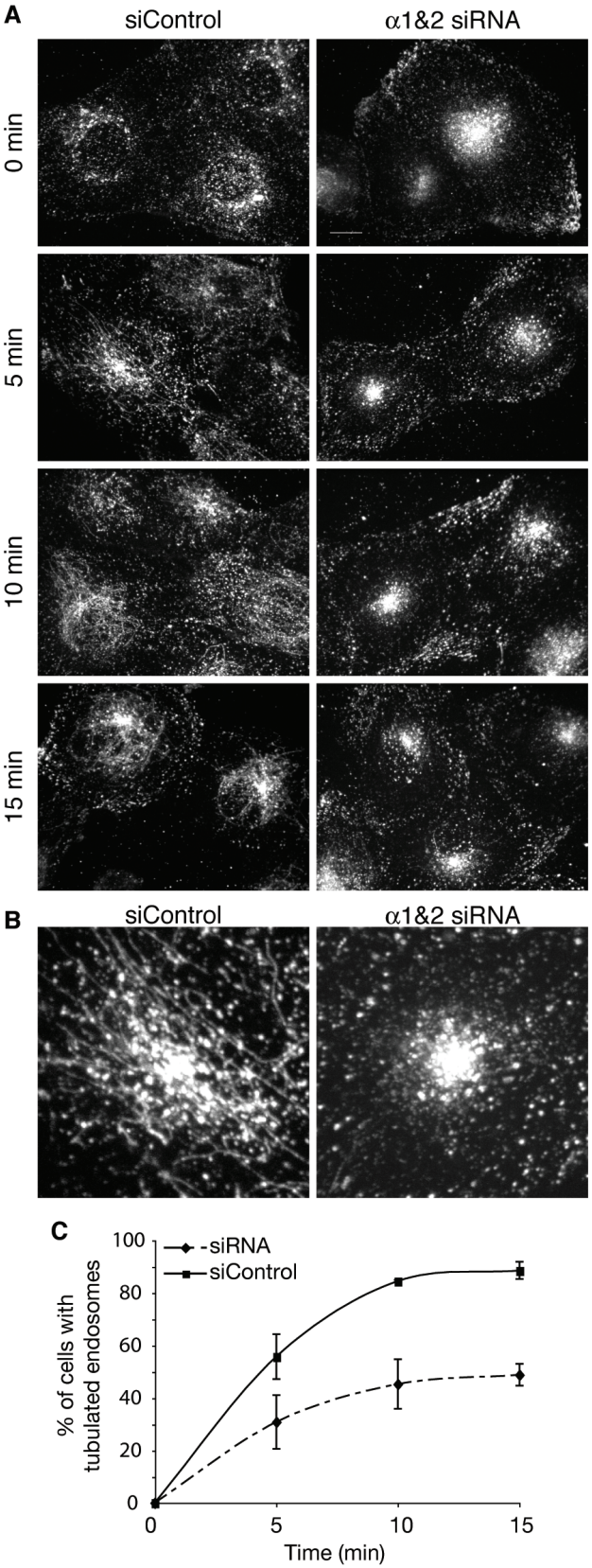
A
siControl
α1&2 siRNA
0 min
5 min
10 min
15 min
B
siControl
α1&2 siRNA
C
-siRNA
siControl
% of cells with tubulated endosomes
100
80
60
40
20
0
0
5
10
15
Time (min)

Figure 4-9: Overexpression of α2 induces endosome tubule formation. (**A**) Representative images of control HeLa cells and HeLa cells transfected with α2. Cells were incubated with Tf-TRITC for 45 min to label endocytic compartments. (**B**) Fraction of total endosomes with tubules in untransfected cells or cells transfected with either α2 or catalytically inactive α2 S48A. ($\geq$2000 endosomes counted/condition). Experimental results from Bret Judson.

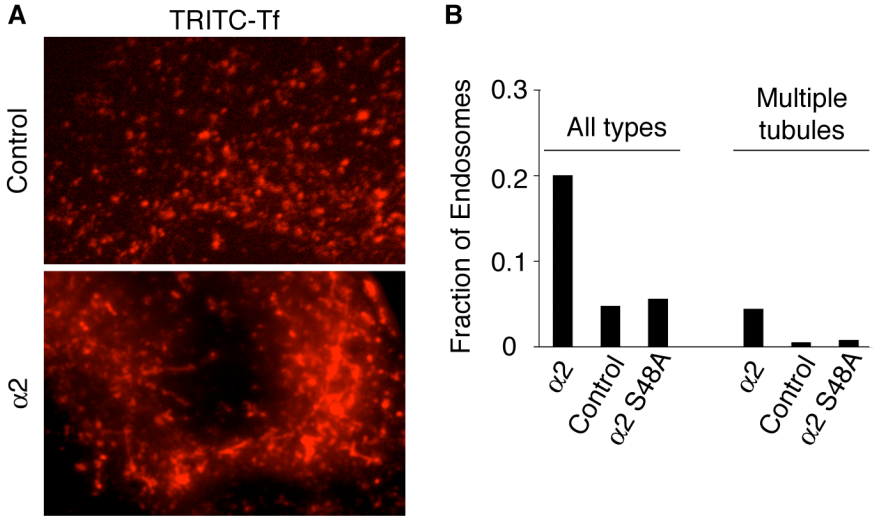
A
TRITC-Tf
Control
α2
B
Fraction of Endosomes
0.3
0.2
0.1
0
All types
Multiple tubules
α2
Control
α2 S48A
α2
Control
α2 S48A

tubule formation was dependent on catalytic activity because overexpression of a catalytic mutant (α2 S48A) did not result in an increase of tubulated endosomes.

Overexpression of PAFAH Ib α1 or α2 Alters Trafficking Through the Endocytic Recycling Compartment

To investigate whether the overexpression of α1 and α2 may enhance endocytic trafficking, we examined the effect of α1 or α2 overexpression on trafficking of Alexa 488-labeled Tf (Tf-488). We overexpressed either wild type α1 or α2, constructs containing mutations in active site serines, or LIS1-binding deficient mutants and followed Tf-488 during a pulse-chase time course. Only α1 is shown and discussed here, as results for α1 and α2 were comparable. Cells were incubated with media containing Tf-488 (pulse) for 45 min followed by replacement of the media with unlabeled Tf (chase) for 40 min. The internalization of fluorescent Tf in 15 min was equivalent between control and all α1-overexpressing cells (Figure 4-10; 4-11 A). Following a 45 min pulse of Tf-488 in untransfected cells or cells transfected with LIS1-binding mutants, α1 E38D or α1 S47A/E38D, Tf-488 was localized to puncta throughout the cell as well as clustered in the juxtanuclear ERC (Figure 4-10; 4-11). However, in cells expressing α1 wild type or α1 S47A, Tf localized only to puncta in the periphery. Similarly, TfRs were found peripherally distributed in α1 or α1 S47A transfected HeLa cells but TfR distribution was not affected in cells expressing LIS1 binding mutant constructs (Figure 4-11 C).

To compare Tf recycling, a chase with unlabeled Tf for 10, 20 min or 40 min was conducted. In control cells and cells expressing LIS1-binding mutant versions of α1, Tf-488 accumulated in the central ERC; and over the 40 min of

Figure 4-10: Overexpression of α1 re-routes Tf and the TfR traffic from early endosomes, bypassing the central endocytic recycling compartment, back to the plasma membrane due to LIS1 binding. HeLa cells were transiently transfected with α1-HA or α1 mutants and pulse-labeled with Alexa 488-Tf (Tf-488) for 15 and 45 min, followed by chase in transferrin-free media for 20 or 40 min to observe transferrin internalization and recycling.
Scale bar = 10μm.

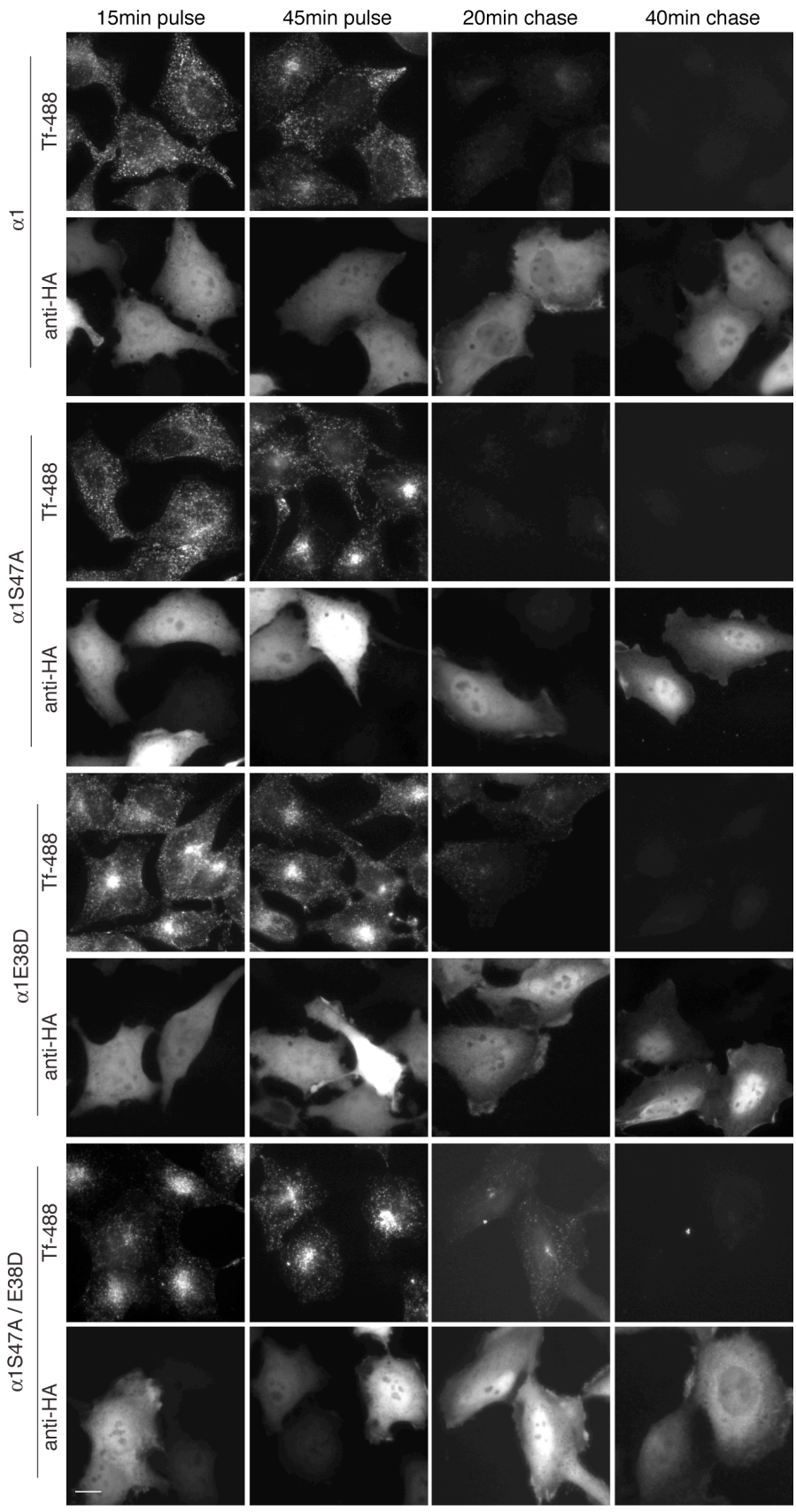
15min pulse
45min pulse
20min chase
40min chase
α1
anti-HA
Tf-488
α1S47A
anti-HA
Tf-488
α1E38D
anti-HA
Tf-488
α1S47A / E38D
anti-HA
Tf-488

Figure 4-11: Overexpression of α1 changes the distribution of Tf and the TfR, and double mutant α1 S47A/E38D slows Tf recycling. (**A**) The fluorescence intensity of Alexa 488-Tf was measured for pulse and chase time points in untransfected (control) HeLa cells and cells expressing indicated proteins. α1 S47A/E38D compared to control or α1 E38D is significantly different with $p < 0.0001$ as analyzed by a T-test. (**B**) Quantification of the percent of cells with central (ERC) Tf fluorescence after a 45 min pulse of Alexa 488-Tf (Tf-488). (**C**) Percent of cells with central Tf receptor (anti-TfR) fluorescence. Anti-TfR was used without co-labeling with anti-HA, as the antibodies were both from mice. Therefore, cell counts include both transfected and untransfected HeLa cells. Error bars = SEM.

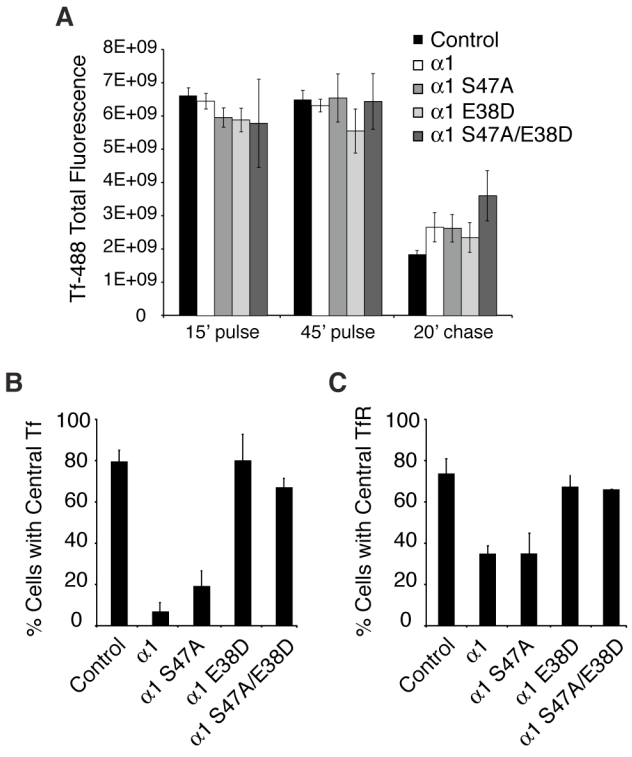
A
Tf-488 Total Fluorescence
8E+09
7E+09
6E+09
5E+09
4E+09
3E+09
2E+09
1E+09
0
15' pulse
45' pulse
20' chase
Control
α1
α1 S47A
α1 E38D
α1 S47A/E38D
B
% Cells with Central Tf
100
80
60
40
20
0
Control
α1
α1 S47A
α1 E38D
α1 S47A/E38D
C
% Cells with Central TfR
100
80
60
40
20
0
Control
α1
α1 S47A
α1 E38D
α1 S47A/E38D

chase, Tf-488 signal was progressively lost due to the recycling of Tf out of the cell and its release into the medium (Figure 4-10). The overexpression of α1 or α1 S47A did not have an effect on the kinetics of Tf recycling but rather affected the route of Tf, as fluorescent Tf never accumulated in the ERC (Figure 4-10; 4-11 A, B). These results suggest that overexpression of α1 or α2, likely by disrupting LIS1 activation of dynein (337, 338), reduced the transport of Tf from peripheral early sorting endosomes to the central ERC, thus bypassing the ERC during the recycling to the cell surface. The overexpression of α1 E38D also did not interfere with the recycling of Tf, since fluorescence of Tf-488 during chase time points was comparable to control cells (Figure 4-11 A). There was, however, a noticeable difference in recycling kinetics with the double mutant α1 S47A/E38D. During chase time points, α1 S47A/E38D showed higher Tf-488 fluorescence in the cell, suggesting delayed recycling kinetics, compared to α1 E38D and control cells.

Discussion

These results reveal a novel mechanism for mediating endosome membrane trafficking and morphology with a new functional role for cytoplasmic PAFAH Ib α1 and α2. Overexpression of α1 or α2 had three clear phenotypic consequences: 1) re-distribution of early and late endosomes toward the cell periphery, 2) stimulation of Tf/TfR export from early sorting endosomes to the plasma membrane, bypassing the ERC, and 3) stimulation of endosome tubule formation. These phenotypes were opposite to effects seen with loss of α1 and α2: 1) re-distribution of early endosomes, late endosomes, and lysosomes to the cell center, 2) a delay in Tf recycling to the cell surface, and 3) inhibition of BFA-stimulated endosome tubules.

The altered organelle distribution observed by overexpression or knockdown of α1 and α2 could be explained by, respectively, increased or decreased interactions with LIS1. This would affect the fraction of LIS1 available to bind and activate dynein for minus end-directed microtubule transport (331, 337). In effect, the overexpression or knockdown would decrease or increase, respectively, transport of endosomes and lysosomes towards the centrosome, which is a dynein-dependent function activated by LIS1 (65, 66, 360, 381). Our results are in agreement with reports that overexpression of α1 and α2 affect LIS1 binding and regulation of dynein in endosome and lysosome transport (338).

The effects of α1 and α2 overexpression and knockdown on Tf recycling may also be partially explained by interactions with LIS1. Pulse-chase experiments demonstrate that overexpression of wild type and catalytically inactive α1 and α2, prevent transport of Tf from peripheral early sorting endosomes to the ERC (step C in Figure 4-12) but not the release of internalized Tf from the cell. These results strongly suggest that Tf was recycled directly from early sorting endosomes rather than from the ERC (step B of Figure 4-12). In fact, a portion of the endocytosed membrane and receptors are normally recycled from early sorting endosomes directly back to the plasma membrane (143, 144). This apparent re-routing of Tf and TfR did not occur with the overexpression of LIS1-binding defective constructs, strongly suggesting that Tf and TfR may be shuttled directly from early endosomes to the plasma membrane due to decreased dynein activation by LIS1. This indicates that dynein activation by LIS1 is important for transport from early endosomes to the endocytic recycling compartment, a trafficking step that is dynein-dependent and membrane tubule-mediated (115, 350, 385).

Figure 4-12: Diagram of the effect of α1 and α2 overexpression and knockdown on endosome distribution and trafficking. (**A**) Normal trafficking routes of endocytosed cargo are shown. Step A: cargo is endocytosed at the plasma membrane and delivered to early sorting endosomes. Step B: A portion of cargo to be recycled is delivered from early endosomes to the plasma membrane. This transport involves kinesin motors. The position of early and late endosomes in the cell as well as the transport of cargo destined for degradation (non-recycled) are both dynein-dependent. Step C: The predominant route of recycled cargo, such as transferrin, is from early endosomes to the centrally located endocytic recycling compartment. This is a dynein and membrane tubule-mediated process. Red arrows depict tubule-mediated trafficking. Recycled cargo then travels as in Step D, from the ERC to the plasma membrane. This step uses kinesin motors. (**B**) The effects seen with knockdown of α1 and α2 on endosomes. Early and late endosomes cluster in the center of the cell via a LIS1-mediated effect, presumably through the activation of dynein motors. Additionally, knockdown delays recycling of Tf from the center of the cell, slowing step D. (**C**) The effects of α1 or α2 wild type overexpression are depicted. Early and late endosomes were seen in the cell periphery due to LIS1 binding, which likely prevented activation of dynein. This would inhibit step C and decrease cargo recycling at step D, increasing the amount of cargo recycled through step B.

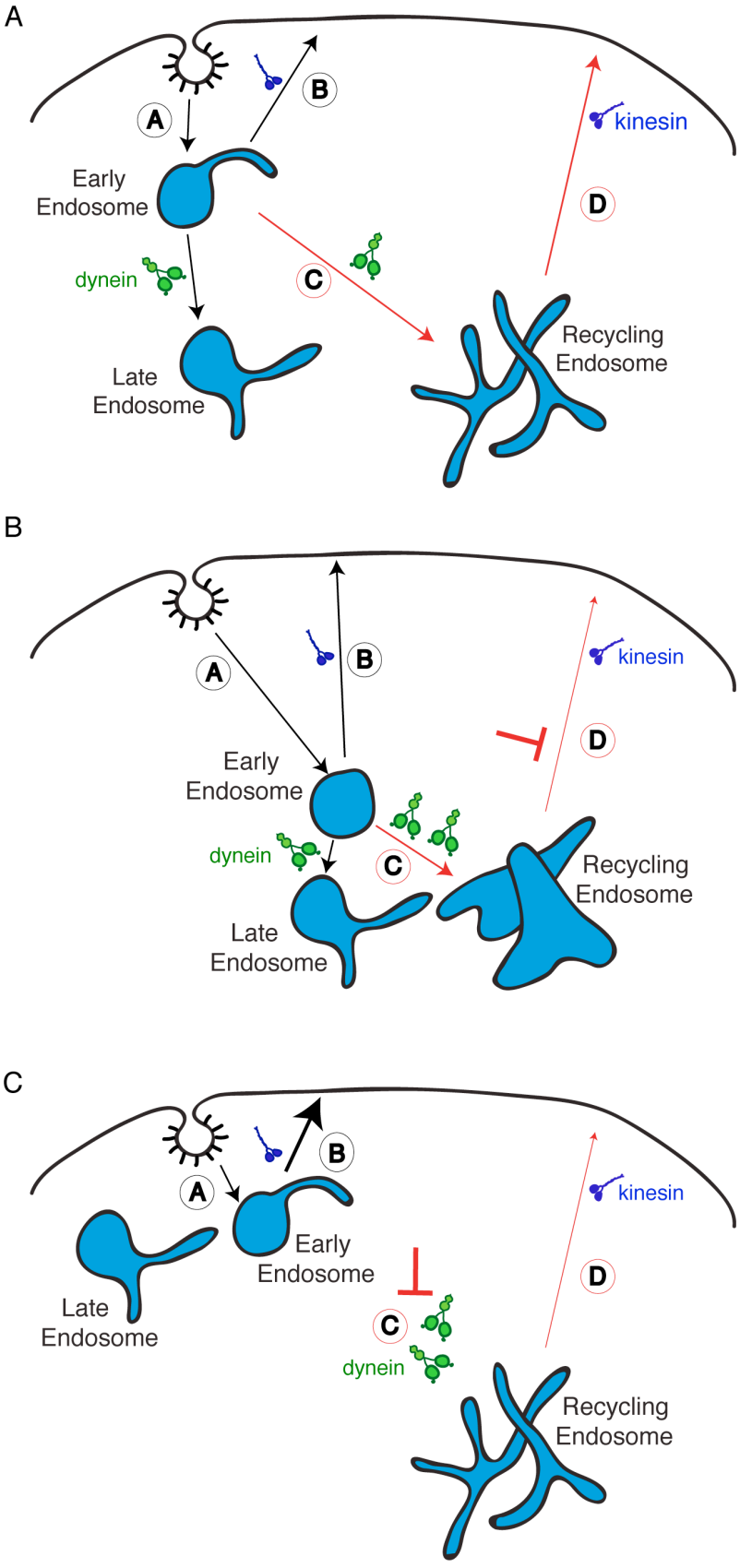
A
A
B
kinesin
Early
Endosome
D
dynein
C
Recycling
Endosome
Late
Endosome
B
A
B
kinesin
D
Early
Endosome
dynein
C
Recycling
Endosome
Late
Endosome
C
B
A
kinesin
Early
Endosome
D
Late
Endosome
C
dynein
Recycling
Endosome

These results also are reminiscent of dynein inactivation by the overexpression of dynamitin, which also shifted the route of Tf recycling directly from peripheral sorting endosomes but did not affect the kinetics of recycling (349). The binding of LIS1 by excess α1 or α2 (from overexpression) would, in effect, decrease the activation of dynein-mediated transport of cargo, including Tf transport from the early sorting endosomes to the ERC (Figure 4-12 C).

The catalytically inactive LIS1-binding mutant, α1 S47A/E38D, did not re-route Tf but did delay Tf recycling compared to control cells and α1 E38D overexpressing cells. This catalytically inactive mutant (α1 S47A/E38D) may act as a dominant negative, which has been suggested by recent studies (259). Catalytically inactive subunits may dimerize with endogenous subunits, creating inactive, 'poisoned' dimers. A dominant negative effect by the catalytic mutant is consistent with knockdown experiments, which also showed a delay in Tf recycling. If catalytically inactive α1 (S47A) or α2 (S48A) act as dominant negatives, one would predict that the α1 S47A would also delay Tf recycling. A possible explanation to this apparent inconsistency is depicted in Figure 4-12: α1 and α2 are important for the membrane trafficking from early endosomes to recycling endosomes (step C) and/or from the ERC to the plasma membrane (step D) but not necessarily in the 'short' recycling pathway directly from the early sorting endosomes to the plasma membrane (step B). This is an appealing possibility that fits well with our observations. The overexpression of α1 or α2, which are able to bind LIS1, appear to dramatically inhibit dynein-dependent function, blocking early to recycling endosome transport (step C) and re-routing Tf to recycle from early endosomes to the plasma membrane (step B). Therefore, no apparent dominant negative phenotype would be seen, as the trafficking steps

regulated by α1 and α2 would already be blocked by reduced dynein function. This suggests that α1 and α2 are important for transport from early endosomes to the ERC (step C) and/or from the ERC to the plasma membrane (step D).

Previous studies have shown that BFA enhances endosome membrane tubule formation (382, 384), effects that are inhibited by PLA_2 antagonists (245). Consistent with this idea, we found that overexpression of catalytically active, but not inactive, α1 or α2 increased the number of tubulated peripheral endosomes. Additionally, α1 and α2 knockdown inhibited Tf-labeled endosome tubules. Changes in membrane tubule formation seen in overexpression and knockdown, can be explained by the direct membrane altering action of PAFAH Ib PLA_2 subunits, α1 or α2, as catalytically inactive forms of α1 or α2 (α1 S47A and α2 S48A) did not increase endosome membrane tubules. The hydrolytic activity of PAFAH Ib α1 or α2 may contribute to the formation of membrane tubules by removal of the acyl chains from the *sn*-2 position of phospholipids, resulting in a shift from cylindrical or cone shaped phospholipids to inverted-cone shaped lysophospholipids (242). Localized accumulation of lysophospholipids creates tighter packing of the acyl chains in one leaflet of the endosome membrane bilayer, resulting in outward curvature of the membrane that could then grow into a tubule (198, 217). Alternatively, the lipid-modifying activity of α1 and α2 may feed into lipid-modifying pathways that can either directly affect membrane curvature or indirectly by recruiting proteins that bend membranes.

The exact physiological role of PAFAH Ib has been unclear. Studies have suggested various roles for PAFAH Ib in regulating LIS1/β and its interactions with dynein (331, 337, 338). To identify other functional roles for

PAFAH Ib, researchers have produced α1 and α2 knockout mice (326, 330). Surprisingly, male and female $\alpha1^{-/-}$ and female $\alpha2^{-/-}$ mice were grossly normal, but male $\alpha2^{-/-}$ mice were infertile with spermatogenesis defects. These defects appeared at earlier stages of meiosis in double knockout mice. Although PAF levels have been shown to influence sperm function (386, 387), the results of knockout studies, and lack of observable phenotypes, cause one to wonder about the exact physiological role of PAFAH Ib in other tissues. Of course, there may be functional redundancy, as other enzymes could compensate for the absence of α1 and α2 in the knockout mice.

There is growing evidence that cytoplasmic PLA_2 enzymes contribute to the formation of membrane tubules and regulate trafficking for other organelles (78, 244, 246, 249). In the past year, three phospholipases have been shown to be involved in Golgi structure and function. The cytoplasmic Ca^{2+}-dependent enzyme, $cPLA_2\alpha$, was shown to be recruited to the Golgi following an increase in secretory load and to enhance intra-Golgi membrane tubules that facilitate anterograde transport through the Golgi stack (256). $cPLA_2\alpha$, was also found to be required for export of junctional proteins in polarized endothelial cells (258). $iPLA_1\gamma$, was shown to be required for retrograde trafficking from the Golgi (260). Finally, in other studies, we have found that PAFAH Ib α1 or α2 are also localized to the Golgi complex where they mediate tubule formation and secretory trafficking (259). These results, along with studies here, establish that α1 or α2 function at multiple organelles.

In summary, our studies identify a specific cytoplasmic PLA_2, PAFAH Ib, that is capable of inducing membrane tubule formation and altering endocytic membrane trafficking pathways. Furthermore, these results demonstrate a physiological role for PAFAH Ib in mediating intracellular

membrane trafficking. Future research should address how PAFAH Ib selectively interacts with endosome and Golgi membranes, and if it interacts with other molecules, e.g., Rabs, sorting nexins, phosphoinositides, to facilitate efficient endosomal sorting. Nevertheless, this work and the recent work of others demonstrate the importance of lipid-modifying enzymes in both secretory and endocytic trafficking.

CHAPTER 5

Gβ1γ2 Activates Phospholipase A_2-Dependent Golgi Tubule Formation

Abstract

Heterotrimeric G proteins transduce the ligand binding of heptahelical transmembrane G protein coupled receptors into a variety of intracellular signaling pathways. Recently, heterotrimeric Gβγ subunit signaling at the Golgi complex has been shown to regulate the formation of transport carriers that deliver cargo from the Golgi to the plasma membrane. This regulation has been shown to increase protein kinase D-activated fission of TGN membranes. While several components of this signaling have been identified, the machinery directly involved in membrane fission as well as the proteins required in the initial formation of these transport carriers are unknown. Here we provide evidence that Gβ1γ2 signaling also stimulates Golgi membrane tubule formation using a reconstitution assay with isolated Golgi complexes. We show that an inhibitor of Gβγ activation of PLA_2 enzymes inhibits in vitro Golgi membrane tubulation. Additionally, purified Gβγ protein stimulates membrane tubules in the presence of low (sub-threshold) cytosol concentrations, and this stimulation of Golgi membrane tubules was repressed when PLA_2 enzymes were inhibited with ONO-RS-082. These studies indicate that Gβ1γ2 signaling activates PLA_2 enzymes required for Golgi membrane tubule formation.

Introduction

Cargo transport from the *trans* Golgi network (TGN) to the plasma

membrane involves both membrane bound vesicles and membrane tubules. Cargo destined for the plasma membrane, such as VSV-G, has been visualized to travel from the TGN in long, thin membrane-bound transport carriers (108, 181, 186, 189). Additionally, vesicle markers have been shown to partially colocalize with these membrane tubule extensions, from which vesicles may bud (186, 189, 388). The formation of vesicular and tubular transport carriers from the mammalian Golgi complex require regulation for precise spatial and temporal trafficking within a cell. The regulation of vesicular transport carriers by small GTPases, such as Arf1, Arls, and Rabs, as well as kinases, including Src family members, LIM kinase, protein kinase C (PKC), and protein kinase D (PKD) has been examined (71, 97, 119, 389-391). The outward budding of a nascent vesicle initially requires positive membrane curvature that is also necessary for forming membrane tubule carriers. However, little is known about the mechanisms that regulate the positive curvature and the formation of membrane tubules at the TGN.

A series of pharmacological studies using phospholipase A_2 (PLA_2) antagonists indicate that phospholipases are an essential component of membrane tubule formation (78, 244, 249, 364). Recent studies have since identified specific phospholipase (PLA) enzymes that contribute to different levels of Golgi membrane tubule formation: $cPLA_2\alpha$, $iPLA_1\gamma$, and platelet activating factor acetylhydrolase Ib (256, 258-260). These phospholipases have partially overlapping function and contribute to distinct aspects of Golgi structure and trafficking. However, it is not known how these PLA enzymes are individually regulated, nor is it understood how membrane tubules in general are regulated.

The large, heterotrimeric G protein family has been implicated in the

regulation of Golgi trafficking and architecture (392-397). Additionally, previous pharmacological studies suggest that heterotrimeric G protein signaling activates PLA_2 enzymes involved in Golgi membrane tubule formation (362). Heterotrimeric G proteins are composed of α, β, and γ subunits, each of which exists in a variety of isoforms. A trimer of Gαβγ associates with transmembrane G protein coupled receptors (GPCRs). In an inactive state, the Gα subunit binds to GDP and the Gβγ subunits, yielding a Gαβγ trimer, which is associated with GPCRs. Upon GPCR activation, a conformational change triggers the alpha subunit to exchange GDP for GTP. This switch leads to dissociation of Gαβγ from the GPCR and dissociation of Gα from Gβγ, each of which is able to stimulate respective signaling cascades.

Golgi structure and vesicle budding have been shown to be regulated by heterotrimeric G proteins, composed of various combinations of Gα, Gβ and Gγ subunit isoforms. Early studies with ilimaquinone (IQ), a metabolite of marine sponges that vesiculates the Golgi complex, revealed a role for Gαs and Gαi-3 as well as Gβγ subunits at the Golgi (392, 394, 396, 398). Gαi-3 and Gαq have also been implicated in the control of Golgi architecture and trafficking (395). Specific Gβγ subunits Gβ1γ2 and Gβ2γ3, upon overexpression in mammalian cells, dramatically affect Golgi membrane structure and alter trafficking, likely through activation of PKCη and PKD at the TGN (392, 397). The activation of PKC and, subsequently, PKD is important for the fission of vesicles at the TGN, and a kinase dead version of PKD (PKD-KD) has been shown to cause dramatic tubulation of the TGN (399). Additionally, recent studies suggest that particular Gβγ isoforms are capable, upon GPCR stimulation, of translocating from the plasma membrane to the Golgi complex, where the Gβγ may trigger vesiculation of the Golgi

complex as well as increased transport (400, 401). The localization of Gβ1γ2 specifically to the Golgi complex resulted in fragmentation of the Golgi and TGN, and inactivation of endogenous Gβγ significantly affected secretory trafficking (393).

In addition to roles in stimulating vesiculation, Gβγ has been implicated in regulating brefeldin A (BFA)-stimulated membrane tubules. Golgi and endosome membrane tubules stimulated by BFA were inhibited by the biscolaurine alkaloid isotetrandrine (ITD) (362), an inhibitor of Gβγ-mediated PLA_2 enzyme activation (402-404). This membrane tubule inhibition by ITD is believed to be an effect of preventing activation of PLA_2 enzymes through yet unknown Gβγ subunits. Put together, it is likely that Gβγ simultaneously activates pathways that promote PLA_2 enzyme activity to generate positive curvature (for both membrane tubules and vesicle formation) as well as activate machinery for vesicles fission.

Reported here is the use of a cell free reconstitution assay (405) to further test the idea that a Gβγ signaling pathway can activate PLA_2-dependent membrane tubule formation. This method permits direct examination of individual components for contributions to Golgi membrane tubule formation.

Methods and Materials

Reagents

Sprague-Dawley male rats were obtained from Charles River Breeding Laboratories, Inc. Isotetrandrine (ITD) and ONO-RS-082 (ONO) were purchased from BioMol Research Laboratories, Inc. Recombinant Gβ1γ2 provided by our collaborator Dr. J. Garrison (University of Virginia Health

Sciences, Charlottesville, VA).

Golgi Complex Isolation

Intact Golgi complexes from rat liver can be enriched following procedures described in (62). A male Sprague-Dawley rat of 100-150 g was euthanized with CO_2, and the liver was immediately removed and kept on ice. The rest of the procedure was performed at 4ºC and on ice. The liver was rinsed with ice-cold homogenization buffer (0.25 M sucrose, 10 mM Tris, pH 7.4) until clear. The liver was minced until fine with a razorblade and any connective tissue removed. The pureed liver was weighed, and homogenization buffer was added to yield 20% weight/volume suspension. The suspension was passed through a Balch/Rothman homogenizer with a 0.2460-inch ball bearing four times. The resulting homogenate was spun in a SS-34 at 5,000 rpm (3,000 x g) for 10 min at 4ºC to pellet nuclei and any unruptured cells. The post-nuclear supernatant was then mixed with an equal volume of 2.3 M sucrose (10 mM Tris, pH 7.4), resulting in a final 1.4 M sucrose concentration, and 15 mL was added to the bottom of Beckman SW28 ultracentrifuge tubes (38 mL capacity). This was overlaid with sucrose step gradients (containing 10 mM Tris, pH 7.4) as follows: 8 mL 1.2 M sucrose, 8 mL 1.0 M sucrose, 4 mL of 0.9 M sucrose, and 3 mL of 0.8 M sucrose. The gradients were spun at 25,000 rpm (90,000 x g) in a Beckman SW28 rotor for 2.5 h with no brake at 4ºC. Golgi membranes were collected with a Pasteur pipette at the 1.0 M/0.9 M interface and frozen in aliquots at -80ºC.

Preparation of Bovine Brain Cytosol

Bovine brain cytosol was prepared as described by (369). The protease

stock solutions were prepared fresh as follows: 10 mg/mL phenylmethylsulfonyl fluoride (PMSF, 500x) in isopropanol, 1 mg/mL pepstatin A in methanol (18250x), 1 mg/mL aprotinin in water (625x), 50 mg/mL 1, 10 phenantholine in ethanol (625x), 0.25 mg/mL leupeptin in water (625x). Ethylene glycol tetraacetic acid (EGTA) was dissolved in water and solubilized with the addition of NaOH, for a final 0.38 g/mL solution.

Fresh calf brains were obtained from a slaughterhouse and immediately put into 4ºC buffer of 320 mM sucrose, 25 mM Tris, pH 7.4 and kept on ice for transport. All procedures where done at 4ºC and on ice as much as possible. Meninges and blood vessels were removed and then brain tissue was coarsely chopped with a razorblade in a small amount of homogenization buffer, which contains: 25 mM Tris, 500 mM KCl, 250 mM sucrose, 1 mM dithiothreitol (DTT), 2 mM EGTA, pH 7.4 with 2 μg/mL aprotinin, 0.5 μg/mL leupeptin, 2 μM pepstatin A, 0.5 mM 1, 10-phenanthroline, and 1 mM PMSF. The minced brain was mixed with 2.5 times the weight (g) in volume (mL) of homogenization buffer and homogenized in a Waring blender for 30 sec two times on high. Homogenized material was then spun in a GSA rotor at 9,000 rpm (13,000 x g) for 30 min at 4ºC. The supernatant was collected, PMSF was added to a final 1x concentration, and was then spun in a Type 35 rotor at 35,000 rpm (143,000 x g) for 2.25 h at 4ºC. The supernatant was collected and more (1x) PMSF was added. Over an hour, 1.5 times the volume was added of saturated ammonium sulfate, pH 8.0 at 4ºC for a final 60% ammonium sulfate, and then mixed for an additional hour at 4ºC. The solution was then spun in a GSA rotor at 8,000 rpm (11,555 x g) for 45 min at 4ºC. The supernatent was discarded, and each pellet was resuspended in 10 mL of dialysis buffer (25 mM Tris, 50 mM KCl, pH 8.0)

containing 0.5 mM DTT and (1x) protease inhibitors. This suspension was placed into molecular weight 14 kDa cutoff dialysis tubing and placed into dialysis buffer + DTT for 1 h at 4°C, then dialyzed overnight in dialysis buffer (without DTT) at 4°C. Dialysate was collected and PMSF added (to 1x), then spun in a Ti 50.2 rotor for 1 h at 45,000 rpm (90,000 x g) at 4°C. The supernatant (BBC) was then collected, additional PMSF added and frozen in aliquots at -80°C.

In Vitro Golgi Tubulation Assays

In vitro Golgi tubulation assays were preformed as described in Banta et al (369). All frozen reagents were rapidly thawed at 37°C and then kept on ice until use. Gβγ was in the following buffer: 20 mM Tris base, pH 8.0, 1 mM EDTA, 1 mM DTT, 150 mM NaCl, and 0.1% Chaps (w/v). BBC was spun in a TLA 100.3 rotor at 70,000 rpm for 20 min to remove precipitate. Reaction mixtures containing BBC, purified protein, and/or inhibitors mixed with tubulation assay buffer (50 mM KCl, 1 mM $MgCl_2$, 25 mM Tris, 10 mM HEPES, pH 7.4) and ATP (final 50 μM) were prepared as indicted in the results. Golgi aliquots and reaction mixtures were prewarmed to 37°C for 15 min, after which the reaction mix was gently mixed 1:1 into the Golgi aliquots, and then incubated for 15 min at 37°C. Ten microliters of each sample was spotted onto Formvar- and carbon-coated EM grids for 15 min, followed by staining 3 times for 4 sec with 2% phosphotungstic acid, pH 7.2. Grids were stored in the dark until viewing by a FEI Morgagni 268 transmission electron microscope. Upon viewing, Golgi were scored as tubulated or not tubulated, based on the presence of one or more membrane tubule (60-90 nm diameter) extensions.

Results

A preparation of bovine brain cytosol (BBC) stimulates Golgi membrane tubules in a reconstitution assay (369), which can be inhibited by PLA_2 inhibitors (78). Here we describe the use of this in vitro reconstitution assay to assess the contribution of Gβ1γ2 and subsequent stimulation of PLA_2 enzymes to the formation of Golgi membrane tubules.

Isotetrandrine Inhibits Cytosol-Stimulated Golgi Membrane Tubules In Vitro

Previous studies have shown that ITD inhibits BFA-stimulated Golgi membrane tubules in mammalian cells (362). To determine if ITD similarly inhibits cytosol-stimulated Golgi tubules in vitro, we tested a range of ITD concentrations with varying BBC concentrations. ITD exhibited a dose-dependent inhibition of BBC-stimulated membrane tubules and showed a positive correlation between concentration of cytosol and the IC_{50} for membrane tubule inhibition (Figure 5-1). This IC_{50} of membrane tubule inhibition is dependent on the individual preparation of BBC, as there is natural variation between different preparations of BBC. We found an IC_{50} range from 25-100 μM with cytosol concentrations that achieve maximum number of tubulated Golgi. Therefore, for each BBC preparation, the appropriate IC_{50} was determined before further experimentation.

Isotetrandrine Inhibits Golgi-Associated Components

The exact target of ITD is unknown (402-404), therefore we tested whether the target of ITD was cytosolic or membrane-associated. The extent of Golgi membrane tubule inhibition was compared between ITD addition to the Golgi membranes themselves—presumably inhibiting a protein directly

Figure 5-1: Dose-dependent inhibition of cytosol-stimulated Golgi membrane tubules. (**A**) Example negative stain electron micrographs of tubulated and non-tubulated Golgi from the in vitro reconstitution assay. Bovine brain cytosol (BBC, 1.5 mg/mL) was incubated with the indicated concentration of ITD and added to isolated Golgi complexes. Control Golgi were incubated with 0.2 mg/mL BSA. Scale bars = 500 nm. (**B**) Quantification of the percent of Golgi complexes with membrane tubules, normalized to the maximum percent of Golgi with tubules in the presence of each BBC concentration shown. Averages are shown from minimum of 3 replicates, error bars = SEM.

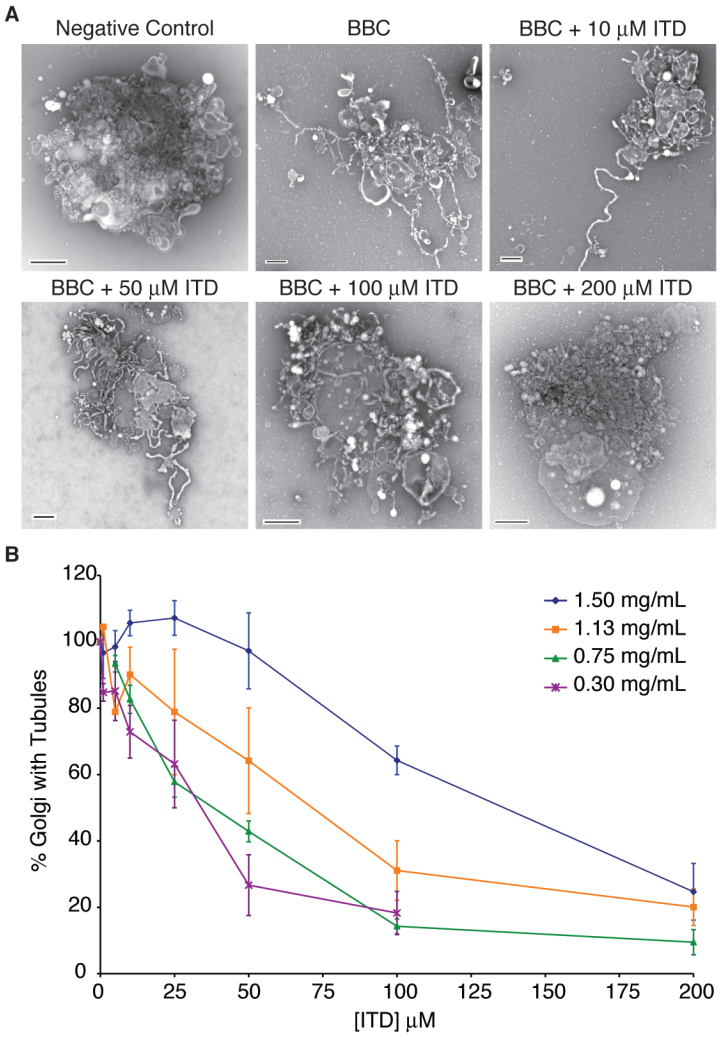
A
Negative Control
BBC
BBC + 10 μM ITD
BBC + 50 μM ITD
BBC + 100 μM ITD
BBC + 200 μM ITD
B
% Golgi with Tubules
[ITD] μM
1.50 mg/mL
1.13 mg/mL
0.75 mg/mL
0.30 mg/mL
0
20
40
60
80
100
120
0
25
50
75
100
125
150
175
200

associated with the membranes—versus ITD addition to the cytosol—inhibiting a cytosolic target. Either the BBC or Golgi membranes were pretreated with isotetrandrine, and then combined. ITD was more efficacious when Golgi membranes were pretreated, consistent with the idea that ITD inhibits a Golgi-associated target (Figure 5-2).

Gβ1γ2 Rescues ITD Inhibition

The pharmacological effect of ITD is to inhibit Gβγ activation of PLA_2 enzymes (402-404). To determine if ITD inhibits a pathway stimulated by Gβγ, as suggested by the previous pharmacological studies, Gβ1γ2 was added to the ITD-treated tubulation mixture and tested for its ability to stimulate Golgi membrane tubules. BBC-stimulated Golgi tubulation was inhibited to near-background levels by ITD (Figure 5-3). Addition of increasing amounts of purified Gβ1γ2 protein to Golgi membranes treated with 25 μm ITD resulted in nearly complete restoration of membrane tubule formation to control levels (Figure 5-3).

Gβ1γ2 Stimulates Golgi Membrane Tubules

ITD inhibition of cytosol-stimulated Golgi membrane tubulation could be rescued by addition of purified Gβ1γ2, therefore we wanted to address whether Gβγ itself could stimulate membrane tubules in the reconstitution assay. Since Gβγ contains a myristoylated tail and is soluble in low concentrations of CHAPS, we first tested the affect of the Gβγ buffer on Golgi membranes and found no effect (Figure 5-4 A). Of the various Gβγ isoforms Gβ1γ2 was selected, as it is the most abundant isoform in bovine brain and has been shown previously to affect Golgi architecture and trafficking (393, 397).

Figure 5-2: ITD inhibits Golgi-membrane associated proteins. Various concentrations of ITD were either pre-incubated at 37°C for 15 min with BBC or Golgi membranes before combining the cytosol and Golgi, followed by further incubation at 37°C for 15 min. (**A**) Representative negative stain Golgi treated with ITD, which was pre-incubated as labeled. Scale bars = 500 nm. (**B**) Quantification of the percent of Golgi with membrane tubules, normalized to BBC alone (1.5 mg/mL). ITD concentrations shown are the final concentration after mixing the Golgi and cytosol. Error bars = SEM.

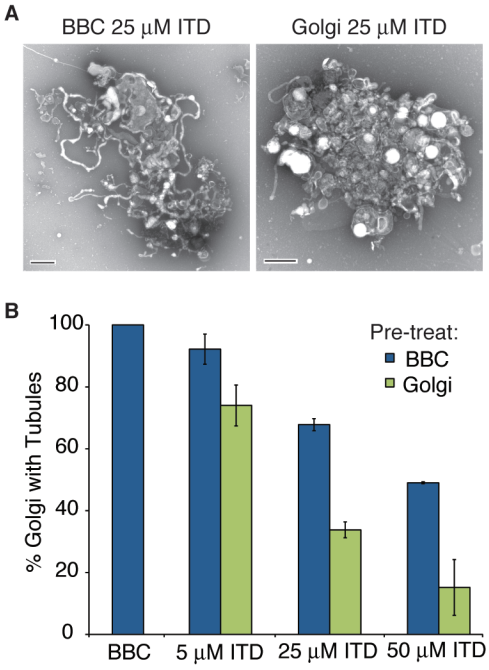
A
BBC 25 μM ITD
Golgi 25 μM ITD
B
% Golgi with Tubules
100
80
60
40
20
0
Pre-treat:
BBC
Golgi
BBC
5 μM ITD
25 μM ITD
50 μM ITD

Figure 5-3: Gβ1γ2 rescues ITD inhibition of cytosol-stimulated Golgi membrane tubules. Quantification of the fraction of Golgi with tubules, relative to the maximum percent of Golgi with tubules seen with BBC (1.5 mg/mL) alone. Final concentrations (after mixing the pre-incubated Golgi and cytosol) are shown for purified Gβγ. ITD final concentration was 25 μM. Error bars = SEM.

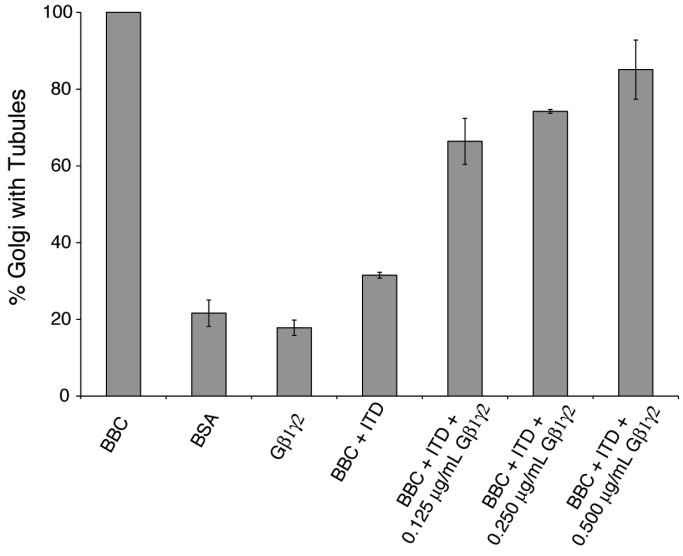
% Golgi with Tubules
100
80
60
40
20
0
BBC
BSA
Gβ1γ2
BBC + ITD
BBC + ITD + 0.125 µg/mL Gβ1γ2
BBC + ITD + 0.250 µg/mL Gβ1γ2
BBC + ITD + 0.500 µg/mL Gβ1γ2

Figure 5-4: Gβ1γ2 stimulates cytosol-dependent Golgi membrane tubulation. (**A**) Representative EM micrographs of Golgi from the reconstitution assay. Golgi were treated with BBC (1.5 mg/mL), a BSA control (0.2 mg/mL), Low BBC (0.15 mg/mL), or Low BBC + Gβ1γ2 (0.5 μg/mL Gβγ). Each condition was in the presence of the Gβγ buffer. Scale bar = 500 nm. (**B**) Quantification of the percent of Golgi with membrane tubules, normalized to the maximum amount of tubulated Golgi with BBC (1.5 mg/mL). Gβ1γ2 purified protein alone does not stimulate Golgi membrane tubules above background levels (no BBC control). In the presence of low cytosol concentrations (Low BBC 0.15 mg/mL), the addition of Gβ1γ2 stimulates membrane tubules. Error bars = SEM.

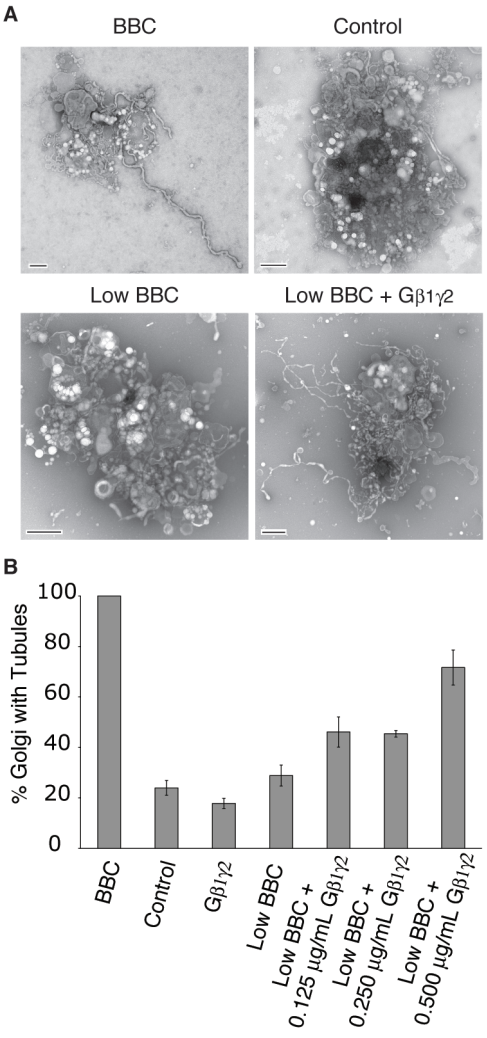
A
BBC
Control
Low BBC
Low BBC + Gβ1γ2
B
% Golgi with Tubules
100
80
60
40
20
0
BBC
Control
Gβ1γ2
Low BBC
Low BBC + 0.125 µg/mL Gβ1γ2
Low BBC + 0.250 µg/mL Gβ1γ2
Low BBC + 0.500 µg/mL Gβ1γ2

Gβγ, when added alone to Golgi membranes, was insufficient to stimulate membrane tubules above background (Figure 5-4). Either Gβ1γ2 does not stimulate membrane tubules or a cytosolic component (e.g. a PLA_2) is required to induce membrane tubule formation. Near background levels of membrane tubule formation are seen with low concentrations of BBC (sub-threshold levels), which can be used in combination with other factors that promote membrane tubule formation to achieve maximum Golgi membrane tubules (249). Therefore we tested whether Gβγ signaling requires a cytosol component by adding Gβγ to sub-threshold cytosol levels. Indeed, we found that the addition of Gβ1γ2 in increasing amounts stimulated the formation of membrane tubules in the presence of low BBC (Figure 5-4).

Gβ1γ2 -*Stimulated Golgi Membrane Tubules are PLA_2 Dependent*

The above studies show that BBC contains a component that is stimulated by Gβ1γ2, likely a protein downstream of the target of ITD. Previous studies have demonstrated that BBC-stimulated Golgi membrane tubules require PLA_2 enzyme activity (244), and ITD is suggested to inhibit Gβ1γ2 activation of PLA_2 enzymes (406), so we tested whether Gβ1γ2-stimulation of membrane tubules also requires PLA_2 activity. To examine this, a PLA_2 enzyme antagonist documented to inhibit Golgi membrane tubules, ONO-RS-082 (244), was pre-incubated with cytosol for 15 min prior to addition with Golgi pre-incubated with Gβ1γ2. The results showed that addition of Gβ1γ2 to low cytosol was able to stimulate Golgi membrane tubules, but Gβ1γ2 did not stimulate membrane tubules when cytosol was pretreated with ONO (Figure 5-5). These results indicate that Gβ1γ2 requires PLA_2 activity found in BBC to stimulate Golgi membrane tubules.

Figure 5-5: Gβ1γ2 stimulation of Golgi membrane tubules is PLA_2 activity dependent. BBC (1.5 mg/mL) was pre-incubated with the PLA_2 inhibitor ONO (at final concentration of 25 μM) at 37°C for 15 min, followed by the addition of Gβ1γ2 purified protein (final concentration of 0.4 μg/mL) to BBC before combining the cytosol and Golgi, and additional incubation at 37°C for 15 min. Low BBC was 0.15 mg/mL and the BSA, as a negative control, was at a final 1 mg/mL concentration. (**A**) Representative negative stain Golgi treated with ONO and Gβ1γ2 as labeled. Scale bars= 500 nm.
(**B**) Quantification of the percent of Golgi with membrane tubules, normalized to BBC alone (1.5 mg/mL). Error bars = SEM.

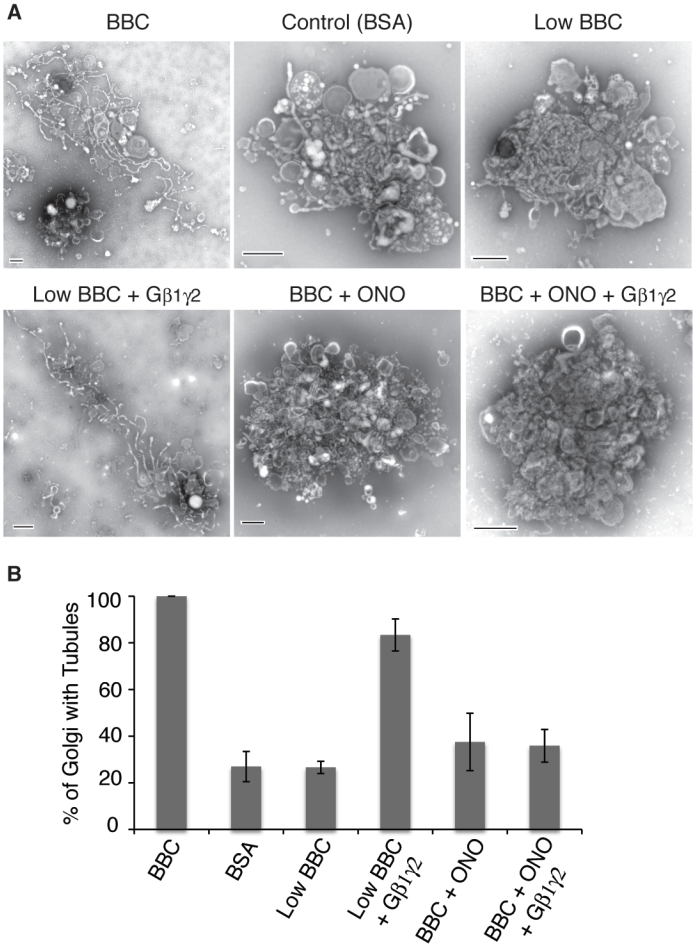
A
BBC
Control (BSA)
Low BBC
Low BBC + Gβ1γ2
BBC + ONO
BBC + ONO + Gβ1γ2
B
% of Golgi with Tubules
100
80
60
40
20
0
BBC
BSA
Low BBC
Low BBC + Gβ1γ2
BBC + ONO
BBC + ONO + Gβ1γ2

Discussion

Here we provide in vitro evidence that heterotrimeric G protein subunits Gβ1γ2 stimulate Golgi membrane tubule formation, which is dependent on PLA_2 activity. Until now, the identified role of Gβ1γ2 at the Golgi complex has been limited to membrane fission in the generation of TGN vesicles. This work is consistent with the hypothesis that Gβγ subunits are additionally important for activation of PLA_2 enzymes that stimulate membrane tubule formation.

Previous studies using the inhibitor ITD implicated Gβγ signaling in the regulation of PLA_2 enzymes. ITD has been used to inhibit inflammatory signaling, by decreasing Gβγ activation of PLA_2 enzymes (404). More recent studies show ITD inhibition of BFA-stimulated Golgi membrane tubule formation, suggesting a broader role of Gβγ regulation of PLA_2 enzymes (362). Here we further explore the hypothesis that ITD inhibits Gβγ activation of PLA_2 enzymes involved in the formation of Golgi membrane tubules, using an in vitro reconstitution assay. We find that ITD inhibits BBC-stimulated membrane tubules from isolated Golgi complexes. This inhibition can be rescued by the addition of purified Gβγ subunits, further supporting the notion that ITD inhibits a Gβγ signaling pathway.

Heterotrimeric Gβγ subunits have recently been shown to localize to the Golgi complex upon GPCR stimulation (393, 401, 407). Once localized to the Golgi complex, Gβ1γ2 stimulates a signaling cascade that increases the TGN diacylglycerol levels necessary for the recruitment of PKD. Upon reaching the Golgi, PKD is subsequently activated by PKCη, leading to phosphorylation of PI4KIIIβ and ceramide transfer protein (CERT). This ultimately leads to enhanced fission and transport of cargo (222, 392, 393, 408,

409).

This signaling cascade includes factors, such as PKD, which have been implicated in vesicle fission (399, 410). However, the current model does not address how the initial positive curvature to form vesicles and membrane tubules is generated to promote the increase in cargo transport upon GPCR stimulation. Increased transport upon Gβγ signaling at the Golgi can be prevented by inactivation of PKD (397). This inhibition of PKD kinase activity results in the exacerbation of long and persistent TGN membrane tubules (399). These results indicate that the machinery involved in the outward bending of Golgi membranes is activated, but the subsequent fission is prevented.

The TGN membrane tubules seen with PKD inactivation can be inhibited by the PLA_2 inhibitor ONO (250). ONO prevents the formation of new PKD kinase dead (PKD-KD) TGN tubules, decreases the number of TGN tubules containing ts045 VSV-G, and inhibits the transport of ts045 VSV-G from the TGN to the plasma membrane (250). Consistent with this, the formation of Gβγ-stimulated tubules was sensitive to ONO inhibition when added to BBC. This suggests that PLA_2 enzyme activity present in the cytosol is required for Gβ1γ2 stimulation of tubules, which are likely stimulated upstream of PKD. While it is possible that a separate signaling pathway regulates the formation of membrane tubules, it is conceivable that stimulation of both positive curvature for outward budding and negative curvature for fission are interconnected signaling pathways activated by Gβγ. The results presented here suggest the latter: Gβγ stimulates the outward curvature of Golgi membranes through PLA_2 activation as well as PKD-dependent fission.

Specific PLA_2 enzymes $cPLA_2\alpha$ and PAFAH Ib are implicated in the formation of Golgi membrane tubules and TGN to plasma membrane transport (256, 258, 259). $cPLA_2\alpha$ has been shown to be important for Golgi membrane tubule formation (256) and has been implicated in the transport of tight junction proteins to the plasma membrane (258). Additionally, PAFAH Ib has been shown to affect the localization of PKD to the TGN and VSV-G kinetics from the Golgi to the plasma membrane (259). It will be interesting in the future to determine whether these specific PLA_2 enzymes, or unidentified PLA enzymes, are part of the $G\beta\gamma$ signaling pathway at the Golgi and how they are interconnected with PKD-activated fission to generate transport carriers.

REFERENCES

1. Dancourt J, Barlowe C. 2010. Protein sorting receptors in the early secretory pathway. Annu Rev Biochem. 79:777-802.

2. Palade G. 1975. Intracellular aspects of the process of protein synthesis. Science. 189(4206):867.

3. Voeltz GK, Rolls MM, Rapoport TA. 2002. Structural organization of the endoplasmic reticulum. EMBO Rep. 3(10):944-950.

4. Kalies KU, Hartmann E. 1998. Protein translocation into the endoplasmic reticulum (ER)--two similar routes with different modes. Eur J Biochem. 254(1):1-5.

5. Neuhof A, Rolls MM, Jungnickel B, Kalies KU, Rapoport TA. 1998. Binding of signal recognition particle gives ribosome/nascent chain complexes a competitive advantage in endoplasmic reticulum membrane interaction. Mol Biol Cell. 9(1):103-115.

6. Wilkinson BM, Regnacq M, Stirling CJ. 1997. Protein translocation across the membrane of the endoplasmic reticulum. J Membr Biol. 155(3):189-197.

7. Bannykh SI, Rowe T, Balch WE. 1996. The organization of endoplasmic reticulum export complexes. J Cell Biol. 135(1):19-35.

8. Budnik A, Stephens DJ. 2009. ER exit sites--localization and control of COPII vesicle formation. FEBS Lett. 583(23):3796-3803.

9. Levine T, Loewen C. 2006. Inter-organelle membrane contact sites: through a glass, darkly. Curr Opin Cell Biol. 18(4):371-378.

10. Barlowe C, Orci L, Yeung T, Hosobuchi M, Hamamoto S, Salama N, Rexach MF, Ravazzola M, Amherdt M, Schekman R. 1994. COPII: a membrane coat formed by Sec proteins that drive vesicle budding from the endoplasmic reticulum. Cell. 77(6):895-907.

11. Mironov AA, Mironov AA, Beznoussenko GV, Trucco A, Lupetti P, Smith JD, Geerts WJC, Koster AJ, Burger KNJ, Martone ME, Deerinck TJ, Ellisman MH, Luini A. 2003. ER-to-golgi carriers arise through direct en bloc protrusion and multistage maturation of specialized ER exit domains. Developmental Cell. 5(4):583-594.

12. Gurkan C, Stagg SM, Lapointe P, Balch WE. 2006. The COPII cage: unifying principles of vesicle coat assembly. Nat Rev Mol Cell Biol. 7(10):727-738.

13. Saraste J, Kuismanen E. 1984. Pre- and post-Golgi vacuoles operate in the transport of Semliki Forest virus membrane glycoproteins to the cell surface. Cell. 38(2):535-549.

14. Saraste J, Svensson K. 1991. Distribution of the intermediate elements operating in ER to Golgi transport. J Cell Sci. 100 (Pt 3):415-430.

15. Schweizer A, Fransen J, Matter K, Kreis T, Ginsel L, Hauri H. 1990. Identification of an intermediate compartment involved in protein transport from endoplasmic reticulum to Golgi apparatus. Eur J Cell Biol. 53(2):185-196.

16. Aridor M, Bannykh SI, Rowe T, Balch WE. 1995. Sequential coupling between COPII and COPI vesicle coats in endoplasmic reticulum to Golgi transport. J Cell Biol. 131(4):875-893.

17. Xu D, Hay JC. 2004. Reconstitution of COPII vesicle fusion to generate a pre-Golgi intermediate compartment. J Cell Biol. 167(6):997-1003.

18. Bannykh SI, Balch WE. 1997. Membrane dynamics at the endoplasmic reticulum-Golgi interface. J Cell Biol. 138(1):1-4.

19. Bannykh SI, Balch WE. 1998. Selective transport of cargo between the endoplasmic reticulum and Golgi compartments. Histochem Cell Biol. 109(5-6):463-475.

20. Munro S, Pelham H. 1987. A C-terminal signal prevents secretion of luminal ER proteins. Cell. 48(5):899-907.

21. Sannerud R, Saraste J, Goud B. 2003. Retrograde traffic in the biosynthetic-secretory route: pathways and machinery. Curr Opin Cell Biol. 15(4):438-445.

22. Pelham HR. 1995. Sorting and retrieval between the endoplasmic reticulum and Golgi apparatus. Curr Opin Cell Biol. 7(4):530-535.

23. Martinez-Menarguez JA, Prekeris R, Oorschot VM, Scheller R, Slot JW, Geuze HJ, Klumperman J. 2001. Peri-Golgi vesicles contain retrograde but not anterograde proteins consistent with the cisternal progression model of intra-Golgi transport. J Cell Biol. 155(7):1213-1224.

24. Bonifacino JS, Glick BS. 2004. The mechanisms of vesicle budding and fusion. Cell. 116(2):153-166.

25. Klumperman J, Schweizer A, Clausen H, Tang B, Hong W, Oorschot V, Hauri H. 1998. The recycling pathway of protein ERGIC-53 and dynamics of the ER-Golgi intermediate compartment. J Cell Sci. 111 (Pt 22):3411-3425.

26. White J, Johannes L, Mallard F, Girod A, Grill S, Reinsch S, Keller P, Tzschaschel B, Echard A, Goud B, Stelzer EH. 1999. Rab6 coordinates a novel

Golgi to ER retrograde transport pathway in live cells. J Cell Biol. 147(4):743-760.

27. Stephens DJ, Pepperkok R. 2001. Illuminating the secretory pathway: when do we need vesicles? J Cell Sci. 114(Pt 6):1053-1059.

28. Appenzeller-Herzog C, Hauri HP. 2006. The ER-Golgi intermediate compartment (ERGIC): in search of its identity and function. J Cell Sci. 119(Pt 11):2173-2183.

29. Lippincott-Schwartz J. 1993. Bidirectional membrane traffic between the endoplasmic reticulum and Golgi apparatus. Trends Cell Biol. 3(3):81-88.

30. Hauri HP, Kappeler F, Andersson H, Appenzeller C. 2000. ERGIC-53 and traffic in the secretory pathway. J Cell Sci. 113 (Pt 4):587-596.

31. Orci L, Montesano R, Meda P, Malaisse-Lagae F, Brown D, Perrelet A, Vassalli P. 1981. Heterogeneous distribution of filipin--cholesterol complexes across the cisternae of the Golgi apparatus. Proc Natl Acad Sci U S A. 78(1):293-297.

32. Cluett E, Kuismanen E, Machamer C. 1997. Heterogeneous distribution of the unusual phospholipid semilysobisphosphatidic acid through the Golgi complex. Mol Biol Cell. 8(11):2233-2240.

33. Dunphy W, Rothman J. 1985. Compartmental organization of the Golgi stack. Cell. 42(1):13-21.

34. Wu X, Zhao X, Baylor L, Kaushal S, Eisenberg E, Greene LE. 2001. Clathrin exchange during clathrin-mediated endocytosis. J Cell Biol. 155(2):291-300.

35. Polishchuk R, Mironov A. 2004. Structural aspects of Golgi function. Cell Mol Life Sci. 61(2):146-158.

36. Neutra M, Leblond CP. 1966. Radioautographic comparison of the uptake of galactose-H and glucose-H3 in the golgi region of various cells secreting glycoproteins or mucopolysaccharides. J Cell Biol. 30(1):137-150.

37. Novikoff AB, Goldfischer S. 1961. Nucleosidediphosphatase activity in the Golgi apparatus and its usefulness for cytological studies. Proc Natl Acad Sci U S A. 47:802-810.

38. Kornfeld R, Kornfeld S. 1985. Assembly of asparagine-linked oligosaccharides. Annu Rev Biochem. 54:631-664.

39. Dunphy W, Fries E, Urbani L, Rothman J. 1981. Early and late functions associated with the Golgi apparatus reside in distinct compartments. Proc Natl Acad Sci U S A. 78(12):7453-7457.

40. Dunphy WG, Rothman JE. 1983. Compartmentation of asparagine-linked oligosaccharide processing in the Golgi apparatus. J Cell Biol. 97(1):270-275.

41. Rambourg A, Clermont Y, Hermo L. 1979. Three-dimensional architecture of the golgi apparatus in Sertoli cells of the rat. Am J Anat. 154(4):455-476.

42. Sasaki T, Motegi N, Higashi S. 1984. Morphological analysis of the Golgi apparatus in rat amelogenesis as revealed by the Ur-Pb-Cu block staining method and freeze-fracture replication. J Electron Microsc (Tokyo). 33(1):19-33.

43. Ladinsky MS, Kremer JR, Furcinitti PS, McIntosh JR, Howell KE. 1994. HVEM tomography of the trans-Golgi network: structural insights and identification of a lace-like vesicle coat. J Cell Biol. 127(1):29-38.

44. Griffiths G, Pfeiffer S, Simons K, Matlin K. 1985. Exit of newly synthesized membrane proteins from the trans cisterna of the Golgi complex to the plasma membrane. J Cell Biol. 101(3):949-964.

45. Rambourg A, Clermont Y. 1990. Three-dimensional electron microscopy: structure of the Golgi apparatus. Eur J Cell Biol. 51(2):189-200.

46. Marsh B, Volkmann N, McIntosh J, Howell K. 2004. Direct continuities between cisternae at different levels of the Golgi complex in glucose-stimulated mouse islet beta cells. Proc Natl Acad Sci U S A. 101(15):5565-5570.

47. Trucco A, Polishchuk RS, Martella O, Di Pentima A, Fusella A, Di Giandomenico D, San Pietro E, Beznoussenko GV, Polishchuk EV, Baldassarre M, Buccione R, Geerts WJ, Koster AJ, Burger KN, Mironov AA, Luini A. 2004. Secretory traffic triggers the formation of tubular continuities across Golgi sub-compartments. Nat Cell Biol. 6(11):1071-1081.

48. Sesso A, Azimovas SR, Ferreira MA. 1994. Freeze-fracture and thin section study of the rough ER-Golgi interface in the pancreatic acinar cell. Resemblance between the intramembranal architecture of the outermost Golgi cisterna and the post-rough ER vesicular and tubular elements. Biol Cell. 81(2):165-176.

49. Tanaka K, Mitsushima A, Fukudome H, Kashima Y. 1986. Three-dimensional architecture of the Golgi complex observed by high resolution scanning electron microscopy. J Submicrosc Cytol. 18(1):1-9.

50. Marsh B. 2005. Lessons from tomographic studies of the mammalian Golgi. Biochim Biophys Acta. 1744(3):273-292.

51. Hawes C, Brandizzi F. 2004. The Golgi apparatus--still causing problems after all these years! Cell Mol Life Sci. 61(2):131-132.

52. Kondylis V, Rabouille C. 2009. The Golgi apparatus: Lessons from Drosophila. FEBS Letters. 583(23):3827-3838.

53. Faso C, Boulaflous A, Brandizzi F. 2009. The plant Golgi apparatus: Last 10 years of answered and open questions. FEBS Letters. 583(23):3752-3757.

54. Papanikou E, Glick BS. 2009. The yeast Golgi apparatus: Insights and mysteries. FEBS Letters. 583(23):3746-3751.

55. Mowbrey K, Dacks JB. 2009. Evolution and diversity of the Golgi body. FEBS Letters. 583(23):3738-3745.

56. Taylor RS, Fialka I, Jones SM, Huber LA, Howell KE. 1997. Two-dimensional mapping of the endogenous proteins of the rat hepatocyte Golgi complex cleared of proteins in transit. Electrophoresis. 18(14):2601-2612.

57. Aridor M, Bannykh SI, Rowe T, Balch WE. 1999. Cargo can modulate COPII vesicle formation from the endoplasmic reticulum. J Biol Chem. 274(7):4389-4399.

58. Rambourg A, Clermont Y, Chretien M, Olivier L. 1993. Modulation of the Golgi apparatus in stimulated and nonstimulated prolactin cells of female rats. Anat Rec. 235(3):353-362.

59. Mollenhauer HH. 1965. An Intercisternal Structure in the Golgi Apparatus. J Cell Biol. 24(3):504-511.

60. Franke WW, Kartenbeck J, Krien S, VanderWoude WJ, Scheer U, Morre DJ. 1972. Inter- and intracisternal elements of the Golgi apparatus. A system of membrane-to-membrane cross-links. Z Zellforsch Mikrosk Anat. 132(3):365-380.

61. Slusarewicz P, Nilsson T, Hui N, Watson R, Warren G. 1994. Isolation of a matrix that binds medial Golgi enzymes. J Cell Biol. 124(4):405-413.

62. Cluett E, Brown W. 1992. Adhesion of Golgi cisternae by proteinaceous interactions: intercisternal bridges as putative adhesive structures. J Cell Sci. 103 (Pt 3):773-784.

63. Barr F, Short B. 2003. Golgins in the structure and dynamics of the Golgi apparatus. Curr Opin Cell Biol. 15(4):405-413.

64. Corthesy-Theulaz I, Pauloin A, Pfeffer SR. 1992. Cytoplasmic dynein participates in the centrosomal localization of the Golgi complex. J Cell Biol. 118(6):1333-1345.

65. Harada A, Takei Y, Kanai Y, Tanaka Y, Nonaka S, Hirokawa N. 1998. Golgi vesiculation and lysosome dispersion in cells lacking cytoplasmic dynein. J Cell Biol. 141(1):51-59.

66. Burkhardt JK, Echeverri CJ, Nilsson T, Vallee RB. 1997. Overexpression of the dynamitin (p50) subunit of the dynactin complex disrupts dynein-dependent maintenance of membrane organelle distribution. J Cell Biol. 139(2):469-484.

67. Ho W, Allan V, van Meer G, Berger E, Kreis T. 1989. Reclustering of scattered Golgi elements occurs along microtubules. Eur J Cell Biol. 48(2):250-263.

68. Brownhill K, Wood L, Allan V. 2009. Molecular motors and the Golgi complex: Staying put and moving through. Semin Cell Dev Biol.

69. Zaal KJ, Smith CL, Polishchuk RS, Altan N, Cole NB, Ellenberg J, Hirschberg K, Presley JF, Roberts TH, Siggia E, Phair RD, Lippincott-Schwartz J. 1999. Golgi membranes are absorbed into and reemerge from the ER during mitosis. Cell. 99(6):589-601.

70. Thyberg J, Moskalewski S. 1992. Reorganization of the Golgi complex in association with mitosis: redistribution of mannosidase II to the endoplasmic reticulum and effects of brefeldin A. J Submicrosc Cytol Pathol. 24(4):495-508.

71. Altan-Bonnet N, Sougrat R, Lippincott-Schwartz J. 2004. Molecular basis for Golgi maintenance and biogenesis. Curr Opin Cell Biol. 16(4):364-372.

72. Altan-Bonnet N, Sougrat R, Liu W, Snapp EL, Ward T, Lippincott-Schwartz J. 2006. Golgi inheritance in mammalian cells is mediated through endoplasmic reticulum export activities. Mol Biol Cell. 17(2):990-1005.

73. Lippincott-Schwartz J, Zaal KJ. 2000. Cell cycle maintenance and biogenesis of the Golgi complex. Histochem Cell Biol. 114(2):93-103.

74. Lucocq JM, Berger EG, Warren G. 1989. Mitotic Golgi fragments in HeLa cells and their role in the reassembly pathway. J Cell Biol. 109(2):463-474.

75. Kreis TE. 1990. Role of microtubules in the organisation of the Golgi apparatus. Cell Motil Cytoskeleton. 15(2):67-70.

76. Warren G. 1993. Membrane partitioning during cell division. Annu Rev Biochem. 62:323-348.

77. Jokitalo E, Cabrera-Poch N, Warren G, Shima DT. 2001. Golgi clusters and vesicles mediate mitotic inheritance independently of the endoplasmic reticulum. J Cell Biol. 154(2):317-330.

78. de Figueiredo P, Polizotto R, Drecktrah D, Brown W. 1999. Membrane tubule-mediated reassembly and maintenance of the Golgi complex is disrupted by phospholipase A2 antagonists. Mol Biol Cell. 10(6):1763-1782.

79. Judson BL, Brown WJ. 2009. Assembly of an intact Golgi complex requires phospholipase A2 (PLA2) activity, membrane tubules, and dynein-mediated microtubule transport. Biochem Biophys Res Commun. 389(3):473-477.

80. Allan BB, Balch WE. 1999. Protein sorting by directed maturation of Golgi compartments. Science. 285(5424):63-66.

81. Pelham H. 2006. Maturation of Golgi cisternae directly observed. Trends Biochem Sci. 31(11):601-604.

82. Glick BS. 2000. Organization of the Golgi apparatus. Curr Opin Cell Biol. 12(4):450-456.

83. Rabouille C, Kondylis V. 2006. TANGOing along the protein secretion pathway. Genome Biol. 7(4):213.

84. Emr S, Glick BS, Linstedt AD, Lippincott-Schwartz J, Luini A, Malhotra V, Marsh BJ, Nakano A, Pfeffer SR, Rabouille C, Rothman JE, Warren G, Wieland FT. 2009. Journeys through the Golgi--taking stock in a new era. J Cell Biol. 187(4):449-453.

85. Gilchrist A, Au C, Hiding J, Bell A, Fernandez-Rodriguez J, Lesimple S, Nagaya H, Roy L, Gosline S, Hallett M, Paiement J, Kearney R, Nilsson T, Bergeron J. 2006. Quantitative proteomics analysis of the secretory pathway. Cell. 127(6):1265-1281.

86. Orci L, Amherdt M, Ravazzola M, Perrelet A, Rothman JE. 2000. Exclusion of golgi residents from transport vesicles budding from Golgi cisternae in intact cells. J Cell Biol. 150(6):1263-1270.

87. Cosson P, Amherdt M, Rothman JE, Orci L. 2002. A resident Golgi protein is excluded from peri-Golgi vesicles in NRK cells. Proc Natl Acad Sci U S A. 99(20):12831-12834.

88. Glick B, Malhotra V. 1998. The curious status of the Golgi apparatus. Cell. 95(7):883-889.

89. Mollenhauer HH, Morre DJ. 1991. Perspectives on Golgi apparatus form and function. J Electron Microsc Tech. 17(1):2-14.

90. Losev E, Reinke CA, Jellen J, Strongin DE, Bevis BJ, Glick BS. 2006. Golgi maturation visualized in living yeast. Nature. 441(7096):1002-1006.

91. Matsuura-Tokita K, Takeuchi M, Ichihara A, Mikuriya K, Nakano A. 2006. Live imaging of yeast Golgi cisternal maturation. Nature. 441(7096):1007-1010.

92. Bonfanti L, Mironov AA, Jr., Martinez-Menarguez JA, Martella O, Fusella A, Baldassarre M, Buccione R, Geuze HJ, Mironov AA, Luini A. 1998. Procollagen traverses the Golgi stack without leaving the lumen of cisternae: evidence for cisternal maturation. Cell. 95(7):993-1003.

93. Becker B, Bolinger B, Melkonian M. 1995. Anterograde transport of algal scales through the Golgi complex is not mediated by vesicles. Trends Cell Biol. 5(8):305-307.

94. Patterson G, Hirschberg K, Polishchuk R, Gerlich D, Phair R, Lippincott-Schwartz J. 2008. Transport through the Golgi apparatus by rapid partitioning within a two-phase membrane system. Cell. 133(6):1055-1067.

95. Jackson CL. 2009. Mechanisms of transport through the Golgi complex. J Cell Sci. 122(Pt 4):443-452.

96. De Matteis MA, Luini A. 2008. Exiting the Golgi complex. Nat Rev Mol Cell Biol. 9(4):273-284.

97. Bard F, Malhotra V. 2006. The formation of TGN-to-plasma-membrane transport carriers. Annu Rev Cell Dev Biol. 22:439-455.

98. Hirst J, Robinson M. 1998. Clathrin and adaptors. Biochim Biophys Acta. 1404(1-2):173-193.

99. Bonifacino JS, Traub LM. 2003. Signals for sorting of transmembrane proteins to endosomes and lysosomes. Annu Rev Biochem. 72:395-447.

100. Rodriguez-Boulan E, Musch A. 2005. Protein sorting in the Golgi complex: shifting paradigms. Biochim Biophys Acta. 1744(3):455-464.

101. Weisz OA, Rodriguez-Boulan E. 2009. Apical trafficking in epithelial cells: signals, clusters and motors. J Cell Sci. 122(Pt 23):4253-4266.

102. Gonzalez A, Rodriguez-Boulan E. 2009. Clathrin and AP1B: Key roles in basolateral trafficking through trans-endosomal routes. FEBS Letters. 583(23):3784-3795.

103. Ang AL, Fölsch H, Koivisto U-M, Pypaert M, Mellman I. 2003. The Rab8 GTPase selectively regulates AP-1B-dependent basolateral transport in polarized Madin-Darby canine kidney cells. J Cell Biol. 163(2):339-350.

104. Ang AL, Taguchi T, Francis S, Fölsch H, Murrells LJ, Pypaert M, Warren G, Mellman I. 2004. Recycling endosomes can serve as intermediates

during transport from the Golgi to the plasma membrane of MDCK cells. J Cell Biol. 167(3):531-543.

105. Folsch H, Ohno H, Bonifacino JS, Mellman I. 1999. A novel clathrin adaptor complex mediates basolateral targeting in polarized epithelial cells. Cell. 99(2):189-198.

106. Fölsch H, Pypaert M, Schu P, Mellman I. 2001. Distribution and function of AP-1 clathrin adaptor complexes in polarized epithelial cells. J Cell Biol. 152(3):595-606.

107. Ladinsky MS, Mastronarde DN, McIntosh JR, Howell KE, Staehelin LA. 1999. Golgi structure in three dimensions: functional insights from the normal rat kidney cell. J Cell Biol. 144(6):1135-1149.

108. Polishchuk E, Di Pentima A, Luini A, Polishchuk R. 2003. Mechanism of constitutive export from the Golgi: Bulk flow via the formation, protrusion, and en bloc cleavage of large trans-golgi network tubular domains. Mol Biol Cell. 14(11):4470-4485.

109. Toomre D, Keller P, White J, Olivo JC, Simons K. 1999. Dual-color visualization of trans-Golgi network to plasma membrane traffic along microtubules in living cells. J Cell Sci. 112 (Pt 1):21-33.

110. Keller P, Toomre D, Díaz E, White J, Simons K. 2001. Multicolour imaging of post-Golgi sorting and trafficking in live cells. Nat Cell Biol. 3(2):140-149.

111. Benting JH, Rietveld AG, Simons K. 1999. N-Glycans mediate the apical sorting of a GPI-anchored, raft-associated protein in Madin-Darby canine kidney cells. J Cell Biol. 146(2):313-320.

112. Schuck S, Simons K. 2004. Polarized sorting in epithelial cells: raft clustering and the biogenesis of the apical membrane. J Cell Sci. 117(Pt 25):5955-5964.

113. Dunn K, McGraw T, Maxfield F. 1989. Iterative fractionation of recycling receptors from lysosomally destined ligands in an early sorting endosome. J Cell Biol. 109(6 Pt 2):3303-3314.

114. Steinman RM, Mellman IS, Muller WA, Cohn ZA. 1983. Endocytosis and the recycling of plasma membrane. J Cell Biol. 96(1):1-27.

115. Maxfield FR, McGraw TE. 2004. Endocytic recycling. Nat Rev Mol Cell Biol. 5(2):121-132.

116. Gruenberg J. 2001. The endocytic pathway: a mosaic of domains. Nat Rev Mol Cell Biol. 2(10):721-730.

117. Doherty GJ, McMahon HT. 2009. Mechanisms of endocytosis. Annu Rev Biochem. 78:857-902.

118. Mayor S, Pagano RE. 2007. Pathways of clathrin-independent endocytosis. Nat Rev Mol Cell Biol. 8(8):603-612.

119. Zerial M, McBride H. 2001. Rab proteins as membrane organizers. Nat Rev Mol Cell Biol. 2(2):107-117.

120. Gruenberg J, Stenmark H. 2004. The biogenesis of multivesicular endosomes. Nat Rev Mol Cell Biol. 5(4):317-323.

121. Grant BD, Donaldson JG. 2009. Pathways and mechanisms of endocytic recycling. Nat Rev Mol Cell Biol. 10(9):597-608.

122. Saftig P, Klumperman J. 2009. Lysosome biogenesis and lysosomal membrane proteins: trafficking meets function. Nat Rev Mol Cell Biol. 10(9):623-635.

123. Gillooly DJ, Morrow IC, Lindsay M, Gould R, Bryant NJ, Gaullier JM, Parton RG, Stenmark H. 2000. Localization of phosphatidylinositol 3-phosphate in yeast and mammalian cells. EMBO J. 19(17):4577-4588.

124. Duclos S, Corsini R, Desjardins M. 2003. Remodeling of endosomes during lysosome biogenesis involves 'kiss and run' fusion events regulated by rab5. J Cell Sci. 116(Pt 5):907-918.

125. Storrie B, Desjardins M. 1996. The biogenesis of lysosomes: is it a kiss and run, continuous fusion and fission process? Bioessays. 18(11):895-903.

126. Stoorvogel W, Geuze HJ, Strous GJ. 1987. Sorting of endocytosed transferrin and asialoglycoprotein occurs immediately after internalization in HepG2 cells. J Cell Biol. 104(5):1261-1268.

127. Geuze H, Slot J, Strous G, Lodish H, Schwartz A. 1983. Intracellular site of asialoglycoprotein receptor-ligand uncoupling: double-label immunoelectron microscopy during receptor-mediated endocytosis. Cell. 32(1):277-287.

128. Bomsel M, Parton R, Kuznetsov SA, Schroer TA, Gruenberg J. 1990. Microtubule- and motor-dependent fusion in vitro between apical and basolateral endocytic vesicles from MDCK cells. Cell. 62(4):719-731.

129. Aniento F, Emans N, Griffiths G, Gruenberg J. 1993. Cytoplasmic dynein-dependent vesicular transport from early to late endosomes. J Cell Biol. 123(6 Pt 1):1373-1387.

130. Hicke L. 2001. A new ticket for entry into budding vesicles-ubiquitin. Cell. 106(5):527-530.

131. Babst M, Katzmann DJ, Snyder WB, Wendland B, Emr SD. 2002. Endosome-associated complex, ESCRT-II, recruits transport machinery for protein sorting at the multivesicular body. Dev Cell. 3(2):283-289.

132. Nickerson DP, Russell MR, Odorizzi G. 2007. A concentric circle model of multivesicular body cargo sorting. EMBO Rep. 8(7):644-650.

133. Raiborg C, Stenmark H. 2009. The ESCRT machinery in endosomal sorting of ubiquitylated membrane proteins. Nature. 458(7237):445-452.

134. Katzmann DJ, Odorizzi G, Emr SD. 2002. Receptor downregulation and multivesicular-body sorting. Nat Rev Mol Cell Biol. 3(12):893-905.

135. Kobayashi T, Gu F, Gruenberg J. 1998. Lipids, lipid domains and lipid-protein interactions in endocytic membrane traffic. Semin Cell Dev Biol. 9(5):517-526.

136. Matsuo H, Chevallier J, Mayran N, Le Blanc I, Ferguson C, Fauré J, Blanc NS, Matile S, Dubochet J, Sadoul R, Parton RG, Vilbois F, Gruenberg J. 2004. Role of LBPA and Alix in multivesicular liposome formation and endosome organization. Science. 303(5657):531-534.

137. Odorizzi G, Babst M, Emr SD. 1998. Fab1p PtdIns(3)P 5-kinase function essential for protein sorting in the multivesicular body. Cell. 95(6):847-858.

138. Sbrissa D, Ikonomov OC, Shisheva A. 2002. Phosphatidylinositol 3-phosphate-interacting domains in PIKfyve. Binding specificity and role in PIKfyve. Endomenbrane localization. J Biol Chem. 277(8):6073-6079.

139. Shisheva A. 2008. PIKfyve: Partners, significance, debates and paradoxes. Cell Biol Int. 32(6):591-604.

140. Gruenberg J, Maxfield F. 1995. Membrane transport in the endocytic pathway. Curr Opin Cell Biol. 7(4):552-563.

141. Griffiths G, Hoflack B, Simons K, Mellman I, Kornfeld S. 1988. The mannose 6-phosphate receptor and the biogenesis of lysosomes. Cell. 52(3):329-341.

142. Mullock BM, Bright NA, Fearon CW, Gray SR, Luzio JP. 1998. Fusion of lysosomes with late endosomes produces a hybrid organelle of intermediate density and is NSF dependent. J Cell Biol. 140(3):591-601.

143. Sheff D, Daro E, Hull M, Mellman I. 1999. The receptor recycling pathway contains two distinct populations of early endosomes with different sorting functions. J Cell Biol. 145(1):123-139.

144. Hao M, Maxfield F. 2000. Characterization of rapid membrane internalization and recycling. J Biol Chem. 275(20):15279-15286.

145. Mayor S, Presley JF, Maxfield FR. 1993. Sorting of membrane components from endosomes and subsequent recycling to the cell surface occurs by a bulk flow process. J Cell Biol. 121(6):1257-1269.

146. Yamashiro DJ, Tycko B, Fluss SR, Maxfield FR. 1984. Segregation of transferrin to a mildly acidic (pH 6.5) para-Golgi compartment in the recycling pathway. Cell. 37(3):789-800.

147. Apodaca G, Katz LA, Mostov KE. 1994. Receptor-mediated transcytosis of IgA in MDCK cells is via apical recycling endosomes. J Cell Biol. 125(1):67-86.

148. Cullen PJ. 2008. Endosomal sorting and signalling: an emerging role for sorting nexins. Nat Rev Mol Cell Biol. 9(7):574-582.

149. Grant BD, Caplan S. 2008. Mechanisms of EHD/RME-1 protein function in endocytic transport. Traffic. 9(12):2043-2052.

150. van Weering JR, Verkade P, Cullen PJ. 2010. SNX-BAR proteins in phosphoinositide-mediated, tubular-based endosomal sorting. Semin Cell Dev Biol. 21(4):371-380.

151. Seaman MN, McCaffery JM, Emr SD. 1998. A membrane coat complex essential for endosome-to-Golgi retrograde transport in yeast. J Cell Biol. 142(3):665-681.

152. Bonifacino JS, Rojas R. 2006. Retrograde transport from endosomes to the trans-Golgi network. Nat Rev Mol Cell Biol. 7(8):568-579.

153. Seaman MN. 2005. Recycle your receptors with retromer. Trends Cell Biol. 15(2):68-75.

154. Bonifacino JS, Hurley JH. 2008. Retromer. Curr Opin Cell Biol. 20(4):427-436.

155. Pfeffer SR. 2009. Multiple routes of protein transport from endosomes to the trans Golgi network. FEBS Letters. 583(23):3811-3816.

156. Jovic M, Sharma M, Rahajeng J, Caplan S. 2010. The early endosome: a busy sorting station for proteins at the crossroads. Histol Histopathol. 25(1):99-112.

157. Munro S. 2003. Cell biology: earthworms and lipid couriers. Nature. 426(6968):775-776.

158. Polishchuk RS, Capestrano M, Polishchuk EV. 2009. Shaping tubular carriers for intracellular membrane transport. FEBS Letters. 583(23):3847-3856.

159. van Meer G, Voelker DR, Feigenson GW. 2008. Membrane lipids: where they are and how they behave. Nat Rev Mol Cell Biol. 9(2):112-124.

160. Bonifacino JS, Lippincott-Schwartz J. 2003. Coat proteins: shaping membrane transport. Nat Rev Mol Cell Biol. 4(5):409-414.

161. Pearse BM. 1976. Clathrin: a unique protein associated with intracellular transfer of membrane by coated vesicles. Proc Natl Acad Sci U S A. 73(4):1255-1259.

162. Novick P, Field C, Schekman R. 1980. Identification of 23 complementation groups required for post-translational events in the yeast secretory pathway. Cell. 21(1):205-215.

163. Kaiser CA, Schekman R. 1990. Distinct sets of SEC genes govern transport vesicle formation and fusion early in the secretory pathway. Cell. 61(4):723-733.

164. Balch W, Dunphy W, Braell W, Rothman J. 1984. Reconstitution of the transport of protein between successive compartments of the Golgi measured by the coupled incorporation of N-acetylglucosamine. Cell. 39(2 Pt 1):405-416.

165. Orci L, Glick BS, Rothman JE. 1986. A new type of coated vesicular carrier that appears not to contain clathrin: its possible role in protein transport within the Golgi stack. Cell. 46(2):171-184.

166. Sudhof TC, Rothman JE. 2009. Membrane fusion: grappling with SNARE and SM proteins. Science. 323(5913):474-477.

167. McMahon HT, Gallop JL. 2005. Membrane curvature and mechanisms of dynamic cell membrane remodelling. Nature. 438(7068):590-596.

168. Peng R, De Antoni A, Gallwitz D. 2000. Evidence for overlapping and distinct functions in protein transport of coat protein Sec24p family members. J Biol Chem. 275(15):11521-11528.

169. Roberg KJ, Crotwell M, Espenshade P, Gimeno R, Kaiser CA. 1999. LST1 is a SEC24 homologue used for selective export of the plasma membrane ATPase from the endoplasmic reticulum. J Cell Biol. 145(4):659-672.

170. Shimoni Y, Kurihara T, Ravazzola M, Amherdt M, Orci L, Schekman R. 2000. Lst1p and Sec24p cooperate in sorting of the plasma membrane ATPase into COPII vesicles in Saccharomyces cerevisiae. J Cell Biol. 151(5):973-984.

171. Moelleken J, Malsam J, Betts MJ, Movafeghi A, Reckmann I, Meissner I, Hellwig A, Russell RB, Sollner T, Brugger B, Wieland FT. 2007. Differential localization of coatomer complex isoforms within the Golgi apparatus. Proc Natl Acad Sci U S A. 104(11):4425-4430.

172. Clermont Y, Rambourg A, Hermo L. 1994. Connections between the various elements of the cis- and mid-compartments of the Golgi apparatus of early rat spermatids. Anat Rec. 240(4):469-480.

173. Clermont Y, Rambourg A, Hermo L. 1995. Trans-Golgi network (TGN) of different cell types: three-dimensional structural characteristics and variability. Anat Rec. 242(3):289-301.

174. Cunningham WP, Morre DJ, Mollenhauer HH. 1966. Structure of isolated plant Golgi apparatus revealed by negative staining. J Cell Biol. 28(2):169-179.

175. Marsh M, Griffiths G, Dean GE, Mellman I, Helenius A. 1986. Three-dimensional structure of endosomes in BHK-21 cells. Proc Natl Acad Sci U S A. 83(9):2899-2903.

176. Lippincott-Schwartz J, Yuan L, Bonifacino J, Klausner R. 1989. Rapid redistribution of Golgi proteins into the ER in cells treated with brefeldin A: evidence for membrane cycling from Golgi to ER. Cell. 56(5):801-813.

177. Cooper MS, Cornell-Bell AH, Chernjavsky A, Dani JW, Smith SJ. 1990. Tubulovesicular processes emerge from trans-Golgi cisternae, extend along microtubules, and interlink adjacent trans-golgi elements into a reticulum. Cell. 61(1):135-145.

178. Sciaky N, Presley J, Smith C, Zaal KJ, Cole N, Moreira JE, Terasaki M, Siggia E, Lippincott-Schwartz J. 1997. Golgi tubule traffic and the effects of brefeldin A visualized in living cells. J Cell Biol. 139(5):1137-1155.

179. Presley JF, Cole NB, Schroer TA, Hirschberg K, Zaal KJ, Lippincott-Schwartz J. 1997. ER-to-Golgi transport visualized in living cells. Nature. 389(6646):81-85.

180. Presley JF, Smith C, Hirschberg K, Miller C, Cole NB, Zaal KJ, Lippincott-Schwartz J. 1998. Golgi membrane dynamics. Mol Biol Cell. 9(7):1617-1626.

181. Hirschberg K, Miller C, Ellenberg J, Presley J, Siggia E, Phair R, Lippincott-Schwartz J. 1998. Kinetic analysis of secretory protein traffic and characterization of golgi to plasma membrane transport intermediates in living cells. J Cell Biol. 143(6):1485-1503.

182. Lippincott-Schwartz J, Roberts TH, Hirschberg K. 2000. Secretory protein trafficking and organelle dynamics in living cells. Annu Rev Cell Dev Biol. 16:557-589.

183. Blum R, Stephens DJ, Schulz I. 2000. Lumenal targeted GFP, used as a marker of soluble cargo, visualises rapid ERGIC to Golgi traffic by a tubulo-vesicular network. J Cell Sci. 113 (Pt 18):3151-3159.

184. Janvier K, Bonifacino JS. 2005. Role of the endocytic machinery in the sorting of lysosome-associated membrane proteins. Mol Biol Cell. 16(9):4231-4242.

185. Polishchuk RS, Polishchuk EV, Marra P, Alberti S, Buccione R, Luini A, Mironov AA. 2000. Correlative light-electron microscopy reveals the tubular-saccular ultrastructure of carriers operating between Golgi apparatus and plasma membrane. J Cell Biol. 148(1):45-58.

186. Puertollano R, Aguilar RC, Gorshkova I, Crouch RJ, Bonifacino JS. 2001. Sorting of mannose 6-phosphate receptors mediated by the GGAs. Science. 292(5522):1712-1716.

187. Orci L, Tagaya M, Amherdt M, Perrelet A, Donaldson J, Lippincott-Schwartz J, Klausner R, Rothman J. 1991. Brefeldin A, a drug that blocks secretion, prevents the assembly of non-clathrin-coated buds on Golgi cisternae. Cell. 64(6):1183-1195.

188. Simpson JC, Nilsson T, Pepperkok R. 2006. Biogenesis of tubular ER-to-Golgi transport intermediates. Mol Biol Cell. 17(2):723-737.

189. Waguri S, Dewitte F, Le Borgne R, Rouille Y, Uchiyama Y, Dubremetz JF, Hoflack B. 2003. Visualization of TGN to endosome trafficking through fluorescently labeled MPR and AP-1 in living cells. Mol Biol Cell. 14(1):142-155.

190. Mukherjee S, Soe T, Maxfield F. 1999. Endocytic sorting of lipid analogues differing solely in the chemistry of their hydrophobic tails. J Cell Biol. 144(6):1271-1284.

191. Klumperman J, Hille A, Veenendaal T, Oorschot V, Stoorvogel W, von Figura K, Geuze H. 1993. Differences in the endosomal distributions of the two mannose 6-phosphate receptors. J Cell Biol. 121(5):997-1010.

192. Geuze HJ, Slot JW, Strous GJ, Peppard J, von Figura K, Hasilik A, Schwartz AL. 1984. Intracellular receptor sorting during endocytosis: comparative immunoelectron microscopy of multiple receptors in rat liver. Cell. 37(1):195-204.

193. Geuze H, Slot J, Strous G, Schwartz A. 1983. The pathway of the asialoglycoprotein-ligand during receptor-mediated endocytosis: a morphological study with colloidal gold/ligand in the human hepatoma cell line, Hep G2. Eur J Cell Biol. 32(1):38-44.

194. Linderman J, Lauffenburger D. 1988. Analysis of intracellular receptor/ligand sorting in endosomes. J Theor Biol. 132(2):203-245.

195. Rome L. 1985. Curling receptors. Trends Biochem Sci. 10:151.

196. Mukherjee S, Ghosh R, Maxfield F. 1997. Endocytosis. Physiol Rev. 77(3):759-803.

197. Roux A, Cappello G, Cartaud J, Prost J, Goud B, Bassereau P. 2002. A minimal system allowing tubulation with molecular motors pulling on giant liposomes. Proc Natl Acad Sci USA. 99(8):5394-5399.

198. Zimmerberg J, Kozlov MM. 2006. How proteins produce cellular membrane curvature. Nat Rev Mol Cell Biol. 7(1):9-19.

199. Stagg SM, Gurkan C, Fowler DM, LaPointe P, Foss TR, Potter CS, Carragher B, Balch WE. 2006. Structure of the Sec13/31 COPII coat cage. Nature. 439(7073):234-238.

200. Antonny B. 2006. Membrane deformation by protein coats. Curr Opin Cell Biol. 18(4):386-394.

201. Pylypenko O, Lundmark R, Rasmuson E, Carlsson SR, Rak A. 2007. The PX-BAR membrane-remodeling unit of sorting nexin 9. Embo J. 26(22):4788-4800.

202. Cozier GE, Carlton J, McGregor AH, Gleeson PA, Teasdale RD, Mellor H, Cullen PJ. 2002. The phox homology (PX) domain-dependent, 3-phosphoinositide-mediated association of sorting nexin-1 with an early sorting endosomal compartment is required for its ability to regulate epidermal growth factor receptor degradation. J Biol Chem. 277(50):48730-48736.

203. Zhong Q, Lazar CS, Tronchere H, Sato T, Meerloo T, Yeo M, Songyang Z, Emr SD, Gill GN. 2002. Endosomal localization and function of sorting nexin 1. Proc Natl Acad Sci U S A. 99(10):6767-6772.

204. Carlton J, Bujny M, Peter BJ, Oorschot VM, Rutherford A, Mellor H, Klumperman J, McMahon HT, Cullen PJ. 2004. Sorting nexin-1 mediates tubular endosome-to-TGN transport through coincidence sensing of high-curvature membranes and 3-phosphoinositides. Curr Biol. 14(20):1791-1800.

205. Peter BJ, Kent HM, Mills IG, Vallis Y, Butler PJ, Evans PR, McMahon HT. 2004. BAR domains as sensors of membrane curvature: the amphiphysin BAR structure. Science. 303(5657):495-499.

206. Gallop JL, Jao CC, Kent HM, Butler PJ, Evans PR, Langen R, McMahon HT. 2006. Mechanism of endophilin N-BAR domain-mediated membrane curvature. Embo J. 25(12):2898-2910.

207. Masuda M, Takeda S, Sone M, Ohki T, Mori H, Kamioka Y, Mochizuki N. 2006. Endophilin BAR domain drives membrane curvature by two newly identified structure-based mechanisms. Embo J. 25(12):2889-2897.

208. Shimada A, Niwa H, Tsujita K, Suetsugu S, Nitta K, Hanawa-Suetsugu K, Akasaka R, Nishino Y, Toyama M, Chen L, Liu ZJ, Wang BC, Yamamoto M, Terada T, Miyazawa A, Tanaka A, Sugano S, Shirouzu M, Nagayama K, Takenawa T, Yokoyama S. 2007. Curved EFC/F-BAR-domain dimers are joined end to end into a filament for membrane invagination in endocytosis. Cell. 129(4):761-772.

209. Voeltz GK, Prinz WA. 2007. Sheets, ribbons and tubules - how organelles get their shape. Nat Rev Mol Cell Biol. 8(3):258-264.

210. Graham TR, Kozlov MM. 2010. Interplay of proteins and lipids in generating membrane curvature. Curr Opin Cell Biol. 22(4):430-436.

211. Itoh T, De Camilli P. 2006. BAR, F-BAR (EFC) and ENTH/ANTH domains in the regulation of membrane-cytosol interfaces and membrane curvature. Biochim Biophys Acta. 1761(8):897-912.

212. Shibata Y, Voss C, Rist JM, Hu J, Rapoport TA, Prinz WA, Voeltz GK. 2008. The reticulon and DP1/Yop1p proteins form immobile oligomers in the tubular endoplasmic reticulum. J Biol Chem. 283(27):18892-18904.

213. Takei K, Slepnev VI, Haucke V, De Camilli P. 1999. Functional partnership between amphiphysin and dynamin in clathrin-mediated endocytosis. Nat Cell Biol. 1(1):33-39.

214. Bielli A, Haney CJ, Gabreski G, Watkins SC, Bannykh SI, Aridor M. 2005. Regulation of Sar1 NH2 terminus by GTP binding and hydrolysis promotes membrane deformation to control COPII vesicle fission. J Cell Biol. 171(6):919-924.

215. Lee SY, Yang JS, Hong W, Premont RT, Hsu VW. 2005. ARFGAP1 plays a central role in coupling COPI cargo sorting with vesicle formation. J Cell Biol. 168(2):281-290.

216. Krauss M, Jia JY, Roux A, Beck R, Wieland FT, De Camilli P, Haucke V. 2008. Arf1-GTP-induced tubule formation suggests a function of Arf family proteins in curvature acquisition at sites of vesicle budding. J Biol Chem. 283(41):27717-27723.

217. Sheetz M, Singer S. 1974. Biological membranes as bilayer couples. A molecular mechanism of drug-erythrocyte interactions. Proc Natl Acad Sci U S A. 71(11):4457-4461.

218. Chernomordik LV, Kozlov MM. 2003. Protein-lipid interplay in fusion and fission of biological membranes. Annu Rev Biochem. 72:175-207.

219. van Meer G, Sprong H. 2004. Membrane lipids and vesicular traffic. Curr Opin Cell Biol. 16(4):373-378.

220. Burger KN. 2000. Greasing membrane fusion and fission machineries. Traffic. 1(8):605-613.

221. Kooijman E, Chupin V, Fuller N, Kozlov M, de Kruijff B, Burger K, Rand P. 2005. Spontaneous curvature of phosphatidic acid and lysophosphatidic acid. Biochemistry. 44(6):2097-2102.

222. Baron CL, Malhotra V. 2002. Role of diacylglycerol in PKD recruitment to the TGN and protein transport to the plasma membrane. Science. 295(5553):325-328.

223. Sato TK, Overduin M, Emr SD. 2001. Location, location, location: membrane targeting directed by PX domains. Science. 294(5548):1881-1885.

224. Kutateladze TG. 2010. Translation of the phosphoinositide code by PI effectors. Nature Chemical Biology. 6(7):507-513.

225. Levine TP, Munro S. 2002. Targeting of Golgi-specific pleckstrin homology domains involves both PtdIns 4-kinase-dependent and -independent components. Curr Biol. 12(9):695-704.

226. Itoh T, Takenawa T. 2002. Phosphoinositide-binding domains: Functional units for temporal and spatial regulation of intracellular signalling. Cell Signal. 14(9):733-743.

227. Di Paolo G, De Camilli P. 2006. Phosphoinositides in cell regulation and membrane dynamics. Nature. 443(7112):651-657.

228. Diaz Anel A. 2007. Phospholipase C beta3 is a key component in the Gbetagamma/PKCeta/PKD-mediated regulation of trans-Golgi network to plasma membrane transport. Biochem J. 406(1):157-165.

229. Goñi FM, Alonso A. 1999. Structure and functional properties of diacylglycerols in membranes. Prog Lipid Res. 38(1):1-48.

230. Shemesh T, Luini A, Malhotra V, Burger K, Kozlov M. 2003. Prefission constriction of Golgi tubular carriers driven by local lipid metabolism: A theoretical model. Biophys J. 85(6):3813-3827.

231. Freyberg Z, Sweeney D, Siddhanta A, Bourgoin S, Frohman M, Shields D. 2001. Intracellular localization of phospholipase D1 in mammalian cells. Mol Biol Cell. 12(4):943-955.

232. Freyberg Z, Siddhanta A, Shields D. 2003. "Slip, sliding away": phospholipase D and the Golgi apparatus. Trends Cell Biol. 13(10):540-546.

233. Ktistakis NT, Brown HA, Waters MG, Sternweis PC, Roth MG. 1996. Evidence that phospholipase D mediates ADP ribosylation factor-dependent formation of Golgi coated vesicles. J Cell Biol. 134(2):295-306.

234. Jovanovic OA, Brown FD, Donaldson JG. 2006. An effector domain mutant of Arf6 implicates phospholipase D in endosomal membrane recycling. Mol Biol Cell. 17(1):327-335.

235. Padrón D, Tall RD, Roth MG. 2006. Phospholipase D2 is required for efficient endocytic recycling of transferrin receptors. Mol Biol Cell. 17(2):598-606.

236. Hashimoto Y, Okiyoneda T, Harada K, Ueno K, Sugahara T, Yamashita A, Shuto T, Suico MA, Kai H. 2008. Phosphatidic acid metabolism regulates the intracellular trafficking and retrotranslocation of CFTR. Biochim Biophys Acta. 1783(1):153-162.

237. Siddhanta A, Backer JM, Shields D. 2000. Inhibition of phosphatidic acid synthesis alters the structure of the Golgi apparatus and inhibits secretion in endocrine cells. J Biol Chem. 275(16):12023-12031.

238. Riebeling C, Morris AJ, Shields D. 2009. Phospholipase D in the Golgi apparatus. Biochim Biophys Acta. 1791(9):876-880.

239. Schmidt JA, Brown WJ. 2009. Lysophosphatidic acid acyltransferase 3 regulates Golgi complex structure and function. J Cell Biol. 186(2):211-218.

240. Bankaitis VA. 2009. The Cirque du Soleil of Golgi membrane dynamics. J Cell Biol. 186(2):169-171.

241. Fernandez-Ulibarri I, Vilella M, Lazaro-Dieguez F, Sarri E, Martinez SE, Jimenez N, Claro E, Merida I, Burger KN, Egea G. 2007. Diacylglycerol is required for the formation of COPI vesicles in the Golgi-to-ER transport pathway. Mol Biol Cell. 18(9):3250-3263.

242. Brown W, Chambers K, Doody A. 2003. Phospholipase A2 (PLA2) enzymes in membrane trafficking: mediators of membrane shape and function. Traffic. 4(4):214-221.

243. Christiansson A, Kuypers F, Roelofsen B, Op den Kamp J, van Deenen L. 1985. Lipid molecular shape affects erythrocyte morphology: a study involving replacement of native phosphatidylcholine with different species followed by treatment of cells with sphingomyelinase C or phospholipase A2. J Cell Biol. 101(4):1455-1462.

244. de Figueiredo P, Drecktrah D, Katzenellenbogen J, Strang M, Brown W. 1998. Evidence that phospholipase A2 activity is required for Golgi complex and trans Golgi network membrane tubulation. Proc Natl Acad Sci U S A. 95(15):8642-8647.

245. de Figueiredo P, Doody A, Polizotto R, Drecktrah D, Wood S, Banta M, Strang M, Brown W. 2001. Inhibition of transferrin recycling and endosome tubulation by phospholipase A2 antagonists. J Biol Chem. 276(50):47361-47370.

246. de Figueiredo P, Drecktrah D, Polizotto R, Cole N, Lippincott-Schwartz J, Brown W. 2000. Phospholipase A2 antagonists inhibit constitutive retrograde membrane traffic to the endoplasmic reticulum. Traffic. 1(6):504-511.

247. Kuroiwa N, Nakamura M, Tagaya M, Takatsuki A. 2001. Arachidonyltrifluoromethy ketone, a phospholipase A(2) antagonist, induces dispersal of both Golgi stack- and trans Golgi network-resident proteins throughout the cytoplasm. Biochem Biophys Res Commun. 281(2):582-588.

248. Tagaya M, Henomatsu N, Yoshimori T, Yamamoto A, Tashiro Y, Fukui T. 1993. Correlation between phospholipase A2 activity and intra-Golgi protein transport reconstituted in a cell-free system. FEBS Lett. 324(2):201-204.

249. Polizotto RS, de Figueiredo P, Brown WJ. 1999. Stimulation of Golgi membrane tubulation and retrograde trafficking to the ER by phospholipase A(2) activating protein (PLAP) peptide. J Cell Biochem. 74(4):670-683.

250. Schmidt JA, Kalkofen DN, Donovan KW, Brown WJ. 2010. A role for phospholipase A2 activity in membrane tubule formation and TGN trafficking. Traffic. Accepted Article(doi:10.1111/j.1399-0004.2010.01115.x).

251. Doody A, Antosh A, Brown W. 2009. Cytoplasmic phospholipase A2 antagonists inhibit multiple endocytic membrane trafficking pathways. Biochem Biophys Res Commun.

252. Evans JH, Spencer DM, Zweifach A, Leslie CC. 2001. Intracellular calcium signals regulating cytosolic phospholipase A2 translocation to internal membranes. J Biol Chem. 276(32):30150-30160.

253. Grewal S, Ponnambalam S, Walker JH. 2003. Association of cPLA2-alpha and COX-1 with the Golgi apparatus of A549 human lung epithelial cells. J Cell Sci. 116(Pt 11):2303-2310.

254. Evans JH, Leslie CC. 2004. The cytosolic phospholipase A2 catalytic domain modulates association and residence time at Golgi membranes. J Biol Chem. 279(7):6005-6016.

255. Evans JH, Gerber SH, Murray D, Leslie CC. 2004. The calcium binding loops of the cytosolic phospholipase A2 C2 domain specify targeting to Golgi and ER in live cells. Mol Biol Cell. 15(1):371-383.

256. San Pietro E, Capestrano M, Polishchuk EV, DiPentima A, Trucco A, Zizza P, Mariggio S, Pulvirenti T, Sallese M, Tete S, Mironov AA, Leslie CC, Corda D, Luini A, Polishchuk RS. 2009. Group IV phospholipase A(2)alpha controls the formation of inter-cisternal continuities involved in intra-Golgi transport. PLoS Biol. 7(9):e1000194.

257. Herbert S, Ponnambalam S, Walker J. 2005. Cytosolic Phospholipase A2-{alpha} Mediates Endothelial Cell Proliferation and Is Inactivated by Association with the Golgi Apparatus. Mol Biol Cell. 16(8):3800-3809.

258. Regan-Klapisz E, Krouwer V, Langelaar-Makkinje M, Nallan L, Gelb M, Gerritsen H, Verkleij AJ, Post JA. 2009. Golgi-associated cPLA2alpha regulates endothelial cell-cell junction integrity by controlling the trafficking of transmembrane junction proteins. Mol Biol Cell. 20(19):4225-4234.

259. Bechler ME, Doody AM, Racoosin E, Lin L, Lee KH, Brown WJ. 2010. The phospholipase complex PAFAH Ib regulates the functional organization of the Golgi complex. J Cell Biol. 190(1):45-53.

260. Morikawa RK, Aoki J, Kano F, Murata M, Yamamoto A, Tsujimoto M, Arai H. 2009. Intracellular phospholipase A1gamma (iPLA1gamma) is a novel factor involved in coat protein complex I- and Rab6-independent retrograde transport between the endoplasmic reticulum and the Golgi complex. J Biol Chem. 284(39):26620-26630.

261. Higgs HN, Glomset JA. 1996. Purification and properties of a phosphatidic acid-preferring phospholipase A1 from bovine testis. Examination of the molecular basis of its activation. J Biol Chem. 271(18):10874-10883.

262. Higgs HN, Han MH, Johnson GE, Glomset JA. 1998. Cloning of a phosphatidic acid-preferring phospholipase A1 from bovine testis. J Biol Chem. 273(10):5468-5477.

263. Tani K, Mizoguchi T, Iwamatsu A, Hatsuzawa K, Tagaya M. 1999. p125 is a novel mammalian Sec23p-interacting protein with structural similarity to phospholipid-modifying proteins. J Biol Chem. 274(29):20505-20512.

264. Shimoi W, Ezawa I, Nakamoto K, Uesaki S, Gabreski G, Aridor M, Yamamoto A, Nagahama M, Tagaya M, Tani K. 2005. p125 is localized in endoplasmic reticulum exit sites and involved in their organization. J Biol Chem. 280(11):10141-10148.

265. Schaloske RH, Dennis EA. 2006. The phospholipase A2 superfamily and its group numbering system. Biochim Biophys Acta. 1761(11):1246-1259.

266. Burke JE, Dennis EA. 2009. Phospholipase A2 structure/function, mechanism, and signaling. J Lipid Res. 50 Suppl:S237-242.

267. Burke J, Dennis E. 2009. Phospholipase A2 biochemistry. Cardiovasc Drugs Ther. 23(1):49-59.

268. Lambeau G, Gelb MH. 2008. Biochemistry and physiology of mammalian secreted phospholipases A2. Annu Rev Biochem. 77:495-520.

269. Boyanovsky BB, Webb NR. 2009. Biology of secretory phospholipase A2. Cardiovasc Drugs Ther. 23(1):61-72.

270. Hiraoka M, Abe A, Shayman JA. 2002. Cloning and characterization of a lysosomal phospholipase A2, 1-O-acylceramide synthase. J Biol Chem. 277(12):10090-10099.

271. Hiraoka M, Abe A, Shayman JA. 2005. Structure and function of lysosomal phospholipase A2: identification of the catalytic triad and the role of cysteine residues. J Lipid Res. 46(11):2441-2447.

272. Abe A, Shayman JA. 1998. Purification and characterization of 1-O-acylceramide synthase, a novel phospholipase A2 with transacylase activity. J Biol Chem. 273(14):8467-8474.

273. Hiraoka M, Abe A, Lu Y, Yang K, Han X, Gross RW, Shayman JA. 2006. Lysosomal phospholipase A2 and phospholipidosis. Mol Cell Biol. 26(16):6139-6148.

274. Chiba H, Michibata H, Wakimoto K, Seishima M, Kawasaki S, Okubo K, Mitsui H, Torii H, Imai Y. 2004. Cloning of a gene for a novel epithelium-specific cytosolic phospholipase A2, cPLA2delta, induced in psoriatic skin. J Biol Chem. 279(13):12890-12897.

275. Clark JD, Lin LL, Kriz RW, Ramesha CS, Sultzman LA, Lin AY, Milona N, Knopf JL. 1991. A novel arachidonic acid-selective cytosolic PLA2 contains a Ca(2+)-dependent translocation domain with homology to PKC and GAP. Cell. 65(6):1043-1051.

276. Dessen A, Tang J, Schmidt H, Stahl M, Clark JD, Seehra J, Somers WS. 1999. Crystal structure of human cytosolic phospholipase A2 reveals a novel topology and catalytic mechanism. Cell. 97(3):349-360.

277. Underwood KW, Song C, Kriz RW, Chang XJ, Knopf JL, Lin LL. 1998. A novel calcium-independent phospholipase A2, cPLA2-gamma, that is prenylated and contains homology to cPLA2. J Biol Chem. 273(34):21926-21932.

278. Lemmon MA. 2008. Membrane recognition by phospholipid-binding domains. Nat Rev Mol Cell Biol. 9(2):99-111.

279. Leslie CC. 1991. Kinetic properties of a high molecular mass arachidonoyl-hydrolyzing phospholipase A2 that exhibits lysophospholipase activity. J Biol Chem. 266(17):11366-11371.

280. Reynolds NJ, Talwar HS, Baldassare JJ, Henderson PA, Elder JT, Voorhees JJ, Fisher GJ. 1993. Differential induction of phosphatidylcholine hydrolysis, diacylglycerol formation and protein kinase C activation by epidermal growth factor and transforming growth factor-alpha in normal human skin fibroblasts and keratinocytes. Biochem J. 294 (Pt 2):535-544.

281. Mosior M, Six DA, Dennis EA. 1998. Group IV cytosolic phospholipase A2 binds with high affinity and specificity to phosphatidylinositol 4,5-bisphosphate resulting in dramatic increases in activity. J Biol Chem. 273(4):2184-2191.

282. Six DA, Dennis EA. 2003. Essential Ca(2+)-independent role of the group IVA cytosolic phospholipase A(2) C2 domain for interfacial activity. J Biol Chem. 278(26):23842-23850.

283. Pettus BJ, Bielawska A, Subramanian P, Wijesinghe DS, Maceyka M, Leslie CC, Evans JH, Freiberg J, Roddy P, Hannun YA, Chalfant CE. 2004. Ceramide 1-phosphate is a direct activator of cytosolic phospholipase A2. J Biol Chem. 279(12):11320-11326.

284. Lin LL, Wartmann M, Lin AY, Knopf JL, Seth A, Davis RJ. 1993. cPLA2 is phosphorylated and activated by MAP kinase. Cell. 72(2):269-278.

285. Hefner Y, Borsch-Haubold AG, Murakami M, Wilde JI, Pasquet S, Schieltz D, Ghomashchi F, Yates JR, 3rd, Armstrong CG, Paterson A, Cohen P, Fukunaga R, Hunter T, Kudo I, Watson SP, Gelb MH. 2000. Serine 727 phosphorylation and activation of cytosolic phospholipase A2 by MNK1-related protein kinases. J Biol Chem. 275(48):37542-37551.

286. Uozumi N, Kume K, Nagase T, Nakatani N, Ishii S, Tashiro F, Komagata Y, Maki K, Ikuta K, Ouchi Y, Miyazaki J, Shimizu T. 1997. Role of cytosolic phospholipase A2 in allergic response and parturition. Nature. 390(6660):618-622.

287. Uozumi N, Shimizu T. 2002. Roles for cytosolic phospholipase A2alpha as revealed by gene-targeted mice. Prostaglandins Other Lipid Mediat. 68-69:59-69.

288. Lucas KK, Svensson CI, Hua XY, Yaksh TL, Dennis EA. 2005. Spinal phospholipase A2 in inflammatory hyperalgesia: role of group IVA cPLA2. Br J Pharmacol. 144(7):940-952.

289. Bonventre JV, Huang Z, Taheri MR, O'Leary E, Li E, Moskowitz MA, Sapirstein A. 1997. Reduced fertility and postischaemic brain injury in mice deficient in cytosolic phospholipase A2. Nature. 390(6660):622-625.

290. Bao S, Miller DJ, Ma Z, Wohltmann M, Eng G, Ramanadham S, Moley K, Turk J. 2004. Male mice that do not express group VIA phospholipase A2 produce spermatozoa with impaired motility and have greatly reduced fertility. J Biol Chem. 279(37):38194-38200.

291. Ackermann EJ, Kempner ES, Dennis EA. 1994. Ca(2+)-independent cytosolic phospholipase A2 from macrophage-like P388D1 cells. Isolation and characterization. J Biol Chem. 269(12):9227-9233.

292. Tang J, Kriz RW, Wolfman N, Shaffer M, Seehra J, Jones SS. 1997. A novel cytosolic calcium-independent phospholipase A2 contains eight ankyrin motifs. J Biol Chem. 272(13):8567-8575.

293. Jenkins CM, Mancuso DJ, Yan W, Sims HF, Gibson B, Gross RW. 2004. Identification, cloning, expression, and purification of three novel human calcium-independent phospholipase A2 family members possessing triacylglycerol lipase and acylglycerol transacylase activities. J Biol Chem. 279(47):48968-48975.

294. Lio YC, Dennis EA. 1998. Interfacial activation, lysophospholipase and transacylase activity of group VI Ca2+-independent phospholipase A2. Biochim Biophys Acta. 1392(2-3):320-332.

295. Kienesberger PC, Oberer M, Lass A, Zechner R. 2009. Mammalian patatin domain containing proteins: a family with diverse lipolytic activities involved in multiple biological functions. J Lipid Res. 50 Suppl:S63-68.

296. Glynn P. 1999. Neuropathy target esterase. Biochem J. 344 Pt 3:625-631.

297. Kretzschmar D, Hasan G, Sharma S, Heisenberg M, Benzer S. 1997. The swiss cheese mutant causes glial hyperwrapping and brain degeneration in Drosophila. J Neurosci. 17(19):7425-7432.

298. van Tienhoven M, Atkins J, Li Y, Glynn P. 2002. Human neuropathy target esterase catalyzes hydrolysis of membrane lipids. J Biol Chem. 277(23):20942-20948.

299. Mcintyre TM, Prescott SM, Stafforini DM. 2008. The emerging roles of PAF acetylhydrolase. The Journal of Lipid Research. 50(Supplement):S255-S259.

300. Tjoelker LW, Wilder C, Eberhardt C, Stafforini DM, Dietsch G, Schimpf B, Hooper S, Le Trong H, Cousens LS, Zimmerman GA, et al. 1995. Anti-

inflammatory properties of a platelet-activating factor acetylhydrolase. Nature. 374(6522):549-553.

301. Tjoelker LW, Eberhardt C, Unger J, Trong HL, Zimmerman GA, McIntyre TM, Stafforini DM, Prescott SM, Gray PW. 1995. Plasma platelet-activating factor acetylhydrolase is a secreted phospholipase A2 with a catalytic triad. J Biol Chem. 270(43):25481-25487.

302. Arai H. 2002. Platelet-activating factor acetylhydrolase. Prostaglandins Other Lipid Mediat. 68-69:83-94.

303. Snyder F. Platelet-activating factor and related lipid mediators. New York, NY: Plenum Press; 1987.

304. Lotner GZ, Lynch JM, Betz SJ, Henson PM. 1980. Human neutrophil-derived platelet activating factor. J Immunol. 124(2):676-684.

305. Mariano F, Bussolati B, Migliori M, Russo S, Triolo G, Camussi G. 2003. Platelet-activating factor synthesis by neutrophils, monocytes, and endothelial cells is modulated by nitric oxide production. Shock. 19(4):339-344.

306. Ishii S, Kuwaki T, Nagase T, Maki K, Tashiro F, Sunaga S, Cao WH, Kume K, Fukuchi Y, Ikuta K, Miyazaki J, Kumada M, Shimizu T. 1998. Impaired anaphylactic responses with intact sensitivity to endotoxin in mice lacking a platelet-activating factor receptor. J Exp Med. 187(11):1779-1788.

307. Kato K, Clark GD, Bazan NG, Zorumski CF. 1994. Platelet-activating factor as a potential retrograde messenger in CA1 hippocampal long-term potentiation. Nature. 367(6459):175-179.

308. Hamasaki Y, Mojarad M, Saga T, Tai HH, Said SI. 1984. Platelet-activating factor raises airway and vascular pressures and induces edema in lungs perfused with platelet-free solution. Am Rev Respir Dis. 129(5):742-746.

309. Vadas P, Gold M, Perelman B, Liss GM, Lack G, Blyth T, Simons FE, Simons KJ, Cass D, Yeung J. 2008. Platelet-activating factor, PAF acetylhydrolase, and severe anaphylaxis. N Engl J Med. 358(1):28-35.

310. Prescott SM, Zimmerman GA, Stafforini DM, McIntyre TM. 2000. Platelet-activating factor and related lipid mediators. Annu Rev Biochem. 69:419-445.

311. Ishii S, Nagase T, Shimizu T. 2002. Platelet-activating factor receptor. Prostaglandins Other Lipid Mediat. 68-69:599-609.

312. Stremler KE, Stafforini DM, Prescott SM, McIntyre TM. 1991. Human plasma platelet-activating factor acetylhydrolase. Oxidatively fragmented phospholipids as substrates. J Biol Chem. 266(17):11095-11103.

313. Stafforini DM, McIntyre TM, Carter ME, Prescott SM. 1987. Human plasma platelet-activating factor acetylhydrolase. Association with lipoprotein particles and role in the degradation of platelet-activating factor. J Biol Chem. 262(9):4215-4222.

314. Gardner AA, Reichert EC, Topham MK, Stafforini DM. 2008. Identification of a domain that mediates association of platelet-activating factor acetylhydrolase with high density lipoprotein. J Biol Chem. 283(25):17099-17106.

315. Wilensky RL, Macphee CH. 2009. Lipoprotein-associated phospholipase A(2) and atherosclerosis. Curr Opin Lipidol. 20(5):415-420.

316. Garza CA, Montori VM, McConnell JP, Somers VK, Kullo IJ, Lopez-Jimenez F. 2007. Association between lipoprotein-associated phospholipase A2 and cardiovascular disease: a systematic review. Mayo Clin Proc. 82(2):159-165.

317. Matsuzawa A, Hattori K, Aoki J, Arai H, Inoue K. 1997. Protection against oxidative stress-induced cell death by intracellular platelet-activating factor-acetylhydrolase II. J Biol Chem. 272(51):32315-32320.

318. Hattori M, Adachi H, Tsujimoto M, Arai H, Inoue K. 1994. The catalytic subunit of bovine brain platelet-activating factor acetylhydrolase is a novel type of serine esterase. J Biol Chem. 269(37):23150-23155.

319. Hattori K, Hattori M, Adachi H, Tsujimoto M, Arai H, Inoue K. 1995. Purification and characterization of platelet-activating factor acetylhydrolase II from bovine liver cytosol. J Biol Chem. 270(38):22308-22313.

320. McMullen TW, Li J, Sheffield PJ, Aoki J, Martin TW, Arai H, Inoue K, Derewenda ZS. 2000. The functional implications of the dimerization of the catalytic subunits of the mammalian brain platelet-activating factor acetylhydrolase (Ib). Protein Eng. 13(12):865-871.

321. Ho Y, Swenson L, Derewenda U, Serre L, Wei Y, Dauter Z, Hattori M, Adachi T, Aoki J, Arai H, Inoue K, Derewenda Z. 1997. Brain acetylhydrolase that inactivates platelet-activating factor is a G-protein-like trimer. Nature. 385(6611):89-93.

322. Hattori M, Arai H, Inoue K. 1993. Purification and characterization of bovine brain platelet-activating factor acetylhydrolase. J Biol Chem. 268(25):18748-18753.

323. Manya H, Aoki J, Kato H, Ishii J, Hino S, Arai H, Inoue K. 1999. Biochemical characterization of various catalytic complexes of the brain platelet-activating factor acetylhydrolase. J Biol Chem. 274(45):31827-31832.

324. Arai H, Koizumi H, Aoki J, Inoue K. 2002. Platelet-activating factor acetylhydrolase (PAF-AH). J Biochem (Tokyo). 131(5):635-640.

325. Manya H, Aoki J, Watanabe M, Adachi T, Asou H, Inoue Y, Arai H, Inoue K. 1998. Switching of platelet-activating factor acetylhydrolase catalytic subunits in developing rat brain. J Biol Chem. 273(29):18567-18572.

326. Koizumi H, Yamaguchi N, Hattori M, Ishikawa T, Aoki J, Taketo M, Inoue K, Arai H. 2003. Targeted disruption of intracellular type I platelet activating factor-acetylhydrolase catalytic subunits causes severe impairment in spermatogenesis. J Biol Chem. 278(14):12489-12494.

327. Adachi H, Tsujimoto M, Hattori M, Arai H, Inoue K. 1995. cDNA cloning of human cytosolic platelet-activating factor acetylhydrolase gamma-subunit and its mRNA expression in human tissues. Biochem Biophys Res Commun. 214(1):180-187.

328. Adachi H, Tsujimoto M, Hattori M, Arai H, Inoue K. 1997. Differential tissue distribution of the beta- and gamma-subunits of human cytosolic platelet-activating factor acetylhydrolase (isoform I). Biochem Biophys Res Commun. 233(1):10-13.

329. Sheffield PJ, Garrard S, Caspi M, Aoki J, Arai H, Derewenda U, Inoue K, Suter B, Reiner O, Derewenda ZS. 2000. Homologs of the alpha- and beta-subunits of mammalian brain platelet-activating factor acetylhydrolase Ib in the Drosophila melanogaster genome. Proteins. 39(1):1-8.

330. Yan W, Assadi AH, Wynshaw-Boris A, Eichele G, Matzuk MM, Clark GD. 2003. Previously uncharacterized roles of platelet-activating factor acetylhydrolase 1b complex in mouse spermatogenesis. Proc Natl Acad Sci U S A. 100(12):7189-7194.

331. Tarricone C, Perrina F, Monzani S, Massimiliano L, Kim MH, Derewenda ZS, Knapp S, Tsai LH, Musacchio A. 2004. Coupling PAF Signaling to Dynein Regulation; Structure of LIS1 in Complex with PAF-Acetylhydrolase. Neuron. 44(5):809-821.

332. Dobyns WB, Reiner O, Carrozzo R, Ledbetter DH. 1993. Lissencephaly. A human brain malformation associated with deletion of the LIS1 gene located at chromosome 17p13. JAMA. 270(23):2838-2842.

333. Reiner O, Carrozzo R, Shen Y, Wehnert M, Faustinella F, Dobyns WB, Caskey CT, Ledbetter DH. 1993. Isolation of a Miller-Dieker lissencephaly gene containing G protein beta-subunit-like repeats. Nature. 364(6439):717-721.

334. Hirotsune S, Fleck MW, Gambello MJ, Bix GJ, Chen A, Clark GD, Ledbetter DH, McBain CJ, Wynshaw-Boris A. 1998. Graded reduction of

Pafah1b1 (Lis1) activity results in neuronal migration defects and early embryonic lethality. Nat Genet. 19(4):333-339.

335. Pawlisz AS, Mutch C, Wynshaw-Boris A, Chenn A, Walsh CA, Feng Y. 2008. Lis1-Nde1-dependent neuronal fate control determines cerebral cortical size and lamination. Hum Mol Genet. 17(16):2441-2455.

336. Assadi AH, Zhang G, McNeil R, Clark GD, D'Arcangelo G. 2008. Pafah1b2 mutations suppress the development of hydrocephalus in compound Pafah1b1; Reln and Pafah1b1; Dab1 mutant mice. Neurosci Lett. 439(1):100-105.

337. Yamaguchi N, Koizumi H, Aoki J, Natori Y, Nishikawa K, Natori Y, Takanezawa Y, Arai H. 2007. Type I platelet-activating factor acetylhydrolase catalytic subunits over-expression induces pleiomorphic nuclei and centrosome amplification. Genes Cells. 12(10):1153-1161.

338. Ding C, Liang X, Ma L, Yuan X, Zhu X. 2009. Opposing effects of Ndel1 and 1 or 2 on cytoplasmic dynein through competitive binding to Lis1. J Cell Sci. 122(16):2820-2827.

339. Vallee RB, Tsai JW. 2006. The cellular roles of the lissencephaly gene LIS1, and what they tell us about brain development. Genes Dev. 20(11):1384-1393.

340. Kardon JR, Vale RD. 2009. Regulators of the cytoplasmic dynein motor. Nat Rev Mol Cell Biol. 10(12):854-865.

341. Criswell PS, Ostrowski LE, Asai DJ. 1996. A novel cytoplasmic dynein heavy chain: expression of DHC1b in mammalian ciliated epithelial cells. J Cell Sci. 109 (Pt 7):1891-1898.

342. Vaisberg EA, Grissom PM, McIntosh JR. 1996. Mammalian cells express three distinct dynein heavy chains that are localized to different cytoplasmic organelles. J Cell Biol. 133(4):831-842.

343. Soldati T, Schliwa M. 2006. Powering membrane traffic in endocytosis and recycling. Nat Rev Mol Cell Biol. 7(12):897-908.

344. Schroer TA. 2004. Dynactin. Annu Rev Cell Dev Biol. 20:759-779.

345. Allan V. 1996. Motor proteins: a dynamic duo. Curr Biol. 6(6):630-633.

346. Holleran EA, Karki S, Holzbaur EL. 1998. The role of the dynactin complex in intracellular motility. Int Rev Cytol. 182:69-109.

347. King SJ, Schroer TA. 2000. Dynactin increases the processivity of the cytoplasmic dynein motor. Nat Cell Biol. 2(1):20-24.

348. Schroer T. 2000. Motors, clutches and brakes for membrane traffic: a commemorative review in honor of Thomas Kreis. Traffic. 1(1):3-10.

349. Valetti C, Wetzel DM, Schrader M, Hasbani MJ, Gill SR, Kreis TE, Schroer TA. 1999. Role of dynactin in endocytic traffic: effects of dynamitin overexpression and colocalization with CLIP-170. Mol Biol Cell. 10(12):4107-4120.

350. Traer CJ, Rutherford AC, Palmer KJ, Wassmer T, Oakley J, Attar N, Carlton JG, Kremerskothen J, Stephens DJ, Cullen PJ. 2007. SNX4 coordinates endosomal sorting of TfnR with dynein-mediated transport into the endocytic recycling compartment. Nat Cell Biol. 9(12):1370-1380.

351. Hirokawa N, Noda Y. 2008. Intracellular transport and kinesin superfamily proteins, KIFs: structure, function, and dynamics. Physiol Rev. 88(3):1089-1118.

352. Faulkner N, Dujardin D, Tai C, Vaughan K, O'Connell C, Wang Y, Vallee R. 2000. A role for the lissencephaly gene LIS1 in mitosis and cytoplasmic dynein function. Nat Cell Biol. 2(11):784-791.

353. Rehberg M, Kleylein-Sohn J, Faix J, Ho TH, Schulz I, Graf R. 2005. Dictyostelium LIS1 is a centrosomal protein required for microtubule/cell cortex interactions, nucleus/centrosome linkage, and actin dynamics. Mol Biol Cell. 16(6):2759-2771.

354. Sapir T, Elbaum M, Reiner O. 1997. Reduction of microtubule catastrophe events by LIS1, platelet-activating factor acetylhydrolase subunit. Embo J. 16(23):6977-6984.

355. Xiang X, Osmani AH, Osmani SA, Xin M, Morris NR. 1995. NudF, a nuclear migration gene in Aspergillus nidulans, is similar to the human LIS-1 gene required for neuronal migration. Mol Biol Cell. 6(3):297-310.

356. Caspi M, Coquelle F, Koifman C, Levy T, Arai H, Aoki J, De Mey J, Reiner O. 2003. LIS1 missense mutations: variable phenotypes result from unpredictable alterations in biochemical and cellular properties. J Biol Chem. 278(40):38740-38748.

357. McKenney RJ, Vershinin M, Kunwar A, Vallee RB, Gross SP. 2010. LIS1 and NudE induce a persistent dynein force-producing state. Cell. 141(2):304-314.

358. Smith DS, Niethammer M, Ayala R, Zhou Y, Gambello MJ, Wynshaw-Boris A, Tsai LH. 2000. Regulation of cytoplasmic dynein behaviour and microtubule organization by mammalian Lis1. Nat Cell Biol. 2(11):767-775.

359. Tai CY, Dujardin DL, Faulkner NE, Vallee RB. 2002. Role of dynein, dynactin, and CLIP-170 interactions in LIS1 kinetochore function. J Cell Biol. 156(6):959-968.

360. Lam C, Vergnolle MAS, Thorpe L, Woodman PG, Allan VJ. 2010. Functional interplay between LIS1, NDE1 and NDEL1 in dynein-dependent organelle positioning. J Cell Sci. 123(Pt 2):202-212.

361. Vallee R, Tai C, Faulkner N. 2001. LIS1: cellular function of a disease-causing gene. Trends Cell Biol. 11(4):155-160.

362. Chan D, Strang M, Judson B, Brown W. 2004. Inhibition of membrane tubule formation and trafficking by isotetrandrine, an antagonist of G-protein-regulated phospholipase A2 enzymes. Mol Biol Cell. 15(4):1871-1880.

363. Pfeffer SR. 2007. Unsolved mysteries in membrane traffic. Annu Rev Biochem. 76:629-645.

364. Drecktrah D, Brown WJ. 1999. Phospholipase A(2) antagonists inhibit nocodazole-induced Golgi ministack formation: evidence of an ER intermediate and constitutive cycling. Mol Biol Cell. 10(12):4021-4032.

365. Hattori M, Adachi H, Tsujimoto M, Arai H, Inoue K. 1994. Miller-Dieker lissencephaly gene encodes a subunit of brain platelet-activating factor acetylhydrolase [corrected]. Nature. 370(6486):216-218.

366. Kato M, Dobyns W. 2003. Lissencephaly and the molecular basis of neuronal migration. Hum Mol Genet. 12 Spec No 1:R89-96.

367. Kerjan G, Gleeson JG. 2007. Genetic mechanisms underlying abnormal neuronal migration in classical lissencephaly. Trends Genet. 23(12):623-630.

368. Brown WJ, Farquhar MG. 1987. The distribution of 215-kilodalton mannose 6-phosphate receptors within cis (heavy) and trans (light) Golgi subfractions varies in different cell types. Proc Natl Acad Sci U S A. 84(24):9001-9005.

369. Banta M, Polizotto RS, Wood SA, de Figueiredo P, Brown WJ. 1995. Characterization of a cytosolic activity that induces the formation of Golgi membrane tubules in a cell-free reconstitution system. Biochemistry. 34(41):13359-13366.

370. Zhang G, Assadi AH, McNeil RS, Beffert U, Wynshaw-Boris A, Herz J, Clark GD, D'Arcangelo G. 2007. The Pafah1b complex interacts with the reelin receptor VLDLR. PLoS ONE. 2(2):e252.

371. Yeaman C, Ayala M, Wright J, Bard F, Bossard C, Ang A, Maeda Y, Seufferlein T, Mellman I, Nelson W, Malhotra V. 2004. Protein kinase D

regulates basolateral membrane protein exit from trans-Golgi network. Nat Cell Biol. 6(2):106-112.

372. Drecktrah D, de Figueiredo P, Mason RM, Brown WJ. 1998. Retrograde trafficking of both Golgi complex and TGN markers to the ER induced by nordihydroguaiaretic acid and cyclofenil diphenol. J Cell Sci. 111 (Pt 7):951-965.

373. He W, Ladinsky MS, Huey-Tubman KE, Jensen GJ, McIntosh JR, Bjorkman PJ. 2008. FcRn-mediated antibody transport across epithelial cells revealed by electron tomography. Nature. 455(7212):542-546.

374. Miaczynska M, Zerial M. 2002. Mosaic organization of the endocytic pathway. Exp Cell Res. 272(1):8-14.

375. Geuze H, Slot J, Schwartz A. 1987. Membranes of sorting organelles display lateral heterogeneity in receptor distribution. J Cell Biol. 104(6):1715-1723.

376. Rojas R, Van Vlijmen T, Mardones GA, Prabhu Y, Rojas AL, Mohammed S, Heck AJR, Raposo G, van der Sluijs P, Bonifacino JS. 2008. Regulation of retromer recruitment to endosomes by sequential action of Rab5 and Rab7. J Cell Biol. 183(3):513-526.

377. Yamada M, Toba S, Yoshida Y, Haratani K, Mori D, Yano Y, Mimori-Kiyosue Y, Nakamura T, Itoh K, Fushiki S, Setou M, Wynshaw-Boris A, Torisawa T, Toyoshima YY, Hirotsune S. 2008. LIS1 and NDEL1 coordinate the plus-end-directed transport of cytoplasmic dynein. Embo J. 27(19):2471-2483.

378. Park J, Lopez J, Cluett E, Brown W. 1991. Identification of a membrane glycoprotein found primarily in the prelysosomal endosome compartment. J Cell Biol. 112(2):245-255.

379. Heller L, Park J, Brown W. 1994. Biosynthesis and intracellular transport of a membrane glycoprotein (plgp57) of the prelysosome compartment. Mol Membr Biol. 11(2):127-134.

380. Park JE, Draper RK, Brown WJ. 1991. Biosynthesis of lysosomal enzymes in cells of the End3 complementation group conditionally defective in endosomal acidification. Somat Cell Mol Genet. 17(2):137-150.

381. Liang Y, Yu W, Li Y, Yang Z, Yan X, Huang Q, Zhu X. 2004. Nudel functions in membrane traffic mainly through association with Lis1 and cytoplasmic dynein. J Cell Biol. 164(4):557-566.

382. Lippincott-Schwartz J, Yuan L, Tipper C, Amherdt M, Orci L, Klausner RD. 1991. Brefeldin A's effects on endosomes, lysosomes, and the TGN

suggest a general mechanism for regulating organelle structure and membrane traffic. Cell. 67(3):601-616.

383. Wood SA, Brown WJ. 1992. The morphology but not the function of endosomes and lysosomes is altered by brefeldin A. J Cell Biol. 119(2):273-285.

384. Wood SA, Park JE, Brown WJ. 1991. Brefeldin A causes a microtubule-mediated fusion of the trans-Golgi network and early endosomes. Cell. 67(3):591-600.

385. Driskell OJ, Mironov A, Allan VJ, Woodman PG. 2007. Dynein is required for receptor sorting and the morphogenesis of early endosomes. Nat Cell Biol. 9(1):113-120.

386. Roudebush WE, Wild MD, Maguire EH. 2000. Expression of the platelet-activating factor receptor in human spermatozoa: differences in messenger ribonucleic acid content and protein distribution between normal and abnormal spermatozoa. Fertil Steril. 73(5):967-971.

387. Roudebush WE, Diehl JR. 2001. Platelet-activating factor content in boar spermatozoa correlates with fertility. Theriogenology. 55(8):1633-1638.

388. Puertollano R, van der Wel NN, Greene LE, Eisenberg E, Peters PJ, Bonifacino JS. 2003. Morphology and dynamics of clathrin/GGA1-coated carriers budding from the trans-Golgi network. Mol Biol Cell. 14(4):1545-1557.

389. Rosso S, Bollati F, Bisbal M, Peretti D, Sumi T, Nakamura T, Quiroga S, Ferreira A, Caceres A. 2004. LIMK1 regulates Golgi dynamics, traffic of Golgi-derived vesicles, and process extension in primary cultured neurons. Mol Biol Cell. 15(7):3433-3449.

390. Weller SG, Capitani M, Cao H, Micaroni M, Luini A, Sallese M, McNiven MA. 2010. Src kinase regulates the integrity and function of the Golgi apparatus via activation of dynamin 2. Proc Natl Acad Sci U S A. 107(13):5863-5868.

391. Bard F, Mazelin L, Pechoux-Longin C, Malhotra V, Jurdic P. 2003. Src regulates Golgi structure and KDEL receptor-dependent retrograde transport to the endoplasmic reticulum. J Biol Chem. 278(47):46601-46606.

392. Jamora C, Yamanouye N, Van Lint J, Laudenslager J, Vandenheede JR, Faulkner DJ, Malhotra V. 1999. Gbetagamma-mediated regulation of Golgi organization is through the direct activation of protein kinase D. Cell. 98(1):59-68.

393. Irannejad R, Wedegaertner PB. 2010. Regulation of constitutive cargo transport from the trans-golgi network to plasma membrane by golgi-localized G protein {beta}{gamma} subunits. J Biol Chem.

394. Stow JL, de Almeida JB, Narula N, Holtzman EJ, Ercolani L, Ausiello DA. 1991. A heterotrimeric G protein, G alpha i-3, on Golgi membranes regulates the secretion of a heparan sulfate proteoglycan in LLC-PK1 epithelial cells. J Cell Biol. 114(6):1113-1124.

395. Denker S, McCaffery J, Palade G, Insel P, Farquhar M. 1996. Differential distribution of alpha subunits and beta gamma subunits of heterotrimeric G proteins on Golgi membranes of the exocrine pancreas. J Cell Biol. 133(5):1027-1040.

396. Jamora C, Takizawa PA, Zaarour RF, Denesvre C, Faulkner DJ, Malhotra V. 1997. Regulation of Golgi structure through heterotrimeric G proteins. Cell. 91(5):617-626.

397. Diaz Anel A, Malhotra V. 2005. PKCeta is required for beta1gamma2/beta3gamma2- and PKD-mediated transport to the cell surface and the organization of the Golgi apparatus. J Cell Biol. 169(1):83-91.

398. Takizawa PA, Yucel JK, Veit B, Faulkner DJ, Deerinck T, Soto G, Ellisman M, Malhotra V. 1993. Complete vesiculation of Golgi membranes and inhibition of protein transport by a novel sea sponge metabolite, ilimaquinone. Cell. 73(6):1079-1090.

399. Liljedahl M, Maeda Y, Colanzi A, Ayala I, Van Lint J, Malhotra V. 2001. Protein kinase D regulates the fission of cell surface destined transport carriers from the trans-Golgi network. Cell. 104(3):409-420.

400. Akgoz M, Kalyanaraman V, Gautam N. 2006. G protein betagamma complex translocation from plasma membrane to Golgi complex is influenced by receptor gamma subunit interaction. Cell Signal.

401. Saini DK, Karunarathne WKA, Angaswamy N, Saini D, Cho J-H, Kalyanaraman V, Gautam N. 2010. Regulation of Golgi structure and secretion by receptor-induced G protein complex translocation. Proceedings of the National Academy of Sciences. 107(25):11417-11422.

402. Akiba S, Nagatomo R, Ishimoto T, Sato T. 1995. Effect of berbamine on cytosolic phospholipase A2 activation in rabbit platelets. Eur J Pharmacol. 291(3):343-350.

403. Akiba S, Kato E, Sato T, Fujii T. 1992. Biscoclaurine alkaloids inhibit receptor-mediated phospholipase A2 activation probably through uncoupling of a GTP-binding protein from the enzyme in rat peritoneal mast cells. Biochem Pharmacol. 44(1):45-50.

404. Hashizume T, Yamaguchi H, Sato T, Fujii T. 1991. Suppressive effect of biscoclaurine alkaloids on agonist-induced activation of phospholipase A2 in rabbit platelets. Biochem Pharmacol. 41(3):419-423.

405. Cluett E, Wood S, Banta M, Brown W. 1993. Tubulation of Golgi membranes in vivo and in vitro in the absence of brefeldin A. J Cell Biol. 120(1):15-24.

406. Akiba S, Abe T, Sato T. 1995. Increased cytosolic phospholipase A2 activity is not accompanied by arachidonic acid liberation in U46619-stimulated rabbit platelets. Biochem Mol Biol Int. 35(2):275-281.

407. Saini DK, Kalyanaraman V, Chisari M, Gautam N. 2007. A family of G protein betagamma subunits translocate reversibly from the plasma membrane to endomembranes on receptor activation. J Biol Chem. 282(33):24099-24108.

408. Fugmann T, Hausser A, Schoffler P, Schmid S, Pfizenmaier K, Olayioye MA. 2007. Regulation of secretory transport by protein kinase D-mediated phosphorylation of the ceramide transfer protein. J Cell Biol. 178(1):15-22.

409. Hausser A, Storz P, Martens S, Link G, Toker A, Pfizenmaier K. 2005. Protein kinase D regulates vesicular transport by phosphorylating and activating phosphatidylinositol-4 kinase IIIbeta at the Golgi complex. Nat Cell Biol.

410. Bossard C, Bresson D, Polishchuk RS, Malhotra V. 2007. Dimeric PKD regulates membrane fission to form transport carriers at the TGN. J Cell Biol. 179(6):1123-1131.